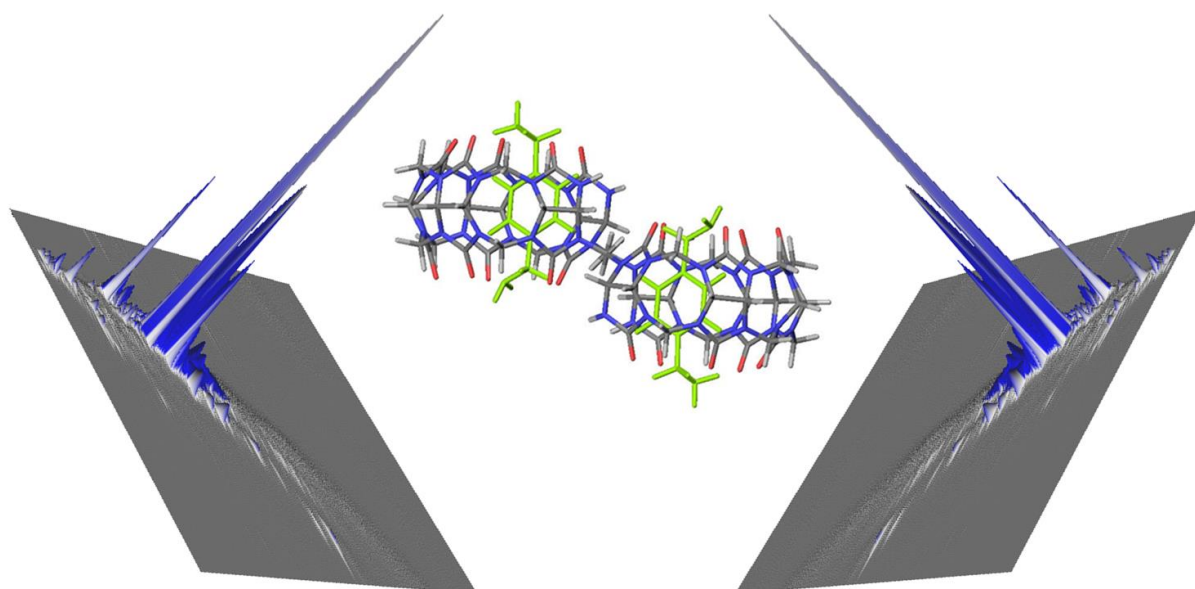




Assessment of the Combination between Mass Spectrometry  
and Computational Chemistry for the investigation of  
Supramolecular Assemblies



Gaseous Flying Boxes as a Case Study

CARROY GLENN

Promoteurs : Prof. Pascal Gerbaux

Prof. Edwin De Pauw

Prof. Jérôme Cornil

Dissertation présentée en vue de l'obtention du  
grade académique de Docteur en Sciences

*Année Académique 2017-2018*

## Acknowledgments

*« Allo?*

*Hey Glenn, Pascal here, how are you?*

*Hey Pascal, I am fine, thank you, what about you?*

*I am OK, look, I might have a solution if you still want to do a PhD, do you want to hear it? »*

This looks closely to the phone call I received from **Pascal Gerbaux** in April 2013. Back then, I was working in the pharmaceutical industry after two failures at the F.R.I.A contest where I tried to obtain a PhD financial support. If I am here today, if I know what I know and if, somehow, I am a little bit good at what I do; the credit first goes to Pascal. Boss, I would like to thank you for believing in me, even though I know I have not been easy to manage all the time. I am proud I have been able to witness and participate to the evolution of the S<sup>2</sup>MOs lab along the years. Now the social rehabilitation begins ( ;- ) but be sure I will never forget those almost 7 years in total spent on your (dark?) side. Thank you very, very much for everything.

*« What?*

*I have a question about "subject A", I don't understand what's happening.*

*Yes but did you think about "subject B", "subject C", have you check your references, internet, books, stars, tarot cards and read the coffee spots?*

*.... I said I don't understand! »*

When you start to work with **Julien De Winter**, you better be patient and learn how to not be easily offended but actually, if you think deeper about it, everything Julien is doing helps you to be better at what you do , to be smarter and a better scientist. When you get to know him, under his sarcasms and bad humors, there is someone helpful and gentle, which will always find a moment to help you at whatever you need him, a tattoo lover (long live Instagram), someone devoted to his work and a true kickass scientist. Now my time is over at the lab, I can say I admire that guy, but won't tell him to much (kidding). Julien, thank you for all the questions and discussions we had, we had some disagreements, but you always responded and I will never forget that.

*« You can be a Jedi [!] but you will not studi [!] »*

**Jerôme Cornil** knows how to make good English tips for myself! Jérôme always impressed me with how he was able to deal with so many different subjects and (experimental/computational) technics. He always came with some insides and solutions when we had meetings for our different publications and issues. Master in jokes and spoonerisms (well, Pascal is also not bad at it), I will always remember those meeting, which were perfect mix of hard work and fun time. Thank you Jérôme for all your help and advices along those years.

*« You can take more processors, they won't see it. \*don't worry face\* »*

I worked with **Vincent Lemaur** from the very start of my master thesis and I feel so lucky I have been able to meet such a nice person. I think nobody will say it differently: Vincent will never say no to help anybody asking even if he is flooded with work and he truly rocks in sciences. Vincent, thank you so much for your patience (#toomanyblankspaceinthefile) and for have been my Master Yoda in computational chemistry for almost 6 years!

*« Well, your thesis is over isn't it? »*

Right after the last congress I had the chance to spoke too, those were the first words I heard from **Edwin de Pauw**. Somehow, he got it right: I had two months to finish my PhD but he also looked confident looking at my work and that was the most important part. Mister De Pauw, we did not meet that much but I cannot thank you enough for saying “yes” to be co-supervisor of this thesis a few years ago. Thank you for your trust.

*« Glenn, it is 3PM, bring the Minion! »*

This is not a breaking news: you have to be a little crazy to become a scientist and my colleagues at the **S<sup>2</sup>MOs** make no exceptions. Thank you Marie, Thomas, Corentin, Emilie, Tiffani, Quentin, Romain, Manu, Sébastien D., Sébastien H., Fabrice, Géry and Eric for all those

great moments spent together whatever it was for talking about sciences, shopping, videos games, music, making jokes, etc. and of course thank you for your support.

In particular, I would like to thank Marie who has been a real support through the first 2 years of my PhD. I will never forget our crazy screaming sessions when we were both working for hours in front of our computers. Thank you for your encouragement and support. After Marie, Emilie came in my office and putting two geeks like us in the same room was maybe not the best idea lol. Emilie, thank you for all our chats on shopping and gaming, for your crazy stupid music and your ugly dogs on facebook (yes, they are ugly, believe it :-P) but also for having my back during this last year. Lastly, thank you Corentin for being so supportive and kind for almost three years.

*« Dude, how are your shoeboxes going on? »*

It is not always easy to make your non-scientist people understand what you do, so yes: I explain my host-guest complexes as shoeboxes since your sneakers will not fit a boots box and vice-versa. Of course, there is many people I would like to thank here but I will focus on some of them.

**Steve** and **Romain** have been my friends for respectively 25 and 13 years, even though they are not chemists, they were always interested about my research and truly helped me going through it, thank you guys, you are rock stars, let's have another 30 plus years of great friendship!

Another rock star is my dear **Orel / Aurélie / Sally / Bébéeéé / Bichetaud**, we have been together for more than 3 years and I feel so lucky to have her in my life. I learn from her every day, self-made woman, true champion and hard-work girl, she is all about passion and getting stuff done. Thank you for helping me being a better man without forgetting the crazy child in me, I am so proud of you and us. I love you "costaud". Where is the gym?

Speaking off self-made women, here comes the best: my mum **Lucia**. There are not enough words to say how much I am proud of her and of the fighter she is. If I am the man I am today, her and my grandparents have all the credit for it. Thank you for supporting me in whatever are the crazy things I do and even if you do not understand them.

Finally yet importantly, there is the man of my life, **Roger**, my grandfather. If I was able to go to the University, it is mostly because of him and my grandmother **Noëlle**. Papy, you have always been an example for me and I cannot thank you enough for the trust you have in the man I have become. Thank you for having been there all the time, from reciting multiplications tables when I was six to the final stages of this PhD.

*« Do or do not, there is no try »*

*Master Yoda.*

I guess this is the best way to describe a PhD, whatever you start it or have to put an end to it. Thank you to the University of Mons (UMONS) and University of Liège (Liège Université) for their financial support.

I can just hope you will enjoy the next two hundred pages as much as I enjoyed writing them. It has been an incredible ride, time for something new.

Thank you all so much.

*Glenn*

## Abstract

Non-covalent interactions result from the associations of different molecules held together by intermolecular forces. Nowadays, supramolecular chemistry is in constant evolution and can probably be considered as one of the main research fields in modern chemistry. Numerous applications in drug delivery, water treatment, catalysis, etc. are already well controlled and more are expected soon.

A peculiar area in the domain of supramolecular assemblies is the host-guest chemistry in which a big chemical receptor, the host, can strongly bind within an inner cavity at least one small molecule, the guest. The structures and physicochemical properties of host-guest assemblies are obviously studied directly in solution with common methods such as NMR and UV-vis spectroscopy. Nevertheless, with the development of soft ionization methods that can preserve non-covalent interactions from the solution to the gas phase, mass spectrometry appears to be an efficient analytical tool in the study of supramolecular assemblies especially with the emergence of ion mobility in association with mass spectrometry. This thesis represents a contribution towards the applicability of MS methods to investigate supramolecular objects, considering that the data generated upon MS are related to gaseous ions and that any shortcut linking the gas phase structures to the condensed phase topologies is definitively not straightforward.

In this PhD, we report different studies carried out on complexes involving cucurbiturils as macrocycle hosts. Cucurbit[*n*]urils are macrocycles obtained by the condensation reaction of *n* glycoluril units ( $n=5$  to 14) and have been extensively studied for the outstanding binding abilities with amino-guest molecules. The selection of cucurbiturils as model host has been motivated due to the rigid character of those macromolecules. For our studies, we used mass spectrometry, associating Electrospray ionization, collision-induced dissociation and ion mobility, with computational chemistry to advantageously study cucurbituril systems in association with different amino compounds. Basically, our studies demonstrated the applicability of MS-based methods to probe the gas phase structures of complex ions, provided computational chemistry is implemented in the workflow to optimize the structures of non-covalent ion candidate to further compare to the experimental data. In particular, the

relative energies of the inclusion/exclusion structures have to be determined for each association under study using theoretical calculations to confirm the experimental observations.

In the first part of this PhD, the influence of the experimental and instrumental conditions on the nature of the detected ions has been investigated with a special emphasis on the in-solution reaction time, saying the time spent by the host and the guest in solution prior to the ionization process, and on the size of the guest, which may affect the in / out ratio of the detected ionized associations. Similarly, the key-role played by the ion optics on the topology of the supramolecular ions transferred from the solution to the gas phase upon Electrospray Ionization has been highlighted.

Secondly, a mass spectrometric study has been performed on a click reaction using the inner cavity of a cucurbit[6]uril host as a catalyzer. According to our results using CID, ion mobility and energy resolved-CID experiments, we observed that the cycloaddition reaction within the CB[6] cavity is an extremely fast process and that the rate determining step in the overall cycloaddition process as measured in solution is the egression of the cycloadduct products from the cavity.

In the final section of this PhD thesis, we report a joint experimental and theoretical study carried on a bitopic cucurbituril receptor (ns-CB[10]). We first demonstrated upon MS measurements that the creation of the ternary complexes is under homotropic allosteric control. We also reported that CID experiments, with the control of the kinetic energy, must be also carefully used when trying to deduce relative binding affinities from CID energy thresholds.

Overall, in the present PhD research work, the advantages and drawbacks of mass spectrometry as an analytical tool for the study of supramolecular chemistry have been highlighted with a special emphasis on the conservation of the complex topology all along the path of the ions from the solution to the detector of the mass spectrometer.

# Table of content

## I. Introduction:

1. Outlook .....	1
2. Supramolecular Chemistry .....	3
2.1 Non-covalent Interactions .....	5
2.1.1 Van Der Waals Interactions.....	6
2.1.2 $\pi$ - $\pi$ stacking .....	7
2.1.3 Hydrophobic interactions.....	8
2.1.4 Hydrogen bonds .....	10
2.1.5 Dative and ionic bonds .....	11
2.1.6 Exotic non-covalent bonds .....	12
2.2 Host-Guest Complexes .....	14
2.3 Investigation Methods for Non-Covalent Associations.....	17
2.3.1 UV-Visible Spectroscopy.....	18
2.3.2 Nuclear Magnetic Resonance (NMR) Spectroscopy .....	20
2.3.3 Isothermal Titration Calorimetry .....	23
2.3.4 Extraction Method .....	26
3. Supramolecular Mass Spectrometry .....	28
3.1 Electrospray Ionization .....	29
3.2 Selected examples of the use of Electrospray in supramolecular chemistry.....	32
3.2.1 Supramolecular associations.....	33
3.2.2 Complete virus ionization.....	37
3.2.3 Gas phase reactivity of supramolecular assemblies .....	38
3.3 False positive detection .....	40
4. Ion Mobility Mass Spectrometry (IMMS).....	41
4.1 Description of the Gas Phase Ion Motion .....	41
4.2 Ion Mobility Spectrometry .....	43
4.3 From Ion Mobility to Collisional Cross Section.....	43



4.4	Experimental considerations for ion mobility experiments: arrival time distribution	47
4.5	Ion Mobility Mass Spectrometry: incorporation of Drift-Cell Units	50
4.5.1	Drift Tube Ion Mobility Measurements	50
4.5.2	Traveling- Wave Ion Mobility Measurements	52
5.	The Cucurbituril Macrocycle Family	57
5.1	Synthesis	57
5.2	History	59
5.3	Structural and chemical properties	61
5.4	Host-guest chemistry	64
5.5	Guest complexation mechanism with cucurbiturils	66
5.6	High-affinity binding	68
5.7	Applications	71
5.7.1	CB[n] recognition in biological systems	71
5.7.2	Catalysis in the inner cucurbituril cavity	74
5.7.3	Photoswitching reaction operated using cucurbituril and product self-sorting release	76
	References	80

## II. Aim of the thesis:

	Aim of the thesis	92
	References	93

## III. Experimental part:

1.	Mass Spectrometers	94
1.1	Waters Q-ToF 2	94
1.1.1	Description	94
1.1.2	Experimental procedure	95
1.2	Waters Synapt G2-Si	96
1.2.1	Description	96
1.2.2	Experimental procedure	97
1.3	Homemade IMS/MS setup of the ILM research group in Lyon	98

2.	Overview of the Mass Spectrometer Acquisition Modes .....	100
3.	Energy-Resolved Collision Induced Dissociation .....	101
4.	Collision Cross Section Calibration Method for TWIMS Analysis.....	104
5.	Nuclear Magnetic Resonance Measurements.....	107
6.	Materials.....	108
7.	Theoretical calculations .....	108
	References .....	109

#### **IV. Results and discussion:**

**Chapter 1:** Influence of Equilibration Time in Solution on the Inclusion/Exclusion Topology Ratio of Host-Guest Complexes Probed by Ion Mobility and Energy-Resolved Collision-Induced Dissociation.

1.1	Introduction .....	111
1.2	Results and discussion .....	113
1.3	Conclusions .....	125
	References .....	126

**Chapter 2:** Flying cages in Traveling Wave Ion Mobility: insidious effect of the instrumental parameters on the topology of the host-guest complexes.

2.1	Introduction .....	129
2.2	Results and discussion .....	131
2.2.1	<i>Adamantylamine•CB[6] and diaminohexane@CB[6] as exclusion and inclusion model complexes .....</i>	<i>132</i>
2.2.2	<i>Aniline•CB[6] or aniline@CB[6] as exclusion or inclusion complexes.....</i>	<i>137</i>
2.2.3	<i>Halogeno-aniline•CB[6] or halogeno-aniline@CB[6] as exclusion or inclusion complexes .....</i>	<i>145</i>
2.2.4	<i>PXD•CB[6] or PXD@CB[6] as exclusion or inclusion complexes .....</i>	<i>149</i>
2.2	Conclusions .....	151
	References .....	153

### **Chapter 3:** Probing the cucurbituril-catalysed 1,3-cycloaddition by mass spectrometry.

3.1	Introduction .....	156
3.2	Results and discussion .....	157
3.3	Conclusion.....	164

References .....	165
------------------	-----

### **Chapter 4:** Homotropic allostery: in-depth structural analysis by mass spectrometry and computational chemistry of the gas-phase non covalent complexes associating a double-cavity cucurbit[n]uril-type host and size-selected protonated amino compounds.

4.1	Introduction .....	167
4.2	Results and discussion .....	170
4.2.1	<i>ESI time-of-flight (TOF) measurements</i> .....	170
4.2.2	<i>Collision-induced dissociation experiments</i> .....	175
4.2.3	<i>Ion mobility spectroscopy experiments (IMS)</i> .....	177
4.2.4	<i>Structural analysis of the ternary complex ions (+2 / +3) by computational chemistry</i> .....	180
4.2.5	<i>Experimental and theoretical investigation of the size specificity of the complexation reaction.</i> .....	185
4.3	Conclusions .....	187

References .....	189
------------------	-----

### **Chapter 5:** Energy-resolved Collision-induced Dissociation of Non-Covalent Ions: Charge- and Guest-dependence of the Decomplexation Reaction Efficiencies.

5.1	Introduction .....	192
5.2	Results and discussion .....	195
5.2.1	Experimental results: mass spectrometry study of the host/guest associations .....	195
5.2.2	Estimation of the dissociation barriers .....	203
5.2.3	CID reactions of the 2+ ternary complexes.....	212
5.2.4	CID reactions of the 3+ ternary complexes.....	214
5.3	Conclusions .....	215

References .....	217
------------------	-----

## **V. Conclusion & outlook:**

Conclusion & Outlook.....	219
---------------------------	-----

## **VI. Annexes:**

1. Mass Spectrometry: additional notes .....	223
1.1 Tandem Mass Spectrometry .....	223
1.2 Triwave.....	224
2. Density Functional Theory .....	227
2.1 The Thomas-Fermi Model .....	228
2.2 The Hohenberg and Kohn Theorems .....	228
2.3 The Kohn-Sham Method .....	230
2.4 Exchange-correlation Energy Assessment methods .....	232
2.4.1 Local Density Approximation (LDA) .....	232
2.4.2 General Gradient Approximation (GGA).....	233
2.4.3 Hybrid Functional.....	233
2.5 The B97D Functional .....	234
2.5.1 Description of the B97D energetic terms .....	234
2.5.2 Description of the dispersion forces energetic term .....	236
References .....	237

## Accomplishments

# I. Introduction

Outlook

Supramolecular Chemistry

Supramolecular Mass Spectrometry

Ion Mobility Mass Spectrometry

The Cucurbituril Macrocyclic Family

## 1. Outlook

In modern chemistry, mass spectrometry (MS) methods are increasingly used to study non-covalent complexes extracted from the solution phase to the rarefied gas phase. The development of new ionization source such as the electrospray allowed such interactions to be preserved through the phase transfer [1]. In the gas phase, ions do not interfere with each other chemically. Consequently, dynamic processes do not play a role anymore and the properties of the supramolecular objects can be monitored, with a special interest in the determination of the composition, i.e. stoichiometry of the association. New insights can be gained from the examination of the gas phase stability and reactivity. However, huge differences can be expected when compared to the solution phase properties so that the use of MS-based methods to study non-covalent associations must be handled with great care, especially when trying to deduce the solution properties from the MS data [1, 2].

Nowadays, MS-based methods appear more and more prone to provide fast and accurate information about supramolecular systems [1]. Mass spectrometry can go far beyond the analytical characterization of the complexes in terms of their exact mass, charge state, and stoichiometry. Indeed, mass spectrometry offers quite a large panel of methods that can provide structural information on the complexes. In particular, the “secondary structure” of the non-covalent associations, i.e. the relative position of the non-covalently bound subunits in the complex can be efficiently probed by collision-induced dissociation [3], associative ion/molecule reactions (H/D exchange) [4] and ion mobility [5] experiments. Relative binding energies of non-covalent associations in the gas phase can also be inferred by MS-based methods by performing ligand exchange reactions in the gas phase [6]. Critical energies of fragmentation for non-covalent complexes in the gas phase are also often estimated by performing energy-resolved CID experiments and determining the center-of-mass energy required for the decomposition / decomplexation reaction to occur [7]. However, such experiments do not afford any thermochemical data such as binding energies but threshold energies are estimated.

In addition, the use of computational chemistry in association with mass spectrometry permits a better understanding of the properties of the supramolecular association in the gas-phase. Indeed, secondary structures alongside with relative binding-guest energies can be determined through the evaluation of optimized geometries of the complex ions. Straightforward comparison with MS data, such as experimental collisional cross-sections, are also doable thanks to the evaluation of theoretical cross-sections calculated from optimized structures. Finally, absolute binding energies for gas-phase non-covalent complexes are nicely evaluated by using computational chemistry. [6,8]

Herein, a deep inside in the gas phase properties of the cucurbit[n]urils containers has been handled. Cucurbit[n]urils are macrocyclic receptors constructed by the association of  $n$  glycoluril repeat units [9]. These pumpkin-shaped molecules present a hydrophobic inner cavity and two identical carbonyl portals, making them suitable for encapsulation of hydrophobic molecules or of the hydrophobic part of molecules in aqueous media. The main drawback of cucurbiturils is their low solubility in water requiring low pH or high ionic strength to ensure their dissolution upon carbonyl portal protonation or cationization [10]. On the other hand, the cucurbit[n]uril (CB[n]) family of molecular containers has attracted huge interest due to their outstanding recognition properties, to the exceptional strength of their interaction ( $k_a$  up to  $10^{17}M^{-1}$ ) with various guests and to the numerous applications offered by the encapsulation propensity of the cucurbituril family members [11]. Cucurbiturils are extensively demonstrated to form stable inclusion complexes with various protonated alkyl- and aryl(di)amines [9-11].

Lastly, the structural modifications of non-covalent complexes due to experimental and/or instrumental parameters have to be treated with a special emphasis. Indeed, in solution, (supra)molecules are characterized by certain conformations, which might not be preserved during the ionization/desolvation processes due to external stimuli (temperature, pH) or inherent voltages used within the mass spectrometer. Understanding the impact of those parameters is critical when attempting to consider MS as an additional tool for structural characterization of non-covalent objects. Then, one of the main objectives of the present PhD thesis is to assess how the gaseous structures can be envisaged as a probe of the condensed phase structure, despite the dramatic changes in environment undergone by the molecules upon Electrospray ionization and transfer within the high vacuum of the mass spectrometer.

## 2. Supramolecular Chemistry

Resolving around intermolecular interactions, supramolecular chemistry has constantly evolved over the last decades, to finally become one of the main research field in modern chemistry.

The basic concepts of this new research area have been formulated in the late nineteenth century. Back then, in 1891, **A. Villiers** discovered the first macrocycle compound: a cyclodextrin [12]. Later on, in 1893, **Alfred Werner** proposed a first definition of coordination chemistry [13] while **Emil Fischer** introduced the “lock and key” concept between enzyme and substrate in 1894 [14]. Nevertheless, more than 40 years were needed to see the apparition of the German Word for “Supramolecule” in the literature when **Karl Wolf** introduced the word “*Übermolekül*” (1937) to describe the interactions of coordinately saturated species like dimers of carboxylic acids [15]. Indeed, supramolecular chemistry has not been directly recognized as a research area in its own right for two reasons: (1) the scientists’ perception, which consisted to believe that the molecular properties were weakly influenced by their environment; and (2) the lack of available methods to explain the dynamic nature of the long range interactions relevant to supramolecular systems [16].

A definition of supramolecular chemistry has been given by **Jean-Marie Lehn** as followed: “*chemistry of molecular assemblies and of the intermolecular bond*” in 1979 [6]. Actually, in 1987, Lehn was awarded the Nobel Prize, alongside with **Donald Cram** and **Charles Pedersen** for their works on cryptands [18-20] (**figure I.1**).



**Figure I.1:** Nobel prizes in Chemistry, laureates of 1987 [21].



From this moment, supramolecular chemistry has been in constant expansion as revealed by **figure 1.2**, which represents the number of referenced articles dealing with supramolecular chemistry over the years.

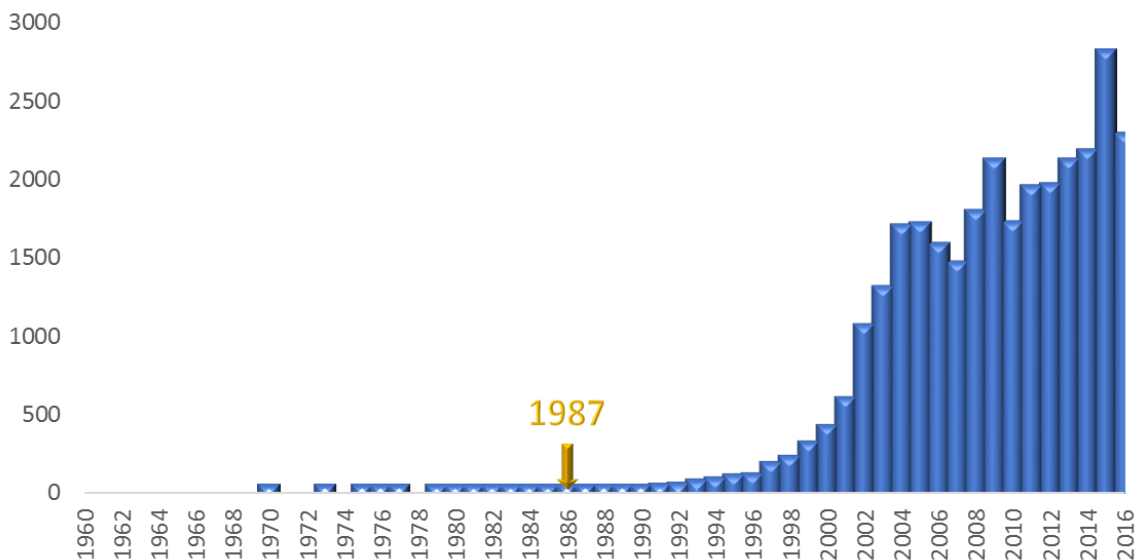


**Figure 1.2:** number of referenced articles when looking for “supramolecular chemistry” as key word (website consulted in March 06, 2017) [22]. 1987: year of the Nobel Prize of Lehn, Cram and Pedersen.

**Jean-Marie Lehn** gave a more elegant definition of supramolecular chemistry in 1995, presenting this new domain as the:

---

*“Chemistry beyond the molecule, bearing on the organized entities of higher complexity that result from the association of two or more chemical species held together by intermolecular forces.” [23].*

---

In conclusion, supramolecular chemistry is defined by the non-covalent interactions between molecules and their structural complementarity. Furthermore, the notion of “self-assembly” [24] has been introduced in order to describe the property of complementary molecules to spontaneously make associations in solution.

At this point, it is important to note that the reactions leading to the establishment of supramolecular interactions are reversible. Accordingly, the formation of supramolecular assemblies does not only depend on the complementarity between the partner structures but also on how the environment and external stimuli will influence the kinetics of the complexation or decomplexation reaction. Therefore, options exist to finely tune the release mechanism of trapped-guest [25].

The next section aims to cover some of the intermolecular interactions commonly responsible of the formation of supramolecular assemblies.

### 2.1 Non-covalent Interactions

Different types of intermolecular interactions exist and are characterized by different range of energy values. Those non-covalent bonds allow for the formation of supramolecular assemblies even though their energies are weak in comparison to ionic (>45 kcal/mol) or covalent bonds ( $\approx 90$  kcal/mol for a single C-C bond). Actually, ionic bonds are defined as “strong interactions” created on the basis of a high electronegativity difference between the covalently bounded atoms [26]. In fact, one or several electron(s) are transferred from the less electronegative atom to the one with the higher electronegativity. Covalent bonds, also named molecular bonds, involve the sharing of one or more electron pairs between atoms for each atom attaining a stable electronic configuration.

Contrariwise, the non-covalent bonds, detailed here after, do not necessitate an electron transfer from one molecule to another [26]. Non-covalent bonds range from tens of kcal/mol for coordinative bonds to only a few kcal/mol for van der Waals interactions [16]. They can be divided into several different classes and the following sections only present a brief overview of the most common interactions found when studying supramolecular associations. **Table I.1** summarizes the different non-covalent bonds presented in an ascending order of the interaction energy values.

**Table I.1:** summary of some of the most common supramolecular interactions and their energy range [26].

<b>Interaction type</b>	<b>Energy (kcal.mol<sup>-1</sup>) in chloroform</b>
<b>van der Waals interactions</b>	0.1 – 1
<b><math>\pi</math>-<math>\pi</math> stacking</b>	2 – 5
<b>Hydrophobic interactions</b>	1 – 10
<b>Hydrogen bonds</b>	Weak: < 1 Moderate: 1 – 4 Strong: 5 – 10
<b>Ionic bond</b>	>45

### 2.1.1 Van Der Waals Interactions

Van der Waals interactions (VDW) represent the weakest supramolecular interactions (0.1 - 1 kcal/mol). Those interactions arise from the permanent or induced dipoles within molecules [27]. VDW forces are a superposition of attractive and repulsive interactions, which evolves with the distance  $r$  between atoms, respectively in an  $r^6$  and  $r^{-12}$  dependence according to the *Lennard-Jones* potential [28].

Actually, this type of non-covalent bond gathers three interactions presented in **figure I.3**: (A) Keesom Forces, (B) Debye forces and (C) London forces, each of them depending on the kind of dipole involved in the interaction between the partners [28].

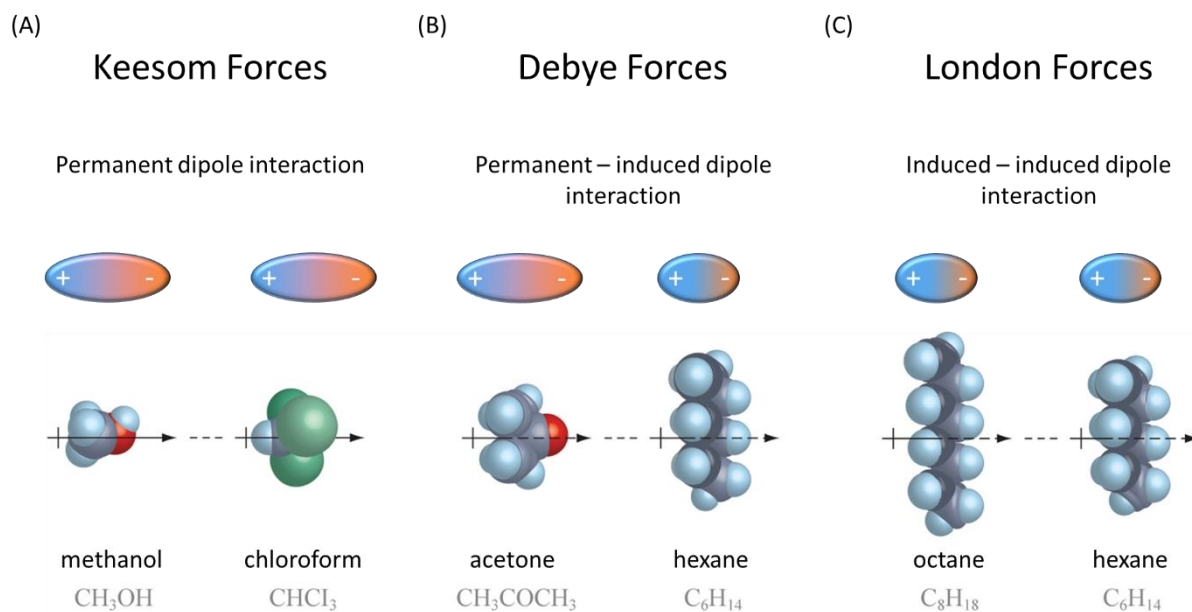


**Figure I.3:** representation of the van der Waals interactions: (A) Keesom forces, (B) Debye forces and (C) London forces (adapted from reference [29]).

### 2.1.2 $\pi$ - $\pi$ stacking

$\pi$ -systems (such as benzene) may weakly interact with other  $\pi$ -systems through  $\pi$ -stacking interactions. Nevertheless, those interactions are quite complex since two systems will not interact in a perfect face-to-face manner [30]. In that case, all partial charges on the facing atoms would repulse each other. Actually, two different orientations exist (**figure I.4**): (A) face-to-face and (B) edge-to-face (3-5 kcal.mol<sup>-1</sup>). This last orientation is stabilized by a favorable attraction between one benzene  $\pi$ -cloud and the positive hydrogen atoms of the other.

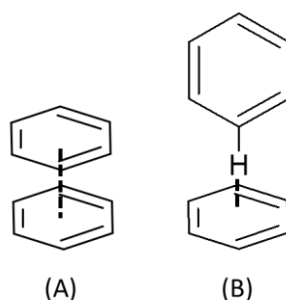


**Figure I.4:** representation of the  $\pi$ -stacking interactions: (A) face-to-face, (B) edge-to-face.

### 2.1.3 Hydrophobic interactions

Hydrophobic interactions, or hydrophobic effect, result from the association of non-polar molecules in a polar solvent. The goal of this clustering is to minimize the energetically unfavorable surface between polar/protic and nonpolar/aprotic molecules [16].

Such interactions are generally demonstrated by the formation of micelles in water, resulting from the association of the hydrophobic parts of amphiphilic molecules in order to no longer interact with the polar solvent (*figure 1.5*) [31]. In that way, only the polar parts of the molecules will be exposed to the polar solvent.

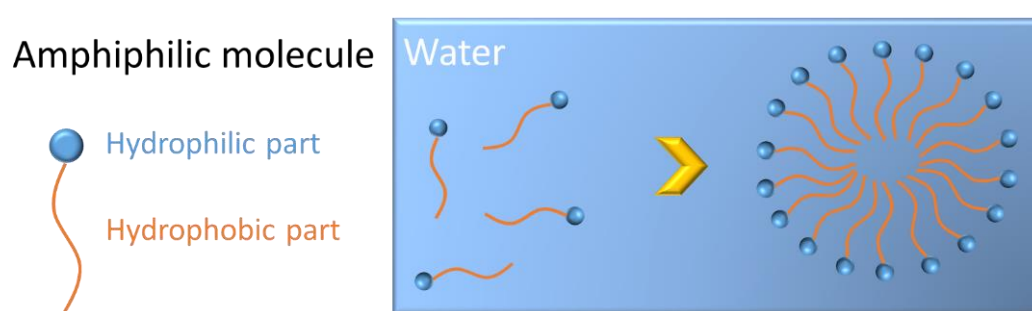


**Figure 1.5:** general representation of the hydrophobic effect in water.

In the case of supramolecular complexes, a more complete definition has been proposed by **Franck Biedermann et al.** in 2014 [32], which describes the contribution of the hydrophobic effect as a driving force for the guest encapsulation process.

This definition involves the liberation of multiple water molecules, called “high energy water molecules” from the host cavity when one guest molecule will make its way through the macrocycle to finally form an inclusion complex. This high-energy water release will contribute to an enhancement of the entropy while the rearrangement of both the solvent molecules (old and new water molecules together) and the host-guest association generate a gain in enthalpy. An example of this revisited version of the hydrophobic effect is represented in *figure 1.6* through the formation of a ternary compound (2 guests for one host) of cucurbit[8]uril [33].

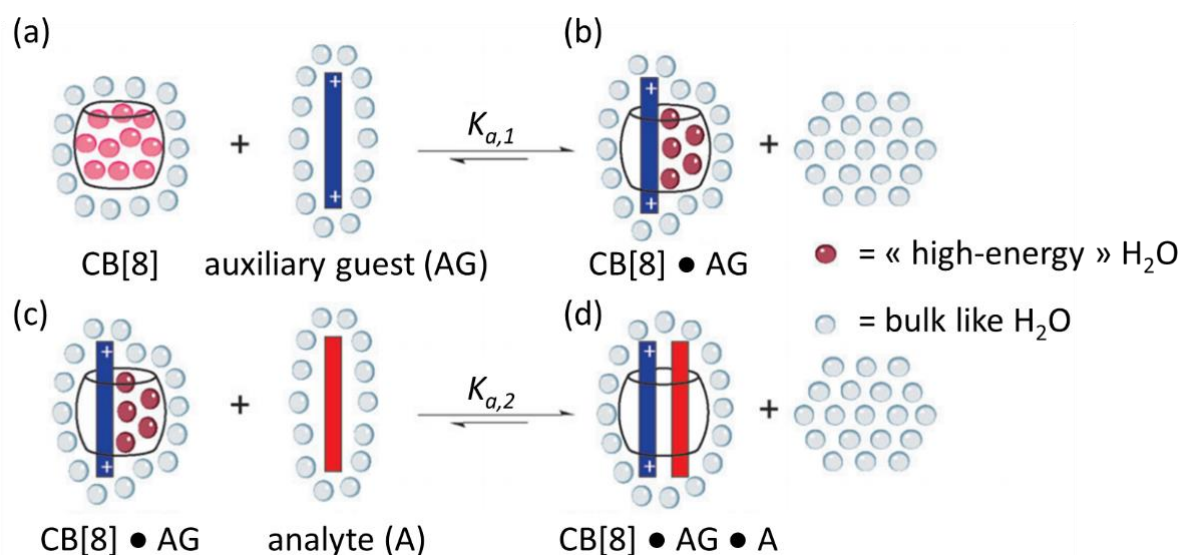


**Figure 1.6:** formation of a ternary complex of CB[8] in aqueous solution. The first binding ( $K_{a,1}$ ) increases the energetic frustration of the residual cavity water. Therefore, the second binding is energetically favored (adapted from reference [33]).

In this example: **(a)** the CB[8] host and the auxiliary guest (AG) are surrounded by solvent molecules. The solvent molecules (water) are represented in light blue while the solvent molecules filling the host cavity are represented in red. Due to the ingress of AG inside the cavity of CB[8] **(b)**, a part of the red “high energy” water molecules contained in the host cavity will be released and therefore participate to the driving force of the ingress process of AG. Following the same principle, the release of the last “high energy” water molecules contained in the binary complex CB[8]•AG **(c)** will contribute to the driving force of the ingress process of the analyte (A) **(d)**. The formation of the first binary complex **(b)** results in a strong exothermic reaction ( $\Delta H$  up to  $-60 \text{ kJ}\cdot\text{mol}^{-1}$ ) for the complexation of aromatic guest, in particular if that guest is large enough to displace all cavity water molecules for the CB[8] host (AG= naphthalene for example) [32-33].

2.1.4 Hydrogen bonds

Hydrogen bonds are one of the most important non-covalent bonds when studying supramolecular associations [34]. In addition to their important role in biochemistry (protein folding, DNA structure, etc.), they were also greatly employed in the design of artificial supramolecules.

Hydrogen bonds (**figure 1.7**) arise from the interaction between an electron deficient acceptor (atom H) and a highly electronegative donor atom (oxygen, nitrogen, etc.).

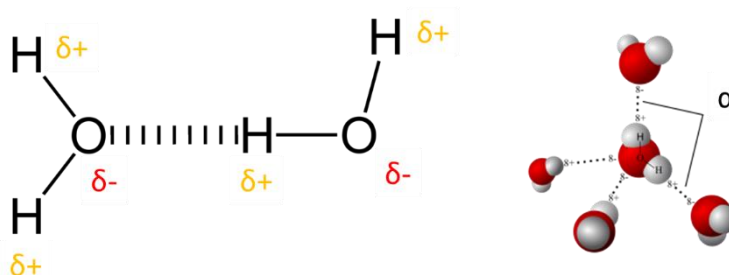


**Figure 1.7:** representation of hydrogen bonds in water [35].

Two reasons explain the pivotal role of hydrogen bonds in host-guest chemistry. The first one is that many host-guest complexes have been studied in non-competitive solvents enhancing the strength of the hydrogen bonds. The second reason is related to a very important intrinsic property of the hydrogen bond: its directionality [16]. Indeed, it allows the chemist to control / modulate the geometry of the complexes and even to design specific host for a peculiar guest.

Hydrogen bonds (H-bonds) are characterized by two parameters:

- The distance between the donor and acceptor atoms.
- The angle between H-bonds ( $\alpha$  on **figure 1.7**).

Accordingly, one should distinguish strong H-bonds from moderate and weak H-bonds. Strong H-bonds yield to binding energies of 5 up to 10 kcal.mol<sup>-1</sup> for an angle between 175 – 180° and a heteroatom distance that varies from 1.5 to 2.5Å [36]. Moderate bonds possess binding energies of 1 to 4 kcal.mol<sup>-1</sup>, for a distance between 2.5 and 3.2Å and an H-bond angle of 130 – 180° while weak H-bonds present a binding energy < 1 kcal.mol<sup>-1</sup> for long donor-acceptor

distance up to 4Å and angles values between 90 and 150°. In addition, this classification expressed the more covalent and inflexible nature of strong H-bonds, while moderate and weak ones are more flexible and display a more electrostatic character [16]. Lastly, hydrogen bonding between neutral molecules should always be distinguished from charged hydrogen bonds. Indeed, H bonding interactions involving ions are significantly stronger. For example, the strongest H-bond known involves  $F-H \cdots F$  and presents a binding energy of 38 kcal.mol<sup>-1</sup> [16].

### 2.1.5 Dative and ionic bonds

Dative and ionic bond-types are both high-energy non-covalent interactions (up to 90 kcal.mol<sup>-1</sup>) characterized by a higher covalent nature than other supramolecular interactions.

Ion-ion interactions (ionic bond) result from the high electronegativity (En) difference between the atoms and implies the transfer of one electron from the less electronegative atom to the higher electronegative atom. Accordingly, an ionic bond corresponds to an electrostatic attraction between two oppositely charged ions [37]. As an example, the NaCl compound (**figure 1.8**) can be cited where Na is positively charged (Na<sup>+</sup>, cation, En=1) and Cl is negatively charged (Cl<sup>-</sup>, anion, En=2.8). The distance between the two opposite charges will become a geometric factor for supramolecular aggregates even though no particular direction is privileged for ionic interaction [16] as shown on the adjacent picture of a NaCl crystal [38].

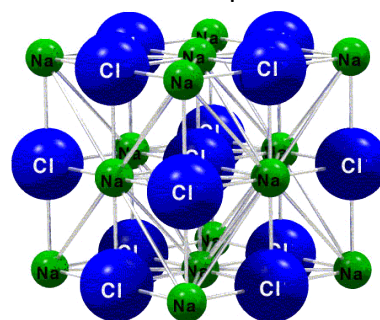


**Figure 1.8** : NaCl crystal



### 2.1.6 Exotic non-covalent bonds

Beside the most famous supramolecular interactions cited above, some interactions are more peculiar. Some of them are briefly presented in the next sections.

#### 2.1.6.1 Multipole forces

Multipole forces result from short contact interactions of intrinsic dipoles together. As an example, the crystal structure of alloxan (pyrimidine-2,4,5,6-tetraone)[39] (**figure I.9**) features a grid of short, almost orthogonal intermolecular  $C=O\cdots C=O$  contacts with distances of about 2.8 Å and  $C=O\cdots C$  angles in the range between 155° and 163°. Regarding the chemical structure of alloxan, one would expect molecules to form a hydrogen-bonded structure, given the existence of two acidic NH units per molecule. In fact, the perpendicular nature of the  $C=O\cdots C=O$  interaction is best described as electrostatic, where the partial positive charge residing on the C atom of the intrinsically polar carbonyl unit represents an electrostatic center of attraction for the partially negatively charged O atom of an adjacent  $C=O$  fragment [40]. Such electrostatic interactions between intrinsically dipolar units can be highly directional and may be the cause of very short contact distances, bearing some structural resemblance to interactions between nucleophiles and carbonyl groups (see sections I.2.1.1 and I.2.1.4).

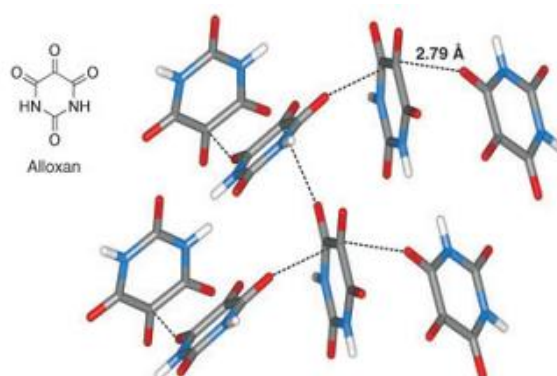


**Figure I.9:** Crystal structure of alloxan (CSD-code: ALOXAN) featuring orthogonal intermolecular  $C=O\cdots C=O$  contacts [39]. Color code: C: gray; O: red; N: blue; H: white.

Beside their important role in small molecules crystals, multipoles forces deeply influence the secondary structure in protein-ligand interactions [41]. For example, the C-F...C=O short orthogonal interaction profile can be found in the complex of the potent serine protease inhibitor ZK-807834 bound to the active site of its biological target, factor Xa (**figure I.10**) [41].

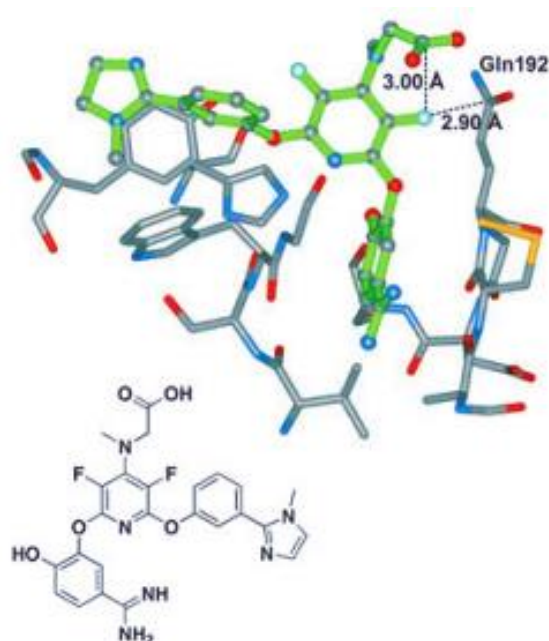


**Figure I.10:** X-ray crystal structure showing a short, orthogonal C-F...C=O contact between the serine protease inhibitor ZK-80784 and factor Xa as well as another intramolecular C-F...C=O close contact of the inhibitor [41]. Color code: inhibitor skeletons: green; C: gray; O: red; N: blue; S: yellow; F: cyan.

In this complex, one fluorine atom of the central pyridine of the inhibitor core is close contact ( $d(\text{F}\cdots\text{C}) = 2.90 \text{ \AA}$ , angle (F-C-O) =  $91^\circ$ , angle (C-F-C) =  $153^\circ$ ) with the side chain amide carbonyl unit of Gln 192. At the same time, the fluorine atom enters into a second intramolecular close contact with almost ideal sheared parallel geometry ( $d(\text{F}\cdots\text{C}) = 3.0 \text{ \AA}$ , angle (F-C-O) =  $88^\circ$ , angle (C-F-C) =  $90^\circ$ ) with a nearby carboxyl unit present in the inhibitor.

In fact, the contributions of orthogonal dipolar interactions (saying multipole interactions) to the secondary structure of proteins and to molecular recognition in biochemical systems have been recognized and an increasing number of cases are now identified.

2.1.6.2 Halogen bonding

Halogen bonding results from the attractive non-covalent interaction between the electrophilic site of a bound halogen atom and a Lewis base [42]. Recently, **Diederich** et al reported the detection of a halogen bonded capsule in the solid state, in solution and in the gas phase (**figure I.11**) [43].

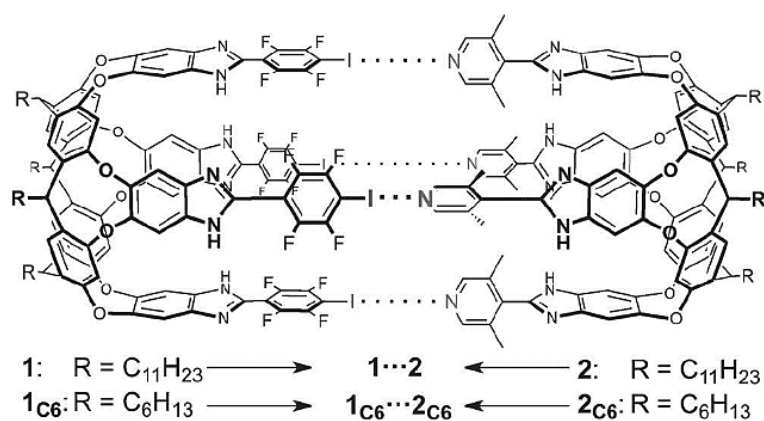


**Figure I.11:** Halogen-bonded supramolecular capsules. 1...2 (R = n-undecyl) studied in solution and in the gas phase. 1<sub>C6</sub>...2<sub>C6</sub> (R = n-hexyl) studied in the solid state [43].

In this example, the halogen bonded donor **1** and acceptor (Lewis base) **2** are constructed from resorcin[4]arene cavitands. The halogeno-bonded capsule **1...2** has been observed in solution and in the gas phase and is characterized by a substantial association constant of  $K_a = 5370 \text{ M}^{-1}$  ( $\Delta G^0 = -4.85 \text{ kcal mol}^{-1}$ ).

2.2 Host-Guest Complexes

In supramolecular chemistry, host-guest chemistry defines the association of two or more molecules or ions held together by non-covalent bonds. In general, the “host” molecule possesses a central cavity, which can include at least one smaller molecule called “guest”. Consequently, the guest molecule will be isolated from the bulk solvent located outside of the container host. Therefore, it is important to design suitable host depending on which substrates will bind the host central cavity.

Fabricating synthetic containers, in order to highly control the guest-binding process and change its reactivity, has been a great challenge for the last forty years [44, 45]. A special regard has been dedicated to the development of molecules characterized by high selectivity interactions such as cryptands, crown ethers, cyclodextrines and more recently cucurbiturils and calixarenes (**figure I.12**). Those compounds are designed to interact with smaller “guest molecules” through non-covalent interactions.

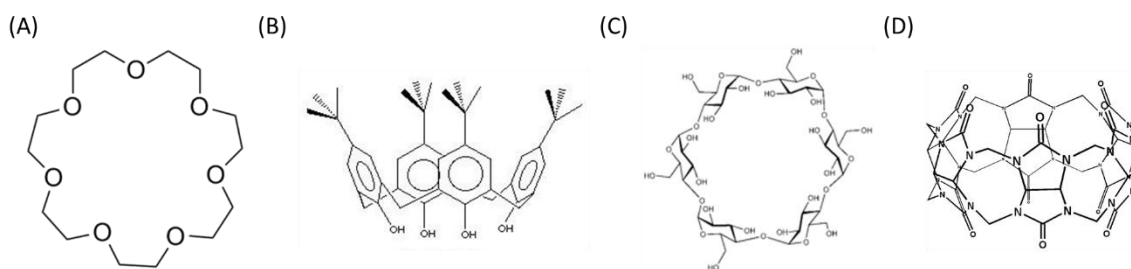


**Figure I.12:** representation of different molecular hosts: (A) Crown ether, (B) Calixarene, (C) Cyclodextrine and (D) Cucurbituril.

The interest in the synthesis of macro-containers has been highlighted in 1971 with the pioneering work of **Breslow** on cyclodextrins as enzyme mimics [46]. Back then, Breslow catalyzed the para-chlorination of anisole trapped inside  $\alpha$ -cyclodextrin and introduced the representation of an inclusion complex as shown in **figure I.13 a**. The full structure of anisole is presented on the figure while the cyclodextrin host is schematically represented by a barrel shape. This simple representation resumes the principle of host-guest chemistry on its own where the “small” anisole molecule is fully encapsulated inside the “big” host cavity.

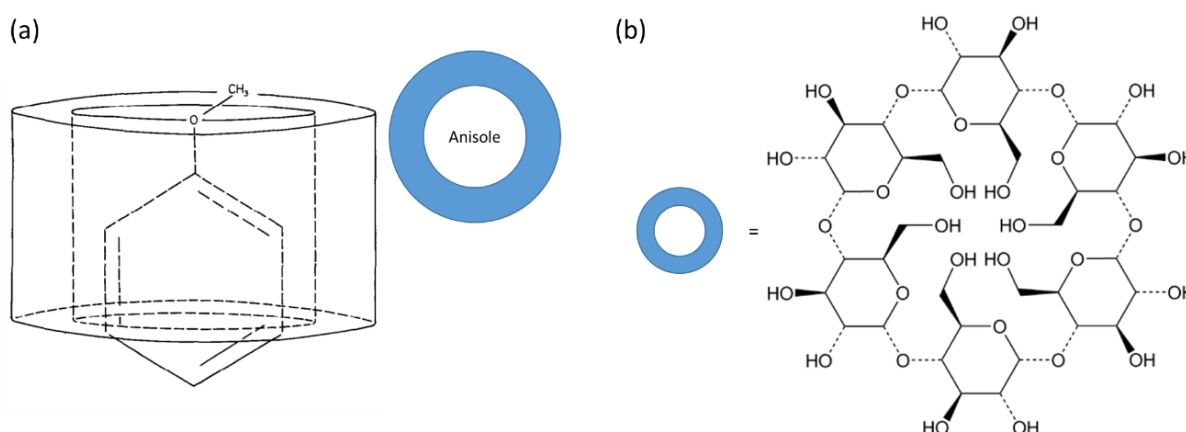


**Figure I.13:** (a) schematic drawing of the anisole- $\alpha$  cyclodextrin complex (adapted from reference [46]). (b) Structure of the  $\alpha$ -cyclodextrin host[47].

From that point, specific host synthesis has constantly progressed with the design of hundreds of new molecules such as calixarenes and resorcinarenes [48], carcerands [49] and many more.

According to a recent review [50], the most representative non-covalent bonds in host-guest chemistry are hydrogen-bonded associations and metal coordination, which both offer huge interior spaces. For example, **figure 1.14** presents a metallo-supramolecular compound constituted of 72 components ( $M_{24}L_{48}$ ) [51], 48 identical ligands organized around 24 palladium metal ions ( $Pd^{2+}$ ) which has been revealed using mass spectrometry. Closely related, the hydrogen bonded hexamers of resorcinarene (60 H-bonds) and pyrogallarene presents an inner cavity volume of about  $1200 \text{ \AA}^3$  [52].

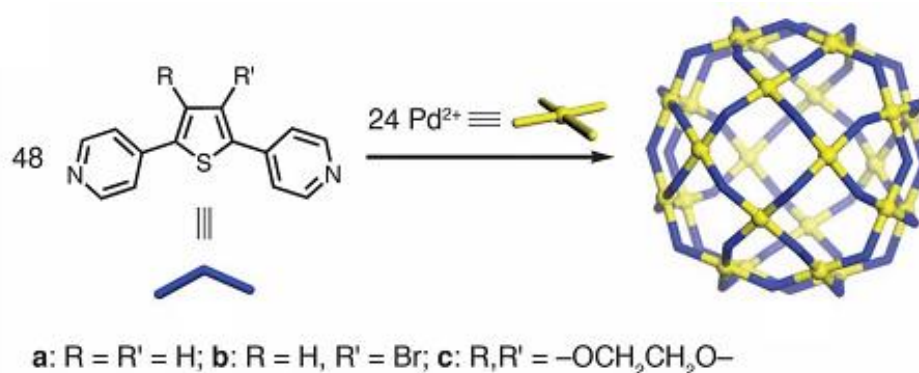
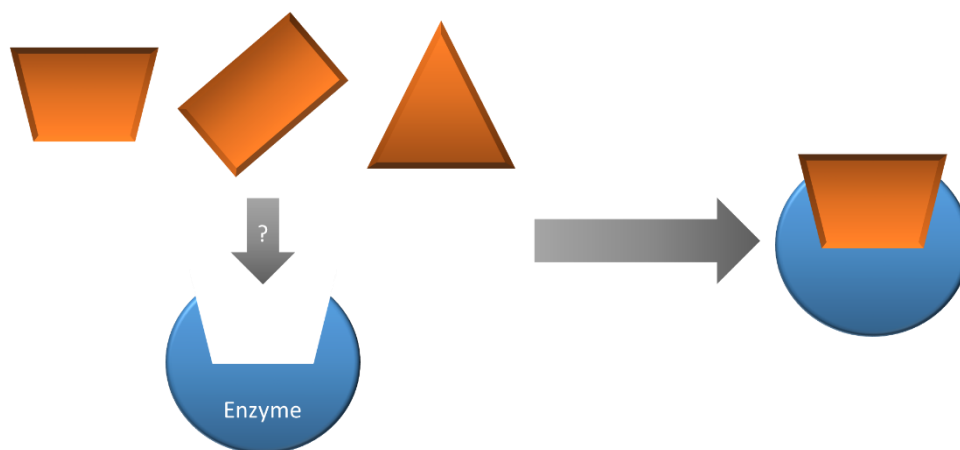


**Figure 1.14:** structure of the metallo-supramolecular compound  $M_{24}L_{48}$  [51].

All previous sections aimed to present some different types of interactions and phenomena related to supramolecular chemistry. Nevertheless, it is now important to stress that supramolecular associations do not only depend on individual non-covalent bonds but also on the structural complementarity, the charge distribution and the surrounding environment of the molecules involved into the binding event [16]. Consequently, selective binding is a combination of steric fit, matching of the charge distribution and spatial arrangement that results in maximizing the attractive forces between host and guest while minimizing repulsive forces. In other words, binding events depends on molecular complementarity between the host and guest compounds as much as it depends on the environment.

This necessity in structure complementarity has been extensively demonstrated according to Fischer's Lock-and-key principle in the interaction of enzymes with a substrate [53]. As presented in **scheme 1.1**, an enzyme will only bind to a substrate that will correctly fit its active

site geometry, saying a substrate that will exhibit the complementary structure of the enzyme active site, while other less adapted substrates will not interact with the enzyme. This simple representation reveals the specificity of an enzyme or host molecule for a peculiar substrate or guest molecule.



**Scheme I.1:** representation of the Lock-and-Key principle of Fischer [53].

Alongside with the synthesis of more specific synthetic hosts, high-performance characterization methods have also been developed. The next section will cover some of the most used methods to describe supramolecular structures.

### 2.3 Investigation Methods for Non-Covalent Associations

In order to characterize supramolecular interactions, different methods are available. The next sections will only cover a few of those methods by a brief presentation of the information they can offer concerning supramolecular complexes. Nevertheless, several books and reviews are dealing with those characterization methods, providing many details and examples to demonstrate how powerful these tools can be for the study of supramolecular associations. Among all these works, some have been of great interest in the redaction of this PhD and are cited in the reference section [54-56].

2.3.1 UV-Visible Spectroscopy

Ultraviolet-visible spectroscopy, also called absorption spectroscopy, is a spectroscopic method involving the absorption of photons in the UV and visible wavelength domain (100-700 nm, an even near infrared up to 1400 nm) by molecules, ions or complexes. The absorption of photons will induce electronic transitions within the sample. Absorption spectroscopy is complementary to fluorescence spectroscopy, in that fluorescence deals with transitions from the excited state to the ground state, while absorption measures transitions from the ground state to the excited states [57].

In the field of host-guest chemistry, UV-visible spectroscopy can be used either as a qualitative as well as quantitative characterization method. In the first case, UV-visible spectroscopy can be used to highlight the complexation of a guest molecule by a supramolecular container by observing the variation of absorption when progressively adding one of the two compounds [58]. As an example, **figure I.15** presents the UV-visible absorption spectrum of Novocain as a function of the  $\beta$ -cyclodextrine concentration [59]. Here, the complex formation is highlighted by the increment of the Novocain absorption intensity in addition to a shift towards higher wavelength (over 289 nm) when adding more cyclodextrine host to the guest solution. The inclusion of Novocain into the cyclodextrine cavity explains the wavelength shift since the inclusion provides a low-polarity environment to the guest chromophore.

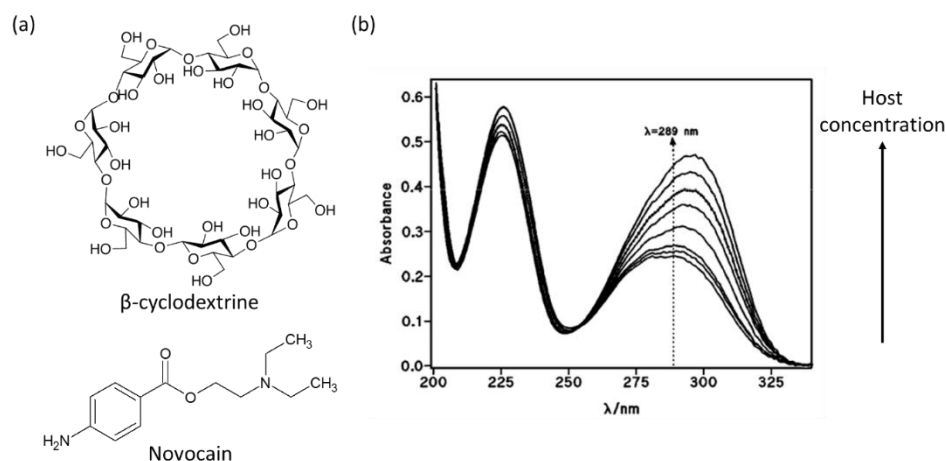


**Figure I.15:** (a) chemical structures of the host  $\beta$ -cyclodextrine and Novocain guest. (b) evolution of the UV-visible absorption spectra of Novocain ( $5.10^{-5}\text{M}$ ) upon addition of  $\beta$ -cyclodextrine (adapted from reference [59]).

For the quantitative part, UV-visible spectroscopy can be used to determine the in-solution binding constant of a supramolecular association alongside with the complex stoichiometry and its thermodynamic parameters (enthalpy, entropy and Gibbs free energy) [58, 60].

**Figure 1.16** presents different data obtained using spectrophotometric method for the determination of caffeic acid self-complexation (**figure 1.16 a**) [61]. Here,  $K_{dB}$  is the equilibrium dimerization constant (**figure 1.16 b**), B1 and B2 are monomers and dimers of caffeic acid, respectively.  $K_{dB}$  can be obtained from a numerical analysis of the experimental concentration dependence of the molar absorptivity of caffeic acid, here in acetonitrile and water solutions, **figure 1.16 c**. The value of the dimerization constant has been computed by nonlinear regression based on the Lavenberg-Marquardt algorithm by Origin software and equals  $2.95 \times 10^3 \text{ M}^{-1}$  in water. The authors showed that heating the aqueous solution of caffeic acid deeply modifies the absorption spectra of the molecules [61]. As temperature increases, the absorption intensity increases which reflects a dissociation of the molecular associated forms in the solutions. **Figure 1.16 d** shows the graph of  $\ln K_{dB}$  as a function of  $1/T$ , which is linear. The magnitude of the enthalpy of compound under study can be estimated from the slope according to van't Hoff equation (**figure 1.16 e**):  $\frac{d \ln(K_{dB})}{d(\frac{1}{T})} = -\frac{\Delta H}{R}$  where,  $\Delta H^\circ$  is the molar enthalpy change,  $R = 8.31 \text{ J.mol}^{-1}.\text{K}^{-1}$ , the universal gas constant and  $T$  the temperature in Kelvin. The entropy is derived from Gibbs free energy and enthalpy. The Gibbs free energy can be expressed as  $\Delta G = -RT \ln K_{dB}$ . The calculated values of Gibbs free energy, enthalpy, and entropy of caffeic acid self-association are  $-34.06$ ,  $-63.20 \text{ k J.mol}^{-1}$  and  $-88.84 \text{ k J.mol}^{-1}$  respectively.



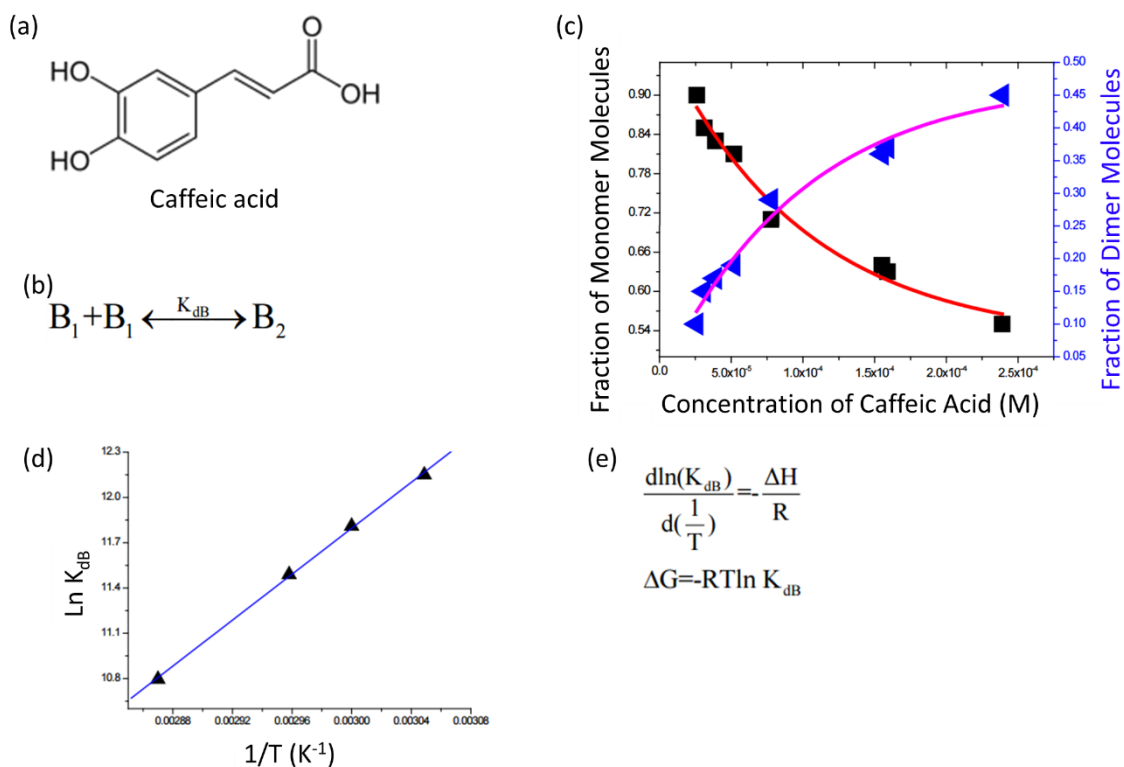


**Figure I.16:** (a) structure of the caffeic acid, (b) dimerization reaction of caffeic acid, (c) the mole fraction of monomer and dimer versus total concentration of caffeic acid in water solution studied by UV-Visible spectroscopy, (d) Van't Hoff plots for self-association of caffeic acid at concentration  $C=5.83 \times 10^{-5}$  M, (e) calculation of the thermodynamic data (adapted from reference [61]).

### 2.3.2 Nuclear Magnetic Resonance (NMR) Spectroscopy

Nuclear Magnetic Resonance spectroscopy (NMR) exploits the magnetic properties of certain atomic nuclei. This experimental method relies on the nuclear magnetic resonance phenomenon that occurs with some nuclei when they are placed in a magnetic field [62]. Using NMR, detailed information about structures and chemical environment of organic molecules can be found starting from either solution or solid samples. Therefore, NMR analyses are mostly used to identify substances due to the unique character of the NMR signature.

As in the case with UV-visible spectroscopy, the formation of a host-guest complex can also be highlighted using NMR spectroscopy. **Figure I.17** presents the proton-NMR spectrum ( $^1\text{H}$

NMR) recorded for the complexation of the host chromene (alone in 3) with aminocaprylic acid as the guest (alone in 1) [63]. In this study, **Fedorova et al.** performed  $^1\text{H}$  NMR titrations upon successive addition of  $\omega$ -aminocaprylic acid to a solution of chromene in acetonitrile. Spectral changes were observed until the molar ratio of 1: 1 is reached (**figure I.17 b2**); further addition of the amino acid does not change the resonance frequencies.

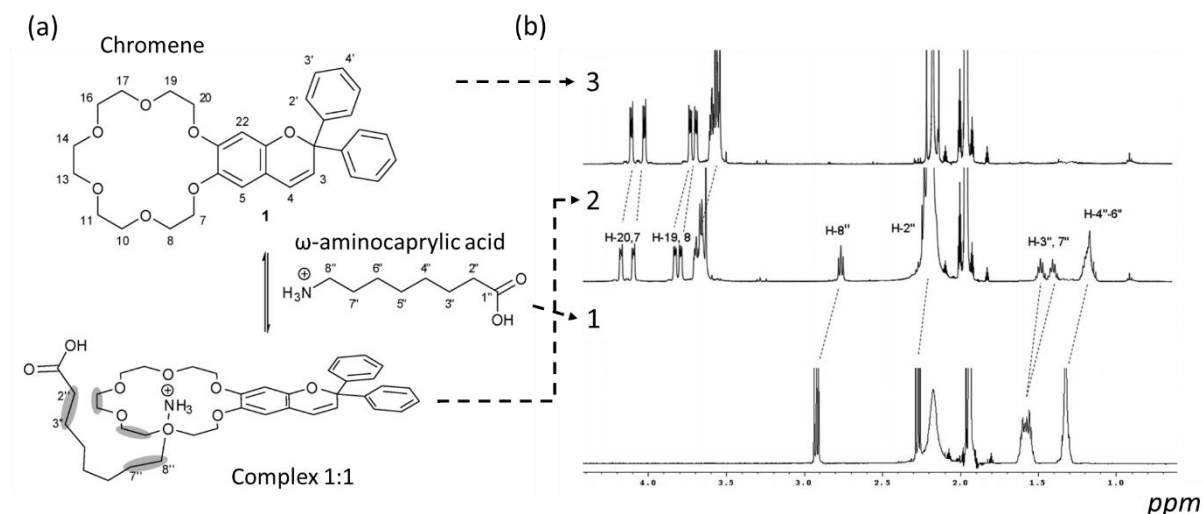


**Figure I.17:** (a) proposed spatial arrangement of the complex involving a chromene derivative (2,2-diphenyl-7,8,10,11,13,14,16,17,19,20-decahydro-2H-[1,4,7,10,13,16]hexaoxacyclooctadeca[2,3-g]chromene) and the acid guest (b)  $^1\text{H}$  NMR spectra (aliphatic region) of the amino acid (1), the 1:1 complex (2) and chromene (3).

For the chromene host, the most pronounced changes in proton resonances can be observed in the proximity of the methylene protons of the crown ether unit (H7-20 and 8-19) whereas the resonances associated to the chromene moiety barely change. On the other hand, the characteristic upfield shift of the guest  $\omega$ -aminocaprylic acid resonances (up to 0.22 ppm) and splitting of H-3'' and H-7'' multiplet signals of the guest indicate the formation of an inclusion complex.

Here again, NMR spectroscopy can be used either as a qualitative and quantitative characterization method. Indeed, in the latter case, NMR can be used to determine the in-solution binding constant of a supramolecular association alongside with the complex stoichiometry and its thermodynamic parameters [64]. The methodology employed will be the same as that using UV-Visible spectroscopy: the host or guest concentration will be

modified in order to study the modification in chemical shifts upon the formation of the complex. From those data, different algorithm methods will be used in order to finally obtain the thermodynamic parameters of the complex formation [65].

Furthermore, besides common experiments, the NMR method is also used to measure the molecular diffusion of non-covalent assemblies; this method is referred to “diffusion NMR” [66]. Molecular diffusion is the random translational motion of particles due to their initial thermal energy and is related to the size of the diffusing compound [67].

Briefly, a typical experiment to measure molecular diffusion, actually to measure the self-diffusion coefficient of a compound, consists in acquiring a set of spectra employing different values of the field gradient strength, or the length of the gradient pulse, while the other parameters of the NMR experiment are held constant. Then, by plotting the intensity of the echo (or response) versus one of those two parameters, it is possible to obtain the self-diffusion coefficient from the decay of the echo intensity [68]. As an example, the encapsulation of benzene inside a tetraureacalix[4]arene dimer (*figure I.18 a*) has been proven using diffusion NMR method [69]. When the calixarene dimer is prepared in a mixture of  $C_6H_6$  and  $C_6D_6$ , a new peak at 4.4 ppm is observed in the  $^1H$  NMR spectrum (*figure I.18 b*). In fact, the middle part of the figure (*figure I.18 b*) depicts the signal decay (echo) as a function of the diffusion gradient strength (named G). The diffusion coefficients extracted therefrom for the peak associated to the complex (4.4 ppm) along with that of the peak of bulk benzene (7.17 ppm) and one representative peak of the dimer (at 1.95 ppm) are represented in *figure I.18 c*. The complex (at 4.4 ppm), is found to have a much lower diffusion coefficient than “free” benzene (at 7.17 ppm). Indeed, the peak at 4.4 ppm is found to have the same diffusion coefficient as the peaks representing the dimer ( $D= 0.34 \cdot 10^{-5} \text{ cm}^2\text{s}^{-1}$ ). Herein, the use of diffusion NMR demonstrates how easy it is to reach the conclusion that the entire capsule diffuses as a single entity since both the ternary complex (1 guest benzene for 1 calixarene dimer) and the empty dimer capsules are characterized by the same diffusion coefficient.

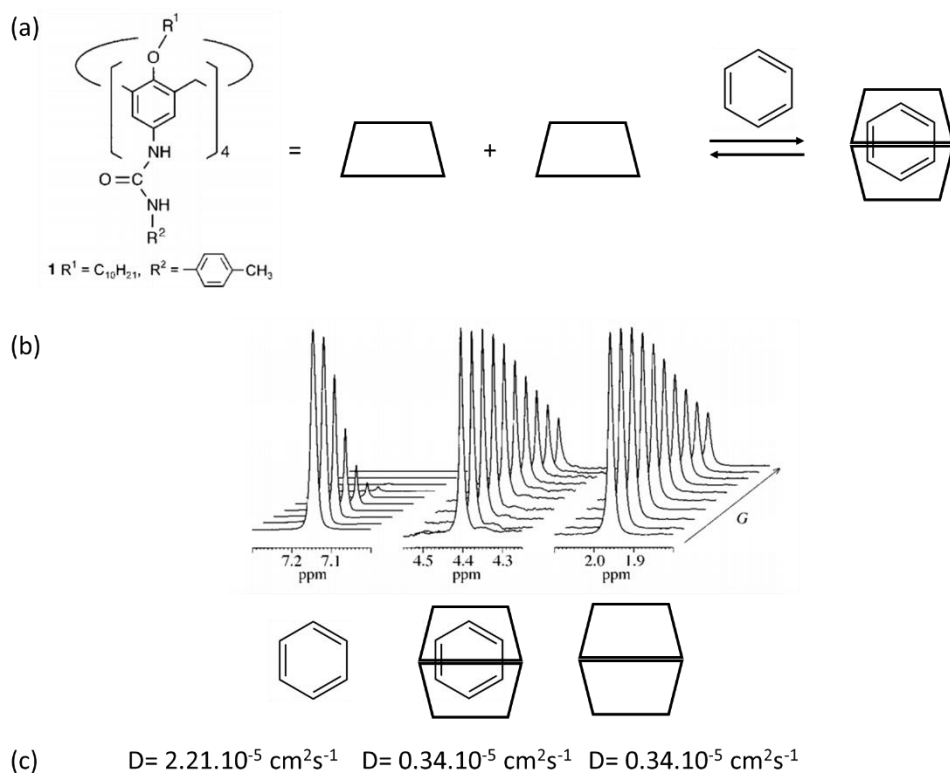


**Figure I.18:** (a) structure of the tetraureacalix[4]arene and formation of the ternary complex, (b) 500 MHz  $^1\text{H}$  NMR spectra of diffusion experiment in a 80 : 20 (v/v) benzene–benzene- $d_6$  solution showing the signal intensity decay as a function of the pulsed gradient strength ( $G$ ).

For clarity only the signal of **1** at 1.95 ppm and the signals attributed to “free” and encapsulated benzene at 7.15 and 4.4 ppm, respectively are shown, the extracted diffusion coefficients are presented in (c) (adapted figure from reference [69]).

### 2.3.3 Isothermal Titration Calorimetry

Any physical or chemical reaction induces variation of enthalpy when the reaction occurs. Isothermal titration calorimetry (ITC) is a direct method allowing measurement of the heat energy change (saying change in enthalpy) of a reaction at constant temperature [70]. Since ITC analysis is carried out at a given temperature, it allows the direct measurement of the reaction binding constant ( $K_a$ ), reaction stoichiometry ( $n$ ), enthalpy change ( $\Delta H$ ) and entropy change ( $\Delta S$ , more details below). In other words, ITC experiments provide the complete thermodynamic profile of a molecular association [70].

The in-solution formation of non-covalent complexes results from multiple steps. Each of these steps is associated to a change in the enthalpy due to the making and breaking of non-covalent bonds (such as the interaction between solvent and host prior to the complexation). Therefore, the calorimetric experiment does not just include measurement of the heat associated with the formation of a complex, but also the heat associated with other potential accompanying events such as protonation/deprotonation, solvent rearrangement and conformational changes in the complexes [71].

**Figure I.19 a** depicts the instrumental set-up of a power compensation calorimeter [72]. Both cells are filled: the reference cell with pure solvent while the sample cell contains a solution of one of the two host-guest partner (generally the host). The addition of the guest solution by a computer-driving syringe induces a heat effect that is counter-regulated by the solvent cell to maintain  $\Delta T$  at zero.

As an example, **figure I.19 b**, illustrates the ITC data output, which consists in a number of heat pulses that decreases (from left to right) with the progressive saturation of the host by incremental addition of the guest compound (presented in **figure I.19 c**) [73]. The upper part of **figure I.19 b** presents downward directed pulses indicating the diminution of the feedback current necessary to keep a zero temperature difference with respect to the reference cell due to the exothermic character of the association between the phosphate guest with the cryptand host. The integration of the heat pulses, when plotted versus the nominal molar ratio of the injected compound over the one in the cell, yields a titration curve that exhibits a characteristic sigmoidal shape (bottom part of **figure I.19 b**). Data treatment of the sigmoidal curve allows for the determination of the molar enthalpy  $\Delta H^0$  from the extrapolated step height of the curve. From the same curve, the stoichiometry  $n$  of the binding process can be determined from the position of the inflection point along the molar ratio axis (X-axis) and the binding constant  $K_a$  is derived from the slope at the inflection point of the sigmoid [72].

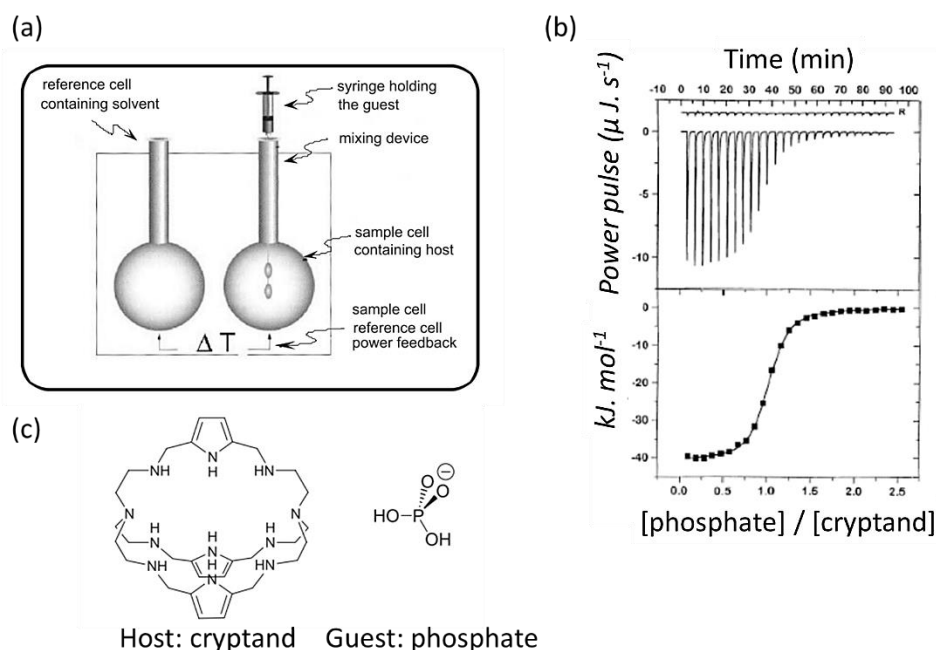


**Figure I.19:** (a) instrumental set-up of a power compensation calorimeter. (b) ITC titration of a cryptand by phosphate guest (pH=7), structures presented in (c) (adapted from reference [73]).

ITC is a versatile, label sensitive and destruction-free, quite rapid (up to three hours) instrumental method that necessitates less than micromolar amounts of compounds to define thermodynamic parameters of reversible molecular associations [72]. Actually, the reliability and accuracy of ITC are unsurpassed. Therefore, ITC is considered as the gold standard in the characterization of intermolecular interactions in solution [72]. Nevertheless, one has to realize that calorimetric spectroscopy is equilibrium-dependent, which is in contrast with some facets of supramolecular chemistry. For example, molecular recognition exists because of non-equilibrium conditions and relies more on kinetic selectivity rather than on thermodynamic phenomena and therefore cannot be described by calorimetry spectroscopy [74].

2.3.4 Extraction Method

Supramolecular chemistry covers different research areas such as molecular recognition, binding and phase transport of chemical compounds that led to several advances in analytical techniques, catalysis, environmental processes etc [44, 75]. Therefore, understanding the binding properties of a host in an organic phase over chemical species diffusing in aqueous solution has been of great interest over the years.

The so-called liquid-liquid extraction enables to assess several supramolecular properties such as binding strength, selectivity, speciation and of course phase transfer associated to supramolecular receptors toward selected cations, anions, zwitterion, salts in two-phase systems (aqueous versus organic phases) [76].

The principle of solvent (liquid-liquid) extraction is presented in **figure 1.20**. The first step corresponds to the extraction process (**a**) and starts with two solutions, aqueous (aq) and organic (org), which are immiscible. The aqueous phase contains the compound of interest (solute) and the organic phase the complexing agent, also called extractant. The phase transfer of the solute is driven by the complex formation between the solute and the extractant and is normally accomplished by mixing the two phases intensively (middle of **figure 1.20 a**). After phase separation, the solute recovery and the extractant regeneration occur from the organic phase (right of **figure 1.20 a**) in a second step by means of a back extraction (schematized in **figure 1.20 b**) [44, 75].

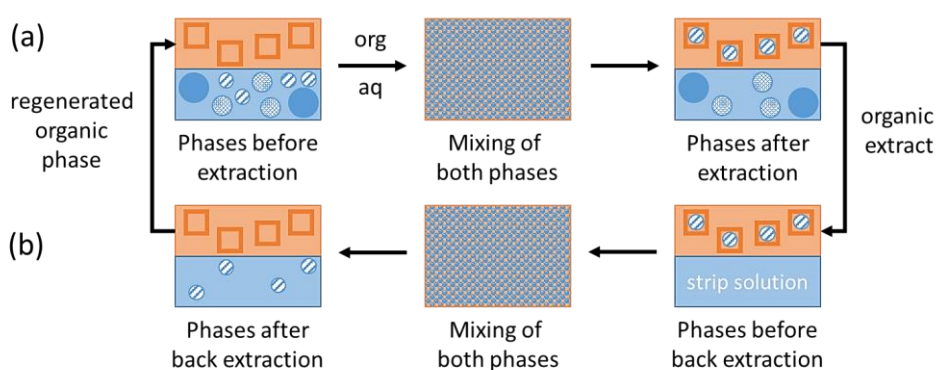


**Figure 1.20:** representation of an extraction process divided in two parts: (a) the extraction, (b) the back extraction.

**Figure I.21** presents an example of the relative selectivity abilities of two different guanidinium compounds (Guadi A and Guadi B) towards different anions ( $\alpha$ ) [77]. Guadi B extracts the strongly hydrophilic  $\text{SO}_4^{2-}$  ion with higher efficiency than  $\text{Br}^-$  or  $\text{HPO}_4^{2-}$ . On the other hand, Guadi A, the monotopic guanidinium derivative, does not present a comparable behavior yielding to an optimum structural arrangement from Guadi B with the sulfate anion (**b**). In fact, this latter result has been confirmed with molecular modeling calculations of the structure of the corresponding 1:1 complex [77] in which the anion is bound by the cooperative action of a salt bridge and at least two strong hydrogen bonds (**figure I.21 b**).

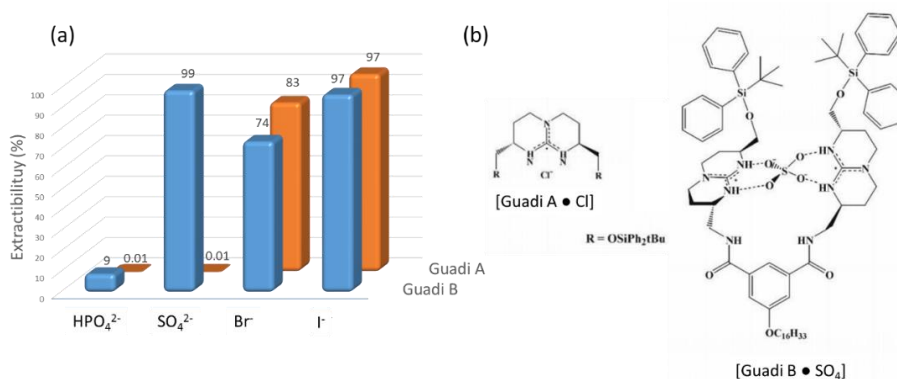


**Figure I.21:** (a) extraction of  $\text{Br}^-$ ,  $\text{I}^-$ ,  $\text{HPO}_4^{2-}$  and  $\text{SO}_4^{2-}$  by guanidinium compounds Guadi A and Guadi B. (b) structures of Guadi A and Guadi B complexed respectively with  $\text{Cl}^-$  and  $\text{SO}_4^{2-}$  in  $\text{CHCl}_3$  (adapted from reference [77]).

In addition to those extraction experiments, isothermal titration calorimetry measurements (ITC, presented in section 1.2.3.3) of sulfate binding by the above receptors in methanol attested the dominating role of solvation during the complex formation [78]. This last example constitutes a good demonstration of how the complementarities of several different characterization methods can be useful in the study of supramolecular assemblies.

The different methods presented in this last section aim to characterize non-covalent associations in solution. Accordingly, the influence of the solvent might sometimes alter the nature or the conformation of the assemblies as well as drive the complexation process. Nevertheless, being able to study supramolecular assemblies without any influence of their environment is dramatically needed in order to define intrinsic properties of those associations. Therefore, mass spectrometry has become a great additional tool to the characterization method armada already available in the field of supramolecular chemistry.



### 3. Supramolecular Mass Spectrometry

Mass Spectrometry (MS) is an experimental method operating in high vacuum (up to  $10^{-9}$  mbar), allowing the detection of gas phase ions of several origins. Since the vaporized compounds are no longer in interaction with their environment, **the molecular intrinsic properties (elemental composition, stoichiometry, secondary structures of non-covalent associations, etc.) can be approached using mass spectrometry**. Indeed, once the molecules have been desolvated and ionized; the gas phase ions do not possess any solvation layer and are isolated in the gas phase. Therefore, isolated compounds of interest can be studied by mass spectrometry without any influence of their environment [79].

In the late nineteenth-century, the prequels of mass spectrometry have been discovered when **Eugen Goldstein** highlighted the influence of a magnetic field over a particles ray emitted from a gas discharge tube [80]. In 1897, **Joseph John Thompson** measured the mass-to-charge ratio of electrons and obtained the Nobel Prize in physics (1906) for his work on discharges in gases and the discovery of electrons [81]. Later on, in 1913, Thompson has been able to separate particles of different mass-to-charge ratios (isotopes  $^{20}\text{Ne}$  and  $^{22}\text{Ne}$ )[82]. Since that moment, mass spectrometry has considerably evolved alongside with its use in modern research as a performant analytical tool (**figure I.22**).

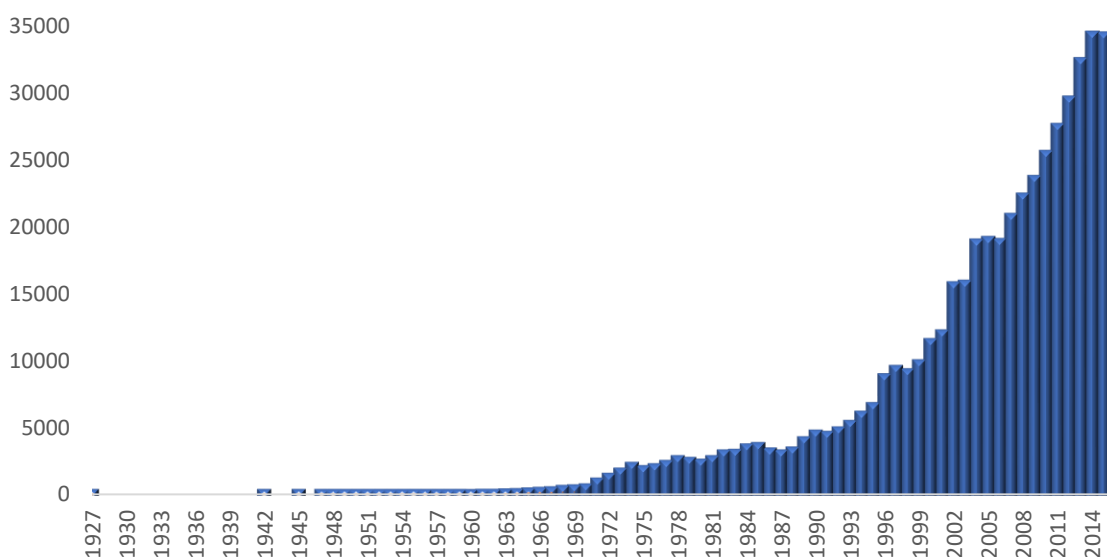


**Figure I.22:** number of referenced articles when looking for “mass spectrometry” as key word (website consulted in March 07, 2017) [83].

Over the last decades, Supramolecular Mass Spectrometry has been constantly used to help answering many questions about characterization (stoichiometry, elemental composition, etc.), structural aspects (connectivities, relative positions, etc.) and reactivity of supramolecular associations in solution and in the gas phase [81, 83].

Mass spectrometry actually offers a large set of methods available to characterize non-covalent associations (see section III), providing the three “S” outlined by McLafferty [84] to this new research field: specificity, sensitivity and speed.

Concerning the research field of supramolecular chemistry, mass spectrometry has been able to adapt to this new research area thanks, in particular, to the development of soft ionization methods such as electrospray (ESI) [85, 86]. Over the last decades, the technical advances in mass spectrometry have allowed for the investigation of many types of different molecular containers in the gas phase [87].

### 3.1 Electrospray Ionization

Supramolecular associations are characterized by weak energy interactions between host and guest molecules. Accordingly, those intermolecular bonds have to be preserved when studying those assemblies in mass spectrometry, in other words when those compounds will be transferred from the solution to the gas phase. Therefore, “hard” ionization methods, such as the Electronic Ionization (EI), cannot be employed when studying non-covalent complexes. Indeed, those methods are accompanied by a high fragmentation ratio, which will probably result in the separation of the host-guest association through the ionization process.

Initially developed for the study of proteins (which cannot either be analyzed using EI method), Electrospray ionization (ESI) has been proposed by **John Fenn** in 1984 [85]. Electrospray is a soft ionization method, which permits the preservation of non-covalent interactions from a solution to the gas phase of a mass-spectrometer. Fenn, alongside with **Koichi Tanaka** (*figure 1.23*), has been awarded a Nobel Prize in chemistry “for their development of soft desorption ionization methods for mass spectrometric analyses of biological macromolecules” in 2002 [88].



**Figure I.23:** Nobel prizes in Chemistry, laureates of 2002 [88].

The Electrospray is a soft, continuous and atmospheric operable ionization source, which allows the analysis of high molecular mass compounds such as proteins, polymers and supramolecular compounds through their corresponding mono or polycharged ions.

Electrospray is triggered by the application of an electric field at atmospheric pressure on a polar sample solution heading through a capillary at a low flow rate (5  $\mu\text{l}/\text{min}$ ) (**figure I.24**) [85]. In addition, the capillary is submitted to a desolvation gas flow ( $\text{N}_2$ ) which contributes to the sample evaporation. The application of the electric field causes an accumulation of charges at the liquid surface located at the end of the capillary leading to the formation of the *Taylor Cone*. The he accumulated ions will be cations if the potential applied on the capillary is positive; oppositely, anions will be accumulated if the applied potential is negative. Accordingly, this potential leads to a separation of the charges in the solution. Once the amount of charges in the *Taylor Cone* overcomes the liquid surface tension, the cone explodes in a spray of highly charged droplets (electrospray) containing analytes and solvent molecules and cations ( $\text{Na}^+$ ,  $\text{K}^+$ , ...) [89].

Those droplets are stable as long as the liquid surface tension balances the coulombic repulsion. Nevertheless, with the temperature in the source (80-120°C), the solvent evaporates and the size of the droplets decreases down to a point where the coulombic repulsion is no more balanced. This limit, called the limit of Rayleigh, leads to the explosion of the droplet in a new spray of smaller charged droplets (Coulomb explosion). Finally, after several droplet explosions, the ions enter the mass spectrometer (around 1 mbar) [89, 90].

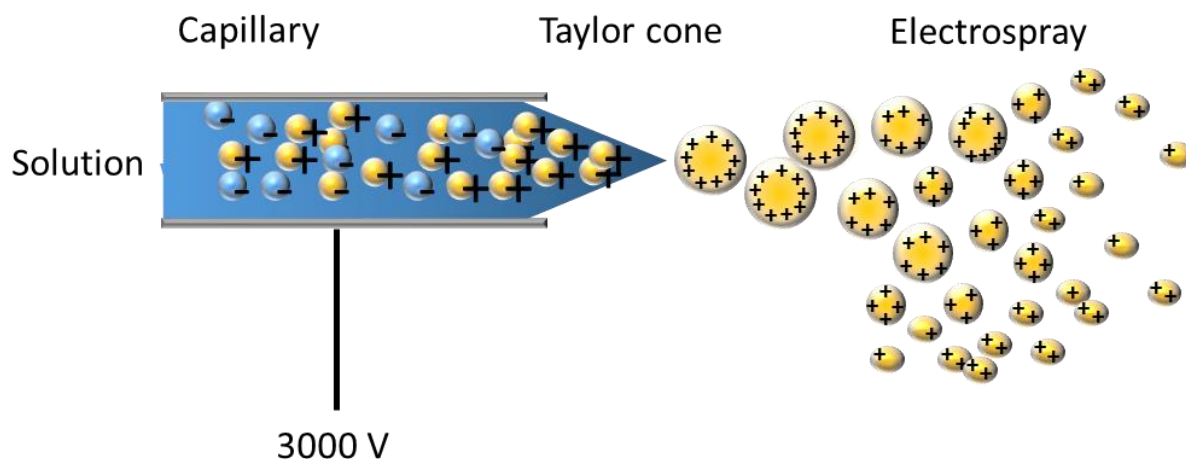


**Figure I.24:** representation of the ESI source in positive mode analysis.

The electrostatic spray ionization process can be described with three different models (**figure I.25**). Once small charged droplets have been produced, **Dole** introduced the “Charged Residue Model” (CRM) to generate gas phase macro ions [85]. For small molecules, another model has been proposed by **Iribarne and Thomson**: the “Ion Evaporation Model” [91, 92]. A third mechanism has been proposed by **Konermann** to explain the formation of unfolded polymer chain ions using ESI: “the Chain Ejection Model” (CEM) [93].

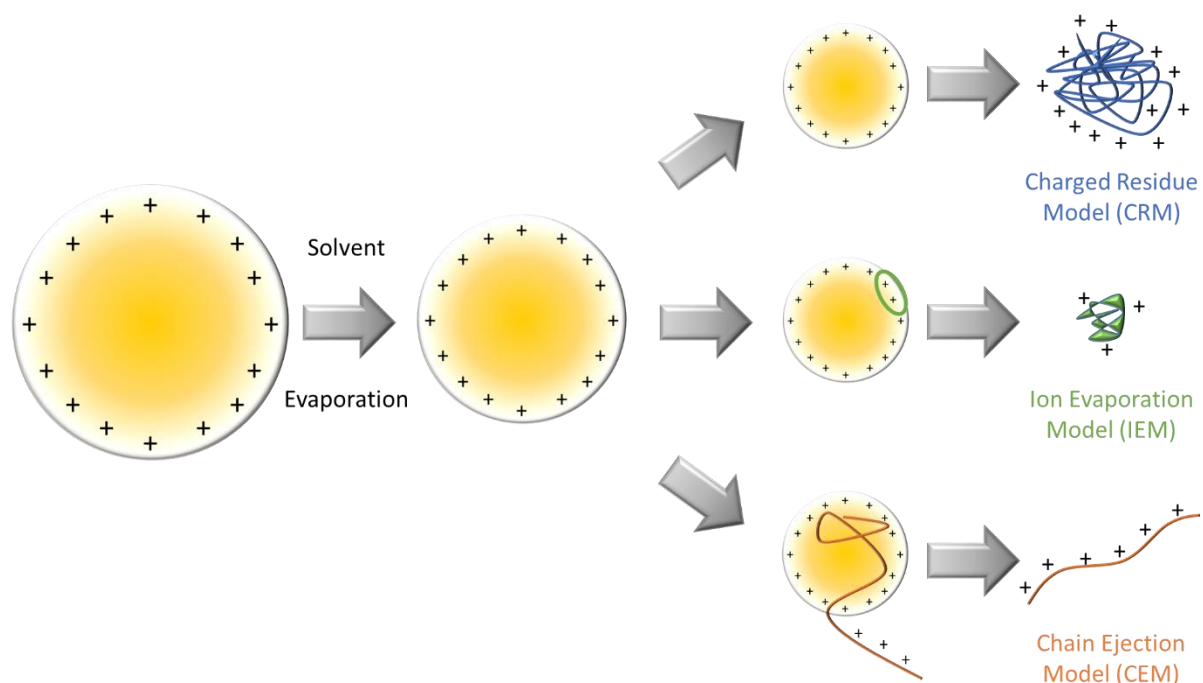


**Figure I.25:** ESI processes by evaporation, explosion method [90] or chain ejection model [93].

In the first case, **Dole** presumes that during the evaporation and Coulomb explosion processes, the ultimate droplets charged on their surface contain only one analyte molecule. Macromolecular ions are then obtained upon evaporation of residual solvent molecules.

In the second case, **Thomson and Iribarne** hypothesize that starting from a certain droplet size, some analyte ions are directly ejected from the droplet in order to reduce the global coulombic repulsion. This process is easier to explain for the liberation of small ions.

For the latter case, the model proposed by **Konermann** (CEM) can be applied to the ionization of polymer chains and proteins. In fact, many non polar moieties of those chains are buried within the charged droplets and form a hydrophobic core that is not accessible by the solvent [94]. This largely hydrophobic character renders unfavorable for unfolded proteins (or polymers) to reside inside the droplet. Instead, in the ultimate droplets, unfolded chains migrate to the droplet surface and one chain terminus gets expelled into the vapor phase. A stepwise sequential ejection of the remaining protein follows until the expulsion of the chain terminus and hence the separation from the droplet occur. The CEM model concerns polymer chains that are (i) disordered, (ii) partially hydrophobic, and (iii) capable of binding excess charge carriers [93, 95, 96].


### 3.2 Selected examples of the use of Electrospray in supramolecular chemistry

As already mentioned, the development of soft ionization methods such as ESI has opened the way of mass spectrometry to the gas phase characterization of supramolecular containers. Therefore, alongside with the use of NMR, UV-visible and other commonly employed analytical methods, mass spectrometry has been increasingly used in the study of non-covalent associations.

Among thousands of examples using mass spectrometry in the field of supramolecular chemistry, the next sections present only a small selection to demonstrate how powerful can be the use of mass spectrometry when studying non-covalent complexes.

### 3.2.1 Supramolecular associations

As cited above, the use of an Electrospray ionization source permits the conservation of supramolecular interactions from the solution to the gas phase of a mass spectrometer. Thereby, all in-source produced ions can be observed when performing a single-stage MS analysis. Such an experiment gives information on the complex stoichiometry, saying the number of guest and host molecules involved in an association (one guest for one host, two guests for one host, etc.)

**Figure 1.26** presents the single stage MS analysis in negative ESI mode of a rotaxane (**figure 1.26 b**) and a mixture of its components (**figure 1.26 c**). The compound structures are presented in **figure 1.26 a** [97]. Rotaxanes are constituted of a macrocycle unit linked to a molecular fragment passing through the macrocycle host. The two compounds can only be separated from each other by a covalent bond breaking since two bulky substituents (larger than the macrocycle cavity) closes the molecular chain on each side (  ) [98]. Therefore, it is important to remark that rotaxane are produced via a synthesis and not a complexation [98]. Accordingly, the synthesized rotaxane (binary complex: one host for one guest compound) is observed in **figure 1.26 b** at  $m/z$  1767. The absence of signals corresponding to the two parts of the association ( $m/z$  805 for the linear chain and  $m/z$  960 for the tetralactame macrocycle) on the mass spectrum attests the efficient synthesis of the rotaxane compound. At the opposite, the spectrum presented in **figure 1.26 c** shows that only the macrocycle and the linear chain are separately detected proving that trying to produce a complexed rotaxane is useless. In fact, the association observed at  $m/z$ 1767 in **figure 1.26 c** only corresponds to a non-specific complex associating the two constituents and not to the formation of a rotaxane [97].

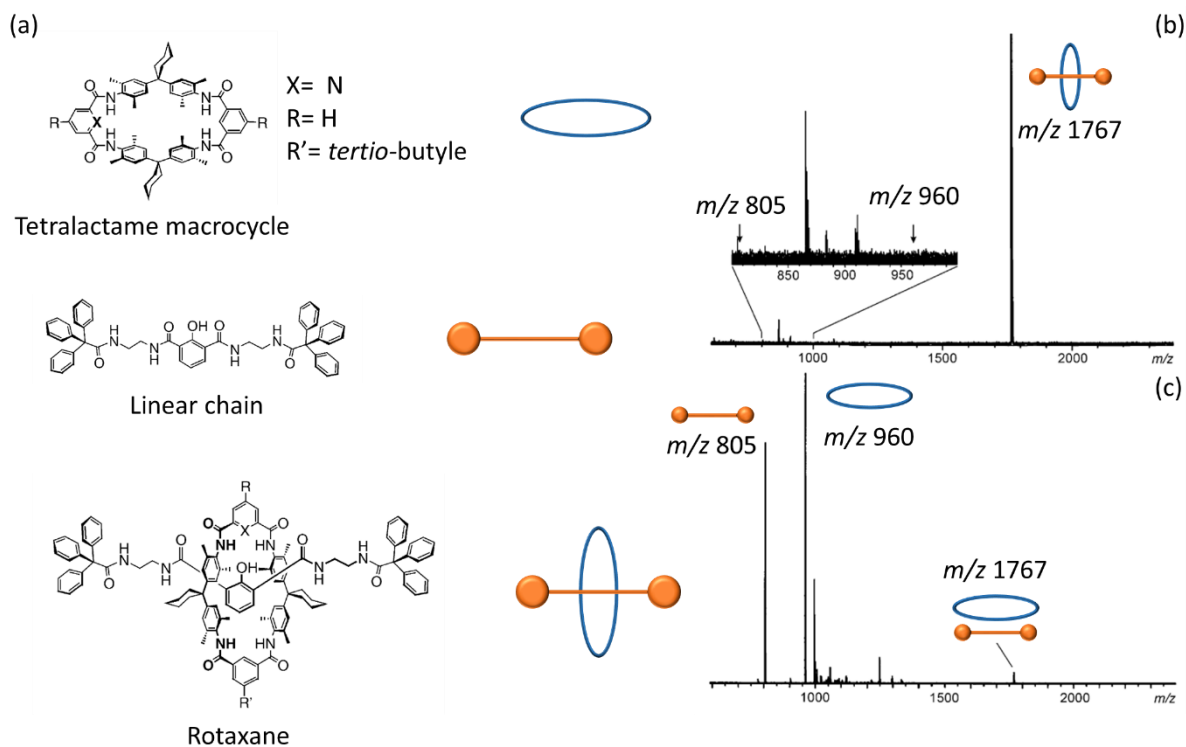


**Figure 1.26:** (a) structures of the rotaxane and its constituents. Single stage MS analysis (ESI negative mode) of (b) a synthesized rotaxane and (c) a mixture of its constituents (adapted from reference [97]).

Through this example, it has been proved that the use of mass spectrometry and the ESI source permit the observations of non-covalent associations in the gas phase. Moreover, using mass spectrometry, the secondary structures of supramolecular associations can also be approached using collisional activation, i.e., tandem mass spectrometry (MSMS) [99]. Briefly, MSMS experiments are constituted of two steps: (i) the selection of a mass to charge ratio (called parent ions) followed by (ii) the fragmentations of those parent ions in a collision cell through collisional activation with a buffer gas to produce “daughter ions”. Based on those daughter ions, the parent ion structure can be determined (for more details on tandem mass spectrometry, please refer to the annex section of this PhD).

Tandem mass spectrometry experiments have been performed on the previously presented rotaxane and a mixture of its constituents (**figure 1.27**).

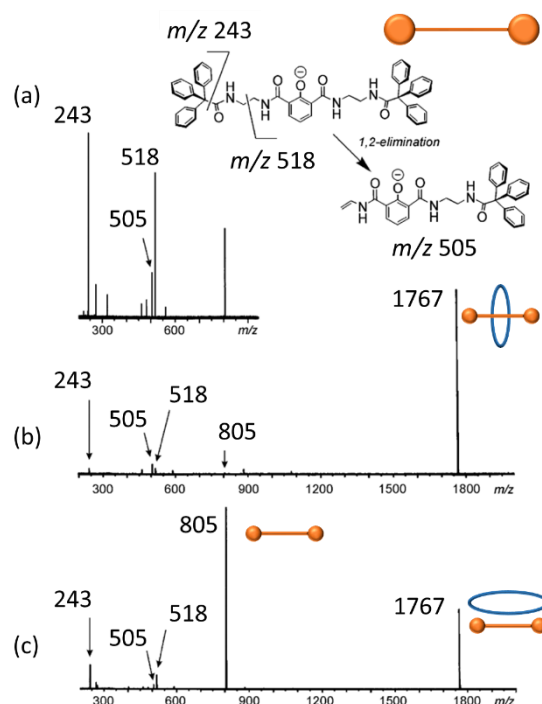


**Figure I.27:** (a) MSMS spectrum and scheme of the linear chain fragmentation pathway. MSMS analysis of (b) the rotaxane and (c) the tetralactame-chain complex (ESI negative mode, adapted from reference [97]).

**Figure I.27 a** presents the fragment ions observed when the linear chain (the guest involved in the rotaxane synthesis) is collisionally activated in the MSMS experiment. When performing MSMS experiments on the rotaxane ( $m/z$  1767, **figure I.27 b**), only few fragments are observed and correspond to fragment ions of the linear chain ( $m/z$  243, 505 and 518). Accordingly, less energy is required to fragment the linear chain than to observe fragmentation of the tetralactame macrocycle ions. Regarding the structural information obtained here when performing MSMS analysis, the observed fragments confirm the successful synthesis of the rotaxane compound since only linear chain fragments are observed and not the intact guest compound ( $m/z$  805). On the other hand, when performing the same experiment on the complex associating the two rotaxane components (**figure I.27 c**), nearly only the intact linear chain is detected ( $m/z$  805) indicating that the compound observed at  $m/z$  1767 in **figure I.27 c** is not a rotaxane but only a “wheel-chain” binary complex formed on the two rotaxane parts.



Beside more common host-guest association studies (crown ethers, cyclodextrines, etc.), the use of electrospray also permitted the characterization of more original associations such as dimer capsules.

In 2011 [100], **Schalley et al.** highlighted the formation of a self-assembled dimers of resorcinarene (**figure 1.28 a**) using a ESI-FTICR (Ionspec QFT-7) [101] mass spectrometer. In this study, mass spectrometry has been used to detect host-guest complexes associating one resorcinarene with ions such as cesium ( $\text{Cs}^+$ ), tetramethyl ammonium ( $\text{TMA}^+$ ) and tetraethyl ammonium ( $\text{TEA}^+$ ) alongside with dimers of resorcinarene with those cations (**figure 1.28 b**).

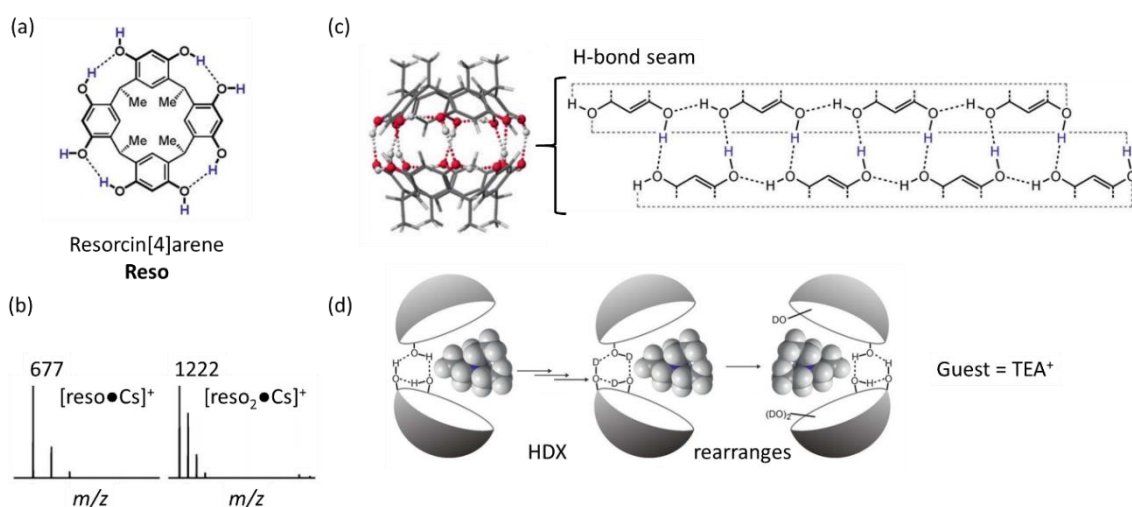


**Figure 1.28:** (a) chemical structure of resorcin[4]arene (reso), (b) ESI-MS spectrum of the association between reso and the cation  $\text{Cs}^+$ , (c) force-field optimized structure of the corresponding hydrogen bonded dimer and zoom on the H-bond seam (before any H/D exchange), (d) H/D exchange in the PacMan-shaped  $[\text{reso}_2 \bullet \text{TEA}]^+$  dimer (adapted from reference [100]).

The use of H/D exchange reactions within the gas phase of the mass spectrometer revealed that the smaller ion  $\text{Cs}^+$ , bounded inside the dimer capsule, does not influence the seam of hydrogen bonding between the two monomers (**figure 1.28 c**). On the other hand, the complexation of bigger ions ( $\text{TEA}^+$  and  $\text{TMA}^+$ ) leads to a partially disrupted H-bonding array between monomers that can be represented by a “PacMan” shape (**figure 1.28 d**) where labile hydrogen slowly exchange, leading to a complete rearrangement of the PacMan shape.

3.2.2 Complete virus ionization

Detection of huge molecules such as viruses (over  $50 \cdot 10^6$  Daltons) has always been challenging. Nevertheless, the development of ESI permitted to achieve significant stride in the characterization of such complicated and heavy biological molecules. Actually, the use of the electrospray ionization method permitted the intact ionization of complete viruses [102].

**Figure 1.29 a** presents the ESI-MS spectrum recorded for the tobacco mosaic virus (TMV, infecting plants especially tobacco). The mass spectrum realized on the TMV particles presents a mass centered distribution between  $39 \cdot 10^6$  and  $42 \cdot 10^6$  Da. This observation is consistent with the theoretical calculated mass of  $40,5 \cdot 10^6$  Da, within the error of the instrument used for this study.

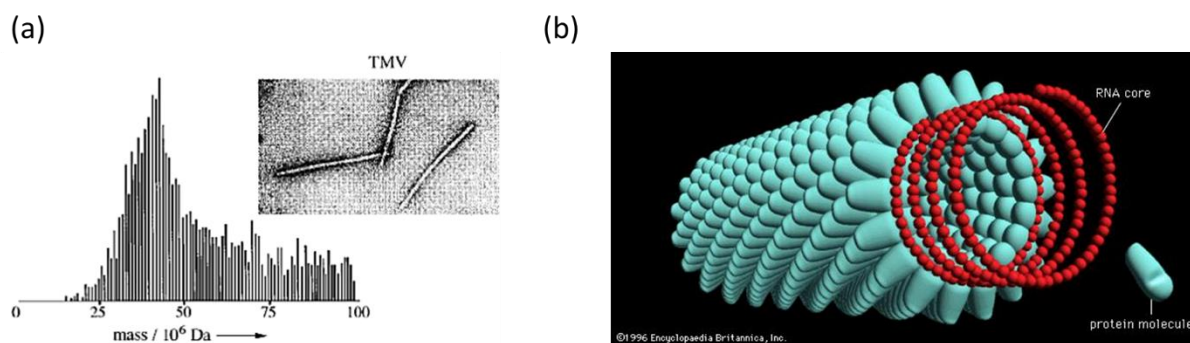


**Figure 1.29:** (a) Mass spectrum of TMV particles analyzed with an Electrospray ionization charge-detection time-of-flight mass spectrometer. Insets: electron micrographs of the cylindrical TMV (approximately 300 nm long and 17 nm in diameter). The known molecular weights of TMV is  $40.5 \cdot 10^6$  Da (adapted from reference [102]). (b) representation of the TMV with the RNA core in red and the protein subunit in blue [103].

TMV molecules are constituted by more than 2100 non-covalently bound protein subunits surrounding a templating RNA strand (schematized in **figure 1.29 b**). The intact ionization of such a monster-macromolecule points out how far the limits of mass spectrometry have been pushed forward in the field of supramolecular chemistry.

### 3.2.3 Gas phase reactivity of supramolecular assemblies

Since electrospray ionization allows the vaporization of non-covalent complexes in the gas phase of a mass spectrometer, several studies have been achieved regarding the gas phase reactivity of those supramolecular associations. In fact, as mentioned by **Schalley** in a review on this subject: *“The significantly higher strength of non-covalent interactions in the absence of competing solvent allows processes to occur that are unable to compete in solution”* [104].

Among those processes, **Beauchamp et al.** [105] highlighted, using an ESI source, the formation of covalent bonds within a vaporized non-covalent complex.

The so-called “mousetrap”, doubly crown-ether-substituted host (C for crown, **figure 1.30**), bears an azodiester group that can quite easily form a carbene upon nitrogen loss. The two [18]crown-6 ethers provide binding sites that can be complexed by diammonium ions bridged with, for example, an alkyl chain long enough to bridge the two crown ether binding sites. Doubly protonated 1,6-diaminohexane (DAH) is a suitable example.

When recording an ESI-MS spectrum of a mixture of C and DAH, doubly charged  $[C\bullet DAH\bullet 2H]^{2+}$  ions appear as the base peak (**figure 1.30**, top). Upon mass-selection and collisional activation in an MS/MS experiment (more details in section III.1.4) (**figure 1.30**, centre), a nitrogen loss is more or less the only fragmentation product observed in the mass spectrum. Therefore, this fragmentation reaction proceeds below the dissociation limit of the complex. Consequently, the expected carbene  $[:C\bullet DAH\bullet 2H]^{2+}$  indeed forms.

The formation of covalent bonds between C and the doubly charged diaminohexane can be examined by an MS<sup>3</sup> experiment, in which the  $[:C\bullet DAH\bullet 2H]^{2+}$  ion is re-isolated and again subjected to collisional activation (**figure 1.30**, bottom). Since the proton affinities of primary amines and crown ethers are not too different ( $\Delta PA \approx 20\text{--}30 \text{ kJ}\cdot\text{mol}^{-1}$ ), a charge-separating fragmentation would easily be possible, provided both components are still bound in a non-covalent way only. In this case, the  $[DAH+H]^+$  ( $m/z$  117) and carbene  $[:C+H]^+$  ( $m/z$  683) fragments would be detected more or less exclusively. However, the MS<sup>3</sup> spectrum clearly shows a large number of fragments that can be assigned to the cleavage of covalent bonds within the complex. This also provides evidence for the formation of a covalent bond between

the two components – likely by insertion reactions of the carbene into one of the covalent bonds in the DAH guest dication.

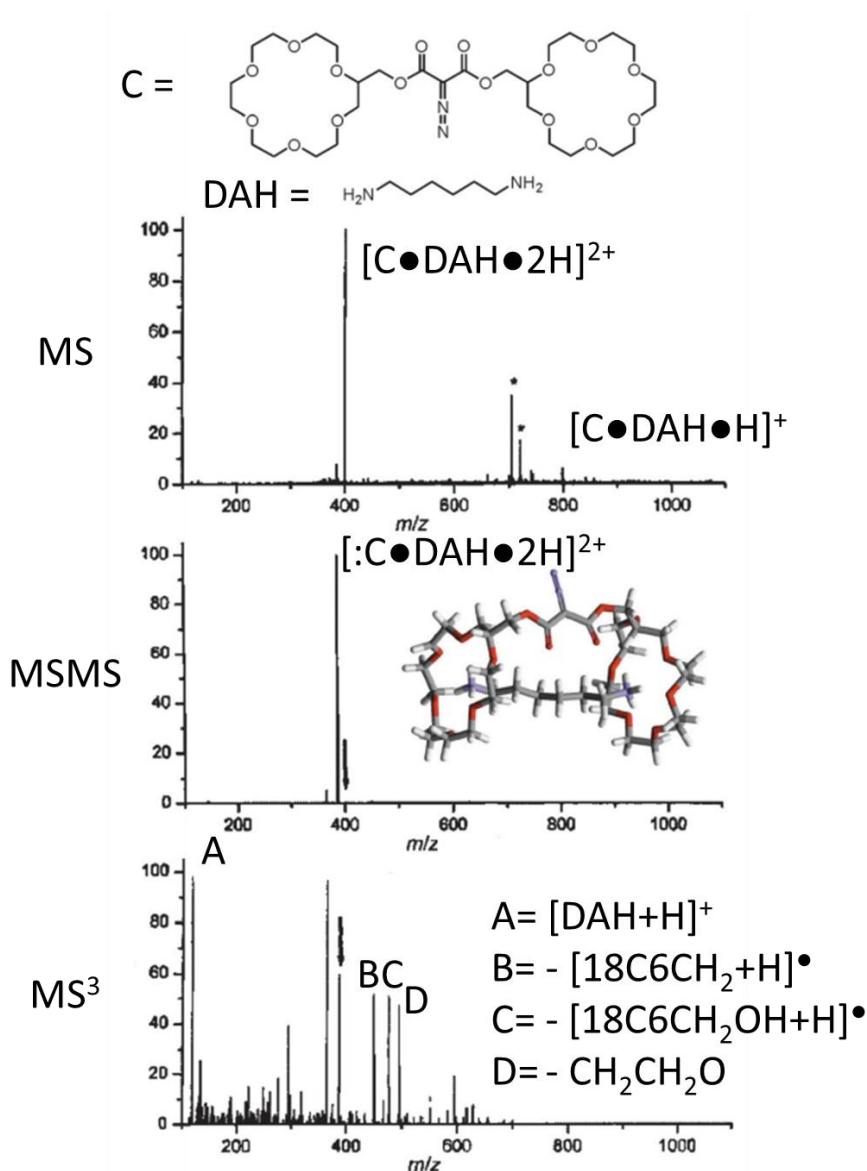


**Figure I.30:** structures of C and DAH followed by the MS (top), MSMS (middle) and MS<sup>3</sup> (bottom) spectra in the study carried by Beauchamp et al. (adapted from reference [105]).

This study provides clear evidences that the much stronger non-covalent interactions in the gas phase allow for covalent bond formation, and other type of gas phase reactivity, competing with complex dissociation. If such a reaction occurs, one can conclude that the activation barriers for the covalent chemistry remain below the dissociation threshold of the complex [105].

### 3.3 False positive detection

The previous sections illustrated some of the major advancements, mass spectrometry has offered in the characterization of intermolecular associations alongside with soft ionization methods. Nevertheless, it is important to stress that the different electrostatic interactions (such as H-bonds, dipole interactions, etc.) are reinforced without solvent contributions [106]. Accordingly, the vaporization inside the ionization source might lead to the formation of non-specific interactions. In this case, the gas-phase experiment will not reflect the reality of the processes that occur in solution.

As an example of those “false positive”, **figure I.31 b** presents the MS-spectrum recorded for the association between the arginine amino acid and the  $\beta$ -cyclodextrine macrocycle (**a**) [106]. The ion corresponding to the monocharged 1:1 host-guest association is observed at  $m/z$  1310. Nevertheless, the  $\beta$ -cyclodextrine host is well known for only significantly complexing aromatic amino acids due to its central cavity hydrophobicity [107].

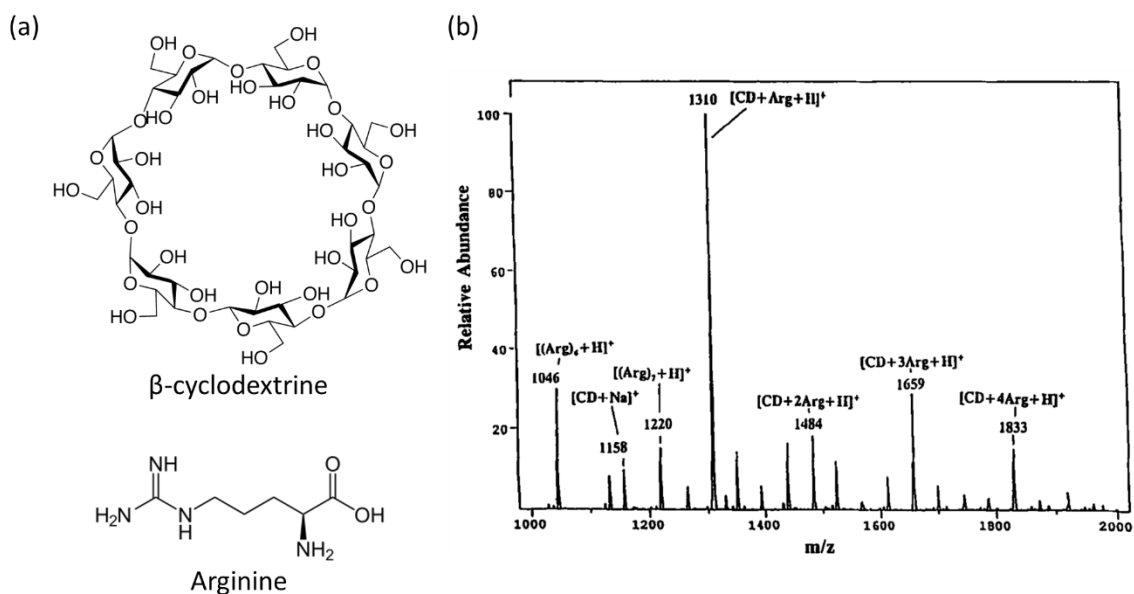


**Figure I.31:** (a) structures of  $\beta$ -cyclodextrine and arginine. (b) MS-spectrum for the association of  $\beta$ -cyclodextrine and arginine in positive mode using an ESI source.

## 4. Ion Mobility Mass Spectrometry (IMMS)

Ion mobility spectrometry (IMS) is an experimental method that, roughly speaking, separates ions, that are accelerated by an electric field, according to their shapes upon collisions against a buffer gas [108 - 111] (also called Plasma Chromatography [108]). The ion sizes are related to their mass (or number of atoms) and their three-dimensional shapes. Therefore, coupling IMS to mass spectrometry (IMMS) enables to sort the ions according two different criteria: their mass and their shape. IMMS experiments gives access to the experimental collisional cross sections ( $CCS_{\text{exp}}$ ) of gas phase ions.

Over the last decade, Ion Mobility Mass spectrometry (IMMS) has been increasingly used and opened new analytical avenues over structural analysis of gas phase ions. Synthetic macromolecules [112], proteins [113], supramolecular complexes [114] and small molecules [115] are a few examples of chemical compounds for which IMMS has proved its efficiency. Before going more in the details of IMMS, some considerations about the gas phase ion motion must be reminded.

### 4.1 Description of the Gas Phase Ion Motion

When considering a localized set of identical ions in a gas of uniform temperature and total pressure and supposing that the ion number density  $n$  - say the number of particles that are present in a particular volume - is low enough to ignore the Coulomb forces of repulsion, then, the ion dispersion in the gas phase is governed by diffusion phenomena. The diffusion process leads to a net spatial transport of the ions produced by their concentration gradient. Accordingly, the ion motion can be described by Fick's law of diffusion (**equation 1**) [116]:

$$J = -D\nabla n$$

**Equation 1**

In this equation,  $J$  is the ionic flux density, which equals the number of ions flowing per unit time through unit area normal to the direction of the flow ( $-\nabla n$ ). The constant of

proportionality  $D$  is called the diffusion coefficient.  $D$  is a joint property of the ions and the gas and is a measure of the transparency of the gas to the diffusing particles [116].

When applying a weak uniform electric field ( $E$ ) throughout the gas, a steady flow of the ions along the field lines will take over the diffusion random motion. Under the influence of  $E$ , the ion cloud will acquire an averaged velocity called the drift velocity ( $v_d$ ), which is directly proportional to the electric field (**equation 2**), provided the field is kept weak (more details below):

$$v_d = KE$$

**Equation 2**

It is important to stress out that the ion drift velocity is constant throughout the electric field. Indeed, ions are accelerated by the electric field ( $E$ ) and, in the same time, decelerated by collisions with the buffer gas, resulting in a steady state where the ion drift velocity ( $v_d$ ) remains constant. In **equation 2**, the constant of proportionality  $K$  is called the mobility of the ions. Like  $D$ ,  $K$  is a joint property of the ions and the gas through which the motion occurs [116].

A relation exists between  $K$  and  $D$  and is called the *Einstein equation* (**equation 3**) [116-117]. This equation is exact in the limit of weak electric field and concentration (more details below):

$$K = \frac{eD}{k_B T}$$

**Equation 3**

where  $e$  is the electronic charge,  $k_B$  the Boltzmann constant and  $T$  the gas temperature.

The usual units of ion mobility  $K$  are square centimeters per volt per second ( $\text{cm}^2 \cdot (\text{Vs})^{-1}$ ). Since  $K$  is gas dependent, the gas temperature  $T$  and the buffer gas density  $N$  will deeply influence mobility measurement [118].

## 4.2 Ion Mobility Spectrometry

Ion mobility spectrometry is based on the separation of gas phase ions that migrate in a buffer gas such as He or N<sub>2</sub> (**figure 1.32**) under the influence of an electric field in the so-called mobility or drift cell.

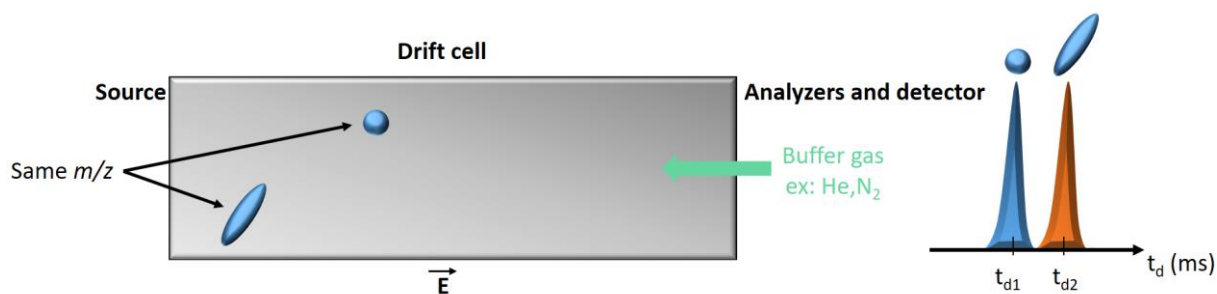


**Figure 1.32:** principle of the ion mobility spectrometry.

Ions will fly through the drift cell (of length  $L$ ) with a characteristic time called the drift time ( $t_d$ ) (see **figure 1.32**), which depends on the ion drift velocity  $v_d$ . Since  $v_d$  depends on two parameters that are the electric field ( $E$ ) and the ion mobility ( $K$ ) as stated in **equation 2**,  $t_d$  can be obtained with **equation 4**:

$$t_d = \frac{L}{V_d} = \frac{L}{KE}$$

**Equation 4**

Since the values of the drift cell length  $L$  and the electric field  $E$  are known, the experimental data generated upon ion mobility spectrometry experiments are the ion drift times. As revealed in **figure 1.32**, ion mobility spectrometry might be used to separate isomers from each other. Indeed, for a same mass to charge ratio, bigger ions will leave the mobility cell later than smaller ions resulting in different values of drift times for each isomer.

## 4.3 From Ion Mobility to Collisional Cross Section

Ion mobility is influenced by collisions with the buffer gas inside the drift tube. The collisions between particles are controlled by the forces between them and the mobility (and  $t_d$  by



extension) must ultimately depend on the ion-neutre interaction forces [118]. This dependence appears in the form of a diffusion collision integral or averaged cross-section ( $\Omega_{avg}$ ) as follows (**equation 5**):

$$K = \frac{3}{16} \frac{q}{N} \sqrt{\frac{2\Pi}{\mu k_B T}} \frac{1}{\Omega_{avg}}$$

**Equation 5**

This equation is known as the **Mason-Schamp** equation where  $q$  is the ion charge and  $\mu$  is the reduced mass. The others parameters have been described in the previous equations. Since measuring ion mobility is the measure of the ion drift time (see **equation 4**), **equation 5** might be rewritten as **equation 6** where the linear dependency between  $t_d$  and the ion collisional cross section is expressed.

$$t_d = \frac{16}{3} \frac{N}{q} \sqrt{\frac{\mu k_B T}{2\Pi}} \Omega_{avg}$$

**Equation 6**

This linear dependency is nevertheless only valid if the following conditions are respected [118]:

1. infinite dilution, which means that ions do not see each other;
2. single collision regime: the free path of the ions must be bigger than their sizes;
3. the ion-neutre collisions have to be elastic (no energy transfer by collisions) since the energy transferred for each collision cannot exceed the thermal energy ( $E_{collision} < kT$ ).

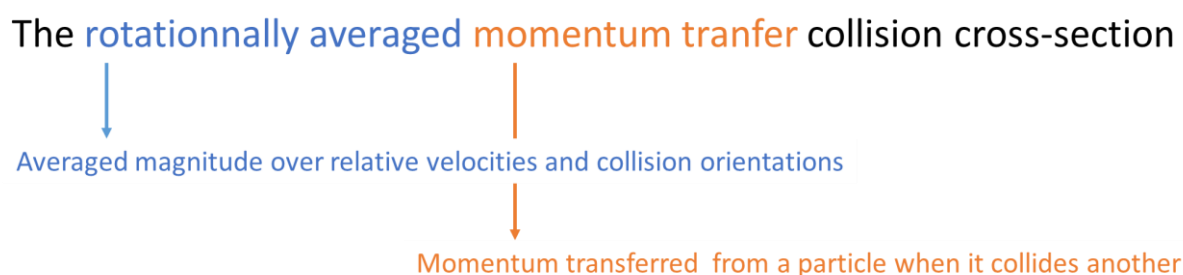
All those conditions can be resumed by one parameter, which is defined as the **low field limit**, validating the **equations 1 to 6**. The low field limit conditions are expressed as follow (**equation 7**) [119]:

$$\frac{E}{N} \ll 3\Omega_{avg}^2 \sqrt{\frac{M}{M+m}} \frac{k_B T}{q}$$

**Equation 7**

where  $M$  and  $m$  are respectively the neutral molecule and the ion masses. The units for the parameter  $E/N$  are the Townsend (Td,  $1\text{Td} = 10^{-17} \text{ V}\cdot\text{cm}^2$ ). According **McDaniel**, the low field limit is respected for  $E/N < 6\text{Td}$  [119]. Under those conditions, the equations presented above (**equations 1-6**) nicely describe the ion motion. The ion mobility value,  $K$ , is a constant and does not depend on the electric field. Indeed, at high field, that corresponds to high values of the electric field  $E$  for the same gas pressure, the ions acquire substantial energy from the field and the elastic nature of the ion/molecule collisions might change. The same phenomenon can be observed if the electric field  $E$  remains constant while the gas pressure is changed [118].

As already mentioned, the collisional cross-section  $\Omega_{\text{avg}}$ , also called “CCS” or noted  $\Omega$ , obtained by ion mobility spectrometry is an averaged value. This CCS corresponds to:



The CCS influences the mobility (**equation 5**) because it represents the effective area for the ion/gas interactions responsible of slowing down the ions by friction [120]. Nevertheless, the collision cross sections also depend on other parameters:

- the number of collisions;
- the temperature (because of the influence of thermal energy over the collision energy);
- the number of vibrators of the buffer gas [121];
- the gas polarizability (different gas meaning different separation) [122].

For the latter, several studies used the polarizability of buffer gases to improve the separation between isomers. As an example, ion mobility (in association with mass spectrometry) has been used to enhance the separation between glycoside cationomers ( $\text{K}^+$  and  $\text{Na}^+$ ) using  $\text{CO}_2$  as the drift gas [123].  $\text{CO}_2$  has been chosen because of its higher polarizability than  $\text{N}_2$  ( $2.93 \text{ \AA}^3$

versus  $1,74 \text{ \AA}^3$  [124]\*). **Figure 1.33** shows the enhancement of separation between cationomers ( $\text{K}^+$ ) of stevioside glycoside (**figure 1.33 a**). In this case, the use of nitrogen as drift gas only permitted the separation of two sets of cationomers (upper part of **figure 1.33 b**) while when performing the separation in  $\text{CO}_2$ , all the four cationomers have been resolved (down part of **figure 1.33 b**).

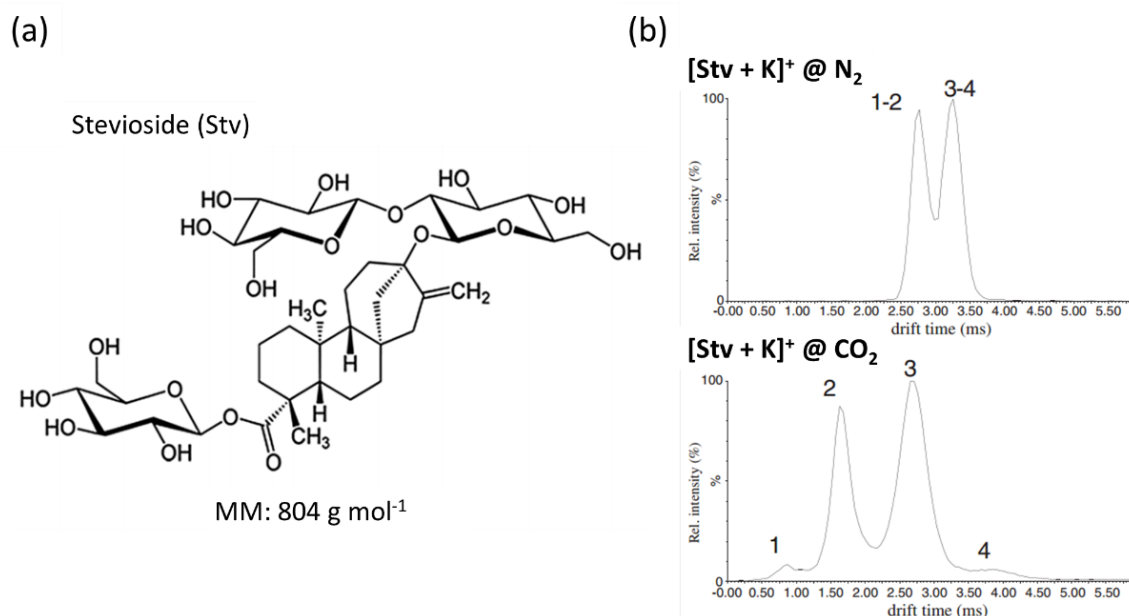


**Figure 1.33:** (a) structure of the stevioside glycoside. (b) Mobilogrammes of the cationized stevioside in  $\text{N}_2$  and  $\text{CO}_2$  as drift gases (adapted figure from reference [123]).

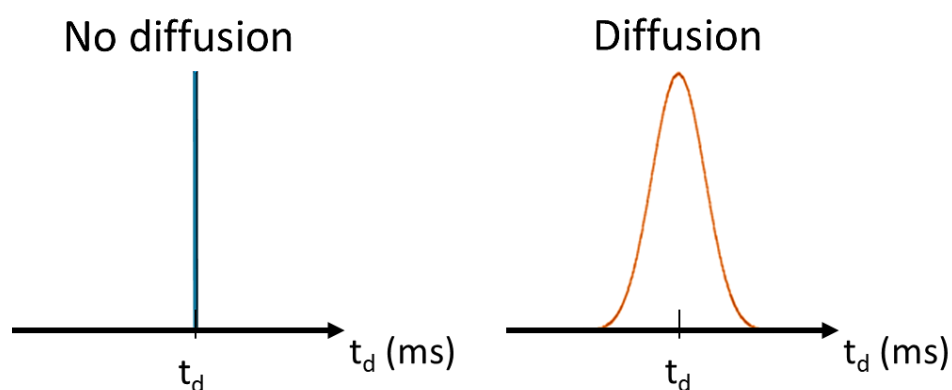
Nevertheless, the difference of polarizability between nitrogen and helium is not sufficient to explain why the CCS obtained using nitrogen as buffer gas are bigger than those obtained using helium. Recently, **Clemmer** and his coworkers emphasize the importance of the buffer gas structure on the experimental CCS determination. In fact, the collision nature within the mobility cell is different when using a polyatomic buffer gas (such as  $\text{N}_2$ ) instead of a monoatomic gas (like He) since those molecules are characterized by different number of vibrators. In the first case, collision will be of inelastic nature while they will be fully elastic for the latter [121]. Accordingly, different collision natures will result in different CCS due to the inelastic / elastic character of the collision happening between the ion and the buffer gas.

\*Using the SI system, the units characterizing polarizability are:  $\text{J.m}^2.\text{V}^{-2}$  and  $1 \text{ \AA}^3 = 1,11 \cdot 10^{40} \text{ J.m}^2.\text{V}^{-2}$  [125].

The determination of the ion collisional cross section permits the acquisition of information regarding the spatial occupation of the studied species; namely their gas phase conformation. Indeed, it is now possible to distinguish isomers from each other, even protomers [126], and to follow conformational rearrangements [111].

#### 4.4 Experimental considerations for ion mobility experiments: arrival time distribution

As already stress here above, performing ion mobility measurements in respect of the low field limit gives first access to the ion drift times, which can be correlated to CSS according to the equation of **Mason-Schamp**. Nevertheless, since the mobility of a group of identical ions is in direct relation with their diffusion (**Einstein's** equation and **Fick's** law), the ion flow will not be characterized by a single drift time but by a distribution. This distribution is called the *arrival time distribution*, also noted ATD. Some ATD have already been presented in the right side of **figure I.32** and **I.33** and here in **scheme I.2**. This distribution is expressed as a Gaussian curve, from which a full width at half maximum can be determined. Therefore, ion mobility spectrometry is characterized by a resolution in the mobility measurement.



**Scheme I.2:** representation of the ATD without diffusion (single drift-time, left side) and with diffusion of the ions in the drift-cell (right side).

Accordingly, the mobility resolution is expressed as follow (**equation 8**)

$$R = \frac{t_d}{\Delta t_{50}}$$

**Equation 8**

where  $R$  is the mobility resolution,  $\Delta t_{50}$  the value of the full width half maximum and  $t_d$  is the top drift time of the arrival time distribution.

Different parameters can influence the shape of the peaks inside the ATD and then influence the mobility resolution. Some of those parameters mostly depends on the device used to perform ion mobility spectrometry (injection-duration, sampling, transfer optics, etc.). However, two other important parameters will deeply influence the arrival time distribution: the ion diffusion and the temperature.

For the first case, diffusion will influence the mobility (and then the ion drift times) according the equation of **Einstein (equation 3)**. Because ion mobility might only be influenced by the diffusion of the ions, the minimal temporal width ( $\Delta t_{50}$ ) of the ion bunch will be given by **equation 9** [127].

$$\Delta t_{50} = 4t_d \sqrt{\frac{k_B T L}{q E} \ln 2}$$

**Equation 9**

Accordingly, the maximum resolution  $R_{max}$  is given by the incorporation of **equation 9** in **equation 8** to give **equation 10**.

$$R_{max} = \frac{1}{4} \sqrt{\frac{q E}{k_B T L \ln 2}}$$

**Equation 10**

From **equation 10**, it can be noticed that the resolution depends also on the electric field and on the temperature. Changes in the temperature deeply influence the resolution in ion mobility. Indeed, enhancing the temperature will increase the collision rate between ions and

gas molecules resulting in a lower mobility of the ions and a larger diffusion (**equation 3**). The result will therefore be a less good mobility resolution (**equation 10**) [128-129].

As an example, **Chirot et al** estimated the temperature dependence of the averaged collisional cross section calculated for alanine-based peptides [128]. As shown in **figure 1.34**, the bigger the temperature increases, the larger becomes the cloud surrounding the averaged collision cross section (solid line). In other words, increasing the temperature broadens the arrival time distribution even leading to potential conformational changes in the gas phase [128]. Indeed, for  $T=500\text{--}600\text{ K}$ , the average collisional cross section displays an inflexion corresponding to the temperature-driven unfolding of the peptides. At the same time, the collisional cross section distribution significantly broadens due to the wider conformational landscape accessible in the unfolded states. The broadening of the ATD is also exhibited in the inset of **figure 1.34** where the calculated ATD becomes much broader when temperature increases from 100 to 300K.

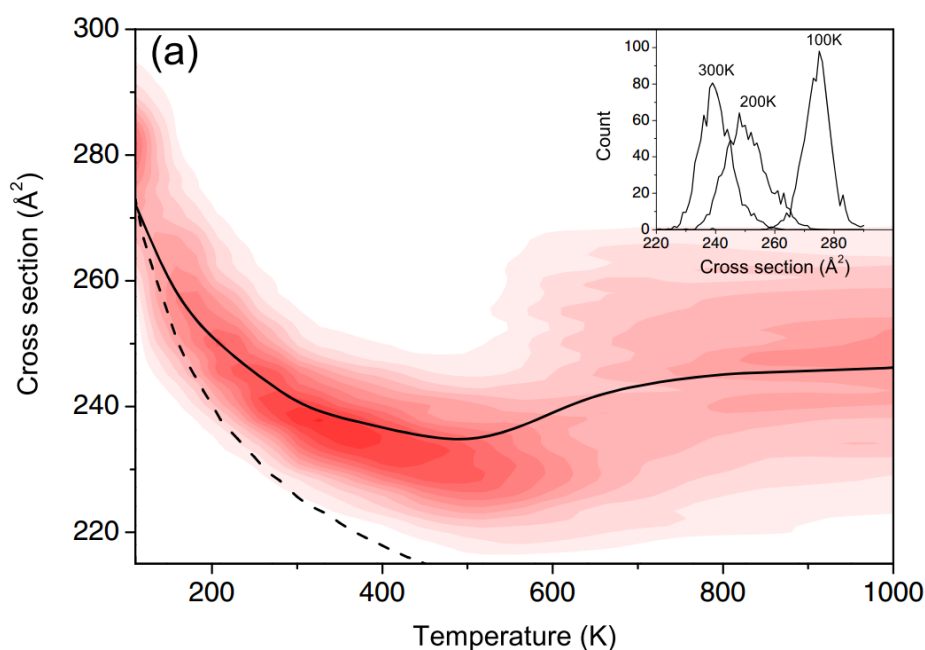


**Figure 1.34:** Averaged collision cross section (solid line) and contour plot of its distribution versus temperature, calculated for an alanine based peptide. The dashed lines illustrate the intrinsic temperature dependence of the cross section for the (frozen) lowest energy structure, and the insets highlight the distributions at chosen temperatures (adapted figure from reference [128]).

## 4.5 Ion Mobility Mass Spectrometry: incorporation of Drift-Cell Units

To obtain the experimental collision cross section values ( $CCS_{exp}$ ), the ion drift times have first to be determined using a drift-cell coupled to a mass spectrometer. In this section, two different mobility-cell setups are associated to mass measurement devices:

- DTIMS cells (Drift Tube Ion Mobility Spectrometry)
- TWIMS cells (Traveling Wave Ion Mobility Spectrometry)

As already mentioned earlier, the association between mass spectrometry and ion mobility adds an extra dimension to the separation of gas phase ions. Indeed, ion mobility mass spectrometry enables to sort the ions according their mass ( $m/z$ ) and their shape ( $CCS_{exp}$ ).

### 4.5.1 Drift Tube Ion Mobility Measurements

In DTIMS, ions are propelled in the drift tube using a static uniform electric field  $E=V/L$  (where  $V$  is the applied voltage across the cell of length  $L$ ) (**figure I.35 a**).

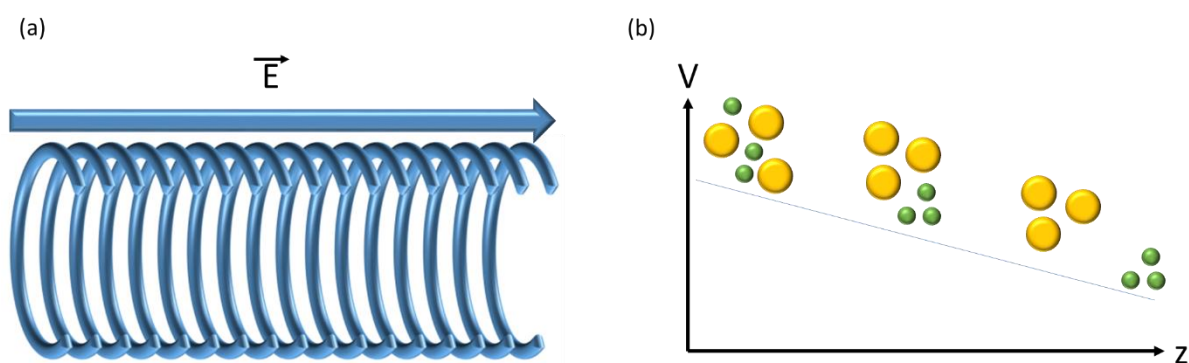


**Figure I.35:** (a) DTIMS cell representation, a homogenous electric field is applied across the tube. (b) Separation of high mobility ions (green) and low mobility ions (yellow) over the homogeneous potential gradient (adapted figure from reference [120]).

The drift-cell is filled with gas, typically helium (He) or nitrogen (N<sub>2</sub>), kept at constant and known pressure. Ions will then be characterized by a drift velocity  $V_d$  which can be determined by measuring the ion drift time  $t_d$  ( $V_d=L/t_d$ ). The drift time of the ions ( $t_d$ ) corresponds to the time spent by the ions inside the drift tube.

When performing ion mobility measurements under the low field limit using a drift tube, the equation of **Mason-Schamp** can be applied so that the measured ion drift times are linearly dependent of their averaged collision cross-section ( $\Omega_{avg}$ ,  $CCS_{exp}$ , **equation 6**). In fact, the different sections presented above (sections I.4.1 to I.4.4) can all be applied to drift tube experiments.

Thanks to the homogenous electric field, the ions will exit the tube as a function of time according to their shape and diffusion yielding to an arrival time distribution (ATD), which can be expressed as followed:

$$ATD = t_d + t_0$$

**Equation 11**

where  $t_d$  is the ion drift time, *i.e.* the time spent inside the drift tube and  $t_0$  is the time spent outside the drift tube and before the ion detection by the detector of the mass spectrometer. This time is also called the dead time. This dead time must be determined for each ion by measuring their arrival times for different drift voltages ( $V$ ). Indeed, when plotting the arrival time ( $t_d$ ) as a function of  $1/V$  (**figure 1.36**), the dead time ( $t_0$ ) corresponds to the Y-intercept and is described as the transfer time  $t_0$  from the end of the mobility cell to the detector (usually through ion optics and the mass analyzer).



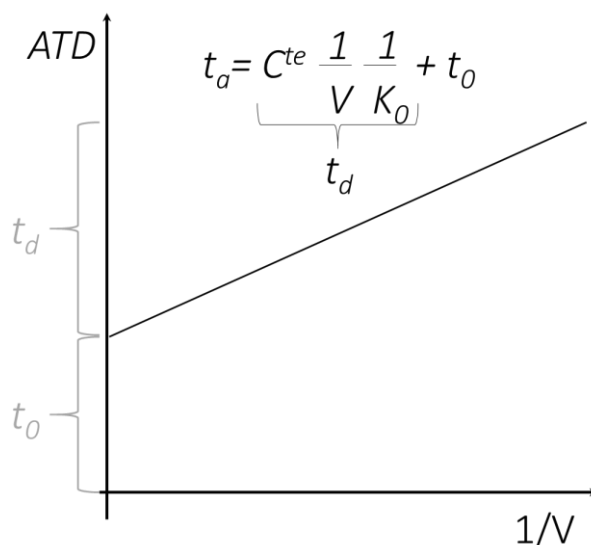


**Figure I.36:** plotting of the arrival time versus the inverse of the applied voltage. The slope is inversely proportional to the reduced mobility  $K_0$  and the Y-intercept gives the dead time  $t_0$  value of the mass spectrometer for a given ion [130].

From  $t_0$  determination, it will now be possible to measure real drift times ( $t_d$ ) from the arrival time distribution. Once the  $t_d$  is obtained, the value will be replaced in **the Mason-Schamp equation** to obtain the ion experimental collision cross section (**equation 6**).

#### 4.5.2 Traveling- Wave Ion Mobility Measurements

Within the **Waters Synapt-G2Si** (see section III), ion mobility separation occurs in a gas filled stacked ring ion guide (SRIG). Initially used as ion guide and collision cell for decades [131], SRIG have been revealed to efficiently separate gas phase ions according to their shape at high cell pressure [132]. Accordingly, the TWIMS technology allows the separation of ions in a stacked ring ion guide (SRIG) in which a pressure in nitrogen is maintained ( $\approx 3.10^{-4}$  mbar). The cell is constituted of annular lenses aligned perpendicularly to the ion direction (**figure I.37** and **figure I.38 a**). Opposite phase RF-voltages are applied to the different lenses in order to create a potential-well to maintain the ion beam trajectory in the

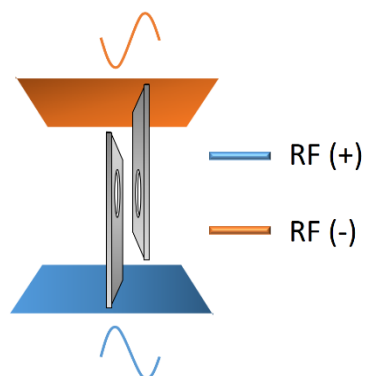


**Figure I.37 :** perpendicular lenses.

center of the mobility cell and reduce the axial dispersion of the ions. In addition, a DC potential travels towards the exit of the SRIG. In fact, the ‘Travelling Wave’ (T-Wave™) is a DC pulse that is applied to the reference voltage on one element pair for a set time, before moving on to the next pair and so forth [133-134]. This “wave” will move the ions towards the exit of the mobility cell (**figure 1.38 b**).

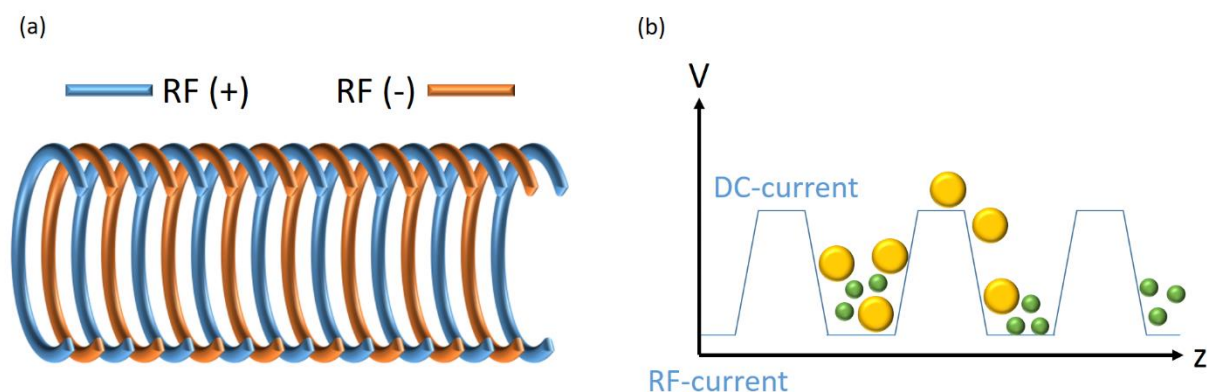


**Figure 1.38:** (a) TWIMS cell representation, the ions are confined by a radio frequency (RF) applied to a stacked ring ion guide. In addition, a direct current voltage is traveling to the exit (T-wave™). (b) Ions of higher mobility (green) are caught up more easily by the waves, whereas larger ions (yellow) are subjected to larger friction with the gas and slip more often behind the waves and therefore exit the mobility cell after a longer time (adapted figure from reference [120]).

In fact, the “traveling wave” restarts every seven pairs of lenses (**figure 1.39**) letting more time to sort the ions according their CCS and charge state to finally obtain packets of ions from a continuous ion flow.

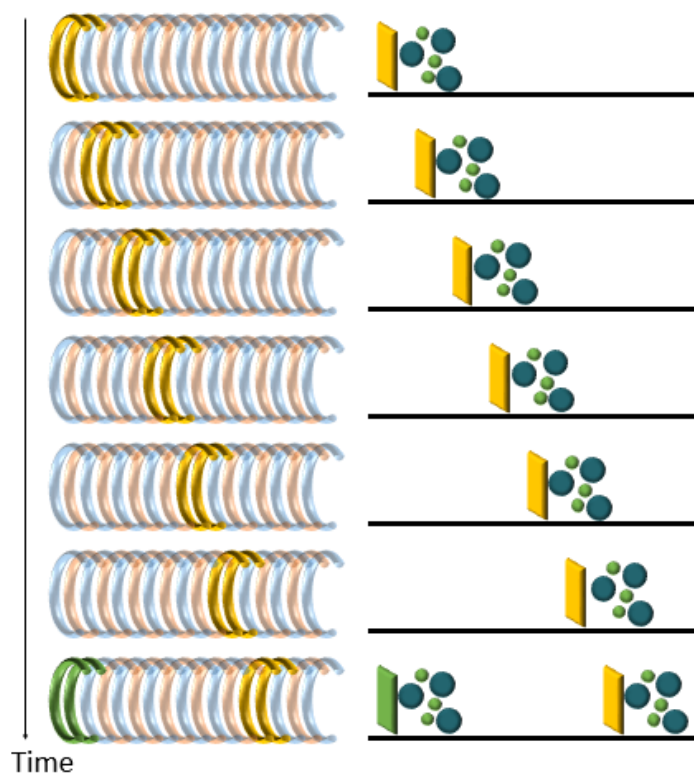


**Figure I.39:** operation of the T-Wave™ (TW), evolution of the DC-pulse (yellow) along pair of lenses. After the migration of the pulse on seven pairs of lenses, a new pulse (or wave) arrives (green).

Inside the TWIMS, ions will be separated according to their charge states and collision cross sections. When the ions are picked up by the ‘travelling wave’ bigger ions will undergo more collisions with the buffer gas and will therefore be more slowed down than smaller ions.

Five main parameters can be tuned on TWIMS mobility cells:

- the wave height, which corresponds to the DC-pulse intensity [132] and is usually set at 40V;
- the wave velocity, which defines how fast the pulse will travel through the pairs of electrodes [133] ( $\approx 1500$  m/s for a  $m/z$  range 50-1200 as typical values for monocharged ions);
- the buffer gas nature (typically nitrogen);
- the buffer gas pressure;
- the analyzed mass range.

Depending of the set parameters, low mobility / big ions are likely to go from the pulse (or wave)  $n$  to the next pulse  $n+1$  by a roll over phenomenon (**figure I.40**, red ions), while high mobility / small ions will “surf” easily on the wave  $n$  and leave the mobility cell quicker (green ions).

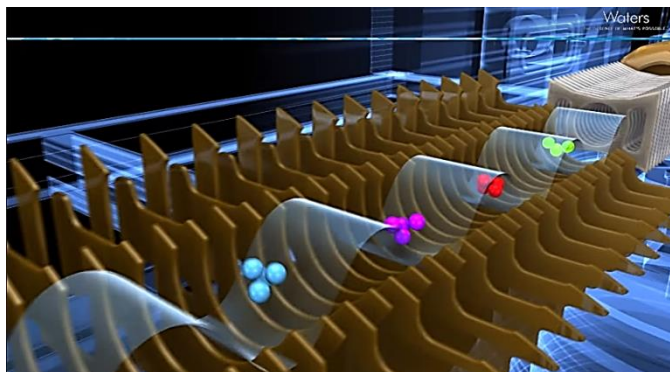


**Figure I.40:** ion separation in T-wave [135].

In other words, the ability of an ion to surf (or keep up with) a travelling wave pulse through the neutral buffer gas is dependent on its mobility  $K$ . Accordingly, under the right conditions of wave height, velocity and gas pressure, mobility separation may be possible within the TWIG [133]. The mobility separation is produced by ions rolling over the top of the travelling waves as they transit the cell, with low mobility ions rolling over more times than the high mobility ions, hence having longer transit (drift) times [133].

Since TWIMS experiment sorts ions according their mobility like in DTIMS, experimental collisional cross sections can be determined from traveling wave measurements. However, contrariwise to DTIMS, the linear dependency between the measured ion drift time and their CCS is no longer available.

In fact, a “roll over” of the ions between the waves characterizes the low mobility ion motion. **Figure I.41** presents a simulation of the chaotic course of two different ions along the TWIMS drift cell: one with a high mobility (**figure I.41 a**) and the other with a weak mobility (**figure I.41 b**) [133]. This representation performed by Giles and his coworkers clearly demonstrates that the ions characterized by a weak mobility follow a much longer trajectory than high mobility ions. Accordingly, their drift times are going to be much longer. Since the TWIMS ion trajectories are chaotic and that the applied electric field constantly changes, it is not possible to linearly correlate the TWIMS ion mobilities with their corresponding drift-times.

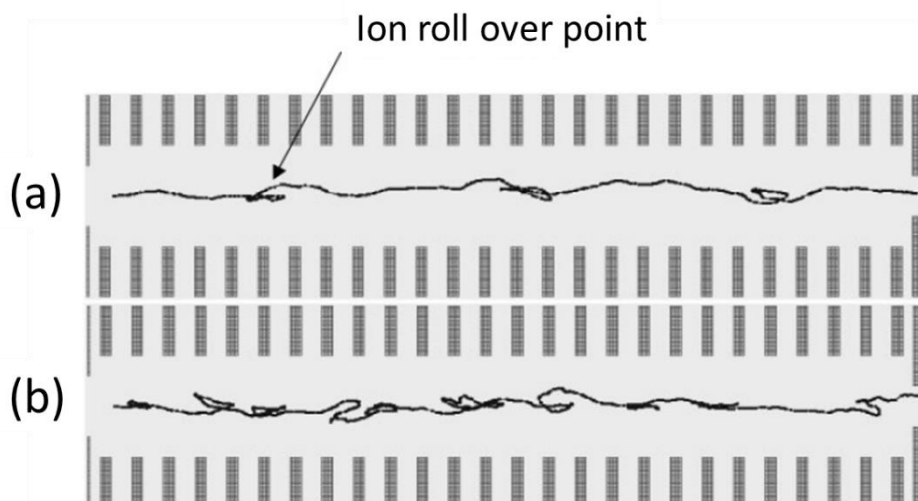


**Figure I.41:** simulation of the trajectories followed by two ions characterized by different mobilities in a Travelling Wave: (a) high mobility ions ( $CCS=300 \text{ \AA}^2$ ) and (b) low mobility ions ( $CCS=400 \text{ \AA}^2$ ). Parameters: wave velocity= 300 m/s, gas pressure = 0.11 mbar (argon), pulse height = 3V [133].

However, different models have been developed to establish a correlation between ion drift times measured in a TWIMS drift cell and their mobility. Since this relation depends on the mobility cell pressure but also on the different potentials applied to the cell (wave height, velocity, etc.) the proportionality between  $t_d$  and the collisional cross section will be different for each analysis [136-137]. Therefore, a calibration must be made with ions of known CCS, which have been precisely determined by DTIMS measurement [134, 138, 139]. The calibration method will be detailed in the experimental section of this report.

## 5. The Cucurbituril Macrocycle Family

This section highlights the cucurbituril macrocycle family at the heart of our PhD work by providing information about their synthesis followed by a brief introduction to the history of those increasingly used supramolecular host and a presentation of their structural properties. In addition, some of their applications in modern chemistry will be presented.

### 5.1 Synthesis

Cucurbiturils are macrocycles obtained by the condensation reaction of  $n$  glycoluril units ( $n=5$  to 14) with formaldehyde under acidic conditions (see **figure I.42 a**) [140]. Actually, depending on the reaction time and temperature, a different mixture of cucurbit[ $n$ ]urils (also noted CB[ $n$ ] or CB $n$ ) can be obtained where  $n$  defines the number of glycoluril units that form the cucurbituril receptor (see example in **figure I.42 b**).

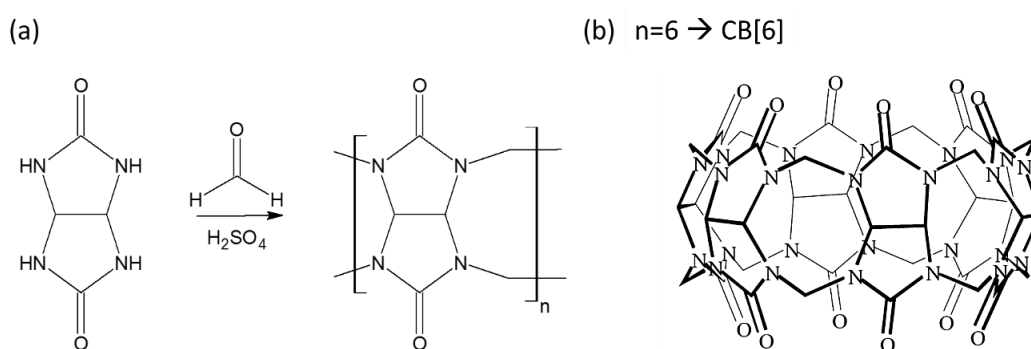


**Figure I.42:** (a) Cucurbituril synthesis. (b) Representation of cucurbit[6]uril (CB[6]) [141].

The cucurbituril formation has not been easy to understand but the work of **Lyle Isaacs and Anthony Day** provided a better comprehension of the CB[ $n$ ] formation mechanism [142]. Indeed, in a review published in 2011, **Isaacs** decomposed the cucurbituril formation mechanism into three different steps (**figure I.43**) [143]. First, the formation of a glycoluril dimer (with two methylene bridges, just like in a cucurbituril) followed by the growth of this dimer into oligomers ( $n\text{C}$ ) of different length (**figure I.43 a**). Once the oligomer is long enough ( $n=5-6$  glycoluril units in  $n\text{C}$ ), the macrocyclization reaction is possible according to two different ways:

- the formation of methylene bridged compounds, namely cucurbiturils (CB[n]) by two successive condensation reaction with one equivalent of formaldehyde at a time (**b**),
- the step-growth condensation between two equivalents of **nC** ( $n=3,5$ ) with one equivalent of formaldehyde to yield bis-nor-seco-CB[n] (**c**). The prefix “nor-seco” is the IUPAC nomenclature that signifies the removal of a methylene group from a parent structure. Accordingly, the prefix “bis” is employed to stress the removal of two methylene bridges from a usual CB[n] structure.

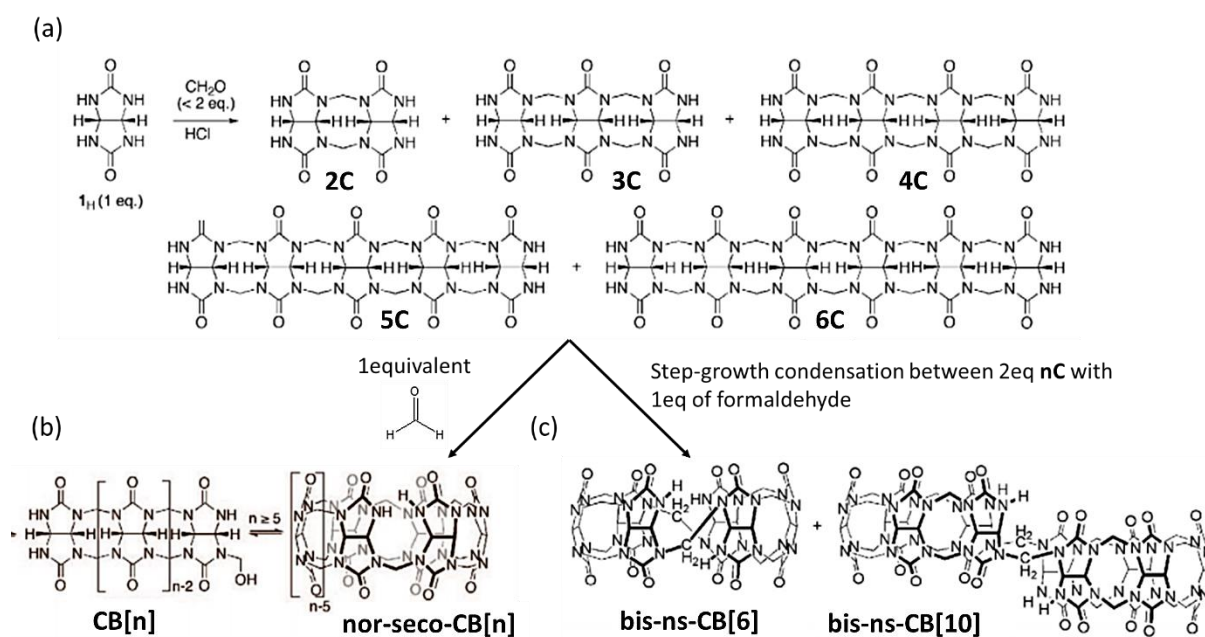


**Figure I.43:** (a) oligomerization of glycoluril units. (b) Macrocyclization of CB[n]. (c) Formation of bis-ns-CB[n] (adapted from reference [143]).

As a consequence, the CB[n]-forming reaction proceeds from glycoluril through oligomers and nor-seco-cucurbiturils as kinetic intermediates and eventually finds its way toward the irreversible formation of CB[5]–CB[7] as thermodynamic products. Indeed, for  $n \geq 8$ , **Day et al** demonstrated the reversible character of the final macrocyclization step [144].

## 5.2 History

Nowadays, cucurbiturils are increasingly studied in modern chemistry as revealed by **figure I.44**. Nevertheless, the history of those macrocycles goes back to the early twentieth century. In 1905, the synthesis of the parent cucurbituril CB[6] has been reported by **Behrend, Meyer** and **Rusche**; they actually named the compound as the “polymer of Behrend” [145].

The molecular structure of CB[6] has been only defined in 1981 by X-ray crystallography by **Mock** and his coworkers [146]. Back then, the chemists had renewed the same synthesis as the one proposed by Behrend eighty years earlier. **Mock et al** decided to name the compound as “cucurbituril” since the structure of CB[6] looked to them as a pumpkin which belongs to the botanical family *cucurbitaceae* [146]. In 1984, the first cucurbituril host-guest compound has been reported in which the CB[6] cavity contains para-xylylenediammonium as the guest molecule [147].

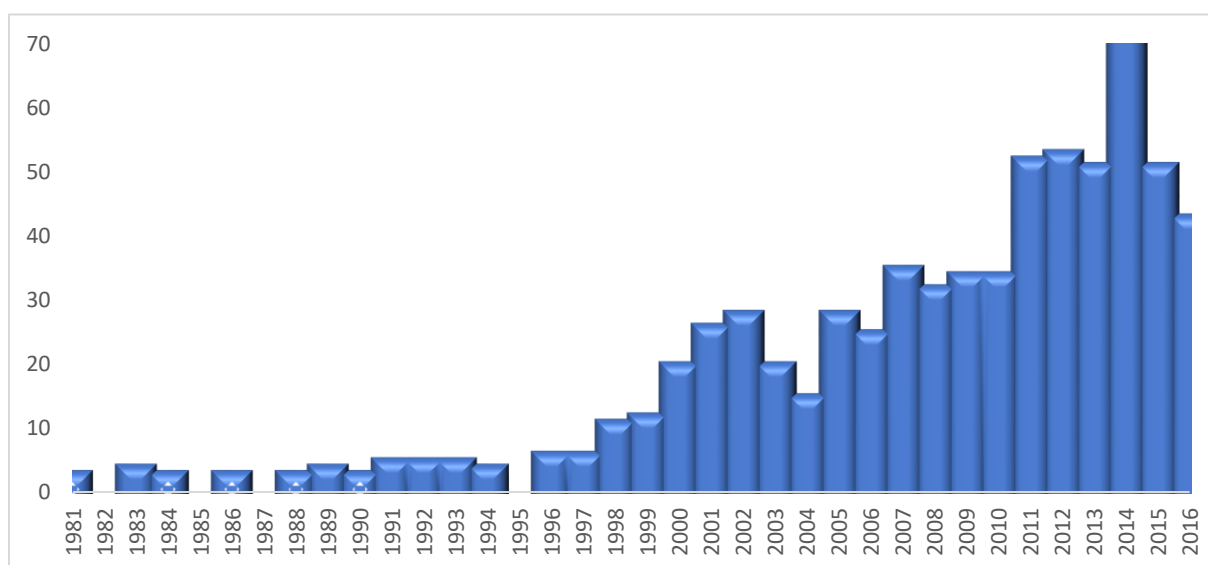


**Figure I.44:** number of referenced articles when looking for “cucurbituril” as key word [148].

Starting back to the early 21<sup>st</sup> century, several cucurbituril synthesis pathways have been developed. **Table I.2** gathers some of the essential milestones that have been achieved in the synthesis of new cucurbituril homologues [149]. The group of **Kim** as well as the one of **Day** varied the reaction conditions (*e.g.*, 80–100 °C, HCl or 9 M H<sub>2</sub>SO<sub>4</sub>, 10–100 h), which proved to be essential to successfully isolate other homologues than CB[6], including CB[5], CB[7], CB[8], and the mixture CB[10]·CB[5]. Nevertheless, even by varying conditions, CB[6] remained the



major product [150-153]. More recently, in 2013, the structure of the largest cucurbituril member CB[14] has been reported by **Tao et al** [153]. Alongside with conventional homologues, the synthesis of functionalized, inverted and nor-seco-CB[n] have been carried on, which pushed cucurbiturils to various new applications due to the host solubility enhancement and their enhanced cavity sizes (see sections I.5.3 and I.5.4) [154].

**Table I.2:** *timeline of the development of cucurbit[n]uril and related cyclic macrocycles (adapted from reference [149]).*

Year	Compound Name	Research Group
1905	CB[6] (not structurally identified)	Behrend [145]
1981	CB[6]	Mock [146]
2000	Isolation of CB[5], CB[7], CB[8]	Kim [150]
2002	Isolation of the mixture CB[10]-CB[5]	Nakamura, Day [152,155]
2003	Partially substituted CB[n]	Isaacs, Kim, Day [156]
2004	hemicucurbit[n]uril (n=6 and 12)	Day, Tao [157]
2005	CB[10], inverted cucurbit[n]uril (n=6 and 7)	Isaacs, Kim, Buschmann [158-160]
2006	ns-CB[10]	Isaacs [161]
2007	Bis-ns-CB[6]	Isaacs, Tao [162]
2009	Partially substituted CB[6]	Tao [163]
2012	Monofunctionalized CB[6] and CB[7]	Scherman, Isaacs [164]
2013	CB[14]	Tao [165]
2014	Monofunctionalized CB[6] at methylene bridge	Sindelar [166]

### 5.3 Structural and chemical properties

The cucurbituril size increases with the number of monomer glycoluril units (see **figure I.45**). **Table I.3** lists the structural parameters of common CB[n] homologues (in Å) [149]. In contrast to other macrocyclic molecules, cucurbiturils have a very rigid structure, which renders the definition of the cavity parameters (**table I.3**) particularly informative. Indeed, depending of the cavity size, CB[n] homologues will be predictably specific of guest molecules (see next sections).

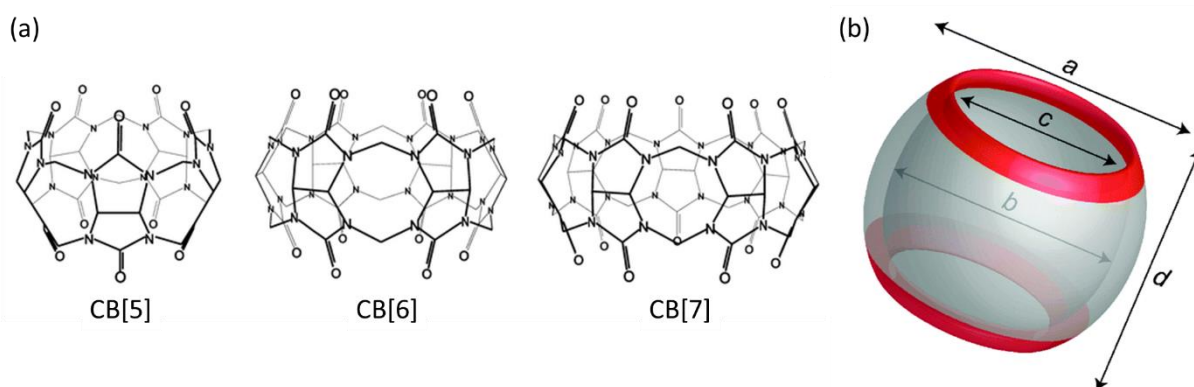


**Figure I.45:** (a) Structures of the CB[n] homologues for  $n=5, 6$  and  $7$ . (b) Representation of the geometrical parameters presented in table I.3 (adapted from reference [149]).

**Table I.3:** structural parameters of CB[n] homologues (in Å).

	Outer diameter (a)	Inner cavity (b)	Portal size (c)	Height (d)
CB[5]	13.1	4.4	2.4	9.1
CB[6]	14.4	5.8	3.9	9.1
CB[7]	16.0	7.3	5.4	9.1
CB[8]	17.5	8.8	6.9	9.1
CB[9]	19.0	10.3	8.6	9.1
CB[10]	20.0	11.7	10.0	9.1

All CB[n] (n = 5–10) have the same height ( $d = 9.1 \text{ \AA}$ ) but show large variations in cavity width and portal size when the number of monomer units increases (respectively b and c in **table I.3**). Accordingly, the inner cavity volumes also increase from CB[5] to CB[10] as revealed by **table I.4** [167].

**Table I.4:** calculated volumes ( $\text{\AA}^3$ ) of the inner cavities of CB[n] homologues.

	Inner cavity volume ( $\text{\AA}^3$ )
CB[5]	68
CB[6]	142
CB[7]	242
CB[8]	367
CB[9]	515
CB[10]	691

Due to their highly symmetric structure, cucurbiturils present two negative rims and an electron deficient cavity as revealed by the electrostatic potential map of CB[8] in **figure I.46** [149].

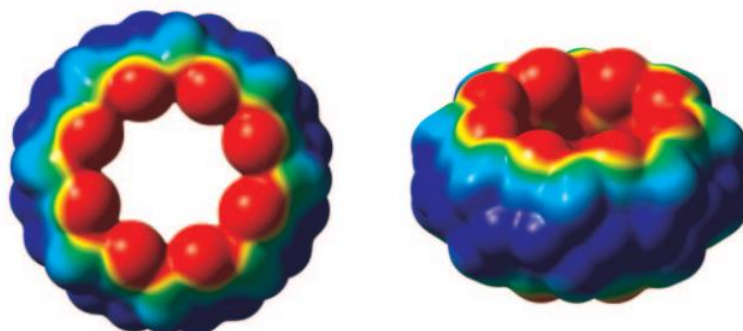


**Figure I.46:** Electrostatic potential map (top and side view) of CB8, revealing the negatively charged carbonyl rims (in red) and the electron-deficient equatorial region (in blue) [149].

The inner cavity of CB[n] homologues has neither functional groups nor electron pairs pointing towards the inside part (**figure 1.45**). Therefore, it cannot be engaged in hydrogen-bonding interactions, which – alongside with the non-dipolar nature of the macrocycle itself – provides an intuitive rationale for the high hydrophobicity of the cavity [149].

The major drawback of cucurbiturils when defining their applications comes from their poor solubility in water (**table 1.5**) [140]. CB[6] and CB[8] are almost unsolvable while CB[5] and CB[7] are characterized by relatively poor water solubility. In fact, the solubility of the cucurbituril macrocycles is usually lower than that of cyclodextrine compounds. At the opposite, the cucurbituril solubility is considerably enhanced in acidic solutions [168].

**Table 1.5:** solubility (S), thermal stability and acidic properties of CB[n] [140].

	S <sub>water</sub> (mM)	S <sub>HCl 3M</sub> (mM)	Stability (°C)	pKa
CB[5]	20-30	60	>420	3.02
CB[6]	0.018	61	425	
CB[7]	20-30	700	370	
CB[8]	<0.01	1.5	<420	

However, the poor solubility of CB[n] in water and other common organic solvents has been tackled recently by synthesizing cucurbituril derivatives (**table 1.2**). Indeed, recent studies showed that introducing alkyl groups on the equator of CB[6] leads to an enhancement of its solubility in water and other organic solvents. As an example, the fully substituted cyclohexyl-CB[6] (**figure 1.47**) presents a water solubility  $10^4$  time superior to CB[6] [169].

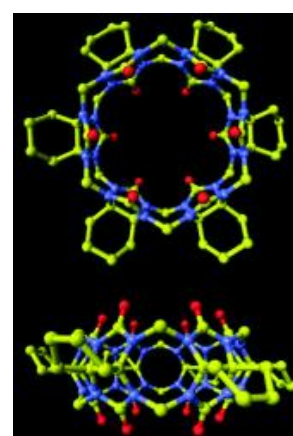


**Figure 1.47 :** cyclohexyl-CB[6].

In **table I.5**, it can be noticed that the CB[n] family is characterized by a high thermal stability, i.e., higher than 370°C for every cucurbituril host. With a pKa value of 3.02 for each homologue, CB[n] are defined as weak acidic compounds.

Finally, cucurbiturils are cation-receptor due to the high electron density at the carbonyl portals [149]. The next section will summarize the binding properties of cucurbiturils through host-guest associations.

#### 5.4 Host-guest chemistry

The host-guest chemistry of CB[n] has already been reviewed extensively [11, 140, 149, 167, 170, 171]. The hydrophobic effect, with emphasis on the release of the high-energy water molecules (see section I.2.1.3), as well as hydrogen bonds interactions (see section I.2.1.4) have been addressed as the main driving forces for the binding of different guests by CB[n]. In fact, cucurbiturils present high specificity for ammonium ions which is largely due to the electrostatic ion-dipole interactions involving the negatively charged oxygen atoms at the carbonyl rims (see **figure I.46**) and the hydrogen atoms of the guest molecule ammonium moiety.

In the mid-eighties, the combined work of **Mock** and **Freeman** reported the first studies concerning the complexation of alkylammonium and alkyldiammonium ions with CB[6] in aqueous formic acid and the determination of the guest binding affinities [146, 147]. Back then, as already mentioned in section I.5.2, **Freeman** reported the first X-ray diffraction structure of a host-guest complex involving a cucurbituril host and the *p*-xylylenediammonium as the guest (**figure I.48**).

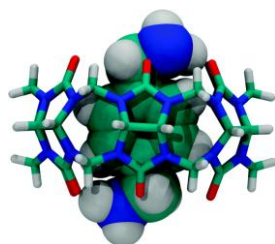


**Figure I.48:** X-ray structure of the *p*-xylylenediammonium ion encapsulated within CB6, the first X-ray diffraction structure of a CBn complex [147].

**Mock et al** also reported the first guest selectivity study of CB[6] between various alkyl- and aryl- substituted ammonium ions [172]. These studies revealed a chain-length dependent selectivity of CB[6] towards diammonium compounds (**figure I.49 a**). Diammonium ions (**▲**) with a pentano or hexano bridge bind significantly stronger to CB[6] than those with shorter or longer lengths. However shorter alkyl-ammonium ions (**●**), with a single ammonium part, present enhanced affinities toward CB[6] than their longer homologues. Actually, for 1,6-diammoniumhexane, the alkyl chain undergoes a folding process to adopt a more compact conformation in order to optimize cavity filling and to additionally maximize ion–dipole interactions (**figure I.49 b**).

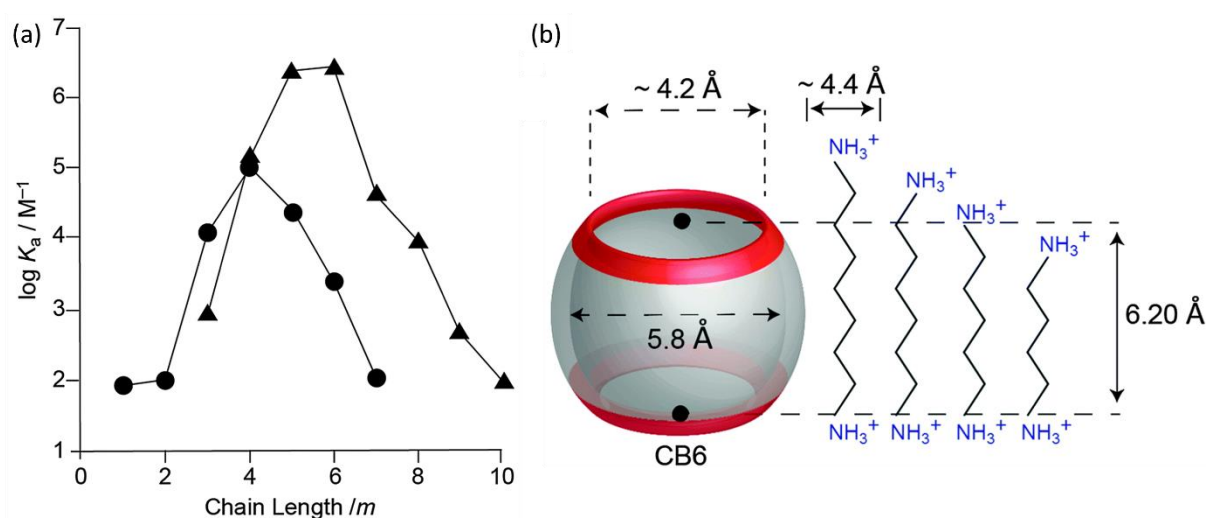


**Figure I.49:** (a) Relationship between the binding constant ( $\log K_a$ ) versus chain length  $m$  for  $H(CH_2)_mNH_3^+$  (●) and  $^+H_3N(CH_2)_mNH_3^+$  (▲). (b) Dimensional comparison between CB[6] and various  $\alpha, \omega$ -alkane diammonium ions (adapted from reference [149, 172]).

In addition to the guest size dependence, cucurbiturils also exhibit shape complementarity. As an example, **Nau et al** demonstrated that CB[6] form inclusion complexes with n-pentane and isopentane but not with neopentane even though those three guests are equally large ( $96 \text{ \AA}^3$ ), see **figure I.50** [173]. The absence of binding of neopentane is actually due to a kinetic effect, in which the tight cucurbituril portals block the ingress of the more bulky neopentane guest. Indeed, **Mock and Shih** already showed that neopentylammonium guest does not form inclusion complexes with CB[6] [172].

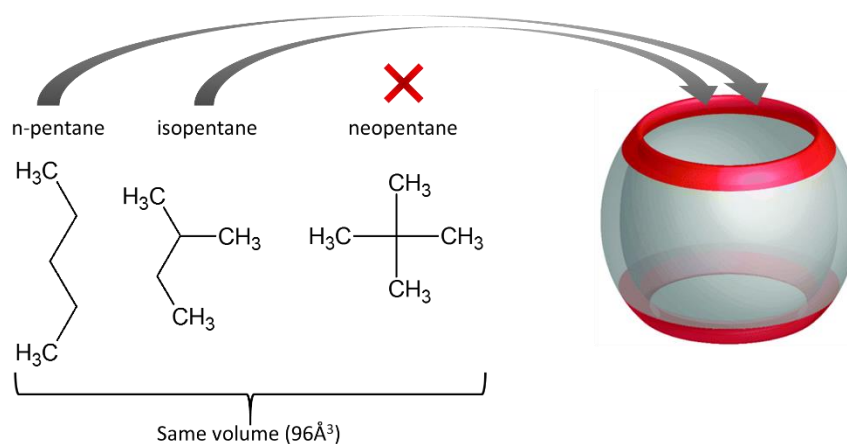
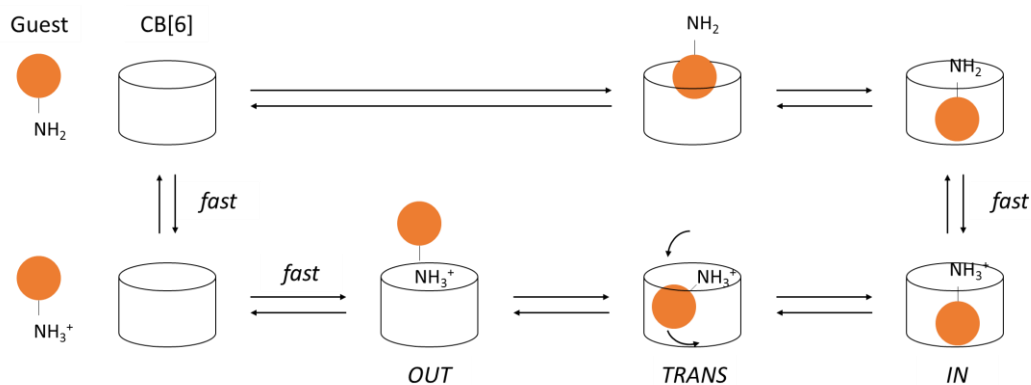


**Figure I.50:** structures of the guest-compounds: *n*-pentane, isopentane and neopentane. Grey arrows represent which isomer interacts with the CB[6] cavity (right side of the figure) while the red cross defines which compound does not form inclusion complexes with the host (adapted from reference [173]).

### 5.5 Guest complexation mechanism with cucurbiturils

In 1986, **Mock** and **Shih** already recognized the possibility of two different modes of binding for an ammonium ion guest: an inclusion complex versus exclusion complex (respectively *IN* and *OUT* in **scheme 1.3**) [172]. In the latter case, only the guest ammonium moiety is in interaction with the CB[*n*] host through H-bonds with the oxygen atoms of the host carbonyl portal while the rest of the guest backbone remain outside the host-cavity. The equilibrium between both the isomeric complexes depends mainly on the size and shape of the attached groups. Indeed, depending on which CB[*n*] homologue is used for the complexation, the size of the carbonyl portals might not always be adapted for the inclusion of bulky guests (see section I.5.6 for more details).

Nevertheless, in 2001, **Nau** and co-workers suggested that the transition state connecting the exclusion complex to the inclusion complex can be described by a flip-flop process in solution (*TRANS* on **scheme 1.3**) in which the appended backbone pivots into the cavity without breaking its N-H...O hydrogen bonds [174].



**Scheme 1.3:** proposed mechanism for the complexation of a amino-compound with CB[6] (adapted from reference [174]).

On the first line of **scheme 1.3**, the neutral guest enters by a direct penetration of the organic backbone into the non polar cavity. However, according to the study carried by **Nau** and his group, this pathway is unfavorable for the ammonium ion (second line of **scheme 1.3**) which first forms rapidly an intermediate association complex (OUT), in which only the ammonium site interacts with the carbonyl rim while the organic residue is still exposed to the aqueous phase. Thus, the ingress process of the organic residue occurs in a flip–flip manner, namely through a different transition state (*TRANS*) than for the neutral guest.

The transition state for conversion of the association to the inclusion complex requires a significant distortion of the host portal, which renders this pathway slower than for the neutral amine. However, the flip–flip process avoids a complete loss of the stabilizing ion–dipole interactions since the transition state allows the ammonium ion to remain at least partly hydrogen bonded with the oxygen atoms of the portal.

The involvement of different transition states in the complexation of neutral or protonated guest receives strong support from the rate constants for the departure of the guest (egression), which differ by more than a factor of 300 for the protonated and unprotonated complex.

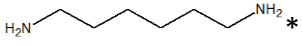
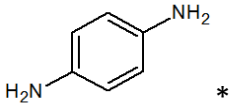
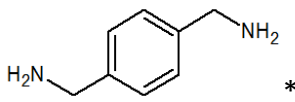
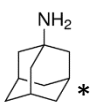
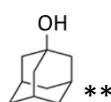
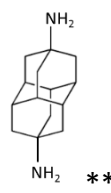
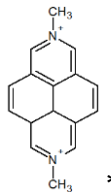
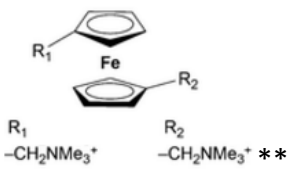


## 5.6 High-affinity binding

Here above, the selectivity of cucurbiturils against amino-guest compounds has been demonstrated. Accordingly, CB[n] are able to bind many guest molecules that present differences both in size and shape. The outcome of this complementarity is expressed by very high affinity binding constants ( $10^3 - 10^{17} \text{ M}^{-1}$ ) for the resulting host-guest complex. **Table 1.6** summarizes a small selection of measured binding constants ( $K_a$ ) for the formation of 1:1 inclusion complexes of the hosts CB[6] and CB[7] with different guest molecules (see **table 1.6** for structures).

Due to its larger cavity, the CB[7] host easily binds larger molecules such as 2,7-dimethyldiazapyrenium ( $4 \cdot 10^7 \text{ M}^{-1}$ ), adamantane, diadamantane and ferrocene derivatives (\*\*\*) whereas no complexes are detected when trying to associate those compounds to the CB[6] cavity. Even if cucurbiturils make strong interactions with amino compounds, they can also strongly interact with guest presenting no amine moiety. As an example, **table 1.6** presents the association between CB[7] and 1-hydroxyadamantane ( $K_a = 2 \cdot 10^{10} \text{ M}^{-1}$ ).

**Table I.6:** binding constants ( $M^{-1}$ ) of inclusion compounds involving CB[6] and CB[7]. ND: non-detected. Values obtained from references: \* [175] and \*\* [149].

Complexed guest	Guest@CB[6] ( $K_a (M^{-1})$ )	Guest@CB[7] ( $K_a (M^{-1})$ )
	$4 \cdot 10^8$	$9 \cdot 10^7$
	$2 \cdot 10^3$	$2 \cdot 10^6$
	$5 \cdot 10^2$	$1 \cdot 10^9$
	ND	$4 \cdot 10^{12}$
	ND	$2 \cdot 10^{10}$
	ND	$3 \cdot 10^{11}$
	ND	$4 \cdot 10^7$
 $R_1$ $-CH_2NMe_3^+$	ND	$3 \cdot 10^{15}$

Recently, **Isaacs** and his coworkers have reported the highest binding constant ever measured for the formation of a binary (1:1) complex in water between CB[7] and diamantane diammonium ion. The binding constant value has been determined using  $^1\text{H}$  NMR competition experiments in  $\text{D}_2\text{O}$  with  $K_a = 7,2 \cdot 10^{17} \text{ M}^{-1}$  [176]. The crystal structure of this association is presented in **figure I.51** where the complete inclusion of the diamantane guest in the host cavity is shown. The near perfect size and shape complementarity between the rigid CB[7] and the diamantane derivative leads to this record association constant [176].

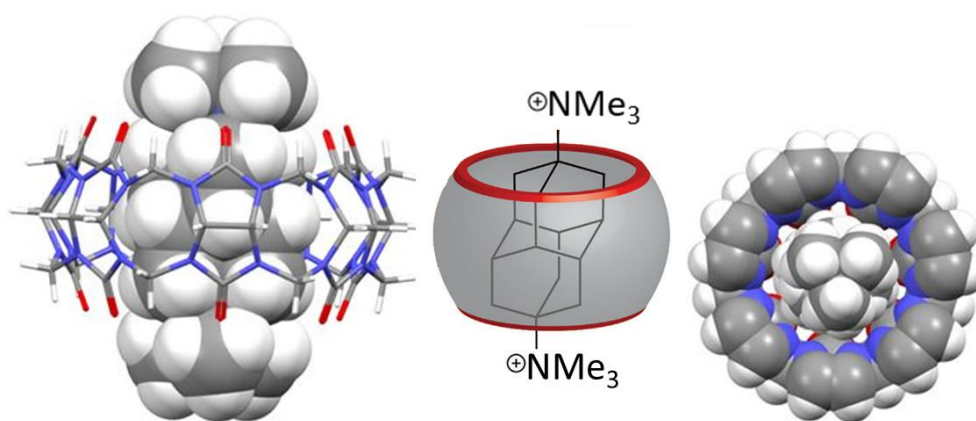


**Figure I.51:** representations of the X-ray crystal structure of the CB[7]·diamantane diammonium complex (adapted from reference [176]).

The tight packing of the diamantane diammonium in the cavity of CB[7] is structurally reflected in a significantly expanded cavity (increase in the diameter by  $\sim 0.3 \text{ \AA}$  and increase in the volume from 242 to 258  $\text{\AA}^3$ ) [176].

According to **Nau** in a recent review [149], the fact that a quaternary trimethylammonium group presents (when measured under identical conditions) a better binding motif than a ternary or primary ammonium group (**figure I.51** versus **table I.6**) demonstrates that the presence of hydrogen bonding interactions is not always the driving force in the ingress process of guests into CB[n] hosts. Nevertheless, as already mentioned above, multiple hydrogen bonds alongside with the complementarity between the host and guest molecules still contribute to the association stability.

## 5.7 Applications

In parallel to the fast development of cucurbituril homologues, numerous uses of CB[n] macrocycles are developed and extensively reviewed [11, 149, 171]. This section will present only a notable selection of recent applications involving cucurbituril compounds.

### 5.7.1 CB[n] recognition in biological systems

Molecular recognition and detection of biomolecules, especially peptides and proteins, in aqueous solution, has always been challenging. Over the last decade [11, 177], cucurbiturils have been increasingly used as supramolecular sensors to assess the presence of peculiar biomolecules in aqueous solution.

The pioneering work of **Urbach et al** revealed the sensing properties of cucurbiturils for amino acid when they reported the ability of the binary complex CB[8]-MV (methyl viologen, see **figure 1.52 a** for structure) to recognize and complex tripeptides containing two glycine (G) and a tryptophan residues (W) [178]. Back then, it has been demonstrated that the WGG tripeptide presents the highest  $K_a$  when binding the CB[8]-MV binary complex (6-fold higher than GWG and 40-fold higher than GGW) (**figure 1.52 b**). Actually, in the ternary association CB[8]-MV-GGW, electrostatic interactions of the C-terminus play a large part in the binding affinity in addition to the repulsion between the carbonyl portals of CB[8] and the carboxylate of the peptides. Binding of the tryptophan residue to the CB[8] cavity is accompanied by charge-transfer complexation with MV and a resulting fluorescence quenching of the indole group (**figure 1.52 c**). The quenching of fluorescence upon binding provides an additional handle for the development of optical sensors for specific peptides using cucurbituril compounds.

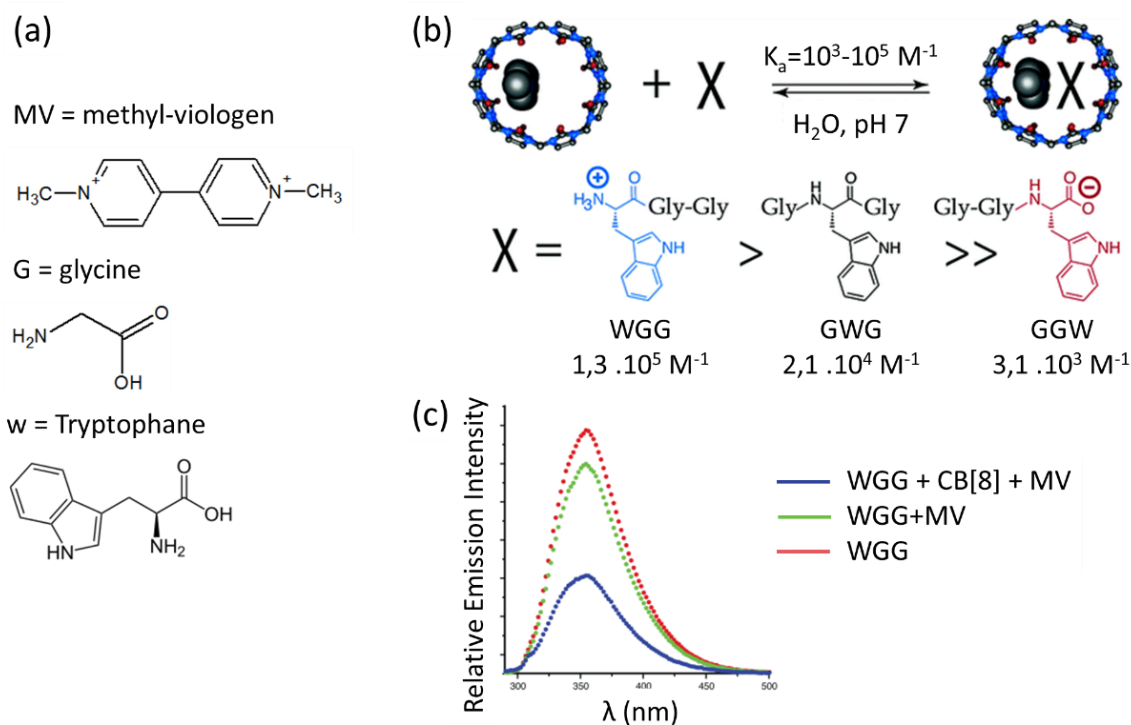


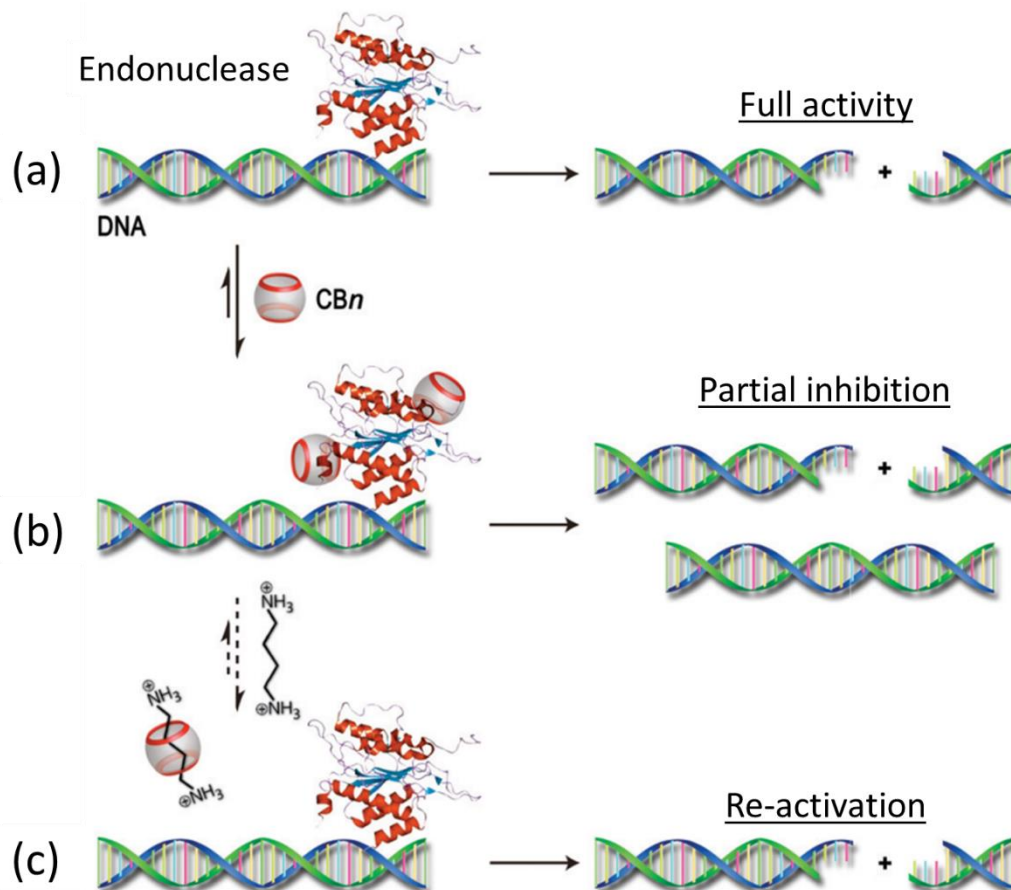
**Figure I.52:** (a) structures of the guest MV and amino-acid residues. (b) Scheme of the association CB[8]-MV-X and their corresponding association constants (c) Fluorescence emission spectra for WGG unbound (red) and in the presence of one equivalent of MV (purple) or CB8-MV (blue). All spectra were obtained with excitation at 279 nm at 25 °C at a concentration of 12.5  $\mu\text{M}$  in 10 mM sodium phosphate, pH 7.0. (adapted from reference [178]).

Despite recognition of small peptides and amino acids, cucurbiturils also bind efficiently proteins and can also moderate biochemical reactions [178, 179, 180]. For example, recently, the group of **Carvalho** showed the inhibition of the enzymatically catalyzed restriction of DNA by cucurbiturils (CB[6] and CB[7], **scheme I.4**) [181].

A restriction fragment is a DNA fragment resulting from the cutting of a DNA strand by a restriction enzyme (restriction endonuclease); the process is called restriction (**scheme I.4 a**) [182].

Using electrophoresis experiments and restriction assays, **Carvalho** and his coworkers demonstrated that the addition of CB[6] or CB[7] to a solution containing DNA and endonuclease efficiently hinders the restriction process [181] (around 50% of inhibition for a host concentration about 6  $\mu\text{M}$  for CB[6] and 90  $\mu\text{M}$  for CB[7], **scheme I.4 b**). In addition, the

restriction reaction can be re-activated by the addition of the strongly competitive polycationic binder spermine for CB[6] ( $K_a = 3.3 \times 10^9 \text{ M}^{-1}$ ) or diaminopentane for CB[7] ( $K_a = 20.10^6 \text{ M}^{-1}$ ) (*scheme 1.4 c*).



**Scheme 1.4:** Schematic illustration of (a) the restriction process, (b) the postulated inhibition of DNA restriction enzymes by CB[ $n$ ] hosts and (c) their re-activation by competitive binding with polyamines (adapted from reference [181]).

Accordingly, cucurbiturils have been used to provide supramolecular control of a biocatalytic process [181].

## 5.7.2 Catalysis in the inner cucurbituril cavity

Catalysis reactions using cucurbiturils as micro-reactors have been reviewed extensively in the last few years especially by the groups of **Nau** [149], **Schalley** [183, 184], and **Scherman** [11, 180].

As a remarkable example, **Lee** and his coworkers investigated the retro-Diels-Alder reactions of bicyclic azoalkanes inside CB[n] containers in the gas phase (**figure I.53 a**) [185]. In this study, mass spectrometry has been combined to ion mobility spectroscopy and quantum-chemical calculations to highlight the catalytic properties of the host CB[6], CB[7] and CB[8].

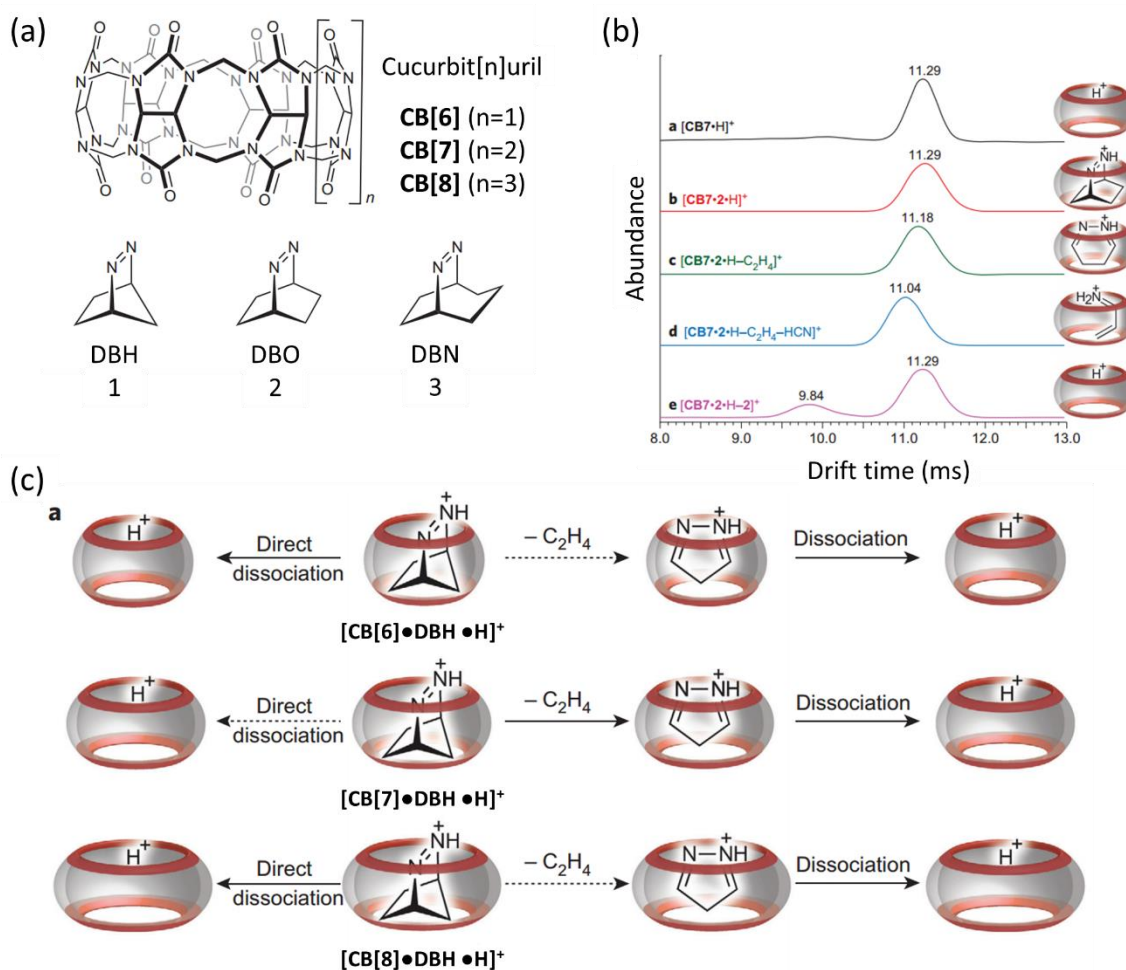


**Figure I.53:** (a) chemical structures of the hosts CB[n] and azoalkane guest: 2,3-Diazabicyclo[2.2.1]hept-2-ene (DBH), 2,3-Diazabicyclo[2.2.2]oct-2-ene (DBO), 6,7-Diazabicyclo[3.2.2]non-6-ene (DBN). (b) Ion mobiligrams of different CB[7] complexes

(involving the DBO guest). (c) Reaction and dissociation pathways of the inclusion complex of DBH inside CB[n] in the gas phase (adapted from reference [185]).

In the study carried by Lee et al, ion mobility experiments were first performed to highlight that the formed complexes between cucurbiturils hosts (CB[6], CB[7], and CB[8]) and the protonated azoalkanes (DBH, DBO, and DBN) are indeed inclusion complexes and not of the exclusion type. For example, in **figure 1.53 b**, it is clearly shown that the protonated free CB[7] (mobilogram a) exhibits the same CCS as the host–DBO complex (mobilogram b); these mobilograms reflect the collisional cross section areas of the “empty” and the “filled” CB[7], respectively. The fact that the cross sections are the same cannot be reconciled with an exclusion complex, because it would display a significantly larger cross section, and thus a larger drift time.

In a systematic approach, the authors examined the fragmentation reaction of each viable complex of differently sized CB[n] and guests. CID experiments were thus carried on the protonated complexes, [CB[n]·guest·H]<sup>+</sup>. The thermal activation of the CB[n]–azoalkane complexes induced in some cases dominant chemical reactions of the encapsulated guests and the formation of [CB[n]·fragment·H]<sup>+</sup> complexes (**figure 1.53 b** mobilograms c and d for example) as opposed to irreversible dissociation of the host–guest complexes. Actually, CID activation of the protonated DBH inside CB[7] afforded the elimination of ethylene with a subsequent dissociation of the intermediary pyrazole complex upon CID (**figure 1.53 c** middle line). In contrast, when DBH is more tightly (inside CB[6]) or more loosely packed (with CB[8]), the simple dissociation pathway into individual guest and host molecules dominated over the inner-cavity chemical reactions (**figure 1.53 c**). Most interestingly, thermal activation of protonated DBO complexed inside CB[7] or CB[8] (no complex was formed for DBO with CB[6]) led first, predominantly, to elimination of ethylene, followed by elimination of hydrogen cyanide, and, ultimately, dissociation of the protonated propenimine complex (**figure 1.54**).



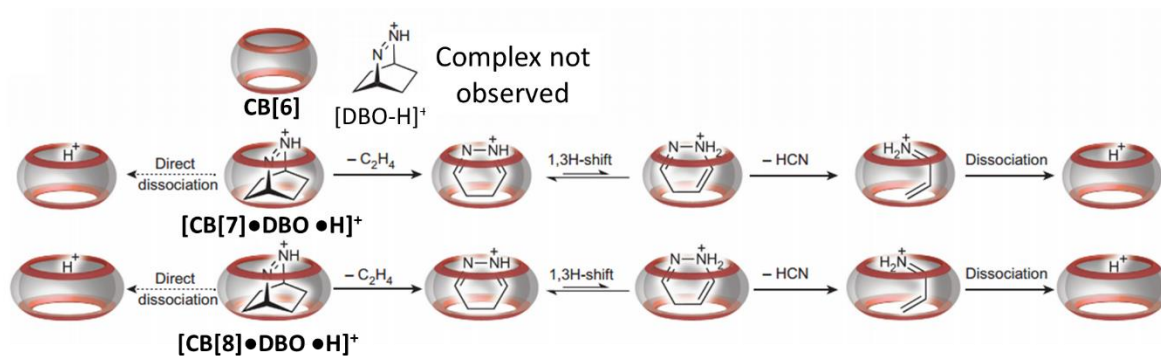


**Figure I.54:** reaction and dissociation pathways of the inclusion complex of DBO inside  $CB[n]$  in the gas phase (adapted from reference [185]).

According to **Lee** and his coworkers, the chemical reactivity of the gas phase complexes was interpreted in terms of three contributing factors:

1. the intrinsic activation energies for chemical reaction of the guest,
2. the constrictive binding displayed by the cucurbituril host,
3. the void space inside the host–guest complex.

By means of DFT calculations, the authors proved that the reaction transition state experiences a stabilization when performing the reaction inside the host cavity because the substrate must expand towards the cavity walls in order to eliminate the nitrogen molecule. Accordingly, these gas phase reactions do provide a puristic case of an inner-phase “catalysis” of a chemical reaction [185].

### 5.7.3 Photoswitching reaction operated using cucurbituril and product self-sorting release

The reversible photo-induced reaction between an anthracene derivative and its dimer using a template effect of the  $CB[8]$  macrocycle has been demonstrated by **Pischel** and his group [186]. The pre-organization of the two guests inside the host cavity (**figure I.54 a**) facilitates inner-cavity photoreactions that would not happen at the dilute concentrations of the free dye molecules [187].

Accordingly, the formation of the inclusion ternary complex (2 guests for one host) between the ammonium-anthracene derivative and the host cucurbituril has been highlighted first, using absorption titration, fluorescence and  $^1\text{H}$  NMR experiments. As presented in **figure I.55 b**, the fluorescence behavior of the anthracene derivative ( $\lambda_{\text{max}} = 494 \text{ nm}$ ) undergoes significant quenching upon titration with the CB[8] host. According to the authors, this is explained by an enhanced non-radiative deactivation caused by  $\pi$ - $\pi$  interactions between the face-to-face organized aromatic guest molecules inside the host cavity. The fitting of the titration data gives a binding constant of  $K_a = 4.5 \times 10^{12} \text{ M}^{-1}$ , which is indicative of a strong supramolecular interaction and a stoichiometry of 0.5 confirming the formation of the ternary complex.

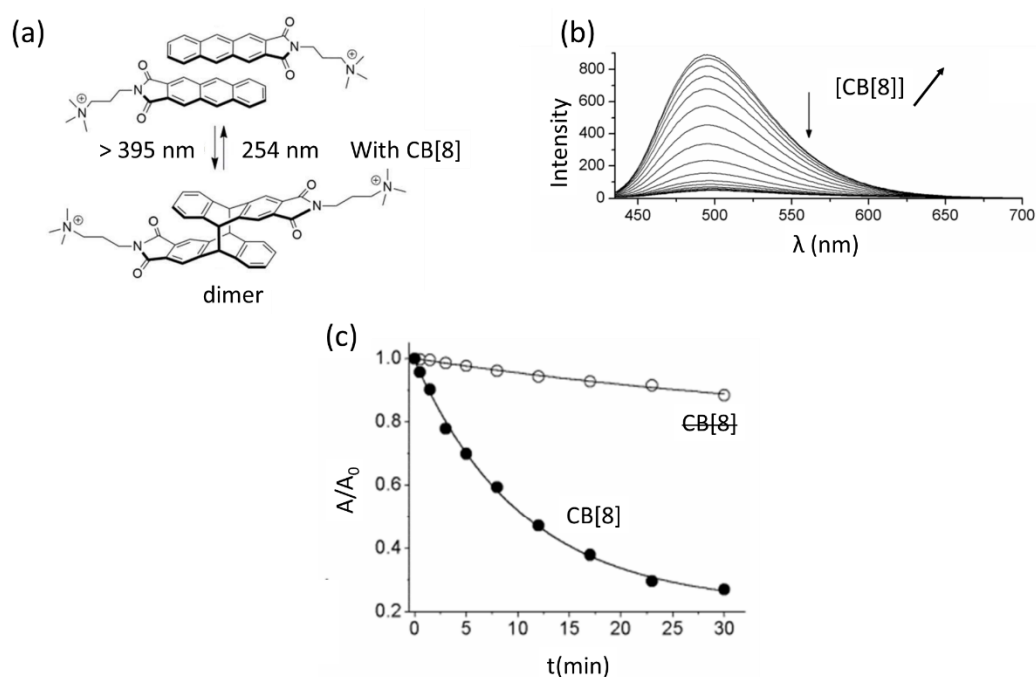
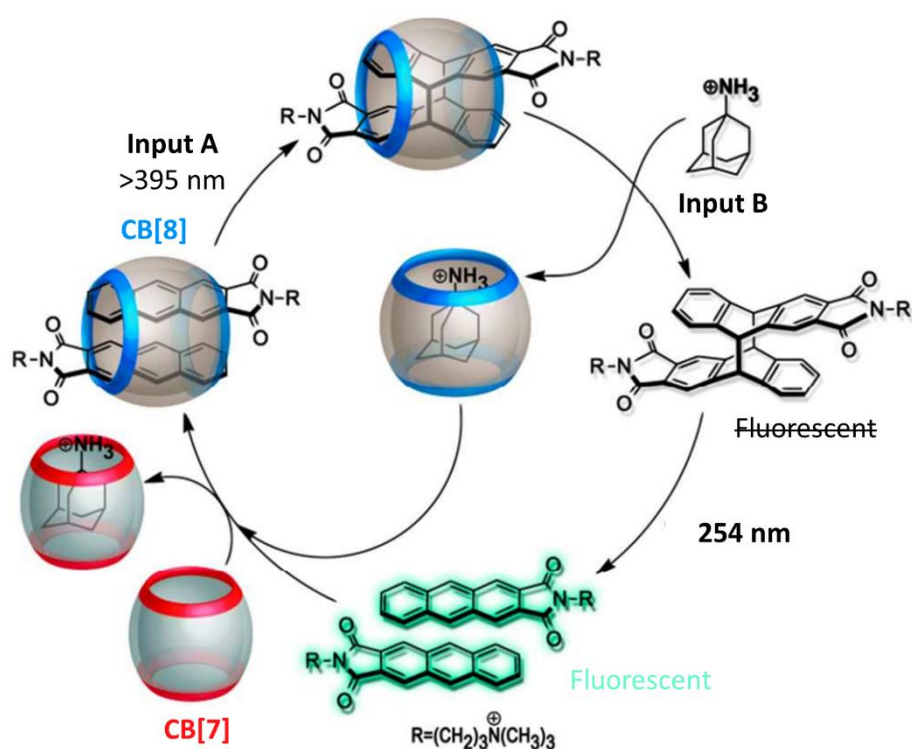


**Figure I.55:** (a) reversible photoswitching between the anthracene derivative and its photodimer. (b) Spectral change of the fluorescence of the anthracene derivative upon titration with CB[8]. (c) Kinetic curves (performed by UV/vis spectroscopy) and mono-exponential fittings for the irradiation of anthracene in absence (empty circles) and presence of CB[8] (filled circles) (adapted from reference [186]).

Once the strong binding of the anthracene guests has been confirmed, the photodimerization can be achieved. To do so, a diluted solution of anthracene derivative ( $10 \mu\text{M}$  in neutral water) in the presence of CB[8] ( $5 \mu\text{M}$ ) has been irradiated at an excitation wavelength  $\lambda_{\text{exc}} > 395 \text{ nm}$ .

The irradiation resulted in a uniform photoreaction that was tracked by UV/vis absorption spectroscopy, liquid chromatography, and  $^1\text{H}$  NMR spectroscopy [186]. After 30 minutes of irradiation (**figure 1.55 c**), 75% of the long-wavelength absorption band of the complex disappears (full circle curve) while the free dye (i.e., in absence of CB[8], empty circle curve) showed only ca. 10% decrease of the long-wavelength absorption band. As a conclusion, a much faster photoreaction (by a factor of ca. 10) occur in the presence of CB[8]. In addition, liquid chromatography associated to mass spectrometric detection confirmed the cucurbituril templated formation of the dimer by the observation of a doubly charged ion at  $m/z$  347. Finally, the recycling of the dimerization/cycloreversion sequence was shown for at least 5 cycles, by submitting the CB[8] complexes to successive irradiations at  $> 395$  nm and 254 nm (**figure 1.55 a**).

However, the different results presented above have always been obtained without removing the CB[8] host from the solution. Therefore, **Pischel et al** developed a peculiar sequence (named keypad lock [186]) in order to liberate the anthracene dimer from the CB[8]cavity. This sequence is presented in **scheme 1.5**.



**Scheme 1.5** supramolecular keypad lock by applying the correct input order and resetting by CB7 (adapted from reference [186]).

The sequence is constituted of two inputs: **inputs A** corresponds to the irradiation step and **input B** to the insertion of adamantylamine to the solution as binding competitor ( $K_a = 8,2 \cdot 10^8 \text{ M}^{-1}$  for the binary complex CB[8]•adamantylamine) [188]. Indeed, the latter is able to displace the monomeric anthracene as well as its dimer from the CB[8] macrocycle leading to the observation of non-complexed photodimer. The dimer is non-fluorescent both in absence and presence of CB[8]. However, the cycloreversion ( $\lambda = 254 \text{ nm}$ ) of the non-complexed dimer back to the anthracene monomer is accompanied by a recovery of the fluorescence, while the same process inside CB[8] leads to no significant fluorescence increase due to efficient quenching (see **figure I.55 b**).

The resetting of the system to its initial state has been highlighted thanks to the reversible nature of the photoreaction and of the involved supramolecular interaction. Indeed, given the fact that the binding constant of adamantylamine to CB[7] is three orders of magnitude larger ( $K_a = 1.2 \times 10^{10} \text{ M}^{-1}$ ) [188] than for CB[8] and that the anthracene derivative has a much smaller binding constant with CB[7] ( $K_a = 3.0 \times 10^5 \text{ M}^{-1}$ ) [186], thermodynamic self-sorting can be used to achieve resetting. Therefore, the addition of CB[7] to the mixture that was obtained after irradiation at 254 nm enables the complexation of adamantylamine by CB[7] and of the anthracene monomer by CB[8], thereby closing the cycle shown in **scheme I.5**. Accordingly, the spectral signature of the ternary complex was re-constituted by addition of CB[7].

## References

1. a) C.A. Schalley, A. Springer, *Mass Spectrometry and Gas-Phase Chemistry of Non-Covalent Complexes*, John Wiley & Sons, Inc., Hoboken, New Jersey, USA, 2009; b) B. Baytekin, H.T. Baytekin, C.A. Schalley, *Org.Biomol.Chem.* 2006; 4: 2825–2841; c) K. Roman, M. Balabin, D. Grünstein, R. Kikkeri, V. Frankevich, P.H. Seeberger, R. Zenobi, *J.Am.Soc.Mass Spectrom.* 2011; 22: 1167-1177.
2. a) J. Sun, E.N. Kitova, N. Sun, J.S.S Klassen, *Anal.Chem.* 2007; 79: 8301-8311; b) V. Gabelica, N. Galic, E. De Pauw, *J.Am.Soc.Mass Spectrom.* 2002; 13: 946-953.
3. a) C.A. Schalley, P. Ghosh, M. Engeser, *Int.J.Mass Spectrom.* 2004; 232: 249-258; b) L. Wang, Y. Chai, C. Sun, D.W. Armstrong, *Int.J.Mass Spectrom.* 2012; 323-324: 21-27.
4. a) E. Kalenius, D. Moiani, E. Dalcanale, P. Vainiotalo, *Chem.Comm.* 2007; 3865-3867; b) D.V. Dearden Y.J. Liang, J.B. Nicoll, K.A. Kellersberger, *J.Mass Spectrom.* 2001; 3: 989-997; c) T. Wyttenbach, M.T. Bowers, *J.Am.Soc.Mass Spectrom.* 1999; 10: 9-14.
5. a) H. Zhang, M. Grabenauer, M.T. Bowers, D.V. Dearden, *J.Phys.Chem.A* 2009; 113: 1508-1517; b) J. De Winter, V. Lemaure, R. Ballivian, F. Chirot, O. Coulembier, R. Antoine, J. Lemoine, J. Cornil, P. Dubois, P. Dugourd, P. Gerbaux. *Chem.Eur.J.* 2011; 17: 9738-9745 ; c) J.B. Renaud, E. Martineau, G.G. Mironov, M.V. Berezovski, P.M. Mayer, *Phys.Chem.Chem.Phys.* 2012; 14: 165-172.
6. a) P. Gerbaux, J. De Winter, D. Cornil, K. Ravicini, G. Pesesse, J. Cornil, R. Flammang, *Chem.Eur.J.* 2008; 14: 11039-11049 ; b) H. Zhang, I.H. Chu, S.Leming, D.V. Dearden, *J.Am.Chem.Soc.* 1991; 113: 7415-7417 ; c) G. Grigorean, J. Ramirez, S. H. Ahn, C. B. Lebrilla, *Anal.Chem.* 2000; 72: 4275 – 4281; d) E. Ventola, K. Rissanen, P. Vainiotalo, *Chem.Eur.J.* 2004; 10: 6152 – 6162.
7. a) C. Lifshitz, *Mass Spectrom.Rev.* 1982; 1: 309-348; b) M.B. More, D. Ray, P.B. Armentrout, *J.Am.Chem.Soc.* 1999; 121: 417-423; c) P. Armentrout, *Int.J.Mass Spectrom.* 2000; 200: 219–241; d) L. Wang, Y. Chai, C. Sun, D.W. Armstrong, *Int.J.Mass Spectrom.* 2012; 323– 324: 21– 27; e) A. Revesz, D. Schröder, J. Svec, M. Wimmerova, V. Sindelar, *J.Phys.Chem.A* 2011; 115: 11378-11386.

8. a) F. Yang, D.V. Dearden, *Isr.J.Chem.* 2012; 51: 511-558; b) J. De Winter, V. Lemaure, O. Coulembier, J. Cornil, P. Dubois, P. Gerbaux. *J.Am.Soc.Mass Spectrom.* 2010; 21: 1159-1168.
9. W. L. Mock, N.-Y. Shih, *J. Am. Chem. Soc.* 1989; 111: 2697–2699.
10. a) J. W. Lee, S. Samal, N. Selvapalam, H. J. Kim, K. Kim, *Chem. Res.* 2003; 36: 621–630; b) K. Kim, N. Selvapalam, Y. H. Ko, K. M. Park, D. Kim, J. Kim, *Chem. Soc. Rev.* 2007; 36: 267–279.
11. a) K.I. Assaf, W.M. Nau, *Chem. Soc. Rev.* 2015; 44: 394-418; b) S.J. Barrow, S. Kasera, M.J. Rowland, J. del Barrio, O.A. Scherman, *Chem. Rev.* 2015; 115 (22): 12320-12406.
12. A. Villiers, *Compt. Rend. Acad. Sci. Paris* 1891; 112: 536.
13. A. Werner, *Z. Anorg. Chem.* 1893; 3: 267.
14. E. Fischer, *Ber. Deutsch. Chem. Ges.* 1894; 27, 2985.
15. K.I. Wolf, H. Frahm, H. Harms, *Z. Phys. Chem. (B)* 1937; 36: 237.
16. C.A. Schalley, *Analytical Methods in Supramolecular Chemistry. Volume 1*, 2012, Wiley-VCH, pages 1-26.
17. J.M. Lehn, *Pure App. Chem.* 1979; 50: 871-892.
18. J.M. Lehn, *Science* 1985; 227: 849-856.
19. D.J. Cram, *Angewandte Chemie* 1988; 27: 1009-1112.
20. C.J. Pedersen, *J. Am. Chem. Soc.* 1967; 89: 7017-7036.
21. Source: [https://www.nobelprize.org/nobel\\_prizes/chemistry/laureates/1987/](https://www.nobelprize.org/nobel_prizes/chemistry/laureates/1987/).
22. Source:  
<https://www.scopus.com/term/analyzer.uri?sid=208E7E2894CCD1E784B0678BAB627CAD.wsnAw8kcdt7IPYLO0V48gA%3a10&origin=resultslist&src=s&s=TITLE-ABS-KEY%28supramolecular+chemistry%29&sort=plf-f&sdt=b&sot=b&sl=39&count=29609&analyzeResults=Analyze+results&txGid=208E7E2894CCD1E784B0678BAB627CAD.wsnAw8kcdt7IPYLO0V48gA%3a6> (visited 17/03/06).
23. J.M. Lehn, *Supramolecular Chemistry: Concepts and Perspectives*; VCH: Weinheim, 1995.
24. C.A. Schalley, A. Lützen, M. Albrecht, *Chem. Eur. J.* 2004; 10: 1072-1080.
25. S. Rieth, K. Hermann, B.-Y. Wang, J.D. Badjic, *Chem. Soc. Rev.* 2011; 40: 1609-1622.
26. V. Rotello, S. Thayumanavan, *Molecular Recognition and Polymers: Control of Polymer Structure and Self-Assembly*. 2008, Wiley, pages 1-440.

27. A.A Abrikosov, L.P. Gorkov, I.E. Dzyaloshinsky, *Electromagnetic Radiation in an Absorbing Medium*, Chapter 6.
28. P. Arnaud, *Cours de Chimie Physique*. Dunod 1988.
29. Source : <http://eng.thesaurus.rusnano.com/wiki/article619>.
30. C.A. Hunter, J.K.M Sanders, *J. Am. Chem. Soc.* 1990; 112: 5525-5534.
31. D. Chandler, *Nature* 2005; 437: 640-647.
32. F. Biedermann, *Angew Chem. Int. Ed.* 2014; 53: 11158-11171.
33. F. Biedermann, M. Vendruscolo, O.A. Scherman, A. De Simone, W.M. Nau, *J. Am. Chem. Soc.* 2013; 135:1 4879-14888.
34. G.A. Jeffrey, *An Introduction to Hydrogen Bonding*, 1997, Oxford University Press, Oxford.
35. A.M. Sweetman, S.P. Jarvis, H. Sang, I. Lekkas, P. Rahe, Y. Wang, J. Wang, N.R. Champness, L. Kantorovich, P. Moriarty, *Nature Communications*. 2014, 5.
36. A. Gerschel, *Liaisons Intermoléculaires*, 1995 CNRS Editions.
37. L. Pauling, *The Nature of the Chemical Bond and the Structure of Molecules and Crystals: An Introduction to Modern Structural Chemistry*, 1960, Cornell University Press.
38. Source: <http://projects.edte.utwente.nl/deeltjesmodel/FS-zouten02.html>.
39. W. Bolton, *Acta Crystallographica* 1964; 17: 147 – 152.
40. R. Pauline, K. Müller, F. Diederich, *Angew. Chem.* 2005; 44: 1788-1805.
41. M. Adler, D. D. Davey, G. B. Phillips, S.-H. Kim, J. Jancarik, G. Rumennik, D. R. Light, M. Whitlow, *Biochemistry* 2000; 39: 12534 – 12542.
42. G.Cavallo,P.Metrangolo,R.Milani, T. Pilati, A. Priimagi, G. Resnati, G. Terraneo, *Chem.Rev.* 2016; 116: 2478 –2601.
43. O. Dumele,B. Schreib,U. Warzok, N. Trapp,C.A. Schalley, F. Diederich*Angew.Chem.Int. Ed.* 2017; 56: 1152 –1157.
44. J.L. Atwood, J.E.D. Davies, D.D. Macnicol, F. Vögtle, J.M. Lehn, *Comprehensive Supramolecular Chemistry* 1996, volume 1-11, Pergamon.
45. a) P. Ballester, A. Vidan-Ferran, P.W.N.L. van Leeuwen, *Advances in Catalysis* 2011; 54: 63-126; b) A. Galan, P. Ballester, *Chem. Soc. Rev.* 2016; 45: 1720-1737; c) M. Yoshizawa, M. Tamura, M. Fujita, *Science* 2006; 312: 251-254.
46. R. Breslow, P. Campbell, *Bioorg Chem.* 1971; 1: 140-156.

47. Source:<http://www.drugfuture.com/pharmacopoeia/usp32/pub/data/images/v32270/cas-10016-20-3.gif>.
48. a) P. Timmerman, W. Verboom, D.N. Reinhoudt, *Tetrahedron* 1996; 52: 2663-2704; b) D.J. Cram, J.M. Cram, *Container Molecules and their Guests*, Royal Society of Chemistry, Hertfordshire, 1997.
49. R. Warmuth, J. Yoon, *Acc. Chem. Res.* 2001; 34: 95-105.
50. Z. Qi, T. Heinrich, S. Moorthy, C.Z. Schalley, *Chem. Soc. Rev.* 2015; 44: 515-531.
51. Q.F. Sun, J. Isawa, D. Ogawa, Y. Ishido, S. Sato, T. Ozeki, Y. sei, K. Yamaguchi, M. Fujita, *Science* 2010; 328: 1144-1447.
52. a) L.R. MacGillivray, J.L. Atwood, *Nature* 1997; 389: 469-472; b) T. Gerkenmeier, W. Iwanneck, C. Agena, R. Fröhlich, S. Kotila, C. Näther, J. Mattay, *Eur. J. Org. Chem.* 1999: 2257-2262.
53. E. Fischer, *Ber. Dtsch. Chem. Ges.* 1894; 27: 2985. Also, see: J.-P. Behr (ed.), *The Lock and Key Principle. The State of the Art – 100 Years On*, Wiley, Chichester 1994.
54. C.A. Schalley, *Analytical Methods in Supramolecular Chemistry, Volume 1 and Volume 2*, Wiley-VCH 2012.
55. D.L. Andrews, *Encyclopedia of Applied Spectroscopy*, Wiley-VCH 2009
56. F. Rouessac, A. Rouessac, *Analyse Chimique (sixth edition)*, Dunod 2004.
57. D.A. Skoog, F.J. Holler, S.R. Crouch, *Principles of Instrumental Analysis (6th ed.)*. Belmont, CA: Thomson Brooks, 2006. pp. 169–173.
58. K. Hirose, *J. of Incl. Phenomena* 2001; 39: 193-209.
59. E. Iglesias, *J. Org. Chem.* 2006; 71: 4383-4392.
60. C.A. Schalley, *Analytical Methods in Supramolecular Chemistry, Volume 1*, Wiley-VCH 2012, pages: 29-43.
61. A. Belay, *International Journal of Biophysics* 2012; 2: 12-17.
62. K.C. Wong, *J. Chem. Educ.* 2014; 91: 1103-1104.
63. S. Paramonov, Y. Fedorov, V. Lokshin, E. Tulyakova, G. Vermeersch, S. Delbaere, O. Fedorova, *Or. Biomol. Chem.* 2012; 10: 671-682.
64. C.A. Schalley, *Analytical Methods in Supramolecular Chemistry, Volume 1*, Wiley-VCH 2012, pages: 44-52.
65. P. Thordarson, *Chem. Soc. Rev.* 2011; 40: 1305-1323.



66. C.A. Schalley, *Analytical Methods in Supramolecular Chemistry, Volume 1*, Wiley-VCH 2012, pages: 197-285.
67. E.L. Cussler, *Diffusion : Mass Transfer in FLuid Systems*, Cambridge University Press, Cambridge 1984.
68. Source: [http://www.uni-muenster.de/imperia/md/content/physikalische\\_chemie/nmr\\_pfg\\_diffusion.pdf](http://www.uni-muenster.de/imperia/md/content/physikalische_chemie/nmr_pfg_diffusion.pdf).
69. L. Frish, S.E. Matthews, V. Böhmer, Y. Cohen, *J. Chem. Soc. Perkin Trans.* 1999; 2: 669-671.
70. L.S. Roselin, M-S Lin, P-H Sin, Y. Chang, W-Y Chen, *Biotechnol. J.* 2010; 5: 85-98.
71. J.E. Ladbury, *Biochem. Soc. Trans.* 2010; 38: 888-893.
72. C.A. Schalley, *Analytical Methods in Supramolecular Chemistry, Volume 1*, Wiley-VCH 2012, pages: 67-104.
73. E. Grell D. Grell, P. Bugnon, B. Dietrich, J.M. Lehn, *J. Therm. Anal. Calorim.* 2004; 77: 483-495.
74. M.L. Bianconi, *Biocalorimetry* (eds. Ladbury, J. E., Doyle, M. L.) Wiley, Chichester, 2004, pages: 175–185.
75. a) J.W. Steed, J.L. Atwood, *Supramolecular Chemistry*, Wiley, Chichester, 2000. b) H.-J. Schneider, A. Yatsimirsky, *Principles and Methods in Supramolecular Chemistry*, Wiley, Chichester, 2000. c) J.L. Atwood, J.W. Steed, *Encyclopedia of Supramolecular Chemistry*, Eds. Marcel Dekker, New York, 2004.
76. C.A. Schalley, *Analytical Methods in Supramolecular Chemistry, Volume 1*, Wiley-VCH 2012, pages: 105-125.
77. a) H. Stephan, K. Gloe, P. Schiessl, F.P. Schmidtchen, *Supramol. Chem.* 1995; 5: 273-280. b) H. Stephan, R. Berger, H. Spies, B. Johannsen, F.P. Schmidtchen, *J. Radioanal. Nucl. Chem.* 1999; 242: 399-403.
78. M. Berger, F.P. Schmidtchen, *Angew. Chem. Int. Ed.* 1998; 37: 2694–2696.
79. B. Baytekin, H.T. Baytekin, C.A. Schalley, *Org. Biomol. Chem.* 2006; 4: 2825-2841.
80. M. Hedenus, *Astronomical Notes* 2002; 323: 569-569.
81. a) K.R. Jennings, *“A History of European Mass Spectrometry*, 2012, IM Publications. b) Source: [https://www.nobelprize.org/nobel\\_prizes/physics/laureates/1906/](https://www.nobelprize.org/nobel_prizes/physics/laureates/1906/).

82. "Joseph John Thomson (1856-1940) Rays of positive electricity". Classic Chemistry.  
Retrieved 2009-12-01.
83. Source:  
<https://www.scopus.com/term/analyzer.uri?sid=114134C0037AD8D642890C4EB633AB1F.wsnAw8kcdt7IPYLOOV48gA%3a461&origin=resultslist&src=s&s=TITLE-ABS-KEY%28mass+spectrometry%29&sort=plf-f&sdt=b&sot=b&sl=32&count=527467&analyzeResults=Analyze+results&txGid=114134C0037AD8D642890C4EB633AB1F.wsnAw8kcdt7IPYLOOV48gA%3a51> (website visited 17/03/07).
84. F.W. McLafferty, *Science* 1981; 214: 280-287.
85. M. Yamashita, J.B. Fenn, *Phys. Chem.* 1984; 88: 4451-4459.
86. Z.P. Yao, T.S.M. Wan, K.P. Kwong, C.T. Che, *Anal. Chem.* 2000; 72: 5383-5393.
87. *Chem. Soc. Rev.* 2015; 44: 515-531, *Chem. Soc. Rev.* 2014; 43: 1800-1812.
88. Source: [https://www.nobelprize.org/nobel\\_prizes/chemistry/laureates/2002/](https://www.nobelprize.org/nobel_prizes/chemistry/laureates/2002/).
89. E. Hoffmann, V. Stroobant, *Spectrométrie de Masse* 2005. Dunod.
90. J. De Winter, *In-depth determination of the connectivity and topology of (co)polymers by state-of-the-art mass spectrometry* 2011, pages 278.
91. J.V. Iribarne, B.A. Thomson, *J. of Chem. Phys.* 1976; 64: 2287-2294.
92. B.A. Thomson, J.V. Iribarne, *J. Of Chem. Phys.* 1979; 71: 4451-4463.
93. L. Konermann, E. Ahadi, A.D. Rodriguez, S. Vahidi, *Anal. Chem.* 2013; 85: 2-9.
94. A.R. Fersht, *Structure and Mechanism in Protein Science*; W. H. Freeman & Co.: New York, 1999.
95. E. Ahadi, K. Konermann, *J. Phys. Chem. B* 2012; 116: 104-112.
96. J.K. Chung, S. Consta, *J. Phys. Chem. B* 2012; 116: 5777-5785.
97. C.A. Schalley, M. Engeser, *Int. J. of Mass Spectrom.* 2004; 232: 249-258.
98. a) J.A. Bravo, F.M. Raymo, J.F. Stoddart, A.J. P. White, D.J. Williams, *Eur. J. Org. Chem.* 1998; 11: 2565-2571; b) T. Harrison, S. Harrison, *J. Am. Chem. Sco.* 1967; 89: 5723-5724.
99. J. Laskin J.H. Futrell, *Mass Spectrom. Rev.* 2005; 24: 1069-1090.
100. H.D. Winkler, E.V. Dzyuba, J.A.W. Sklorz, N.K. Beyeh, K. Rissanen, C.A. Schalley, *Chem. Sci.* 2011; 2: 615-624.

101. Source: <http://www.bcp.fu-berlin.de/chemie/chemie/service/biosupramol/Massenspektrometrie/MS/Geraete/FTICR.html>.
102. a) S.D. Fuerstenau, W.H. Benner, J.J. Thomas, C. Brugidou, B.Bothner, G. Siuzdak, *Angew. Chem. Int. Ed.* 2001; 40: 541-544; b) G. Siuzdak, B. Bothner, M. Yeager, C. Brugidou, C.M. Fauquet, K. Hoey, C.M. Change, *Chem. Biol.* 1996; 3: 45-48.
103. Source : <https://www.britannica.com/science/tobacco-mosaic-virus>.
104. L. Cera, C.A. Schalley, *Chem. Soc. Rev.* 2014; 43: 1800-1812.
105. R.R. Julian, J.A. May, B. Slotz, J.L. Beauchamp, *Angew. Chem. Int. Ed.* 2003; 42: 1012-1015.
106. J.B. Cunniff, P. Vouros, *J. Am. Chem. Soc. Mass Spectrom.* 1995; 6: 437-447.
107. J. Szejtli, B. Zsardon, T. Cserhati, W.L. Hinz, D.W. Armstrong In *Ordered Media in Chemical Separations*, Eds.; American Chemical Society: Washington DC, 1987; Chap. 11.
108. D.E. Clemmer, M. F. Jarrold, *J. Mass Spectrom.* 1997; 32: 577–592.
109. E.A. Mason, E.W. McDaniel, Wiley-VCH Verlag GmbH & Co. KGaA: Weinheim, FRG, 1988, 0–471.
110. B. C. Bohrer, S. I. Merenbloom, S. L. Koeniger, A. E. Hilderbrand, D. E. Clemmer, *Annu. Rev. Anal. Chem. (Palo Alto. Calif)* 2008; 1: 293–327.
111. A. B. Kanu, P. Dwivedi, M. Tam, L. Matz, H. H. Hill., *J. Mass Spectrom.* 2008; 43: 1–22.
112. a) J. De Winter, V. Lemaure, R. Ballivian, F. Chirot, O. Coulembier, R. Antoine, J. Lemoine, J. Cornil, P. Dubois, P. Dugourd, and P. Gerbaux, *Chem. - A Eur. J.* 2011; 17: 9738–9745; b) S. Crotty, S. Gerislioglu, K.J. Endres, C. Wesdemiotis, U.S. Schubert, *Analytica Chimica Acta* 2016; 932: 1-21.
113. a) Beck A, Terral G, Debaene F, Wagner-Rousset E, Marcoux J, Janin-Bussat MC, Colas O, Van Dorselaer A, Cianférani S, *Expert Review of Proteomics* 2016; 13 : 157-183; b) K. Rajabi, A. E. Ashcroft, S.E. Radford, *Methods* 2015; 89: 13-21; c) D.C. Dallas, A. Guerrero, E.A. Parker, R.C. Robinson, J. Gan, J.B. German, D. Barile, C.B. Lebrilla, *Proteomics* 2015; 15: 1026-1038; d) C. Uetrecht, R.J. Rose, E. Van Dujin, K. Lorenzen, A.J.R Heck, *Chem. Soc. Rev.* 2010; 39: 1633-1655.

114. a) Y.T. Chan, X. Li, M. Soler, J.L. Wang, C. Wesdemiotis, G.R. Newkome, *J. Am. Chem. Soc.* 2009; 131: 16395-16397; b) Y.T. Chan, X. Li, J. Yu, G.A. Carri, C.N. Moorefield, G.R. Newkome, C. Wesdemiotis, *J. Am. Chem. Soc.* 2011; 133: 11967-11976.
115. C. Laphorn, F. Pullen, B.Z. Chowdhry, *Mass Spec. Rev.* 2013; 32: 43-71.
116. E.A. Mason, E.W. McDaniel, *Transport Properties of Ions in Gases*, 1988 Wiley-VCH (pages 1-3).
117. E.W. Mc Daniel, E.A. Mason, *The Mobility and diffusion of ions in Gases*, Wiley, New-York, 1973.
118. H.E. Revercomb, E.A. Mason, *Anal. Chem.* 1975; 47: 970-983.
119. E.A. Mason, E.W. McDaniel, *Transport Properties of Ions in Gases*, 1988 Wiley-VCH (pages 4-5, 32-36).
120. V. D'Atri, M. Porrini, F. Rodu, V. Gabelica, *J. Mass Spectrom.* 2015; 50: 711-726.
121. C. Larriva-Andaluz, J. Fernandez-Garcia, M.A. Ewing, C. J. Hogan Jr., D.E. Clemmer, *Phys. Chem. Chem. Phys* 2015; 17: 15019-15029.
122. J.C. May, J.A. McLean, *Int. J. Ion Mobil. Spec.* 2013; 16: 85-94.
123. G.A. Bataglion, G.H. M. F. Souza, G. Heerdt, N.H. Morgon, J.D.L. Dutra, R.O. Freire, M.N. Eberlin, A. Tata, *J. Mass. Spectrom.* 2015; 50: 336-343.
124. E. A. Mason, E. W. McDaniel, *Transport Properties of Ions in Gases*. 1988 Wiley-VCH, Appendix 3.
125. R.G. Forbes, *Surface Sciences* 1977; 64: 367-371.
126. P.M. Lalli, B.A. Iglesias, H.E. Toma, G.F. de Sa, R.J. Daroda, J.C. Silva Filho, J.E. Szulejko, K. Araki, M.N. Eberlin, *J. Mass Spectrom.* 2012; 47: 712-719.
127. Ph. Dugourd, R.R. Hudgins, D.E. Clemmer, M.F. Jarrold, *Rev. Sci. Instrum.* 1997; 68: 1122-1129.
128. F. Chirof, F. Calvo, F. Albrieux, J. Lemoine, Y.O. Tsybin, P. Dugourd, *J. Am. Soc. Mass. Spectrom.* 2012; 23: 386-396.
129. J.P. Neirotti, F. Calvo, D.L. Freeman, J.D. Doll, *J. Chem. Phys.* 2000; 112: 10340-10349.
130. J. De Winter, PhD Thesis (University of Mons) 2010 (page 44).
131. a) D. Gerlich, *In State-Selected and State-to-State Ion-Molecule Reaction Dynamics*, Part 1. Baer M Editions, John Wiley: New-York, 1992. Pages: 1-176; b) M. Morris, P. Thibault, R.K. Boyd, *J. Am. Soc. Mass Spectrom.* 1994; 5: 1042-1063.

132. K. Giles, S.D. Pringle, K.R. Worthington, D. Little, J.L. Wildgoose, R.H. Bateman, *Rapid Commun. Mass Spectrom.* 2004; 18: 2401-2414.
133. A. A. Shvartsburg, R.H. Bateman, *Rapid Comm. In Mass Spectrom.* 2004; 18: 2401-2414.
134. K. Giles, J.L. Wildgoose, D.J. Langridge, I. Campuzano, *Int. J. of Mass Spectrom.* 2010; 298: 10-16.
135. Source: [http://www.waters.com/waters/fr\\_FR/SYNAPT-G2-Si-High-Definition-Mass-Spectrometry/nav.htm?locale=fr\\_FR&cid=134740622](http://www.waters.com/waters/fr_FR/SYNAPT-G2-Si-High-Definition-Mass-Spectrometry/nav.htm?locale=fr_FR&cid=134740622).
136. B.T. Ruotolo, J.L.P. Benesch, A.M. Sandercock, S.J. Hyung, C.V. Robinson, *Nature Protocols* 2008; 3: 1139-1152.
137. M. F. Bush, Z. Hall, K. Giles, J. Hoyes, C. V. Robinson, B. T. Ruotolo., *biology. Anal. Chem.* 2010; 82: 9557–9565.
138. A.A. Shvartsburg, R.D. Smith, *Anal. Chem.* 2008; 80: 9689-9699.
139. F. Lanucara, S.W. Holman, C.J. Gray, C.E. Eyers, *Nat. Chem.* 2014; 6: 281-294.
140. J. Lagona, P. Mukhopadhyay, S. Chakrabarti, L. Isaacs, *Angew. Chem. Int. Ed.* 2005; 44: 4844–4870; *Angew. Chem.* 2005; 117: 4922–4949.
141. Source: <http://journals.iucr.org/b/issues/2004/03/00/av0066/av0066fig3mag.jpg>.
142. a) D. Witt, J. Lagona, F. Damkaci, J. C. Fettinger, L. Isaacs, *Org. Lett.* 2000; 2: 755 – 758; b) A. Chakraborty, A. Wu, D. Witt, J. Lagona, J. C. Fettinger, L. Isaacs, *J. Am. Chem. Soc.* 2002; 124: 8297 – 8306; c) R. J. Blanch, A. J. Sleeman, T. J. White, A. P. Arnold, A. I. Day, *Nano Lett.* 2002; 2: 147 – 149; d) A. I. Day, R. J. Blanch, A. Coe, A. P. Arnold, *J. Inclusion Phenom. Macrocyclic Chem.* 2002; 43: 247 – 250; e) S. Liu, K. Kim, L. Isaacs, *J. Org. Chem.* 2007; 72: 6840 – 6847.
143. L. Isaacs, *Isr. J. Chem.* 2011; 51: 578-591.
144. A.I. Day, A.P. Arnold, R.J. Blanch, B. Snushall, *J. Org. Chem.* 2001; 66: 8094-8100.
145. R. Behrend, E. Meyer and F. Rusche, *Justus Liebigs Ann. Chem.*, 1905; 339: 1-37.
146. W. A. Freeman, W. L. Mock and N.-Y. Shih, *J. Am. Chem. Soc.*, 1981; 103: 7367-7368.
147. W.A. Freeman, *Acta Cryst.* 1984; B40: 382-387.
148. Source: <https://www.scopus.com/term/analyzer.uri?sid=793532D4979D1012DDFF638F448E16B4.wsnAw8kcdt7IPYLOOV48gA%3a10&origin=resultslist&src=s&s=TITLE-ABS->

- KEY%28Cucurbituril%29&sort=plf-f&sdt=b&sot=b&sl=27&count=640&analyzeResults=Analyze+results&txGid=793532D4979D1012DDFF638F448E16B4.wsnAw8kcdt7IPYLO0V48gA%3a13 (website visited 02/23/17).
149. K.I. assaf, W.M. Nau, *Chem. Soc. Rev.*, 2015; 44: 394-418.
  150. J. Kim, I.-S. Jung, S.-Y. Kim, E. Lee, J.-K. Kang, S. Sakamoto, K. Yamaguchi and K. Kim, *J. Am. Chem. Soc.*, 2000; 122: 540-541.
  151. A. Day, A. P. Arnold, R. J. Blanch and B. Snushall, *J. Org. Chem.*, 2001; 66: 8094-8100.
  152. A. I. Day, R. J. Blanch, A. P. Arnold, S. Lorenzo, G. R. Lewis and I. Dance, *Angew. Chem., Int. Ed.*, 2002; 41: 275-277.
  153. X.-J. Cheng, L.-L. Liang, K. Chen, N.-N. Ji, X. Xiao, J.-X. Zhang, Y.-Q. Zhang, S.-F. Xue, Q.-J. Zhu, X.-L. Ni and Z. Tao, *Angew. Chem., Int. Ed.*, 2013; 52: 7252-7255.
  154. a) S. Ghosh and L. Isaacs, *J. Am. Chem. Soc.*, 2010; 132: 4445-4454; b) H.-K. Lee, K. M. Park, Y. J. Jeon, D. Kim, D. H. Oh, H. S. Kim, C. K. Park and K. Kim, *J. Am. Chem. Soc.*, 2005; 127: 5006-5007; c) B. C. Pemberton, R. Raghunathan, S. Volla and J. Sivaguru, *Chem. – Eur. J.*, 2012; 18: 12178-12190.
  155. H. Isobe, S. Sato and E. Nakamura, *Org. Lett.*, 2002; 4: 1287-1289.
  156. a) C. A. Burnett, J. Lagona, A. X. Wu, J. A. Shaw, D. Coady, J. C. Fettinger, A. I. Day and L. Isaacs, *Tetrahedron* 2003; 59: 1961-1970; b) A. I. Day, A. P. Arnold and R. J. Blanch, *Molecules* 2003; 8: 74-84; c) S. Y. Jon, N. Selvapalam, D. H. Oh, J.-K. Kang, S.-Y. Kim, Y. J. Jeon, J. W. Lee and K. Kim, *J. Am. Chem. Soc.* 2003; 125: 10186-10187.
  157. Y. J. Zhao, S. F. Xue, Q. J. Zhu, Z. Tao, J. X. Zhang, Z. B. Wei, L. S. Long, M. L. Hu, H. P. Xiao and A. I. Day, *Chin. Sci. Bull.* 2004; 49: 1111-1116.
  158. S. M. Liu, P. Y. Zavalij and L. Isaacs, *J. Am. Chem. Soc.* 2005; 127: 16798-16799.
  159. H.-J. Buschmann, A. Zielesny and E. Schollmeyer, *J. Inclusion Phenom. Macrocyclic Chem.* 2006; 54: 181-185.
  160. L. Isaacs, S.-K. Park, S. M. Liu, Y. H. Ko, N. Selvapalam, Y. Kim, H. Kim, P. Y. Zavalij, G.-H. Kim, H.-S. Lee and K. Kim, *J. Am. Chem. Soc.* 2005; 127: 18000-18001.
  161. W.-H. Huang, S. M. Liu, P. Y. Zavalij and L. Isaacs, *J. Am. Chem. Soc.*, 2006; 128: 14744-14745.

162. a) W.-H. Huang, P. Y. Zavalij and L. Isaacs, *Angew. Chem., Int. Ed.* 2007; 46: 7425-7427;  
b) L.-B. Lu, Y.-Q. Zhang, Q.-J. Zhu, S.-F. Xue and Z. Tao, *Molecules*, 2007; 12: 716-722.
163. L.-H. Wu, X.-L. Ni, F. Wu, Y.-Q. Zhang, Q.-J. Zhu, S.-F. Xue and Z. Tao, *J. Mol. Struct.* 2009; 920: 183-188.
164. a) N. Zhao, G. O. Lloyd and O. A. Scherman, *Chem. Commun.*, 2012; 48: 3070-3072. b) L. P. Cao and L. Isaacs, *Org. Lett.* 2012; 14: 3072-3075.
165. X.-J. Cheng, L.-L. Liang, K. Chen, N.-N. Ji, X. Xiao, J.-X. Zhang, Y.-Q. Zhang, S.-F. Xue, Q.-J. Zhu, X.-L. Ni and Z. Tao, *Angew. Chem., Int. Ed.*, 2013; 52: 7252-7255.
166. L. Gilberg, M. S. A. Khan, M. Enderesova and V. Sindelar, *Org. Lett.* 2014; 16: 2446-2449.
167. W.M. Nau, M. Florea, K.I. Assaf, *Isr. J. Chem.* 2011; 51: 559-577.
168. K. Jansen, H.J. Buschmann, A. Wego, D. Döpp, C. Mayer, H.J. Holdt, E. Schollmeyer, J. Inclusion Phenom. *Macrocyclic Chem.* 2001; 39: 357-363.
169. a) J. Zhao, H.J. Kim, J. Oh, S.Y. Kim, J. Lee, W.S. Sakamoto, K. Yamaguchi, K. Kim, *Angew. Chem. Int. Ed.* 2001; 40: 4233-4235. b) V. Lewin, J. Rivollier, S. Coudert, D.A. Buisson, D. Baumann, B. Rousseau, F.X. Legrand, H. Kourilova, P. Berthault, J.P. Dognon, M.P. Heck, G. Huber, *Eur. J. Org. Chem.* 2013; 2013: 3857-3865.
170. L. Isaacs, *Acc. Chem. Res.* 2014; 47: 2052-2062.
171. E. Masson, X. Ling, R. Joseph, L. Kyremeh-Mensah, X. Lu, *RSC Adv.* 2012; 2: 1213-1247.
172. W. L. Mock and N.-Y. Shih, *J. Org. Chem.*, 1986; 51: 4440-4446; *J. Am. Chem. Soc.*, 1988; 110: 4706-4710.
173. M. Florea and W. M. Nau, *Angew. Chem., Int. Ed.*, 2011; 50: 9338-9342.
174. C. Marquez, W.M. Nau, *Angewandte Chemie* 2001; 40: 3155-3160.
175. S. Liu, C. Ruspic, P. Mukhopadhyay, S. Chakrabarti, P. Zavalij, L. Isaacs, *J. Am. Chem. Soc.* 2005; 127: 15959-15967.
176. L. Cao, M. Sekutor, P.Y. Zavalij, K. Mlinaric-Majerski, R. Glaser, L. Isaacs, *Angew. Chem. Int. Ed.* 2014; 53: 988-993.
177. H.J. Buschmann, L. Mutihac, R.C. Mutihac, E. Schollmeyer, *Thermochim. Acta* 2005; 430: 79-82.

178. M.E. Bush, M. E., N.D. Bouley, A.R. Urbach, *J. Am. Chem. Soc.* 2005; 127: 14511–14517.
179. a) L.A. Logsdon, A.R. Urbach, *J. Am. Chem. Soc.* 2013; 135: 11414–11416; b) G. Ghale, V. Ramalingam, A.R. Urbach, W.M. Nau, *J. Am. Chem. Soc.* 2011; 133: 7528–7535; c) R.E. McGovern, H. Fernandes, A.R. Khan, N.P. Power, P.B. Crowley, *Nat. Chem.* 2012; 4: 527–533.
180. a) F. Biedermann, U. Rauwald, J.M. Zayed, O.A.A. Scherman, *Chem. Sci.* 2011; 2: 279–286; b) D.T. Dang, J. Schill, L. Brunsveld, *Chem. Sci.* 2012; 3: 2679–2684.
181. C.P. Carvalho, A. Norouzy, V. Ribeiro, W.M. Nau, U. Pischel, *Org. Biomol. Chem.* 2015; 13: 2866–2869.
182. N.A. Campbell, J. B. Reece, *Biology* (Seventh ed.). Benjamin Cummins 2005.
183. Z. Qi, T. Heinrich, S. Moorthy, C.A. Schalley, *Chem. Soc. Rev.* 2015; 44: 515–531.
184. L. Cera, C.A. Schalley; *Chem. Soc. Rev.* 2014; 43: 1800–1812.
185. T.C. Lee, E. Kalenius, A.I. Lazar, K.I. Assaf, N. Kuhnert, C.H. Grun, J. Janis, O.A. Scherman, W.M. Nau, *Nat. Chem.* 2013; 5: 376–382.
186. C.P. Carvalho, Z. Dominguez, J.P. Da Silva, U. Pischel, *Chem. Comm.* 2015; 51: 2698–2701.
187. a) B. C. Pemberton, R. K. Singh, A. C. Johnson, S. Jockusch, J. P. Da Silva, A. Ugrinov, N. J. Turro, D. K. Srivastava and J. Sivaguru, *Chem. Commun.* 2011; 47: 6323–6325. b) C. Yang, T. Mori, Y. Origane, Y. H. Ko, N. Selvapalam, K. Kim and Y. Inoue, *J. Am. Chem. Soc.* 2008; 130: 8574–8575. c) F. Biedermann, I. Ross and O. A. Scherman, *Polym. Chem.* 2014; 5: 5375–5382.
188. J. Vázquez, P. Remón, R. N. Dsouza, A. I. Lazar, J. F. Arteaga, W. M. Nau, U. Pischel, *Chem. Eur. J.* 2014 ; 20 : 9897–9901.



## II. Aim of the thesis

## Aim of the thesis

After reading the Introduction section of thesis PhD thesis, it appears obvious that mass spectrometric methods become mandatory as a complementary technique within the analytical toolbox of the supramolecular chemist. The challenging task is nowadays to define the relation between the condensed phase and the gaseous structures and the potential modifications that could be inherent to the ionization/desolvation processes occurring within the ion source. Such an essential research topic could only be approached through the investigation of the gas phase ion chemistry, say the study of the structures and the (unimolecular) reactivities of the non-covalent associations and their instrumental and experimental dependencies. Nevertheless, most of the researches in the field of supramolecular chemistry only use mass spectrometry to assess the non-covalent association formation, *say complex or no complex*, without any further investigations of their gas-phase properties. Therefore, the limitations of mass spectrometry to study supramolecular assemblies remain foggy. Pioneering work of **Christoph A. Schalley** [1] already demonstrate how gas phase data should be handle with great care when trying to compare gas phase and in-solution behavior of non-covalent complexes but also how powerful can be mass spectrometry in the field of supramolecular chemistry [2].

Initiated with my master thesis, the gas-phase properties of supramolecular assemblies involving cucurbiturils as host molecules have been deeply studied. The selection of cucurbiturils as model host has been motivated by their rigid character and their propensity to specific encapsulation. In the present work, we will investigate the influence of all the experimental and instrumental parameters, before and during the MS analysis, on the structure of the non-covalent associations. To assess the gas phase structures of those ions, we will mainly rely on two complementary experimental methods, namely collision-induced dissociation (CID) and ion mobility.

As far as the experimental parameters are concerned, the influence of the in-solution conditions – solvent, equilibration time and temperature - prior to the ionization process over the gaseous conformations/topologies of the non-covalent ions will be broadly detailed in the next sections. In addition, a better understanding of the host/guest complexes formation

depending on the compounds involved in the association will largely be discussed especially when changing the host molecule size, meaning varying the number of glycoluril units ( $n$ ) involved in the cucurbituril (CBn) host. For the instrumental parameter influence, we will investigate whether the source parameters – voltages and pressure – as well as the ion optic voltages can modify, either by decomposition or isomerization, the nature of the detected (non-covalent) ions.

In addition to mass spectrometry methods, the different systems under study will be theoretically approached using different methods of computational chemistry, with, in particular, the use of Density Functional Theory (DFT) and Molecular Dynamics. Indeed, by essence, mass spectrometry data being obtained in vacuo nicely correlate with theoretical data that are most of the time generated on isolated molecules and supramolecules. Therefore, this adequacy will render the comparison between experimental and theoretical data rather straightforward. In particular, computational chemistry will be advantageously solicited to (i) generate optimized structures, (ii) calculate the relative energies between isomers, (iii) estimate the dissociation/decomplexation threshold to correlate with CID data, and (iv) to calculate the Collision Cross Sections – CCS- that are to be compared with the ion mobility data.

We hope that this PhD thesis will be a modest contribution to the development of mass spectrometry as a performant research tool in the field of supramolecular chemistry demonstrating how the full panel of MS based methods can help determining critical properties of ionized host / guest complexes.

## References

1. C.A. Schalley, A. Springer, Mass Spectrometry and Gas-Phase Chemistry of Non-Covalent Complexes, John Wiley & Sons, Inc., Hoboken, New Jersey, USA, 2009.
2. C.A. Schalley, Analytical Methods in Supramolecular Chemistry. Volume 1, 2012, Wiley-VCH

# III. Experimental part

Mass Spectrometers

Overview of the Mass Spectrometer Acquisition Modes

Energy-Resolved Collision Induced Dissociation

Collision Cross Section Calibration Method for TWIMS Analysis

Nuclear Magnetic Resonance Measurements

Materials

Theoretical Calculations

## 1. Mass Spectrometers

In the context of this thesis, different mass spectrometers have been used. The first part of this section will be dedicated to the description of those machines.

### 1.1 Waters Q-ToF 2

#### 1.1.1 Description

The Waters Q-ToF 2 is equipped with an electrospray ionization (ESI) source, which has been presented in details in the introduction (section I.3.1). Downstream to the detector, the ions will successively fly through two analyzers: a quadrupole ion guide, and an orthogonal acceleration (oa) Time of Flight (ToF) (**figure III.1**), which surround and a hexapole collision-cell. Accordingly, the Q-ToF 2 is a hybrid mass-spectrometer, associating different type of analyses (Q and ToF). The ions are finally detected by the Multi-Channel Plate (MCP) detector after separation within the ToF-analyzer.

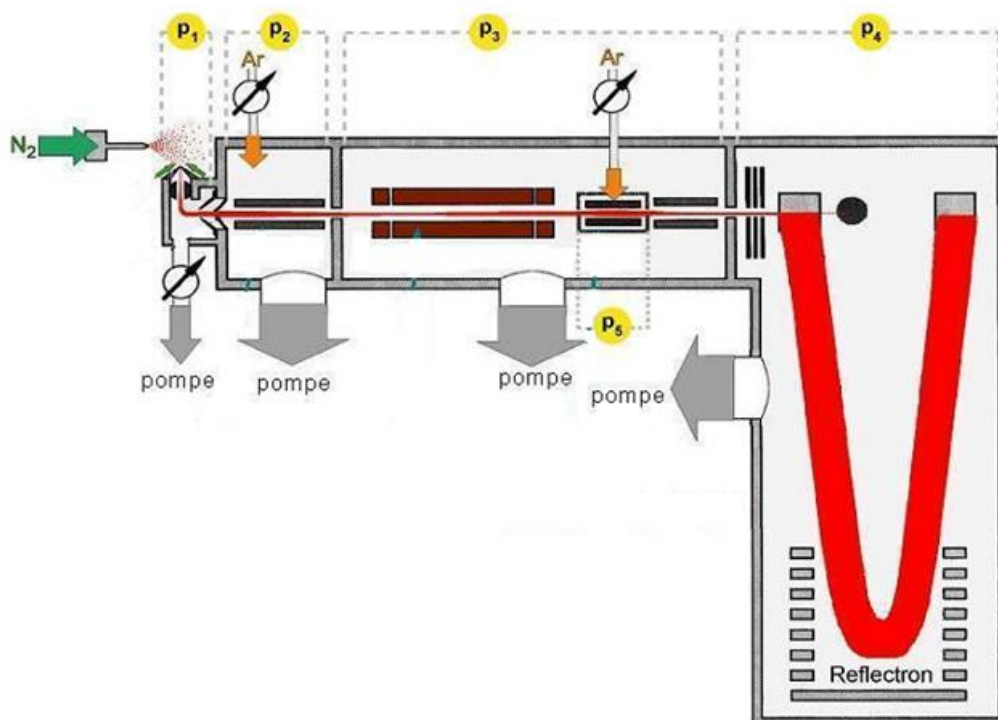


**Figure III.1:** scheme of the Waters Q-ToF 2 mass spectrometer.

### 1.1.2 Experimental procedure

The analyte solutions (host:  $10^{-4}$  M and guest:  $5 \cdot 10^{-4}$  M in water/methanol 80/20) are delivered to the ESI source by a Harvard Apparatus syringe pump at a flow rate of  $5 \mu\text{l min}^{-1}$ . Typical ESI conditions are: capillary voltage 3.1 kV, cone voltage 15-40 V (see figure captions in the Results and discussion section), source temperature  $80^{\circ}\text{C}$ , and desolvation temperature  $120^{\circ}\text{C}$ . Dry nitrogen is used as the ESI gas. Following custom-made modifications of the ion source of the QToF instrument, the pressure in the transmission region that is defined by the volume between the sample cone and the extractor cone is measured by a Pirani ion gauge. Regular pressure, i.e. at full pumping speed, is 1.2 mbar (**figure III.1 and figure III.2**) up to 6 mbar (see figure captions).

For the ESI-MS spectra, the quadrupole (rf-only mode) is set to pass all ions from  $m/z$  50 to 2000, and all ions are transmitted into the pusher region of time-of-flight analyzer where they are mass analyzed with 1s integration time. Data are collected in continuum mode until acceptable averaged results are obtained. For the ESI-MSMS experiments, the ions of interest are mass selected by the quadrupole mass filter. The precursor ion resolution is adjusted to select the complete isotopic cluster to help identifying the charge state of the fragment ions. The selected parent ions are then submitted to collision against argon in the rf-only hexapole collision cell (1mbar), and the laboratory-frame kinetic energy is selected to afford sufficiently intense signals for the fragments. The fragment ions, as well as the non dissociated precursor ions, are finally mass measured with the oa (orthogonal axis) -ToF analyzer.

The Waters Q-ToF presents an Electrospray ion source set in a Z-spray configuration (see **figure III.2**). Therefore, the ions will follow an electric field according to a Z-shape in the transition region between the cones presented above.

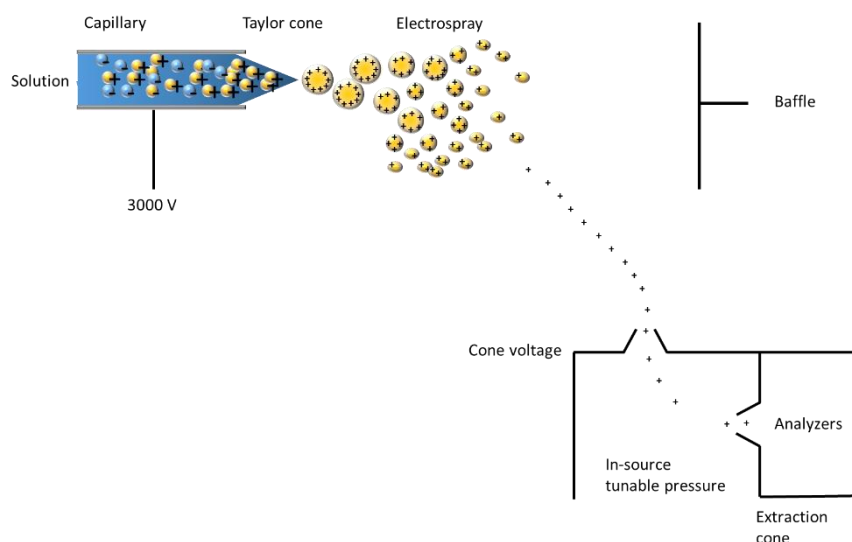


**Figure III.2:** schematic of the Z-spray ionization source of the Waters Q-ToF 2.

For more details about the electrospray, please refer to section I.3.1.

## 1.2 Waters Synapt G2-Si

### 1.2.1 Description

Ion mobility mass spectrometry measurements were performed using a hybrid quadrupole (Q) - traveling wave ion mobility spectrometry (TWIMS) - time-of-flight (ToF) mass spectrometer (Synapt G2-Si, Waters, U.K., **figure III.3**).

The Waters Synapt G2-Si is also equipped with an ESI source and corresponds to a hybrid mass spectrometer. In fact, the ionization source is followed by a Step-Wave<sup>®</sup>, a quadrupole, the so-called Triwave<sup>®</sup> setup and an orthogonal acceleration (oa) Time of Flight (ToF). The Step-Wave<sup>®</sup> is an original update to increase the desolvation and then decrease the chemical noise usually associated to residual solvent molecules. used as an ion guide; whereas the quadrupole can be used as a mass selector for the MSMS mode. The Triwave<sup>®</sup> part roughly corresponds to a collision cell and will be presented in more details in another section (section II.2.2.3). The ions are finally detected after separation associating the Quan-ToF<sup>®</sup> analyzer system. The resolution in CCS determination for the device is around 40.

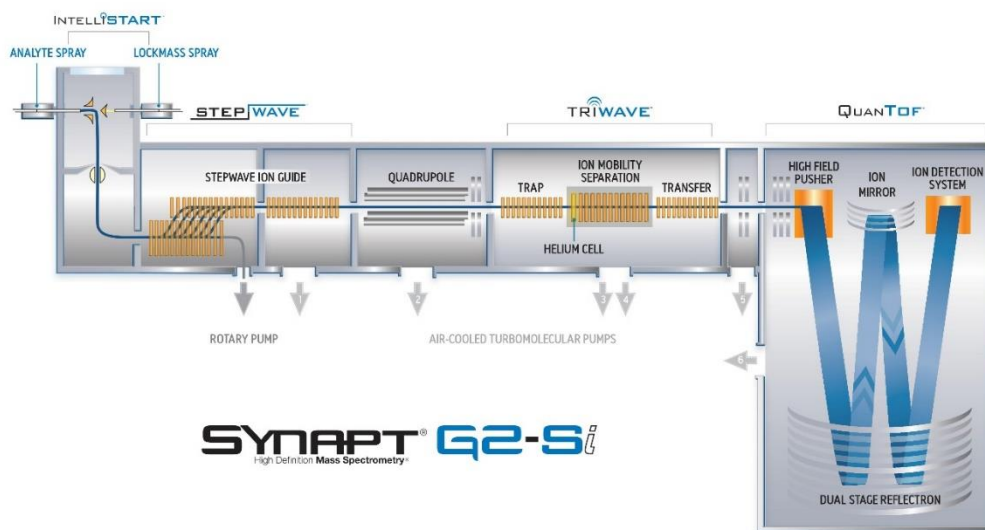


**Figure III.3:** scheme of the Waters Synapt G2-Si mass spectrometer.

### 1.2.2 Experimental procedure

Typical ion source conditions were: capillary voltage, 3.1 kV; sampling Cone, 40 V; source Offset, 80 V; source temperature, 150°C and desolvation temperature, 300 °C. This mass spectrometer was used for the recording of ESI full scan mass spectrum, for the (energy-resolved) collision-induced dissociation (CID) as well as for the ion mobility experiments.

Briefly, the core of the instrument is constituted by the so-called Tri-wave setup that is composed of three successive T-wave elements named the trap, the IMS cell, and the transfer, in which the wave speed and amplitude are user-tunable (see figure captions). The trap and transfer cells are filled with argon whereas the IMS cell is filled with nitrogen. A small RF-only cell filled with Helium is fitted between the trap and the IMS cell. Collision energy may be applied in the trap (trap CE) and in the transfer (transfer CE) to fragment ions respectively before and after the ion mobility separation. For the energy-resolved CID experiments, mass-selected ions are subjected to increased collision energies in the Trap cell. For the energy-resolved CID experiments on ions separated by ion mobility, the ions are decomposed within the transfer cell. Collisional cross sections were obtained following a calibration protocol using polyalanine as calibrant [1].



### 1.3 Homemade IMS/MS setup of the ILM research group in Lyon

**Figure III.4** shows a schematic representation of the ion mobility spectrometry/mass spectrometry (IMS/MS) instrument used,[2] which consists of a home-made drift cell coupled to a commercial quadrupole time-of-flight (QToF) machine (micro-QToF, Bruker Daltonics). Electrosprayed ions enter the instrument through a heated capillary interface held at 473 K, are guided through a first ion funnel, and accumulated in a small cylindrical ion trap. Periodically, ion packets are injected in the drift tube. The ions travel along the drift tube under the influence of a uniform electric field generated by a stack of isolated rings and a voltage divider. A second ion funnel focuses the diffuse ion packet at the exit of the drift tube. Ions exit this second ion funnel into a vacuum chamber through an aperture (diameter=0.7 mm) and are conveyed into the QToF instrument by a series of two ion funnels. Consecutively, they travel through a quadrupole and a collision cell and are accelerated into a perpendicular reflectron time-of-flight analyzer. The drift-tube assembly consists of 101 metal plates and is 1 m long. The drift region is operated between 5.7 and 8.3 V.cm<sup>-1</sup>, which corresponds to a drift voltage of 570–830 V. It is filled with approximately 16 mbar Torr of helium continuously injected at the end of the drift cell at a flow rate of 140 cm.s<sup>-1</sup>. The chamber that houses the first ion funnel is pumped down by a dry rotary pump, thus producing a flow of helium gas between this chamber and the drift cell and preventing neutral molecules from entering the drift cell, while a direct current (DC) electric field pushes the ions through the funnel against the flow. The cylindrical trap is an original feature that was designed to trap ions at intermediary pressures (ca. 10 Torr) [3]. Ions are periodically ejected in the drift cell by applying a voltage of 10 V between the two cap electrodes. The drift cell is operated at a frequency of 3–6 Hz and the time width of the ion packet injected in the cell is 1 ms. The Pusher/Puller of the ToF analyzer is operating at 10 kHz. Synchronization between the ion trap, and the ToF is provided by a National Instrument clock board under the command of custom software. The signal from the detector located at the end of the ToF is amplified and accumulated in a timeto-digital converter (Acqiris) by using the ToF extraction pulse as the start trigger. Data are converted into IM/MS maps post-treatment. IM resolution of the instrument with a drift voltage of 770 V and an ion gate of 1 ms is 50, and mass resolution is

### III. Experimental part

10 000. When using the on-axis detector, ions are mass selected with the quadrupole, and arrival time distributions are accumulated with a multichannel scaler with the ion-trap synchronization as the start trigger.

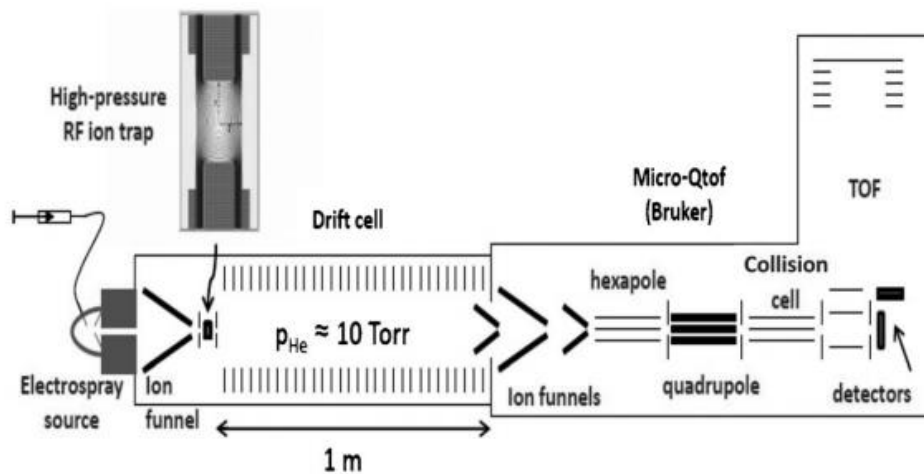


**Figure III.4:** schematic of the homemade IMS/MS setup of the ILM research group of Lyon.

## 2. Overview of the Mass Spectrometer Acquisition Modes

Depending on the mass spectrometer geometry, different analysis modes are available. The **table III.1** summarizes those acquisition modes for the mass spectrometers used in this thesis.

**Table III.1:** overview of the different analyses performed with the  
*Waters Q-ToF 2 and Synapt G2-Si.*

		Source ESI	Quadrupole	Hexapole			ToF	Detector
Q-ToF 2	MS	✓	RF	RF			↗	✓
	MSMS	✓	→	☀			↗	✓
Synapt G2-Si		Source ESI	Quadrupole	Trap	IMS	Transfer	ToF	Detector
	MS	✓	RF	RF	✗	RF	↗	✓
	MSMS	✓	→	☀	✗	RF	↗	✓
	IMMS	✓	RF	RF	✓	RF	↗	✓
	IM-MSMS (Trap)	✓	→	☀	✓	RF	↗	✓
	IM-MSMS (Transfer)	✓	→	RF	✓	☀	↗	✓
	TAP	✓	→	☀	✓	☀	↗	✓

### Table legend:



→ Element in active mode for the analysis



→ Element not used for the analysis



→ Element used as mass selector (fixed)



→ Scanned element



→ Element used as a collision cell

RF

→ Element used as an ion guide (RF-only mode)

### 3. Energy-Resolved Collision Induced Dissociation

Energy-resolved Collision Induced Dissociation (ER-CID) experiments are actually MSMS experiments (see annex section VI.1.1) performed to evaluate the kinetic of fragmentation by probing the decomposition efficiencies of ionized compounds after collision against the collision gas at different kinetic energy [4].

As a reminder, a MSMS experiment consists in accelerating ions with a specific  $m/z$  in a collision cell filled with a collision gas (usually Argon), the collision between the investigated ions and the atoms (molecules) of gas induce an increase of internal energy of the ions by converting a part of translational kinetic energy into internal energy ( $E_{int}$ , vibrational). This increase of internal energy, through all the vibrators, finally induces fragmentation as soon as the energy overcomes the so-called critical energy of dissociation, say the activation or threshold energy for dissociation ( $\epsilon_0$ ). Accordingly, if all those steps occur inside the collision-cell, the energy needed to fragment 50% of the selected parent ions can be evaluated. The RRKM theory (Rice–Ramsperger–Kassel–Marcus) describes the influence of the ion internal energy ( $E_{int}$ ) on the decomposition reaction rate with **equation 1** [5]:

$$k = \nu \left[ \frac{E_{int} - \epsilon_0}{E_{int}} \right]^{n-1}$$

**Equation 1**

where  $k$  is the fragmentation reaction kinetic constant,  $E_{int}$  is the ion internal energy,  $n$  the number of oscillators in the ion,  $\nu$  is the frequency factor and  $\epsilon_0$  is the activation energy for dissociation. This last value corresponds to the minimum energy required for  $k > 0$  (see **figure III.5**). The parameters  $n$  and  $\nu$  depend on the ion structure and the reaction channel [5]. The frequency factor  $\nu$  is defined by the entropy factor of the transition state  $\Delta S^*$  ( $\nu = \left( \frac{E_{int} - \epsilon_0}{h} \right) e^{\Delta S^*/R}$ )

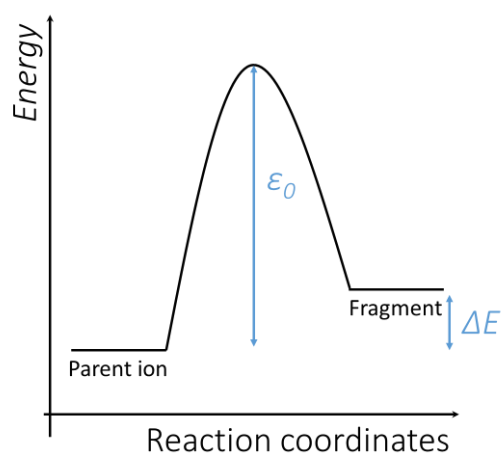


**Figure III.5:** representation of  $\epsilon_0$ .

which decreases when the activated complex is more ordered resulting in a decrease of the frequency factor and of the reaction rate [5].

To perform an energy-resolved CID experiment, the CID spectra of mass-selected ions are recorded by varying the kinetic energy of the ions prior to the collisional activation step [6] in order to evaluate the influence of the accelerating energy on the decomposition efficiencies of ionized compounds.

The result of energy-dependent-CID experiments for a given mass-selected parent ion is a survival yield curve with a sigmoidal-like shape (**figure III.6**) reporting the fraction of the precursor ions which survives in a CID reaction (Survival Yield).

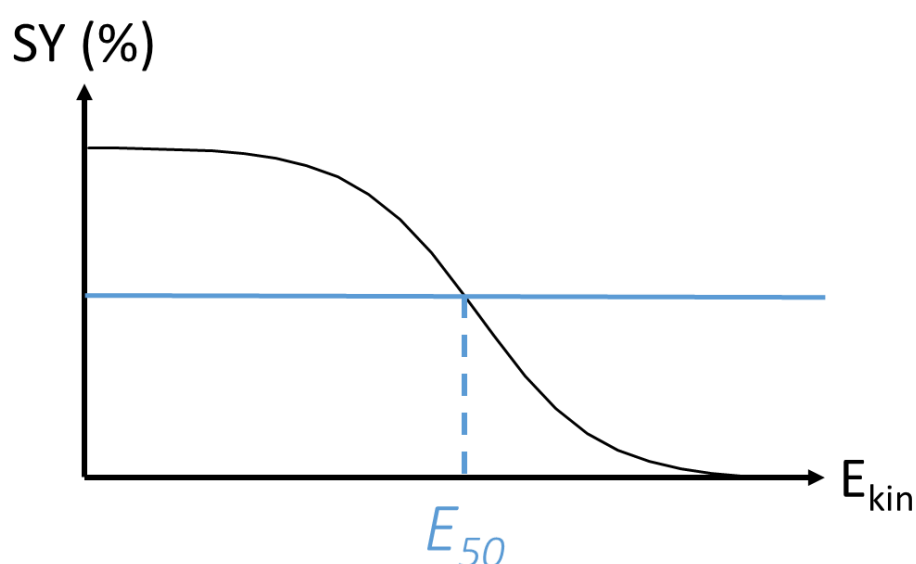


**Figure III.6:** representation of the survival yield (SY) curve obtained by performing an ER-CID experiment.

In the previous description (**figure III.6**), the energy applied to the ions is the collision energy, which is a parameter that can be modified in the mass spectrometer. Nevertheless, this description is not fully correct. Indeed, the total energy acquired by the ions through collisions with the buffer gas cannot be only linked to the collision energy ( $E_{lab}$ ) potential since those collisions are inelastic. Therefore, the  $E_{lab}$  parameter has to be replaced by the center of mass energy ( $E_{CM}$ ) in order to take into account the inelastic nature of the ion-gas collisions (**equation 2**) [5].

$$E_{CM} = \frac{z(E_{lab})m_{gas}}{m_{gas} + m_{ion}}$$

**Equation 2**

In this formula,  $z$  is the ion charge,  $m_{ion}$  is the ion mass,  $m_{gas}$  is the buffer gas mass and  $E_{lab}$  is the collision energy set in the laboratory reference system. The center of mass energy is defined as the maximum energy transferred to an ion per collision with a gas molecule. Additionally, ECM is also an approximation while more than one collision occurs in our system.

## 4. Collision Cross Section Calibration Method for TWIMS

### Analysis

As mentioned earlier, for DTIMS measurement, a linear relationship exists between the measured ion drift-time and their experimental collision cross-section (namely the equation of **Mason-Schamp**).

However, the Waters Synapt G2-Si presented above is equipped with a Traveling Wave Ion Mobility Spectrometry (TWIMS) drift-cell for which a power function correlates the ion drift-time ( $t_D$ ) and their CCS ( $\Omega_{avg}$ ) through **equation 3** [7-8]:

$$\Omega_{avg} = \frac{\sqrt{18}}{16} \frac{q}{\sqrt{\mu k_B T}} \sqrt{\frac{1}{m_I} + \frac{1}{m_N}} \frac{760}{p} \frac{T}{273.2} \frac{1}{N} A t_D^B$$

**Equation 3**

In this equation,  $q$  is the ion charge,  $k_B$  the Boltzmann constant,  $T$  the temperature,  $m_I$  and  $m_N$  are respectively the ion mass and the drift-gas mass,  $P$  is the pressure within the drift-cell,  $N$  is the mobility gas density and  $A$  and  $B$  are constants.

In **equation 4**,  $\Omega_{avg}$  has been simplified into  $\Omega'$ , which corresponds to the ion collisional cross section freed from the charge and reduced mass of the ion-gas system. Consequently, getting freed from the ion-gas system permits to measure cross-sections regardless of the drift-gas used to perform the ion mobility experiments. All constant values are included into  $A'$  [8].

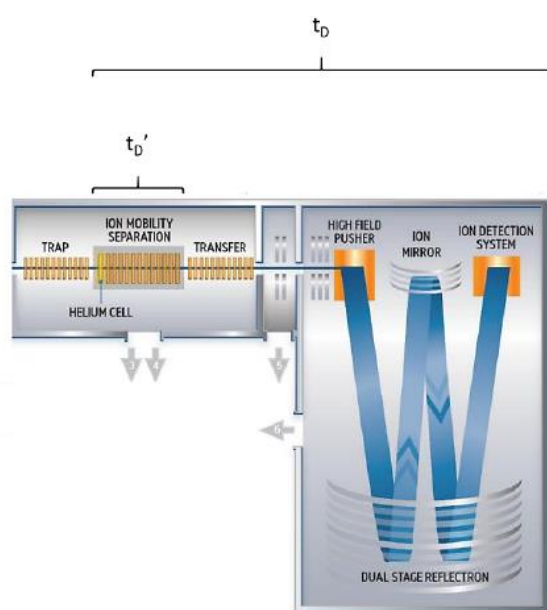
$$\Omega' = A' t_D^B$$

**Equation 4**

The relationship presented in **equation 4** deeply depends on the experimental parameters and on the ion charge state. Accordingly, the constants  $A$  and  $B$  have to be determined using a calibration method in order to convert the TWIMS measured ion drift-times into experimental CCS.

The calibration method presented here below is decomposed in five different steps and the protocol is described within the literature [9]. The purpose of each step is to correct the ion drift-times but also to free the collisional cross-section of the ions from their charge and from the drift-gas employed for measurements. For clarity, each of those five steps will now be detailed:

- I. Firstly, the molecules used for calibration (polyalanines in this case) have to be analyzed within the TWIMS in order to determine the drift-times of each signal/ion. Those drift-times will first be corrected through **equation 5**. This correction allows the determination of the “true” ion drift-times without taking in account the death time of the instrument. Indeed, since the ion drift-times are only measured at the detector of the mass spectrometer, the “true” drift-time of the ions is tainted by a death time corresponding to the time spent by the ions from the end of the mobility cell to the detector (see **figure III.7**).



$$t_D' = t_D - \frac{C\sqrt{m/z}}{1000}$$

**Equation 5**

In this equation,  $t_D'$  is the corrected effective mobility drift-time,  $t_D$  is the experimental drift-time and the constant  $C$  is a parameter defined by the mass spectrometer (namely EDC for enhanced duty cycle). In the case of the Waters Synapt G2-Si used in this PhD,  $C$  equals 1,51. The furnisher provides this value [9].

**Figure III.7:** representation of the effective drift time ( $t_D'$ ) in the Waters Synapt G2-Si.

- II. According to **Ruotolo** [9], the reference CCS  $\Omega_{\text{Ref}}$  must also be corrected to afford a charge and mass independent quantity. Therefore, **equation 6** presents the correction brought to the CCS presented in literature ( $\Omega$ , using helium). In this equation,  $\Omega'$  is the corrected CCS when performing IMS experiments in nitrogen,  $\Omega$



III. Experimental part

is the CCS obtained in helium,  $z$  is the charge of the ion and  $\mu$  is the reduced mass of the ion-N<sub>2</sub> system.

$$\Omega' = \frac{\Omega}{z \sqrt{\frac{1}{\mu}}}$$

**Equation 6**

- III. When plotting  $\ln t_d'$  as a function of  $\ln \Omega'$  (**figure III.8**), the following linear equation is obtained:  $\ln \Omega' = B \ln t_d' + \ln A$

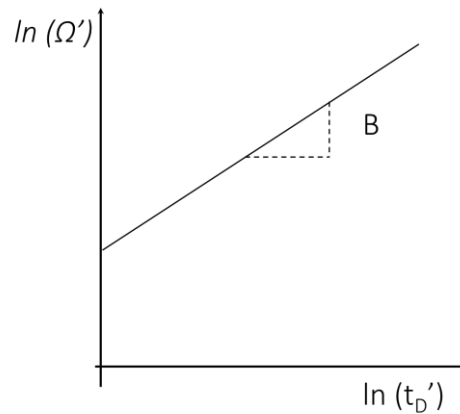


**Figure III.8:** representation of the relation between  $\ln \Omega'$  and  $\ln t_d'$ .

The  $B$  factor is called the exponential factor (see **equation 7** hereafter).

- IV. In order to obtain a linear relationship between  $\Omega$  and  $t_D$ , the effective drift-time  $t_D'$  has to be corrected through **equation 7**. This correction regarding the charge of the ions allows the drift-time to be freed from the drift-gas nature. In this equation  $t_D''$  is the corrected drift-time,  $X$  the exponential factor (obtained in III),  $z$  the ion charge and  $\mu$  the reduced mass of the ion-N<sub>2</sub> system.

$$t_D'' = t_D' X z \sqrt{\frac{1}{\mu}}$$

**Equation 7**

- V. Finally, by plotting  $t_D''$  as a function of  $\Omega$  (**figure III.9**), a linear equation is obtained between the calibrant ion drift-times and their CCS.

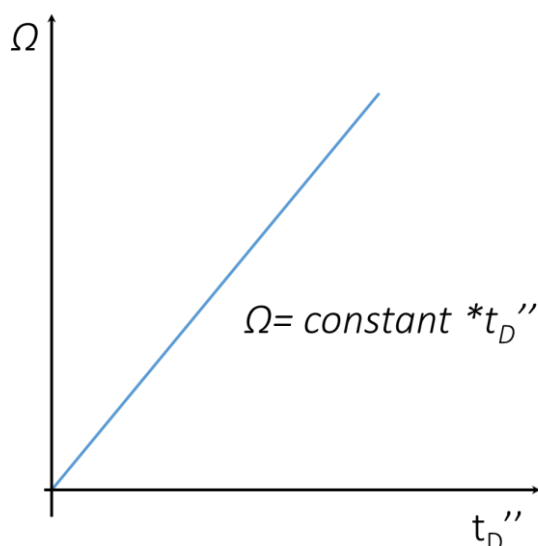


**Figure III.9:** representation of the relation between  $\Omega$  and  $t_D''$ .

This relationship allows for the determination of ion CCS from their TWIMS measured drift-times ( $t_D$ ) corrected to obtain  $t_D''$ . Nevertheless, the relationship obtained through those five steps will be applicable only if the drift-times of the samples are determined using the exact same experimental conditions (wave height, velocity, mass range, pressure, etc.) as those used to obtain the calibrant molecules drift-times. In addition, the analyte ion CCS have to be included within the CCS range covered by the calibration [7-9].

## 5. Nuclear Magnetic Resonance Measurements

The NMR spectra are recorded at room temperature on an AVANCEII 500 spectrometer working at 500 MHz (Bruker, Karlsruhe, Germany). The samples are prepared with a mixture of  $D_2O$  and  $CD_3OD$  and a saturation of the residual water peak is applied on some spectra with the noesypr1d sequence. All spectra are recorded with 64 scans.

## 6. Materials

Para-phenylenediamine (1,4-diaminobenzene - DAPHEN), para-xylylenediamine (PXD), adamantylamine (ADAM), para-toluidine (TOLU), aniline, 2 and 4-chloroaniline, 2 and 4-bromoaniline, 4-iodoaniline, propargylamine, azidoethyl amine, cucurbit[6]uril (CB[6]) and cucurbit[7]uril (CB[7]) were commercially available (Sigma Aldrich) and were used without further purification except when the amino-compounds presented a brown color, they were then distilled. The bis-nor-seco-cucurbit[10]uril (ns-CB[10]) was synthesized following the literature procedure [10]. We would like to thank Professor Lyle Isaacs (Department of Chemistry and Biochemistry, University of Maryland, College Park, MD 20742, USA) for providing us the bitopic cucurbit[10]uril host molecule.

The host stock solution ( $10^{-3}$ M) was prepared in formic acid/water (50:50). The guest stock solutions ( $5 \cdot 10^{-3}$ M) were prepared in methanol/water (80:20) with 1% HCOOH. HPLC-grade solvents were used for all solutions (Sigma-Aldrich). The analyte solutions (host:  $10^{-4}$  M and guest:  $5 \cdot 10^{-4}$  M) were prepared using a solvent mixture composed of water/methanol 80/20.

## 7. Theoretical calculations

All molecular structures reported herein have been optimized at the Density Functional Theory (DFT) level using the B97D functional and a 6-31 G(d,p) basis set. Analysis of the calculated vibrational modes of each optimized structure confirmed that they correspond to energy minima. The reported energies are Gibbs free energies corrected for the Basis Set Superposition Error (BSSE). All DFT-calculations have been performed with the Gaussian09 package [11]. The optimized structures have then been injected in the MOBICAL program using the Trajectory Method [12] to derive Collisional Cross Sections (CCS) readily comparable with the data generated by the ion mobility experiments.

For more details about Density Functional Theory and Mobcal, please refer to the annex section of this PhD manuscript.

## References

1. M. F. Bush, I. D. G. Campuzano and C. V. Robinson, *Anal.Chem.*, 2012; 84: 7124-7130.
2. F. Albrieux, F. Calvo, F. Chirot, A. Vorobyev, Y. O. Tsybin, V. Lepère, R. Antoine, J. Lemoine, P. Dugourd, *J. Phys. Chem. A* 2010 ;114 : 6888 –6896.
3. F. Albrieux, R. Antoine, F. Chirot, J. Lemoine, P. Dugourd, *Eur. J. Mass Spectrom.* 2010, 16, 557–565.
4. K. M. Ervin., *Chem. Rev.* 2001; 101: 391-444.
5. L. Sleno, D.A. Volmer, *J. Mass. Spectrom.* 2004; 39: 1091-1112.
6. a) P. B. Armentrout, *Top. Curr. Chem.* 2003; 225: 233-262; b) A. Pak, D. Lesage, Y. Gimbert, K. Vékey, J.C. Tabet, *J. Mass Spectrom.* 2008; 43: 447–455, c) T.M. Kertesz, L.H. Hall, D.W. Hill, D.F. Grant, *J. Am. Soc. Mass Spectrom.* 2009; 20: 1759–1767.
7. F. Lanucara, S.W. Holman, C.J. Gray, C.E. Eyers, *Nat. Chem.* 2014; 6: 281–294 (2014).
8. D.P. Smith, T.W. Knapman, I. Campuzano, R.W. Malham, J.T. Berryman, S.E. Radford, A.E. Ashcroft, *Eur. J. Mass Spectrom.* 2009; 15: 113-130.
9. B.T. Ruotolo, J.L.P. Benesch, A.M. Sandercock, S. Hyung, C.V. Robinson, *Nat. Prot.* 2008; 3: 1139-1152.
10. a) W.-H. Huang, S. Liu, P. Y. Zavalij, L. Isaacs, *J. Am. Chem. Soc.* 2006; 128: 14744–14745; b) R. Nally, L. Isaacs, *Tetrahedron* 2009; 65: 7249–7258; c) J. B. Wittenberg, M. G. Costales, P. Y. Zavalij, L. Isaacs, *Chem. Commun.* 2011; 47: 9420–9422.
11. Gaussian 09, Revision A.02, M. J. Frisch, G. W. Trucks, H. B. Schlegel, G. E. Scuseria, M. A. Robb, J. R. Cheeseman, G. Scalmani, V. Barone, B. Mennucci, G. A. Petersson, H. Nakatsuji, M. Caricato, X. Li, H. P. Hratchian, A. F. Izmaylov, J. Bloino, G. Zheng, J. L. Sonnenberg, M. Hada, M. Ehara, K. Toyota, R. Fukuda, J. Hasegawa, M. Ishida, T. Nakajima, Y. Honda, O. Kitao, H. Nakai, T. Vreven, J. A. Montgomery, Jr., J. E. Peralta, F. Ogliaro, M. Bearpark, J. J. Heyd, E. Brothers, K. N. Kudin, V. N. Staroverov, R. Kobayashi, J. Normand, K. Raghavachari, A. Rendell, J. C. Burant, S. S. Iyengar, J. Tomasi, M. Cossi, N. Rega, J. M. Millam, M. Klene, J. E. Knox, J. B. Cross, V. Bakken, C. Adamo, J. Jaramillo, R. Gomperts, R. E. Stratmann, O. Yazyev, A. J. Austin, R. Cammi, C. Pomelli, J. W. Ochterski, R. L. Martin, K. Morokuma, V. G. Zakrzewski, G. A. Voth, P. Salvador, J. J. Dannenberg, S. Dapprich, A. D. Daniels, O. Farkas, J. B. Foresman, J. V. Ortiz, J. Cioslowski, and D. J. Fox, Gaussian, Inc., Wallingford CT (2009).
12. M. F. Mesleh, J. M. Hunter, A. A. Shvartsburg, G. C. Schatz and M. F. Jarrold, *J. Phys. Chem.*, 1996; 100: 16082-16086.

## IV. Results and discussion

## Chapter 1:

Influence of Equilibration Time in Solution on the Inclusion/Exclusion Topology Ratio of Host-Guest Complexes Probed by Ion Mobility and Energy-Resolved Collision-Induced Dissociation.

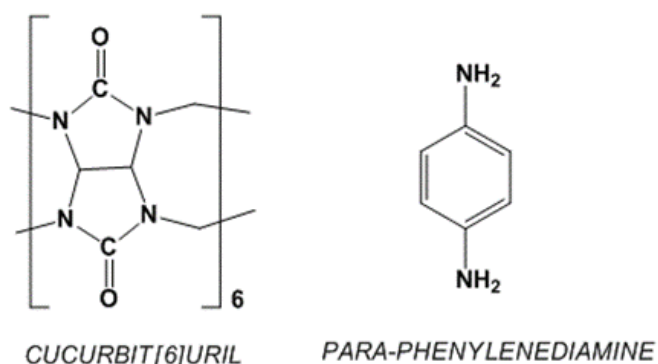
*G. Carroy, C. Daxhelet, V. Lemaur, J. De Winter, E. De Pauw, J. Cornil, P. Gerbaux*

*Chemistry, A European Journal 2016 ; 22 : 4528-4534.*

---

## 1.1 Introduction

The cucurbit[n]uril, CB[n], family of molecular containers has attracted a huge interest in the recent years [1]. Cucurbit[n]urils are macrocyclic molecules constituted by the association of  $n$  glycoluril repeat units, see **scheme IV.1.1**. These pumpkin-shaped molecules present a hydrophobic inner cavity and two identical carbonyl-laced portals and form stable inclusion complexes with various protonated alkyl and aryl (di)amines [1]. The popularity of CB[n]s is largely due to their outstanding recognition properties, and to the exceptional strength of their interaction with various guests. As a typical example, Mock et al determined using NMR experiments that alkylammonium ions bind to CB[6] in acidic aqueous media with binding constants in the  $10^1$ – $10^7$   $M^{-1}$  range [2]. The high affinities are inter alia caused by the high rigidity of the macrocycles and by the coulombic interactions between positively charged substituents of host molecules and the CB[n] rims. In contrast to the behavior of most synthetic receptors in aqueous solution, the CB[6] congener commonly displays slow kinetics of guest association and dissociation which might render the encapsulation kinetically rather than thermodynamically driven [3]. Actually, significant deformations of the rigid portals of the CB[6] receiver were shown to occur in the transition state to allow access to its interior part, thus reducing the kinetic constant for ingress ( $k_{\text{ingress}}$ ) [3].



**Scheme IV.1.1:** Host and guest molecules selected for the present study: cucurbit[6]uril and para-phenylenediamine.

It is now admitted that the association and dissociation of the inclusion complexes between CB[n] and ammonium ions proceed via a transiently formed exclusion complex [4]. Nau et al proposed that the transition state connecting the exclusion complex to the inclusion complex

corresponds to a flip-flop process [5]. They also demonstrated that two mechanisms for ingress are competing for the complexation of amino/ammonium guest, depending on the pH of the solution, with an optimal pH at  $\text{pH} = \text{pKa}$  [5-6]. They further showed on the basis of NMR measurements the huge impact of the temperature and ionic strength on the kinetics and thermodynamics of complexation [6]. As a striking example, for the cyclohexylmethylamine/CB[6] system in  $\text{D}_2\text{O}$  (0.2M  $\text{Na}_2\text{SO}_4$ ), between 25°C and 60°C, the  $k_{\text{ingress}}$  was measured to increase by a factor 200, from 0.79 to  $150 \cdot 10^3 \text{ M}^{-1}\text{s}^{-1}$ . For large guests presenting favorable binding constants with CB[6], no complexation is observed, even with a large guest excess, either at elevated temperature or over prolonged times (up to 1 year), essentially for kinetic reasons [6].

Recently, Dearden and Jarrold examined complexes between cucurbit[6]uril and the ortho-, meta-, and para-phenylenediamine isomers using computational methods together with tandem mass spectrometry and ion mobility [7]. In particular, they obtained evidences for the presence of internal and external complexes within the ion beam constituted by the singly charged binary complexes between para-phenylenediamine and CB[6]. They also noted the exclusive presence of inclusion complexes for the doubly charged binary complexes [7]. Numerous studies dealing with mass-spectrometry (MS) analysis of cucurbituril complexes are reported in the literature, most of them being performed by the groups of Dearden at the Brigham Young University [8] and Nau and coworkers at Jacobs University Bremen [9]. However, to the best of our knowledge, none of these MS-based investigations focused on the kinetics of the complexation reactions. In the present communication, we use ion mobility experiments on a Waters Synapt G2-Si mass spectrometer to monitor the inclusion/exclusion topology ratio all along the reaction time. The assignment of the topology of the ions separated by ion mobility will be achieved on the basis of (energy-resolved) collision-induced dissociation experiments and further corroborated by calculating the collisional cross sections using topologies generated by computational chemistry methods.

Theoretical calculations based on the Density Functional Theory (DFT) using the B97D functional accounting for dispersive forces [10] and a 6-31G(d,p) basis set will be performed to support our experimental observations, with a special emphasis on the determination of the relative energies of the inclusion/exclusion structures and collisional cross sections. CB[6] and para-phenylenediamine (DAPHEN) were selected as the model system, see ***scheme IV.1.1***,



for the present study taking into account that: (i) both the internal and external topologies have already been observed and; (ii) some theoretical data are already reported in the literature [7].

## 1.2 Results and discussion

When a solution containing an equimolar mixture ( $10^{-5}\text{M}$ ) of CB[6] and DAPHEN is sprayed into the gas phase using the ESI source, the full scan source mass spectrum presented in **figure IV.1.1** is typically recorded. This spectrum features several peaks corresponding to different singly (+1) and doubly (+2) charged ions. Three peaks immediately confirm the interaction between the cucurbituril host molecule and the guest molecule DAPHEN and are observed at  $m/z$  1105,  $m/z$  553 and  $m/z$  607, for respectively  $[\text{CB}[6]+\text{DAPHEN}+\text{H}]^+$ ,  $[\text{CB}[6]+\text{DAPHEN}+2\text{H}]^{2+}$  and  $[\text{CB}[6]+2\text{DAPHEN}+2\text{H}]^{2+}$ . For the present discussion, we will only focus on the two binary complexes at  $m/z$  1105 and  $m/z$  553 highlighted in bold in **figure IV.1.1**.

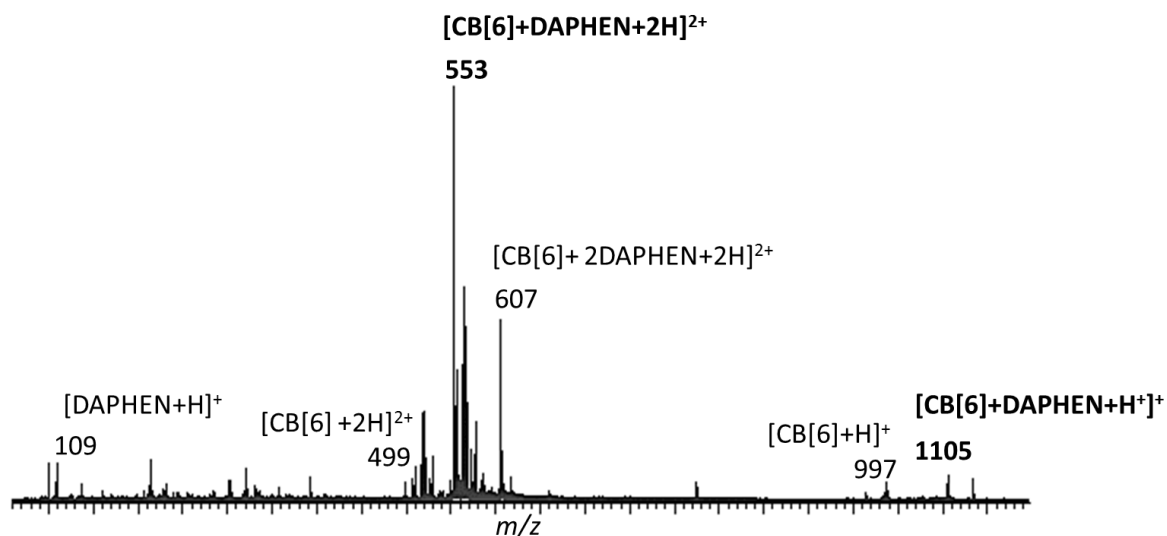


**Figure IV.1.1:** ESI-MS analysis of an equimolar solution of ( $10^{-5}\text{M}$ ) of CB[6] and para-phenylenediamine recorded on a Waters Synapt G2-Si mass spectrometer.

In their 2009 paper, Dearden et al already studied this system using mass spectrometry together with theoretical calculations [7]. Using ion mobility, they showed that the ions at  $m/z$  1105, i.e., the singly charged 1:1 complexes, are detected both as inclusion and exclusion complexes. As gathered in **table IV.1.1**, the experimental collisional cross sections (CCS)

#### IV. Results and discussion

respectively amount to 177 and 200 Å<sup>2</sup> for the internal and external topologies, as confirmed by the theoretical CCS of 184 and 201 Å<sup>2</sup> (left side of **table IV.1.1**). The internal complexes have nearly the same cross section as protonated CB[6] (178 Å<sup>2</sup> in Dearden's publication [7]), confirming that the guest molecule is totally entangled inside the cavity [7]. As far as the 2+ binary complex ions are concerned, only the inclusion topology was observed by Dearden et al with a characteristic CCS of 178 Å<sup>2</sup>. The structures and relative energies of the lowest energy internal and external 1:1 doubly charged complexes presented in **table IV.1.1** were determined at the quantum-chemical level. In reference [7], exact hard sphere collisional cross sections were calculated from the lowest-energy structures obtained using HF/6-31G\* methods (**table IV.1.1**).

**Table IV.1.1:** Inclusion and exclusion complexes associating DAPHEN and CB[6] : relative energies and collisional cross sections. <sup>a</sup> charge state of the detected complex ions; <sup>b</sup> from reference [7]; <sup>c</sup> relative energies obtained at the B3LYP/6-31G\*\*/HF/6-31G\* level of theory in reference [7]; <sup>d</sup> relative energies and collisional cross sections obtained in the present study (see text); <sup>e</sup> not determined (n.d.) in reference [7]; <sup>f</sup> exclusion conformations with the doubly protonated guest lying on one of the two portals; <sup>g</sup> not observed (n.o.) in reference [7]; <sup>h</sup> two different protomers, see text; <sup>i</sup> exclusion conformations with the doubly protonated guest lying on one of the two portals, see text.

		Dearden et al [7]			Results of our study			
Topology		Relative Energy <sup>b</sup> (kcal/mol)	CCS <sub>th</sub> (Å <sup>2</sup> ) <sup>b</sup>	CCS <sub>exp</sub> (Å <sup>2</sup> ) <sup>b</sup>	N	Relative Energy <sup>d</sup> (kcal/mol)	CCS <sub>th</sub> (Å <sup>2</sup> ) <sup>d</sup>	CCS <sub>exp</sub> (Å <sup>2</sup> ) <sup>d</sup>
<b>+1<sup>a</sup></b>	Inclusion	n.d. <sup>e</sup>	184	177	<b>1</b>	0	188	n.o.
	Exclusion	n.d. <sup>e</sup>	201	200	<b>2</b>	23	214	217
<b>+2<sup>a</sup></b>	Inclusion	0	184	178	<b>3</b>	0	190	202
	Exclusion	20 <sup>c,f</sup>	201 <sup>f</sup>	n.o. <sup>g</sup>	<b>4</b>	35 <sup>h</sup>	218 <sup>h</sup>	219
					<b>5</b>	46 <sup>i</sup>	203 <sup>i</sup>	
					<b>6</b>	49 <sup>i</sup>	203 <sup>i</sup>	
<b>7</b>					53 <sup>h</sup>	216 <sup>h</sup>		

Structural optimization calculations have been made here using DFT at the B97D 6-3,1g(d,p) level of theory, that explicitly accounts for the dispersive forces, in contrast to the HF approach. In a recent paper, we successfully used this theoretical method for the study of ternary complexes associating amino guests to a ditopic cucurbituril receptor [14]. Two stable structures for the [CB[6]+DAPHEN+H]<sup>+</sup> complex have also be obtained and are presented in **figure IV.1.2**.

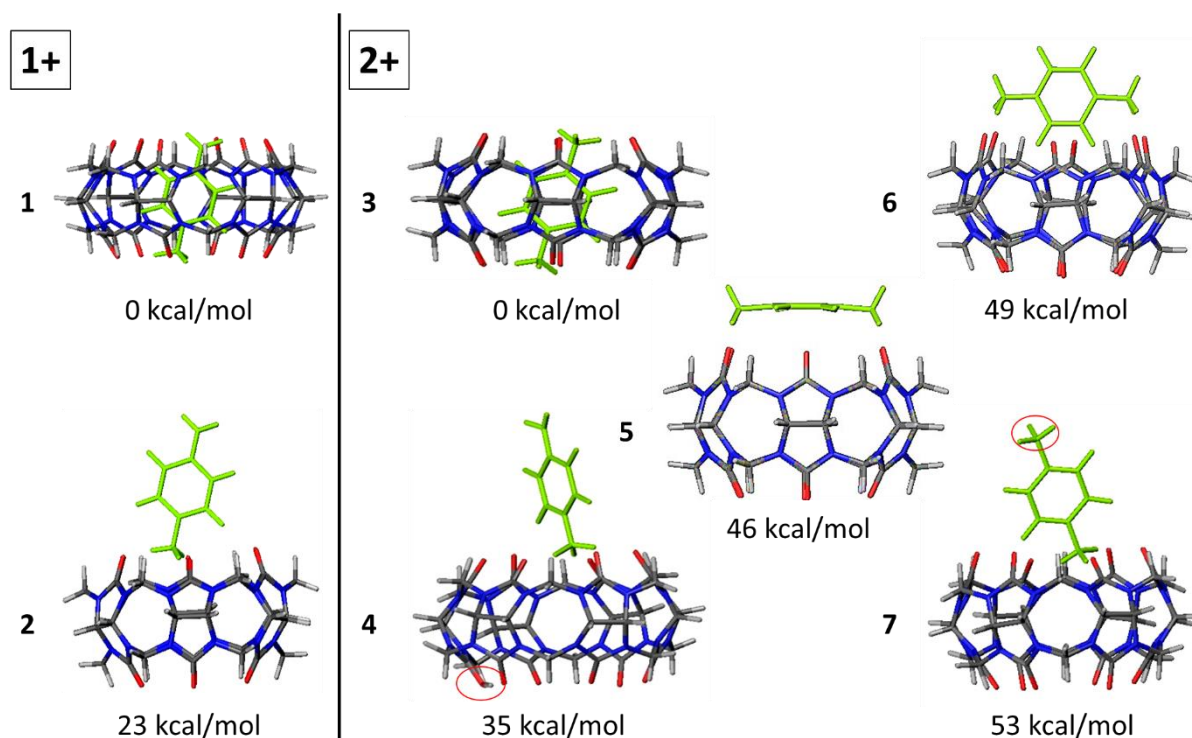


**Figure IV.1.2:** Optimized structures and relative energies (kcal/mol) (B97D, 6-31g(d,p)) for the inclusion and exclusion 1:1 complexes associating para-phenylenediamine to CB[6].

As expected, the inclusion complex (**1**, see **table IV.1.1** and **figure IV.1.2**) represents the global minimum on the potential energy surface lying 23 kcal/mol lower than the exclusion complex (**2**, see **table IV.1.1**). We also determined the CCS that are found to be quite similar from the data in the previous study [7]. In the case of the doubly charged 1:1 complex ions  $[\text{CB}[6]+\text{DAPHEN}+2\text{H}]^{2+}$ , the inclusion topology (**3** in **figure IV.1.2**) is also calculated to be more stable than the exclusion complexes (**4-7**), see **table IV.1.1**. For the exclusion topology, among the different theoretical structures, we identified two different protomers (**4** and **7**), with **4** found to be the more stable, see **table IV.1.1** (right side) and **figure IV.1.2**. Indeed, whereas one of the proton is bound onto the nitrogen atom of the guest molecule, the second proton can either be attached on the second nitrogen atom of the guest or on an oxygen atom of the opposite carbonyl rims of the cucurbituril receptor. The CCS of these three optimized complex ions (**3**, **4**, **7**) are calculated to be respectively 190 and 216/218 Å<sup>2</sup> for the inclusion and exclusion complexes. The negligible difference between the CCS of the protomers for the exclusion topology will certainly preclude their experimental distinction. In their report, Dearden et al proposed, on the basis of their calculations, that, for the doubly charged

exclusion complex ions, the doubly protonated guest molecule is lying on the carbonyl rim with both ammonium groups in close interaction with the carbonyl oxygen atoms (like structure **6**) [7]. At the B97D/6-31G(d,p) level of theory, we also identified two topologies presenting such a spatial arrangement, one with the benzene ring lying parallel to the rim (**5**, 46 kcal/mol above the inclusion topology) and the other with a perpendicular layout (**6**, 49 kcal/mol less stable than the inclusion topology), see **figure IV.1.2**. Nevertheless, none of these two arrangements is the most stable structure for the exclusion complexes, see **table IV.1.1** and **figure IV.1.2**.

When exposed to ion mobility experiments (**figure IV.1.3**), the 2+ 1:1 complexes, detected at  $m/z$  553, are separated into two ion families, according to their inclusion/exclusion topologies. From the measured drift times, the corresponding collisional cross sections are derived by calibrating the drift time scale with standards of known CCS [11]. We measured two CCS at respectively 202 and 219 Å<sup>2</sup> that are in very good agreement with the theoretical CCS for the most stable inclusion (**3**) and exclusion (**4**) complexes, see **table IV.1.1**. We assume that the exclusion topology corresponds to the most stable protomer identified as (**4**) since this conformation is about 20 kcal/mol more stable than (**7**). Interestingly, in their studies, Dearden et al [7] only observed the doubly charged inclusion complexes. On the other hand, and again at odd with Dearden's report, the singly charged 1:1 complexes ( $m/z$  1105) are here only detected with the exclusion topology characterized by a  $CCS_{exp}$  of 217 Å<sup>2</sup>, see **figure IV.1.3**. The discrepancies between our results and the literature data partially originate from different instrumental conditions during the production and the transfer of the ions. As a matter of fact, we are running our experiments inside a Waters Synapt G2-Si instrument, whereas the literature results were obtained on a home-built apparatus consisting of an electrospray source associated in sequence to a temperature-variable drift tube and a quadrupole mass spectrometer [7].

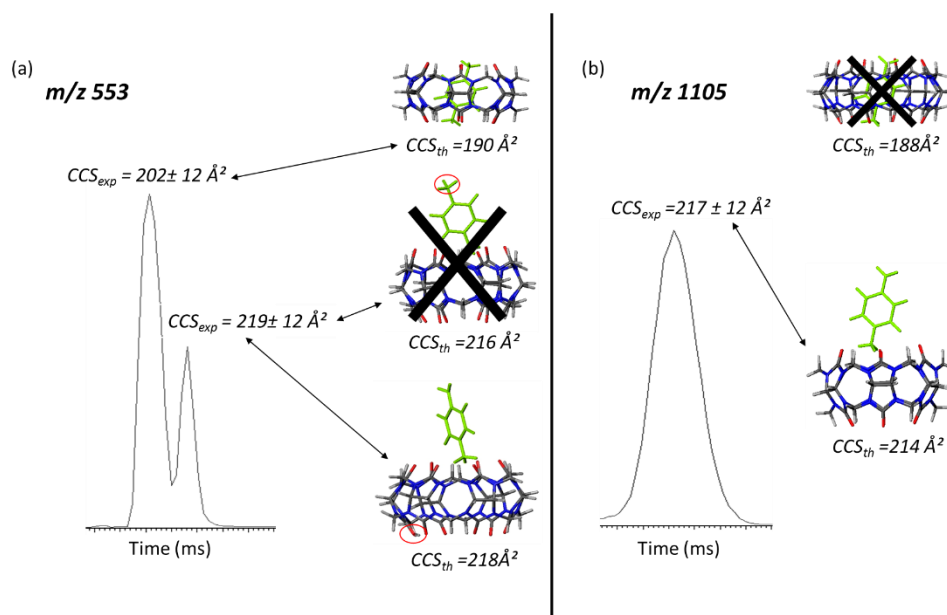


**Figure IV.1.3:** Ion Mobility-Mass Spectrometry plot (IM-MS plot) for the (a) doubly charged 1:1 complexes and (b) singly charged 1:1 complexes associating one *para*-phenylenediamine guest to one CB[6] host.

In addition, when looking carefully at the experimental conditions used in Dearden's paper, we also observed that, whereas we are running experiments under stoichiometric conditions, Dearden et al used at least a two-fold excess of *para*-phenylenediamine, rendering the production of non-specific adduct ions, such as ternary complexes for instance, more likely to occur during the Electrospray process.

Another aspect that must be taken into account is that the ingress processes within the CB[6] cavity are often characterized by really low kinetic constants (see Introduction), rendering the equilibrium state really slow to reach. We thus decided to undertake a kinetic study by considering the evolution of the inclusion/exclusion ratio along the reaction time. This reaction time is defined in the present study as the time between the preparation of the solution (at a given temperature) and the infusion within the Electrospray source (without any dilution) of the mass spectrometer.

As illustrated in **figure IV.1.4**, after 1 hour equilibration time at 25°C, the *m/z* 553 ion beam is mainly constituted by exclusion complexes. However, the inclusion/exclusion ratio is clearly modified over time and, at 25°C, almost 24 hours are required for a quantitative inclusion. As expected, when increasing the temperature to 50°C, the inclusion process is occurring faster

and, after 2 hours, the exclusion complex ions have almost totally disappeared. To the best of our knowledge, this is the very first time that such a kinetic evolution is followed by ion mobility mass spectrometry.

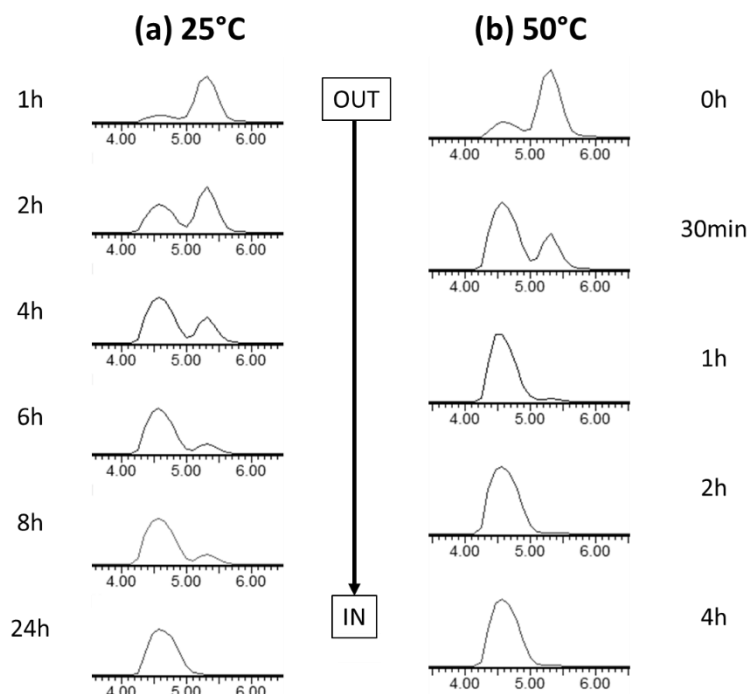


**Figure IV.1.4:** Time evolution (hours) of the IM-MS plot for the doubly charged 1:1 complex ions obtained upon electrospray ionization of a stoichiometric DAPHEN/CB[6] solution thermalized at (a) 25°C and (b) 50°C.

We have also plotted the time evolution of the  $m/z$  553 ion beam relative composition by extracting from the ion mobility plot the surface specific of the inclusion topology and dividing it by the total area associated with both topologies. Doing so, we obtained the kinetic plot in **figure IV.1.5** that reveals that an upper limit of 24 hours (25°C) is required to get the molar fraction of inclusion complexes within the  $m/z$  553 ion beam close to unity. One could imagine deriving this plot from an original analytical method to determine the kinetic parameters of the complexation reaction in solution. Nevertheless, such an extrapolation would certainly be corrupted by the intrinsic differences between the observed inclusion and exclusion complexes. Indeed, whereas we can clearly set that the inclusion complexes are directly extracted from the solution, this is not true for the exclusion complexes that are likely to be mainly stabilized during the final step of the Electrospray process which could lead to the formation of non-specific associations between the phenylene guest and the CB[6] host.

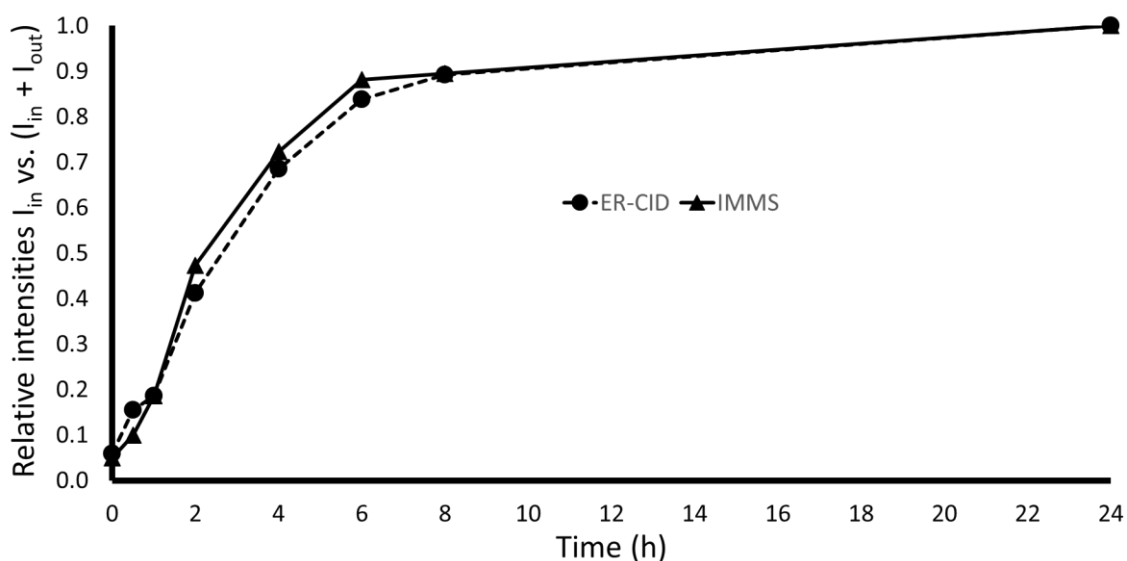


**Figure IV.1.5** Time evolution by ion mobility (IMMS) and energy-resolved CID (ER-CID) of the molar ratio of inclusion complexes of the doubly charged 1:1 complex ions obtained upon electrospray ionization of a stoichiometric DAPHEN/CB[6] solution thermalized at 25°C.

Moreover, depending on the source and ion optic topologies and energetics, both complexes are not likely to be transferred to the same extent from the ion source to the ion mobility cell. Indeed, exclusion complexes are probably more prone to dissociation than their inclusion isomers upon activation, leading to an overestimation of the inclusion/exclusion ratio. With the Tri-Wave technology, we are able to perform an energy-resolved collision-induced dissociation on the exclusion/inclusion complex ions after their separation by ion mobility. This experiment, presented in **figure IV.1.6 a**, clearly confirms the higher stability against CID of the inclusion complexes with an  $E_{50}$  around 2 eV (center of mass energy for 50% drop of the parent ion signal intensity) whereas 50% of the exclusion complexes are already dissociated at 0.8 eV center-of-mass energy. To further shed light on the different behaviors, we analyzed the corresponding CID spectra in **figure IV.1.6**.



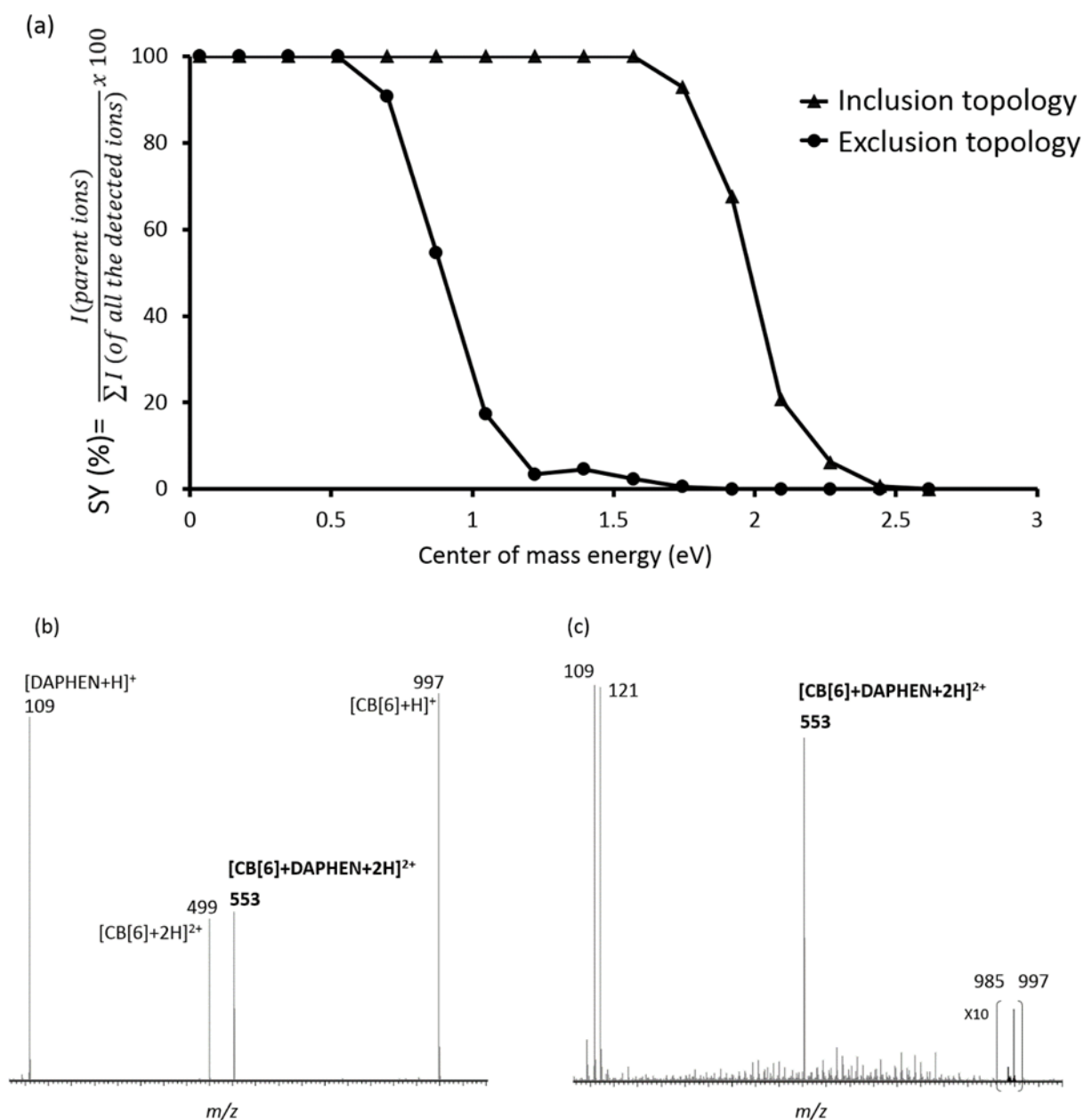


**Figure IV.1.6:** Energy-resolved CID experiments on the doubly charged 1:1 complex ions after ion mobility separation in the Triwave setup of the waters Synapt G2-Si: (a) ER-CID plot, (b) CID spectrum of the exclusion complexes and (c) CID spectrum of the inclusion complexes.

Upon CID, exclusion complexes mainly dissociate by rupture of the non-covalent interactions, see **figure IV.1.6 b**. Indeed, mass-selected  $m/z$  553 ions presenting the exclusion topology dissociate by competitive losses of protonated or neutral phenylenediamine. The neutral guest loss reaction affords doubly protonated CB[6] fragment ions that are detected at  $m/z$  499. The protonated guest loss corresponds to a charge separation process affording fragment

ions at  $m/z$  109 and  $m/z$  997, for respectively the protonated guest and the protonated host molecules.

As revealed in **figure IV.1.6 c**, the CID reactions undergone by the inclusion complexes are clearly different with the occurrence of multiple tiny signals that are likely to arise from the breaking of the covalent bonds constituting the host cage. Also, beside the huge signal at  $m/z$  109 for protonated DAPHEN, abundant  $m/z$  121 fragment ions are detected in the CID mass spectrum and their origin is not straightforward to identify.

We propose that the overall decomposition pathway is initiated by a proton transfer between the ammonium group of the protonated guest to one of the oxygen atom of the carbonyl rim of the host, see **figure IV.1.7 a**. The presence of the proton on the oxygen atom will then induce a backbone cleavage affording an inclusion complex from which the expulsion of the protonated guest molecule, detected at  $m/z$  109 in the CID spectrum, see **figure IV.1.7 b**, can occur. Competitively, within this inclusion complex, the lone electron pair of the amino group can interact with the carbenium group creating a covalent bond between both partners. As proposed in **figure IV.1.7 c**, an intermolecular proton transfer from the ammonium group to an oxygen atom can then occur through a favourable six-membered ring transition state, formally ending up with the transfer of a methylene group from the host macrocycle to the nitrogen atom of the guest molecule. Interestingly, all this sequence of reactions will generate a new inclusion complex associating a doubly protonated formaldimine, i.e. N-[4-aminophenyl]-methanimine, within a norseco-CB[6]. Finally, an additional proton transfer from the ammonium group of the guest to a nitrogen atom of the macrocycle will open the way to the preparation of the  $m/z$  121 and  $m/z$  985 cations, see **figure IV.1.7 d**. The complexity of the pathway together with the necessity to break covalent bonds is of course likely to induce the higher amount of internal energy required for the dissociation of the inclusion [15]. Interestingly, this mechanism also points to the drastic difference between the gas and the condensed phase decomplexation reactions.

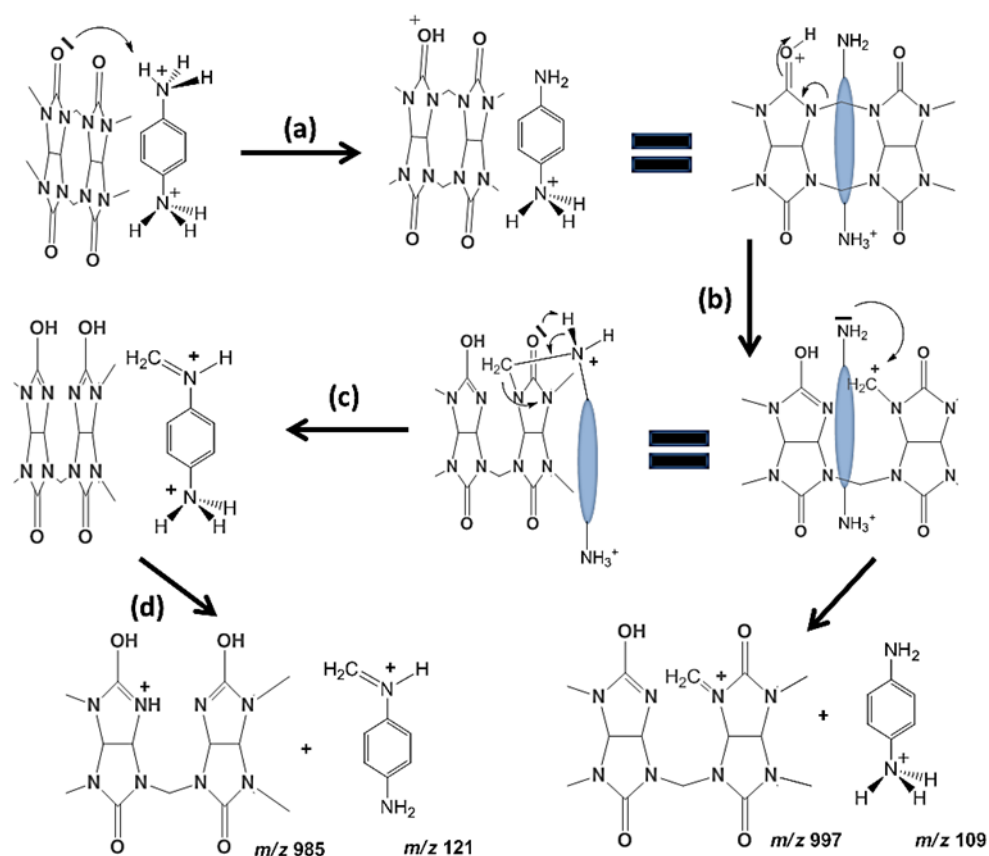


**Figure IV.1.7:** Collision-induced dissociation of 2+ inclusion complex associating para-phenylenediamine to CB[6]: mechanistic proposal for the production of the  $m/z$  109 and 121 cations.

In a recent paper dealing with the distinction of polymer topologies, we used energy-resolved collision-induced dissociation (ER-CID) methods to probe the molar ratio between two isomeric ions provided they are characterized by significantly different  $E_{50}$  [16]. Given the data recorded when associating in sequence ion mobility to ER-CID (**Figure IV.1.6 a**), we decided to submit to ER-CID experiments, without ion mobility separation, the doubly charged  $m/z$  553 ions and analyze the spectra as a function of time. **Figure IV.1.8** clearly reveals that the inclusion/exclusion ratio is related to the residence time in solution (at 25°C) prior to the ESI. The presence of a plateau between two step decreases around respectively 0.8 and 2 eV attests for the coexistence of (at least) two topologies. The plateau can be used to calculate the relative molar abundances between the exclusion and inclusion complexes.

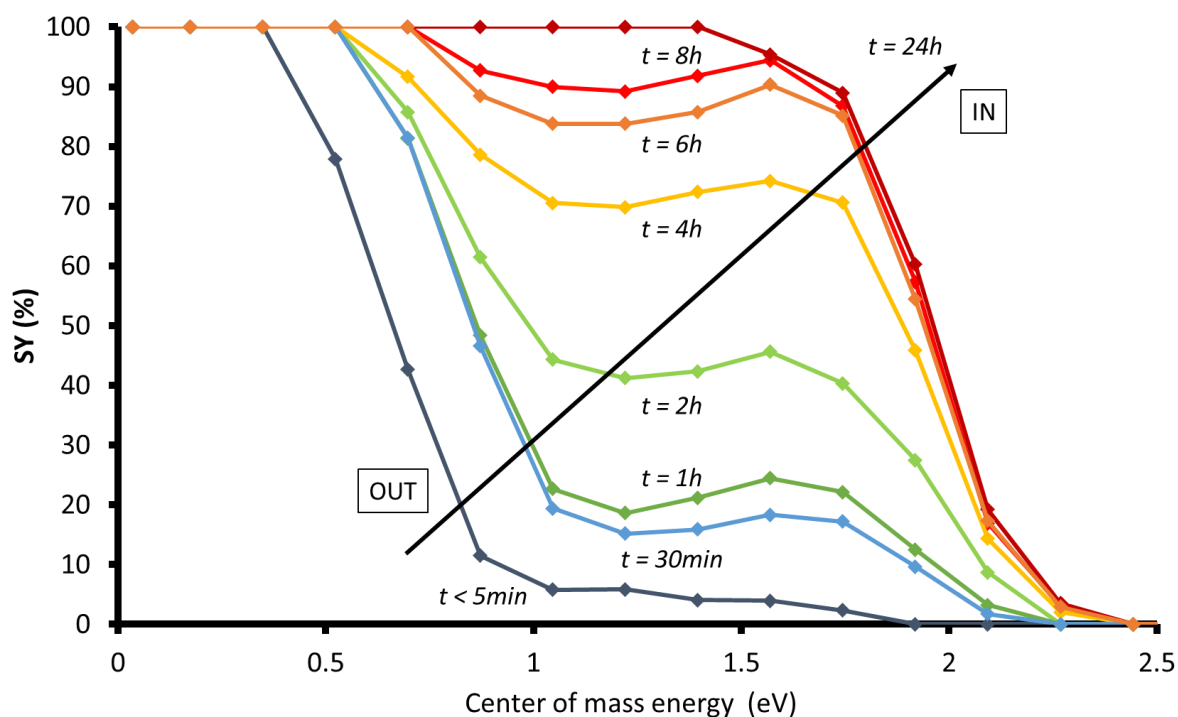


**Figure IV.1.8:** Time evolution of the energy-resolved CID curves for the doubly charged 1:1 complex ions ( $m/z$  553) at 25°C. The increase of the SY with center-of-mass energy at given times is due to the data analysis process. This basically arises from the setting of an intensity threshold (1%) for the fragment ion signals that renders the data processing sensitive to the opening of numerous dissociation routes for the inclusion complexes upon covalent bond breaking of the CB[6] ring (see **figure IV.1.6 c**).

In **figure IV.1.5**, we plotted the so-obtained molar ratio as a function of time in solution; we observe a really nice superimposition with the data generated upon ion mobility experiments, demonstrating the robustness of both methods to measure the relative abundances of complexes with different topologies for a given mass-to-charge ratio.

### 1.3 Conclusions

State-of-the-art mass spectrometry methods such as electrospray ionization, energy-resolved collision-induced dissociation and ion mobility are nowadays increasingly used in the context of host-guest chemistry for the structural characterization of non-covalent assemblies. Most of the MS-based studies are performed in association with condensed phase measurements, in particular nuclear magnetic resonance. It is now well established that the correlation between the data obtained on the gas-phase ionized complexes and the solution data must be analyzed with great care. In the present communication, we demonstrate within a joint experimental and theoretical approach that the ion topologies in gas phase can be affected by the equilibrium time in solution, especially for host-guest systems characterized by slow kinetics of complexation.

As a model system, we selected a member of the cucurbituril family, namely cucurbit[6]uril, whose complexation kinetics has been analyzed in great details by NMR spectroscopy. We used ion mobility and energy-resolved CID to follow the evolution of the ion topologies as a function of time in solution prior to the ESI analysis and highlight the structural time evolution. This study paves the way to further investigations that intend to close the gap between the solution and the gas phase studies in host-guest chemistry.

## References

1. a) J. Lagona, P. Mukhopadhyay, S. Chakrabarti and L. Isaacs, *Angew. Chem.*, 2005; 117: 4922 –4949; *Angew. Chem. Int. Ed.*, 2005; 44: 4844 –4870; b) J. W. Lee, S. Samal, N. Selvapalam, H. J. Kim and K. Kim, *Acc. Chem. Res.*, 2003; 36: 621 –630; c) K. Kim, N. Selvapalam, Y. H. Ko, K. M. Park, D. Kim and J. Kim, *Chem. Soc. Rev.*, 2007; 36: 267– 279; d) L. Isaacs, *Isr. J. Chem.*, 2011; 51: 578– 591; e) E. Masson, X. Ling, R. Joseph, L. Kyeremeh-Mensah and X. Lu, *RSC Adv.*, 2012; 2: 1213– 1247; f) S. Liu, C. Ruspic, P. Mukhopadhyay, S. Chakrabarti, P. Y. Zavalij and L. Isaacs, *J. Am. Chem. Soc.*, 2005; 127: 15959 –15967.
2. W. L. Mock and N.-Y. Shih, *J. Am. Chem. Soc.*, 1989; 111: 2697 – 2699.
3. W. L. Mock and N. Y. Shih, *J. Org. Chem.*, 1986; 51: 4440 –4446.
4. D. R. Hoffmann, W. Knoche, C. Fenn and H.-J. Buschmann, *J. Chem.Soc. Faraday Trans.*, 1994; 90: 1507 – 1511.
5. a) C. Marquez, R.R. Hudgins and W. M. Nau, *J. Am. Chem. Soc.*, 2004; 126: 5806 – 5816; b) K.I. Assaf and W.M. Nau, *Chem.Soc.Rev.*, 2015; 44: 394-418.
6. C. Marquez and W.M. Nau, *Angew.Chem. Int. Ed.*, 2001; 40: 3155-3160.
7. D. V. Dearden, T. A. Ferrell, M. C. Asplund, L. W. Zilch, R. R. Julian and M. F. Jarrold, *J. Phys. Chem.*, 2009; 113: 989–997.
8. F. Yang and D.Dearden, *Isr.J.Chem.*, 2011; 51: 553-558.
9. T.-C. Lee, E. Kalenius, A. I. Lazar, K. I. Assaf, N. Kuhnert, C. H. Grün, J. Jänis, O. A. Scherman and W. M. Nau, *Nature Chemistry*, 2013; 5: 376-382.
10. S. Grimme, *J.Comput.Chem.*, 2006; 27: 1787-1799.
11. M. F. Bush, I. D. G. Campuzano and C. V. Robinson, *Anal.Chem.*, 2012; 84: 7124-7130.
12. Gaussian 09, Revision A.02, M. J. Frisch, G. W. Trucks, H. B. Schlegel, G. E. Scuseria, M. A. Robb, J. R. Cheeseman, G. Scalmani, V. Barone, B. Mennucci, G. A. Petersson, H. Nakatsuji, M. Caricato, X. Li, H. P. Hratchian, A. F. Izmaylov, J. Bloino, G. Zheng, J. L. Sonnenberg, M. Hada, M. Ehara, K. Toyota, R. Fukuda, J. Hasegawa, M. Ishida, T. Nakajima, Y. Honda, O. Kitao, H. Nakai, T. Vreven, J. A. Montgomery, Jr., J. E. Peralta, F. Ogliaro, M. Bearpark, J. J. Heyd, E. Brothers, K. N. Kudin, V. N. Staroverov, R. Kobayashi, J. Normand, K. Raghavachari, A. Rendell, J. C. Burant, S. S. Iyengar, J. Tomasi, M. Cossi, N. Rega, J. M. Millam, M. Klene, J. E. Knox, J. B. Cross, V. Bakken, C. Adamo, J. Jaramillo, R. Gomperts, R. E. Stratmann, O.

#### IV. Results and discussion

- Yazyev, A. J. Austin, R. Cammi, C. Pomelli, J. W. Ochterski, R. L. Martin, K. Morokuma, V. G. Zakrzewski, G. A. Voth, P. Salvador, J. J. Dannenberg, S. Dapprich, A. D. Daniels, O. Farkas, J. B. Foresman, J. V. Ortiz, J. Cioslowski, and D. J. Fox, Gaussian, Inc., Wallingford CT (2009).
13. M. F. Mesleh, J. M. Hunter, A. A. Shvartsburg, G. C. Schatz and M. F. Jarrold, *J.Phys.Chem.*, 1996; 100: 16082-16086.
  14. V. Lemaur, G. Carroy, F. Poussigue, F. Chirot, J. De Winter, L. Isaacs, P. Dugourd, J. Cornil and P. Gerbault, *ChemPlusChem*, 2013; 78: 959 – 969.
  15. H. Zhang, E. S. Paulsen, K. A. Walker, K. E. Krakowiak and D .V. Dearden, *J.Am.Chem.Soc.*, 2003; 125: 9284-9285.
  16. T. Josse, J. De Winter, P. Dubois, O. Coulembier, P. Gerbault, and A. Memboeuf, *Polymer Chemistry*, 2015; 6: 64–69.

## Chapter 2:

Flying cages in Traveling Wave Ion Mobility: insidious effect of the instrumental parameters on the topology of the host-guest complexes.

G. Carroy, V. Lemaire, C. Henaumont, S. Laurent, J. De Winter, E. De Pauw, J. Cornil, P. Gerbaux.

*JASMS 2017, submitted*

---



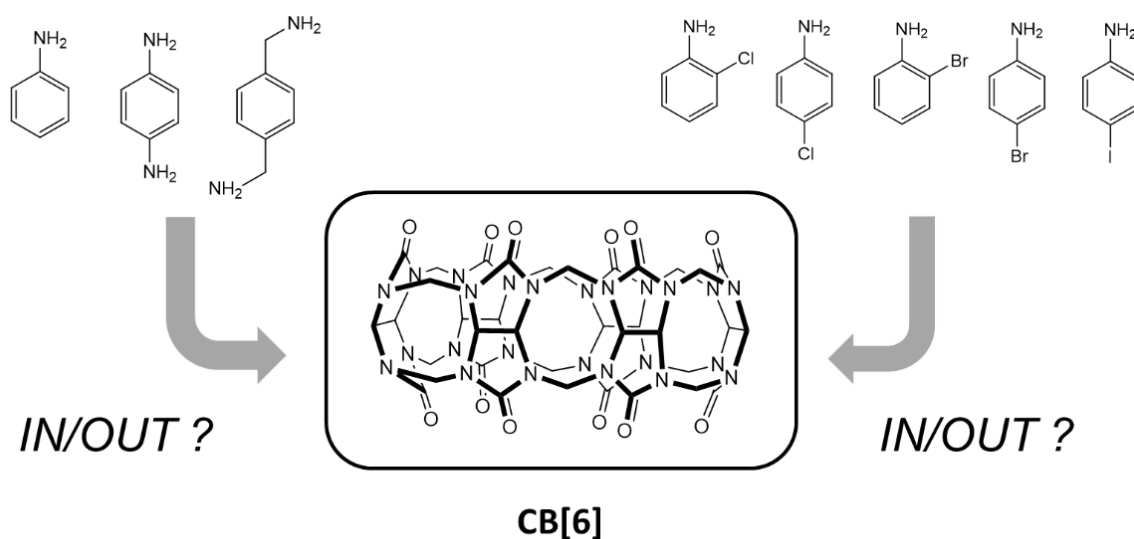
## 2.1 Introduction

Cucurbit[n]urils are macrocyclic receptors constructed by the association of  $n$  glycoluril repeat units [1]. These pumpkin-shaped molecules present a hydrophobic inner cavity and two identical carbonyl portals, making them suitable for encapsulation of hydrophobic molecules or the hydrophobic part of molecules in aqueous media [2]. The main drawback of cucurbiturils is their low solubility in water requiring low pH or high ionic strength to ensure their dissolution upon protonation of the carbonyl portal or cationization [2]. On the other hand, the cucurbit[n]uril (CB[n]) family of molecular containers has attracted a huge interest due to their outstanding recognition properties, exceptional strength of their interaction with various guests, and to the numerous applications offered by the encapsulation propensity of the cucurbituril family members [3]. Cucurbiturils form stable inclusion complexes with various protonated alkyl- and aryl(di)amines [1-3]. Nuclear magnetic resonance (NMR) experiments are most of the time conducted to investigate the host-guest complexes of cucurbiturils. The interior of the cucurbituril cavity represents a  $^1\text{H}$  NMR shielding region, with upfield shifts of more than 1 ppm being common [4]. By NMR integration, 1:1 complexes associating alkyl- or aryl-ammonium ions are most of the time detected with CB[6], the common cucurbituril receptor. Apparently, the exchange between bound and free alkylammonium ions is really slow on the NMR time scale, making the signals from both species observable when an excess of guest is present. Counter-examples are reported when, for instance,  $n$ -propylammonium ions are engaged in complexation studies with CB[6]. In such a case, only an averaged NMR spectrum is observed [4]. The association of protonated arylamines and CB[6] represents a typical example of such a behavior. Indeed, CB[6] is able to accommodate the benzene ring within the hydrophobic cavity, even if benzene has a van der Waals diameter larger than the calculated internal cavity of CB[6]. Mock *et al* suggested that the benzene ring exceeds the strain-free binding capacity of CB[6], with the cage structure getting distorted into an ellipsoid shape upon benzene encapsulation. A decrease by more than 0.4 Å of the diameter of the CB[6] molecule in a direction orthogonal to the guest ring has been measured from the crystal structure of the  $p$ -xylylenediamine complex of CB[6] [2-3]. Therefore, the relatively low binding affinities of the arylamine guests with CB[6] must be understood as a balanced compensation between favorable non covalent interactions and the

stress-strain relationship between the host and the guest [1]. As a typical example, the dissociative constants for the host-guest complexes associating ethanamine and aniline respectively amount to  $10^{-2}$  M and  $10^{-4}$  M [4]. It was also demonstrated that, when the inner cavity of CB[6] is occupied by a benzene ring, there is no extra room for additional ortho- and meta substituents. For the para isomers, both substituents are able to extend toward both carbonyl portals, making the complexation of substituted anilines, specific to the para isomers [1]. In addition, CB[6] usually presents slow kinetic of guest encapsulation since a significant deformation of the portals must occur to let the guest molecule enter the CB[6] cavity. The complexation mechanisms have been also extensively studied and Nau *et al* proposed that the inclusion step corresponds to a flip-flop process, with the exclusion complexes considered as intermediate in the pre equilibrium step [5]. In a recent paper [6], our research groups depicted the outstanding capabilities of the association between mass spectrometry methods, ion mobility spectroscopy and computational chemistry to monitor the slow encapsulation process of the guest *para*-phenylenediamine (DAPHEN) within the CB[6] host. The use of the ESI source allowed us to study the non-covalent associations present in solution within the rarefied gas phase. The binary complex formed between CB[6] and DAPHEN has been used as a model system to demonstrate, by means of ion mobility and collision-induced dissociation measurements, that the inclusion/exclusion topology ratio of gas phase ions  $[CB[6] + DAPHEN + 2H]^{2+}$  ( $m/z$  553) varies as a function of the equilibration time in solution prior to the electrospray process [6].

In direct continuity with this previous study, we report here a detailed study of the complex formation between CB[6] or CB[6] and numerous mono- and diamino benzenic compounds, paying a special attention to the in-solution equilibration time, i.e., the time between the preparation of the solution and the mass spectrometry analysis. The selected guests are presented in ***scheme 1***. These guests all possess an aromatic ring – to be entangled within the hydrophobic cavity - and at least one amino group – to be associated with the carbonyl rim. Aniline has been previously demonstrated to be entangled within the CB[6] cavity with a binding constant of up to  $10^4$  M<sup>-1</sup> [4]. As such, aniline corresponds to the simplest guest to be included in the present investigation. The halogeno-compounds (*ortho*- and *para*-) have been chosen to create a (increasing) steric hindrance on the way to the encapsulation. The *para*-xylylenediamine compound (PXD) basically presents the same structural features as DAPHEN

(two amine moieties, one aromatic ring) but with a different backbone and in particular non conjugated and more flexible amino groups, due to the presence of the methylene bridges. As in our reference article [6], the assignment of the topology of the ions separated by ion mobility will be achieved on the basis of energy-resolved collision-induced dissociation experiments (ER-CID) and further corroborated by calculating the collisional cross-sections from topologies generated with computational chemistry methods using the Density Functional Theory at the B97D level of theory with a 6-31G(d,p) basis set. A special emphasis on the determination of the relative energies of the inclusion/exclusion structures has been set up to confirm our experimental observations. CB[6] and the different guest, have been chosen to better understand the influence of the guest and host sizes on the equilibration time in solution prior to the Electrospray process.



**Scheme IV.2.1:** Molecular structures of the host CB[6] and of the guests from left to right: aniline, para-phenylenediamine (DAPHEN), para-xylylenediamine (PXD), 2-chloroaniline, 4-chloroaniline, 2-bromoaniline, 4-bromoaniline, 4-iodoaniline.

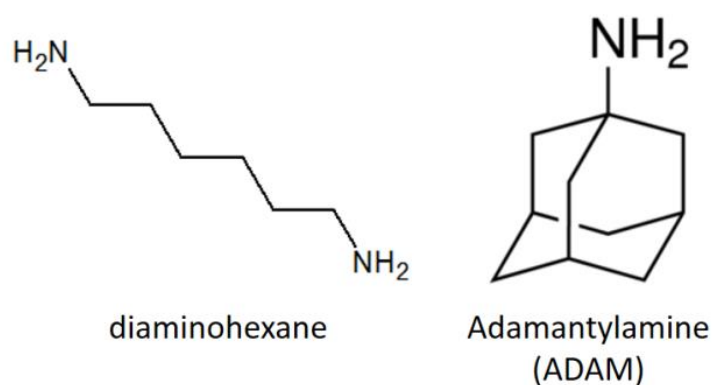
## 2.2 Results and discussion

In a previous report [6], we investigated by mass spectrometry and theoretical chemistry the complexes associating para-phenylenediamine, DAPHEN, with cucurbit[6]uril. By monitoring the time evolution of the Arrival Time Distribution (ATD) derived from ion mobility

experiments, we demonstrated that the full encapsulation of the guest molecule within the host cavity is hindered by the size of the carbonyl portals, leading to a slow kinetic for ingress [6]. DAPHEN presents two major structural features: two amines moieties and one aromatic ring that makes this molecule suitable for complexation within the cucurbituril cavity. For the present study, we would like to investigate the influence of the nature and position of substituents on the phenyl ring on the kinetic of ingress. As a starting point, the pristine aniline molecule has been selected since aniline possesses only one amine function and no other substitution in *ortho* or *para* position of the amino group, which makes it the simplest guest with a structure close enough to DAPHEN. The aniline phenyl ring will then be progressively decorated by halogen atoms (chlorine, bromine and iodine) in *ortho* and/or *para* positions.

2.2.1 Adamantylamine•CB[6] and diaminohexane@CB[6] as exclusion and inclusion model complexes

Adamantylamine (ADAM) and diaminohexane, see **scheme IV.2.2**, are introduced in the present investigation as model guests for the ion mobility experiments since the binary complexes associating ADAM and diaminohexane have already been demonstrated to create specifically exclusion and inclusion complexes with CB[6], respectively [7].



**Scheme IV.2.2:** Molecular structures of model host compounds for the inclusion and exclusion complexes with CB[6]: diaminohexane and adamantylamine.

As presented in **table IV.2.1**, the  $[\text{CB}[6]+\text{diaminohexane}+2\text{H}]^{2+}$  complexes present only one gas phase structure – i.e., a single signal in the Arrival Time Distribution – both at  $t = 5$  min and  $t = 24$  h. This structure is clearly identified as an inclusion topology. The nice agreement between theoretical and experimental CCS in addition with the high  $E_{50}$  value (center-of-mass energy) at 1,59 eV confirm the inclusion character of the detected ions. This inclusion topology possesses by far the most stable structure in comparison with the exclusion candidate, with the exclusion structure being 63,5 kcal/mol less stable than the inclusion one. In **figure IV.2.1**, the CID mass spectrum of the  $m/z$  557 ions is presented. The decomposing complex ions are shown to mostly end up to protonated CB[6] by the loss of protonated diaminohexane. The corresponding signal ( $m/z$  117) is not detected amongst the CID fragments while  $m/z$  100 cations, corresponding to  $\text{NH}_2\text{-(CH}_2\text{)}_5\text{-CH}_2^+$  cations, are detected. This suggests that the decomposition process is more complicated than a simple decomplexation reaction. We previously reported that the decomposition of the inclusion complexes created between 1,4-diaminophenylene and CB[6] occurs via a complicated mechanism involving bond breaking within the cucurbituril backbone. The observation of CB[6] fragment ions points to a similar mechanism, that will not be discussed further in the present study.

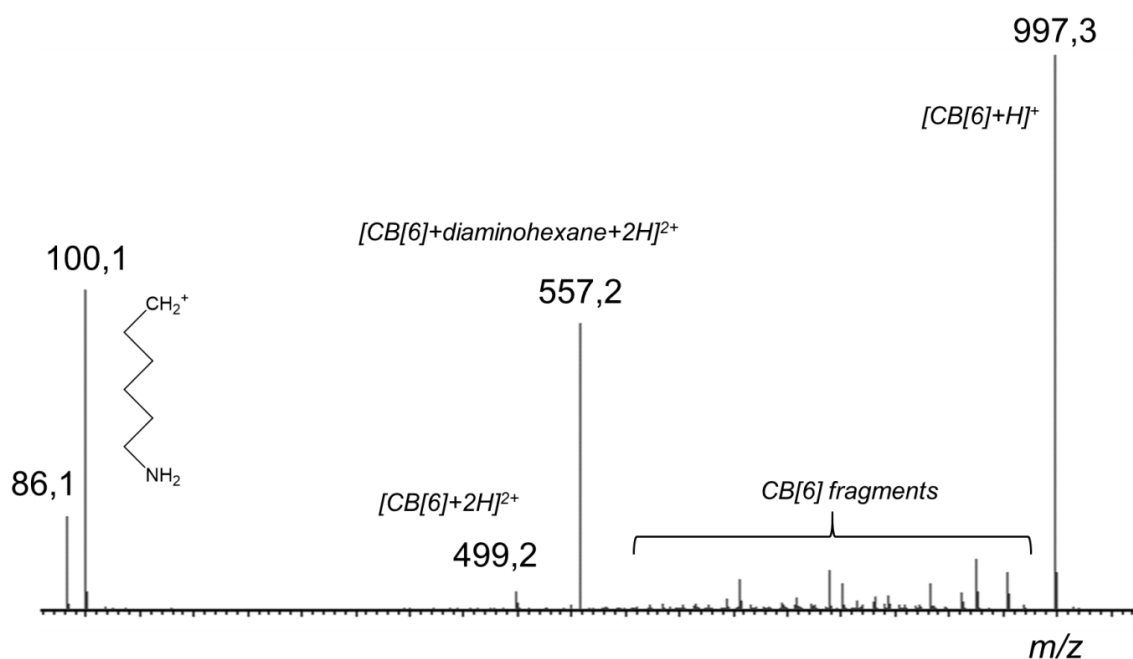


**Figure IV.2.1:** CID analysis (Trap cell) of the  $[\text{CB}[6]+\text{diaminohexane}+2\text{H}]^{2+}$  complex ions ( $m/z$  557,2).



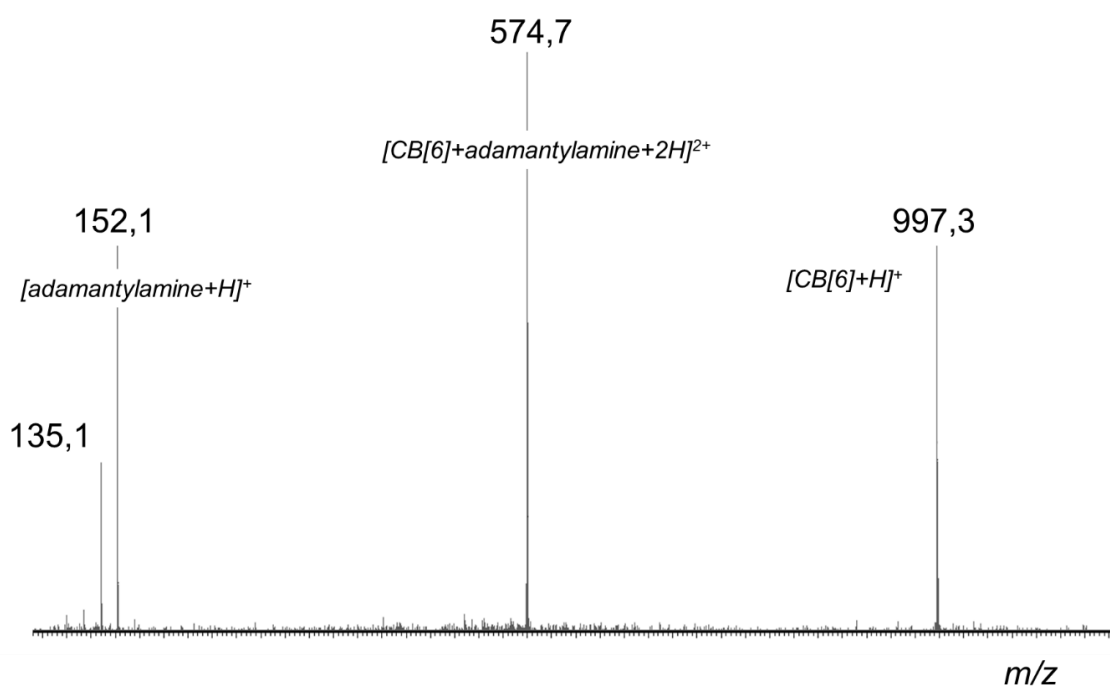























**Table IV.2.1** also presents the results for the  $[\text{CB}[6]+\text{ADAM}+2\text{H}]^{2+}$  ions. The experimental data clearly point to the exclusive presence of an exclusion topology. The identification of an exclusion complex is mainly based on the nice agreement between theoretical ( $217 \text{ \AA}^2$ ) and experimental ( $228 \text{ \AA}^2$ ) CCS. The CCS calculated for the inclusion and exclusion complexes are respectively 196 and  $217 \text{ \AA}^2$ ; this huge difference is readily associated to the large volume of the adamantyl group. Interestingly, the relative energy between both topologies only amounts to 6 kcal/mol. The exclusive occurrence of the exclusion complexes finds its origin in a very low kinetic constant of ingress for the guest encapsulation process. The huge transition barrier for ingress is clearly associated with the requirement of significant deformations of the rigid portals of the CB[6] receiver to allow the adamantyl group entering the cavity. When exposed to energy-resolved CID experiments, those exclusion complexes are characterized by a  $E_{50}$  of about 0,9 eV. This  $E_{50}$  energy around 0.9-1 eV is associated with the dissociation of the H-bonds present between the ammonium group of the guest and the carbonyl oxygen atoms of the receiver portal. In the case of the adamantylamine complexes, based on the high proton affinity of the molecule ( $\text{PA} = 948,8 \text{ kJ/mol}$  vs  $882,5 \text{ kJ/mol}$  for aniline), protonated adamantylamine plus protonated CB[6] are the dominating CID fragments (see **figure IV.2.2**).



**Figure IV.2.2:** CID analysis (Trap cell) of the  $[\text{CB}[6]+\text{adamantylamine}+2\text{H}]^{2+}$  complex ions.

When comparing the fragment ions for the aniline and adamantylamine complex ions, we observed that, depending on the relative PA values, the proton remains on the guest molecule (adamantylamine) or on the receptor macrocycle (aniline). Given the close similarity between the  $E_{50}$  values whatever the nature of the fragment ions, we conclude that the proton transfer reaction (aniline case) is less energy demanding than the overall dissociation of the H-bonds. At variance, for the diamino guest, the  $E_{50}$  value is higher (1,59 eV) in relation to the presence of both the ammonium groups creating H-bonds on both rims of the receptor. This was already observed in our previous report (data from reference [6] also added to **table IV.2.1**) dealing with 1,4-diaminophenylene. However, for the diaminohexane guest, the inclusion complexes are detected immediately after mixing the guest and the host in solution while for the benzenoid counterpart, 24 hours are required for full encapsulation [6].

**Table IV.2.1:** Experimental and theoretical data relevant to the investigated CB[6] / guest systems. The experimental data are composed by the drift time – arrival time value ( $t_A$ ), the determined Collision Cross Section (CCS) and the  $E_{50}$  from energy-resolved CID experiments. The theoretical data present the CCS and the relative energies for different topologies.

Guest molecules	Experimental data			Theoretical data		
	$t_A$ (ms) <sup>a</sup>	$CCS_{exp}$ (Å <sup>2</sup> )	$E_{50}$ (eV) <sup>b</sup>	Topology	$CCS_m$ (Å <sup>2</sup> )	$E_{rel}$ (kcal/mol)
1,6-hexanediamine	4,90	203 IN	1,59	 IN	193	0
				 OUT	222	63,5
adamantylamine	5,90	228 OUT	0,94	 IN	196	6
				 OUT	217	0
Aniline	4,80	206 IN	0,91	 IN	190	0
	5,22	216 OUT	0,84	 OUT	204	17
				 OUT	208	15
2-chloroaniline				 IN	193	0
	5,63	218 OUT	0,69	 OUT	208	5
				 OUT	211	6
4-chloroaniline	5,08	207 IN	0,84	 IN	190	0
	5,63	218 OUT	0,76	 OUT	205	16
				 OUT	216	10
2-bromoaniline	N.D.			 IN	193	0
				 OUT	210	11
				 OUT	207	7
4-bromoaniline	5,08	207 IN	0,79	 IN	190	0
	5,76	224 OUT	0,86	 OUT	209	24
				 OUT	217	17
4-iodoaniline	5,69	229 OUT	0,88	 IN	190	0
				 OUT	218	9
para-xylenediamine	5,08	204 IN	1,63	 IN	192	0
	5,63	218 OUT	0,95	 OUT	215	64
diaminophenylene	5,08	202 IN	1,98	 IN	190	0
	5,63	219 OUT	0,89	 OUT	218	33



2.2.2 Aniline•CB[6] or aniline@CB[6] as exclusion or inclusion complexes

**Figure IV.2.3** presents the global MS-analysis obtained when an equimolar solution ( $10^{-5}$  M) of aniline and CB[6] is submitted to Electrospray ionization. Beside the doubly protonated naked CB[6] at  $m/z$  499, the binary complex associating one aniline guest to one CB[6] host is also detected with two different charge states.  $M/z$  1090 ions correspond to the singly charged complex ions,  $[CB[6]+aniline+H]^+$ , whereas  $m/z$  545 ions are readily identified as the doubly charged species,  $[CB[6]+aniline+2H]^{2+}$ . The signal at  $m/z$  592 corresponds to the doubly charged ternary complexes, associating two aniline molecules to a macrocyclic receptor, affording the  $[CB[6]+2aniline+2H]^{2+}$  ions.

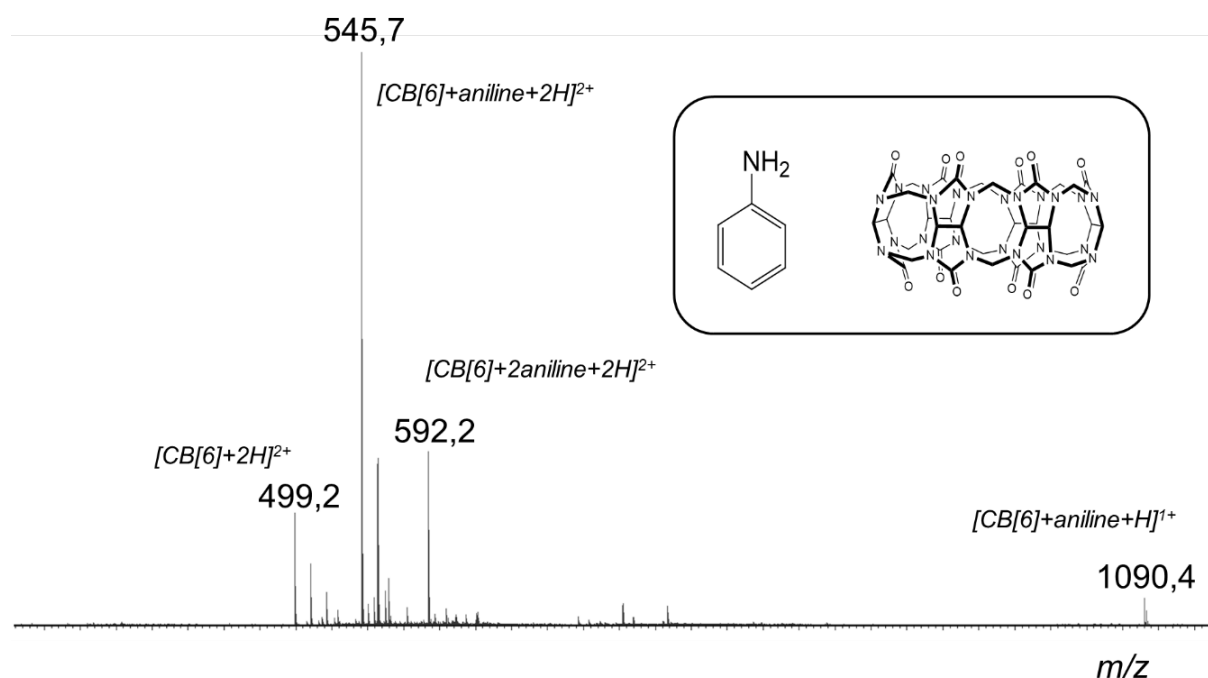


**Figure IV.2.3:** ESI-MS analysis of a freshly-prepared ( $t = 5$  min) equimolar solution ( $10^{-5}$  M) of CB[6] and aniline recorded on a Waters Synapt G2-Si mass spectrometer (Sample Cone Voltage = 40 V).

We would like to stress out here that our principal objective is to study the evolution of the gas phase ion topology as a function of equilibration time in solution. Thus, to gain structural information about the gas phase ions under study, ion mobility spectroscopy experiments in

association with mass spectrometry (IMMS) have been carried out after a residence time in close to 0 ( $t = 5$  min) and after 24h of agitation at 25°C.

**Figure IV.2.4 a** presents the IMMS plots obtained from the full mass spectrum, without any precursor mass selection prior to the ion mobility separation, for the  $m/z$  545 ions for  $t = 5$  min and  $t = 24$  h, namely the  $[\text{CB}[6]+\text{aniline}+2\text{H}]^{2+}$  doubly charged complexes. For both equilibration times, two different drift times are recorded at 4.80 and 5.22 ms, highlighting the presence of two different non-interconverting populations of ions on the time-scale of the ion mobility experiments. Obviously, these two families correspond to ions possessing different topologies. It is worth noting that those two families are still detected after 24h in solution with almost no modification in their relative proportions (**Figure IV.2.4 a**). This already contrasts with the DAPHEN case [6] where only one structure corresponding to an inclusion topology is detected after 24 hours of equilibration time in solution at room temperature. The identification of the topologies that correspond to these different drift times is made below based on the comparison of the experimental and theoretical data (**Figure IV.2.4**). The experimental collisional cross sections ( $\text{CCS}_{\text{exp}}$ ) in **Figure IV.2.4 a** have been obtained after calibration of the Waters Synapt G2-Si. **Figure IV.2.4 b** summarizes the data obtained by the DFT calculations to generate the ion structures and calculate their relative energies and MOBCAL (Trajectory Method) software to calculate the theoretical collision cross sections ( $\text{CCS}_{\text{th}}$ ). A quick comparison between the experimental and theoretical values of CCS (with 5% of experimental errors) would suggest the exclusion character of both detected ions since the  $\text{CCS}_{\text{th}}$  for the inclusion complexes amounts to  $190 \text{ \AA}^2$ , a value that is lower than the measured data. As presented in **Figure IV.2.4 b**, the exclusion topologies are located about 15 kcal/mol higher in energy than the inclusion complex that is identified as the most stable structure for the ions  $[\text{CB}[6]+\text{aniline}+2\text{H}]^{2+}$ .

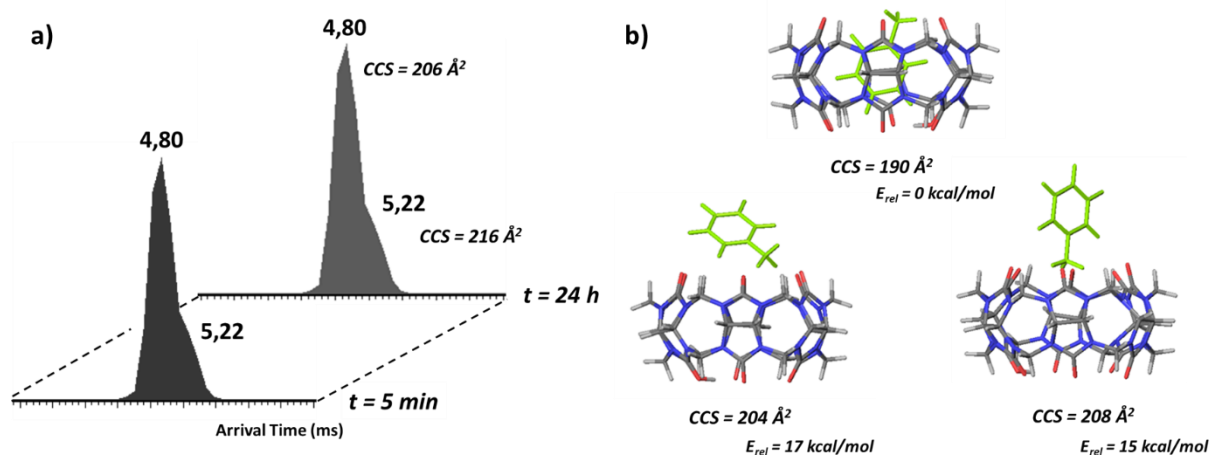


**Figure IV.2.4:** ESI-IMS-MS analysis of an equimolar solution ( $10^{-5}$  M) of CB[6] and aniline (CV = 40 V) for two different equilibration time ( $t = 5$  min and 24 h). (a) Arrival time distribution (ATD) (no mass selection prior the IMS separation) of the  $[CB[6]+aniline+2H]^{2+}$  ions ( $m/z$  545,7) – the  $CCS_{exp}$  and the relative abundances are obtained using, respectively, the calibration and the deconvolution procedures described in the experimental section. (b) Optimized topologies for the  $[CB[6]+aniline+2H]^{2+}$  ions obtained at the DFT level using the B97D functional and the 6-31g(d,p) basis set – the  $CCS_{th}$  are calculated by the trajectory method in the MOBCAL software starting from DFT-optimized geometries.

As a third set of data, the  $E_{50}$  values have been obtained by recording the survival yield curves (see **figure IV.2.5** for a typical example) obtained from the energy-resolved CID experiments (ER-CID) carried on after the mobility cell (in the transfer cell) in order to study each topology separately. The  $E_{50}$  data are converted into center-of-mass energies to allow comparing the different host-guest systems. As presented in **table IV.2.1**, the measured  $E_{50}$  values (ca 0,9 eV) are significantly reduced in comparison to that measured previously for the DAPHEN@CB[6] inclusion complexes ( $\approx 2$ eV) [6].

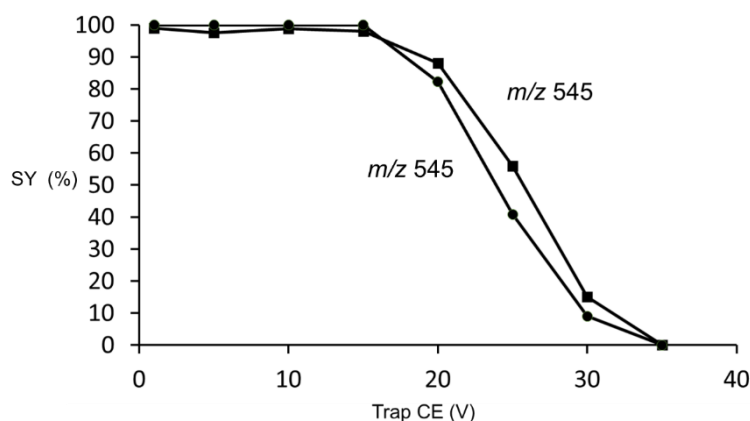


**Figure IV.2.5:** Energy-resolved Collision-induced Dissociation experiments on the  $[CB[6]+aniline+2H]^{2+}$  complexes in the transfer cell after ion mobility separation of the exclusion/inclusions complexes. Determination of the  $E_{50}$  energy.

At this point of the discussion, we must admit that we cannot define unambiguously the structures of both ion families. We believe that, without the second amino group in *para* compared to *DAPHEN*, the aniline guest might probably either: (i) easily flip out of the cavity generating the exclusion topology or; (ii) even continuously “flip” in and out of the cavity leading to an average topology. However, in the latter case, only one signal would have been observed in the ATD, instead of the two detected signals. Embarrassing is also the fact that the ratio between both ATD signals does not evolve from  $t = 5$  min to  $t = 24$ h. Mock *et al* used NMR spectroscopy to characterize the selectivity of cucurbiturils toward several guest compounds [4]. In particular, they demonstrated that aniline is entangled in the CB[6] cavity with a dissociation constant that amounts to  $10^{-4}$  M. In other words, based on the equimolar nature of the aniline/CB[6] solution used in the present MS investigation, we should consider that the complexation of aniline within the CB[6] cavity is quantitative in solution. To support this assumption, we compared the  $^1H$ -NMR spectrum of an aniline/CB[6] solution with the NMR spectrum of pure aniline (see **figure IV.2.6**). We observe the complete disappearance of the aniline signals at  $\delta = 6,55$  (ortho position), 7,05 (meta) and 6,65 (para) ppm in favor of signals at  $\delta = 5,4$  (ortho), 3,9 (meta) and 4,55 (para) ppm for the aniline@CB[6] complex. As reported in the NMR reference paper, the interior of cucurbituril is a proton-shielding region, based on the cumulative effect of the 12 urea residues of cucurbituril, each presenting a face to the interior of the cavity [4].

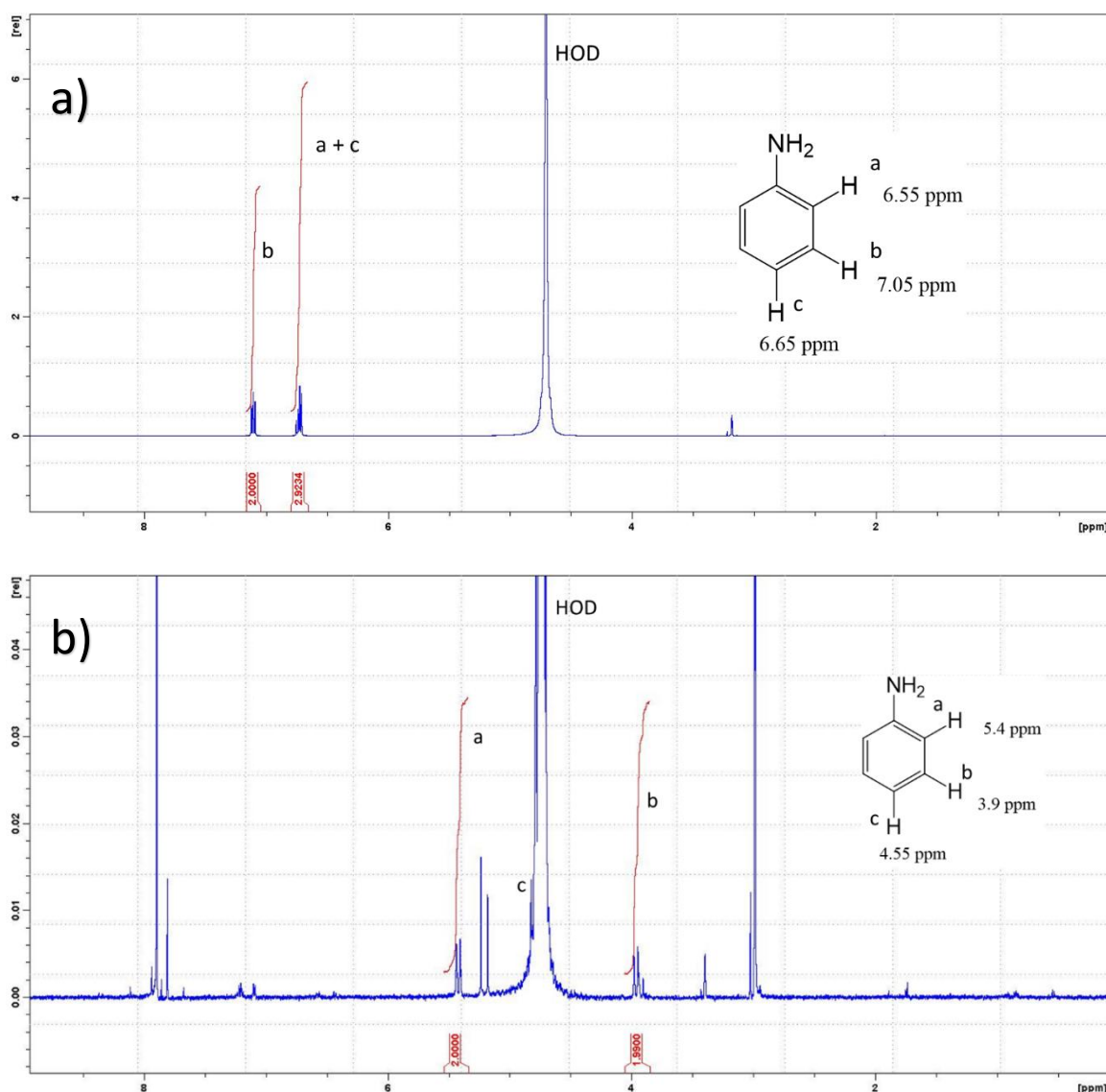


**Figure IV.2.6:**  $^1\text{H-NMR}$  spectra of (a) aniline and (b) an equimolar solution of aniline and CB[6] in  $\text{D}_2\text{O} / \text{CD}_3\text{OD}$ . Only the signals relevant to aniline are identified and integrated.

Thus, thanks to the NMR experiment, we now must consider as the starting point of our MS investigations that, in the aniline/CB[6] solution, inclusion complexes are quantitatively present. Going back to **figure IV.2.4 a**, we then suggest that the ion populations correspond to inclusion and exclusion complexes at respectively  $t_D = 4,80$  and  $5,22$  ms. Since both ion families are separated upon ion mobility, we can state that the inclusion and exclusion complexes do not interconvert during the ion mobility experiment. Further evidence for the presence of the exclusion topology at  $t_D = 5,22$  ms comes from the following sequence of ion manipulations. We submit to collision-induced dissociation (CID) in the trap cell of the triwave setup the mass-selected doubly charged ternary complexes at  $m/z$  592, the

$[\text{CB}[6]+2\text{aniline}+2\text{H}]^{2+}$  ions, in order to generate the  $m/z$  545 binary complexes that are likely to correspond to exclusion complexes. Indeed, the ternary complexes are expected to present both aniline molecules pointing outside the CB[6] cavity in a full exclusion structure. We first confirm that, upon CID, the  $m/z$  592 ions generate the  $m/z$  545 ions by loss of a neutral aniline molecule, see **figure IV.2.7** for the CID spectrum of the  $m/z$  592 ions. The so-produced  $m/z$  545,7 ions are then subjected to ion mobility and the recorded ATD is now characterized by a quasi-unique signal at  $t_D = 5,22$  ms, confirming the exclusion topology of those complex ions (see also **figure IV.2.7**).

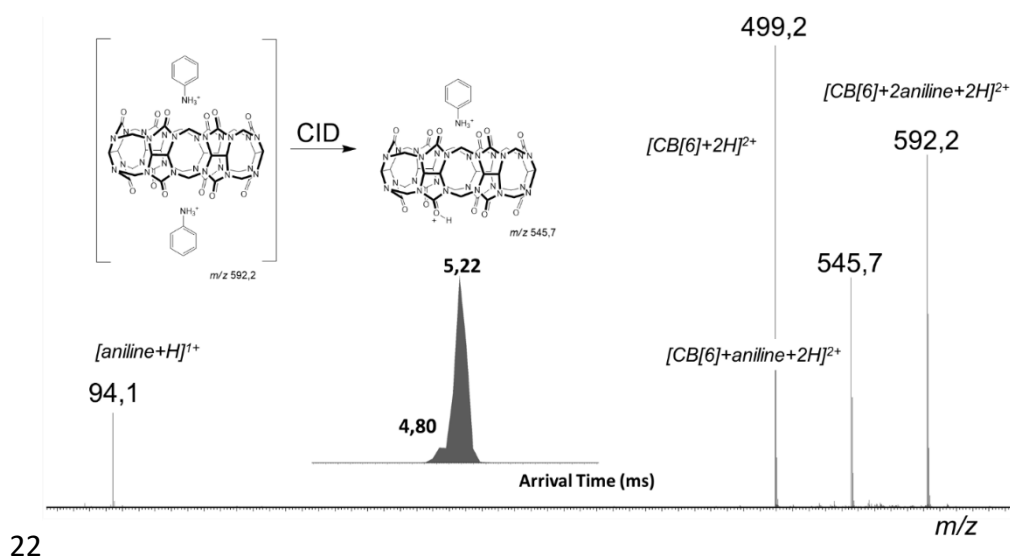


**Figure IV.2.7:** CID analysis (Trap cell) of the doubly charged ternary complexes associating two anilinium cations to one CB[6] receptor ( $m/z$  592,2). The Arrival Time Distribution (inset) reveals that most of the  $m/z$  545,7 ions are exclusion complexes as presented in the chemical equation.

It is then tempting to deduce from this last experiment that decompositions of the  $[\text{CB}[6]+2\text{aniline}+2\text{H}]^{2+}$  ions ( $m/z$  592) either in the ion source or somewhere else during the flight of the ions from the source to the TWIG cell can be responsible for the production of the  $m/z$  545 ions presenting the exclusion topology observed in **figure IV.2.4 a**. Basically, the  $m/z$  592 ions can decompose into  $m/z$  545 at mainly two specific places during their flight from the source to the ion mobility cell: (i) before the quadrupole, the ions are accelerated between the stepwave and the first TWIG and the applied voltage is as the **Sample Cone voltage** in the tune page, see **figure IV.2.8**. This corresponds to a voltage applied to increase sensitivity by

de-clustering the ion adducts; after the quadrupole, the ions are stored in the so-called Trap cell that is floated at a voltage – the **Trap DC Bias** - that is the voltage applied between the trap and the helium cells allowing the ion injection into the mobility cell. The Trap cell can also be used as a CID cell by modifying the **Trap CE** (Trap Collision Energy). First, with regard on those three parameters, we focus on the in-source events by mass-selecting the  $m/z$  545 ions by the quadrupole analyzer and monitoring the evolution of the IN/OUT ratio as a function of the **sample cone** parameter.

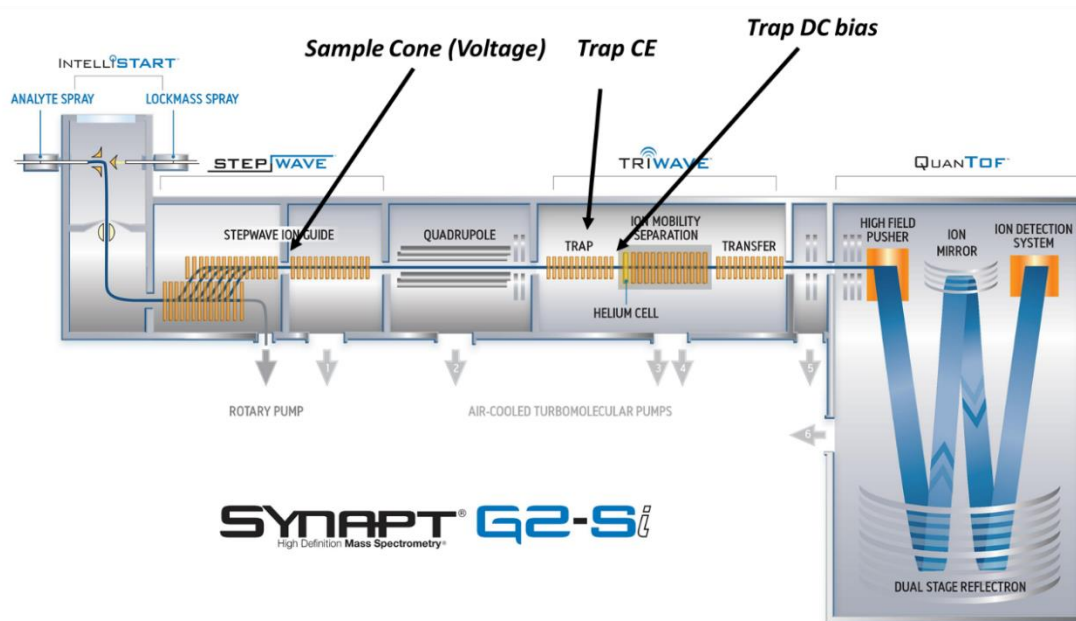


**Figure IV.2.8:** Schematic of the Waters Synapt G2-Si mass spectrometer: identification of the voltages responsible for ion activation.

As presented in **figure IV.2.9 a**, even at the lowest tested sample cone value (10 V), ions presenting the exclusion topology are already detected with a relative abundance of about 10%. The stepwise increase of the sample cone voltage from 10 to 70 V clearly induces the modification of the relative proportions between the IN and OUT topologies with the exclusion complex ions becoming more abundant above *ca* 50 V (**figure IV.2.9 a**). **Figure IV.2.9 b** presents the sample cone voltage dependence of the relative abundances of three different key ions, namely  $[\text{CB}[6]+2\text{aniline}+2\text{H}]^{2+}$  ( $m/z$  592),  $[\text{CB}[6]+\text{aniline}+2\text{H}]^{2+}$  ( $m/z$  545) and  $[\text{CB}[6]+2\text{H}]^{2+}$  ( $m/z$  499). From **figure IV.2.9 b**, we can conclude that, in the sample cone voltage range 10-70 V, no extensive decomposition of the  $[\text{CB}[6]+2\text{aniline}+2\text{H}]^{2+}$  ( $m/z$  592) nor the

[CB[6]+aniline+2H]<sup>2+</sup> (*m/z* 545) ions is observed. Therefore, we can deduce that the IN/OUT evolution is mainly caused by the collision-induced isomerization of the *m/z* 545 inclusion complex ions toward the less stable and less compact exclusion complexes (**figure III.2.2 b**). We then assess the influence of the **Trap DC bias** on the IN/OUT ratio by again mass-selecting the *m/z* 545 ions by the quadrupole analyzer and monitoring the evolution of the IN/OUT ratio as a function of the **Trap DC bias** voltage, taking care to avoid the *m/z* 545 ion decomposition. The data presented in **figure IV.2.7 c** again suggest that the increase in the **Trap DC bias** clearly induces the IN-to-OUT isomerization.

As a final experiment, we probe the influence of the **Trap Collision Energy** (Trap CE) on the Survival Yield (SY) and the IN/OUT ratio of the mass-selected *m/z* 545 ions. The SY corresponds, in a CID mass spectrum, to the ratio between the abundance of the non fragmented parent ions and the abundances of all ions (parent plus fragments) going out of the collision cell. The IN/OUT ratio is measured by injecting the *m/z* 545 emerging from the trap cell into the ion mobility cell. The results of such an experiment are presented in **figure IV.2.9 d**. Basically, the parent ions start to decompose at a **Trap CE** above 10 V. Nevertheless, already at a value of 5 V, the IN-to-OUT ratio is in favor of the exclusion topology, indicating that the IN-to-OUT isomerization requires less internal energy to occur than the complex ion dissociation. It is also remarkable to note that the *m/z* 545 parent ions start to decompose when the proportion of exclusion complex ions reaches a maximum around 12-13 V. This clearly indicates that the collisionally-activated *m/z* 545 inclusion complex ions first undergo the IN-to-OUT isomerization prior to their decomposition. The dominant decomposition reaction corresponds to the loss of neutral aniline and the formation of [CB[6]+2H]<sup>2+</sup> at *m/z* 499.



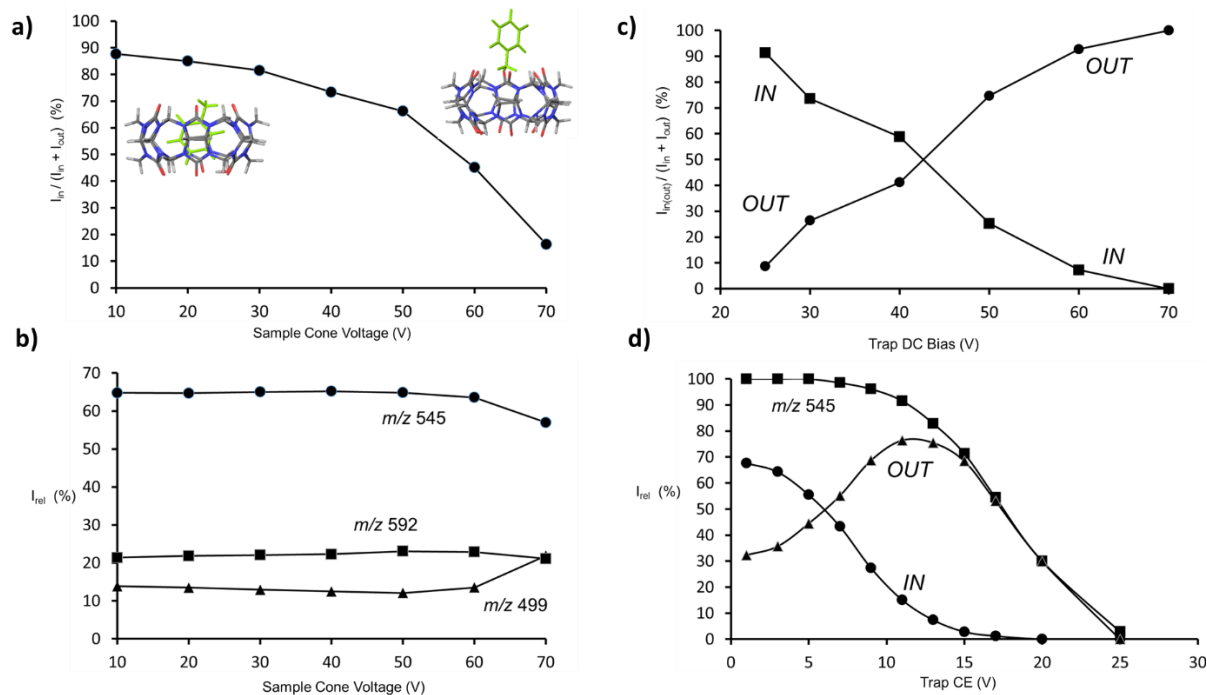


**Figure IV.2.9:** MS analysis of an equimolar solution ( $10^{-5}$  M) of CB[6] and aniline. (a) Influence of the Sample Cone Voltage on the IN/OUT ratio determined by IMS on mass-selected  $m/z$  545 ions (Trap Bias 30V – Trap CE 0,5V). (b) Influence of the Sample Cone Voltage on the relative intensities of the  $m/z$  499, 454 and 592 ions within the ESI-ToF analysis (Trap Bias 30V – Trap CE 0,5V). (c) Influence of the Trap DC Bias on the IN/OUT ratio determined by IMS on mass-selected  $m/z$  545 ions (Sample Cone Voltage 40V – Trap CE 0,5V). (d) Survival Yield of the mass-selected  $m/z$  545 ions with CID in the trap and influence of the Trap DC on the IN/OUT ratio determined by IMS (Sample Cone Voltage 40V – Trap Bias 30V).

### 2.2.3 Halogeno-aniline•CB[6] or halogeno-aniline@CB[6] as exclusion or inclusion complexes

The data acquired for aniline, adamantylamine and diamino-hexane will support the discussion of the experimental/theoretical results for the halogeno-aniline guests (*see scheme IV.2.1*). Briefly, the anilinium guest is enclosed within the cavity of the receptor in the solution phase, but is progressively expelled outside the cavity upon ion activation during the CID experiments but also due to the transfer optics. The  $E_{50}$  amounts to about 0,9 eV for both topologies, demonstrating that the rate determining step on the way to the complex ion dissociation is

the H-bond breaking. This is confirmed when analyzing the adamantylamine guest with a  $E_{50}$  of about 0,9 eV.

All experimental and theoretical data obtained for the systems associating CB[6] to 2-chloroaniline (**2-Cl**), 2-bromoaniline (**2-Br**), 4-chloroaniline (**4-Cl**), 4-bromoaniline (**4-Br**) and 4-iodoaniline (**4-I**) are presented in **table IV.2.1**. First, no influence of the equilibration time over the ion mobility data has been monitored pointing to either no or fast encapsulation of the guest within the cavity.

For the *ortho*-substituted anilines, no complex ions are detected for **2-Br** guest, whereas only one arrival time ( $t_A$ ) is measured at 5,63 ms for the **2-Cl** counterpart. The associated CCS amounts to 218 Å<sup>2</sup> points to the presence of an exclusion topology. This is confirmed by: (i) the  $E_{50}$  value determined at 0,69 eV and; (ii) by the theoretical data with a  $CCS_{th}$  of 211 Å<sup>2</sup> for the exclusion complex ions. The absence of exclusion complex ions for the bromine-containing guest is probably related to the steric hindrance created around the bromine atom in the *ortho* position of the anilinium group.

For the *para* isomers, two traces are observed in the case of **4-Cl** and **4-Br** guests whereas only one topology is detected for the **4-I** molecule. We again use NMR spectroscopy to establish the solution topology of the **4-Cl**/CB[6] complexes and again the data confirm the quantitative encapsulation of the 4-chloroaniline inside the cavity (see **figure IV.2.10**). For the **4-I**/CB[6] system, only a single arrival time is measured at 5,69 ms corresponding to a CCS of 229 Å<sup>2</sup> and a  $E_{50}$  of 0.88 eV (**table IV.2.1**). The direct comparison with the theoretical CCS suggests the presence of an exclusion complex. We again used NMR spectroscopy to access the solution topology of the 4-iodoaniline/CB[6] association. As revealed in **figure IV.2.11**, all H-nuclei NMR signals are slightly deshielded when 4-iodoaniline is mixed with an equimolar amount of CB[6] in solution. This corresponds to either no complexation (the slight deshielding being due to protonation in the acidic conditions used for the CB[6] dissolution) or external association with H-bond creation between the ammonium hydrogen atoms and the oxygen atoms of the carbonyl groups.

## IV. Results and discussion

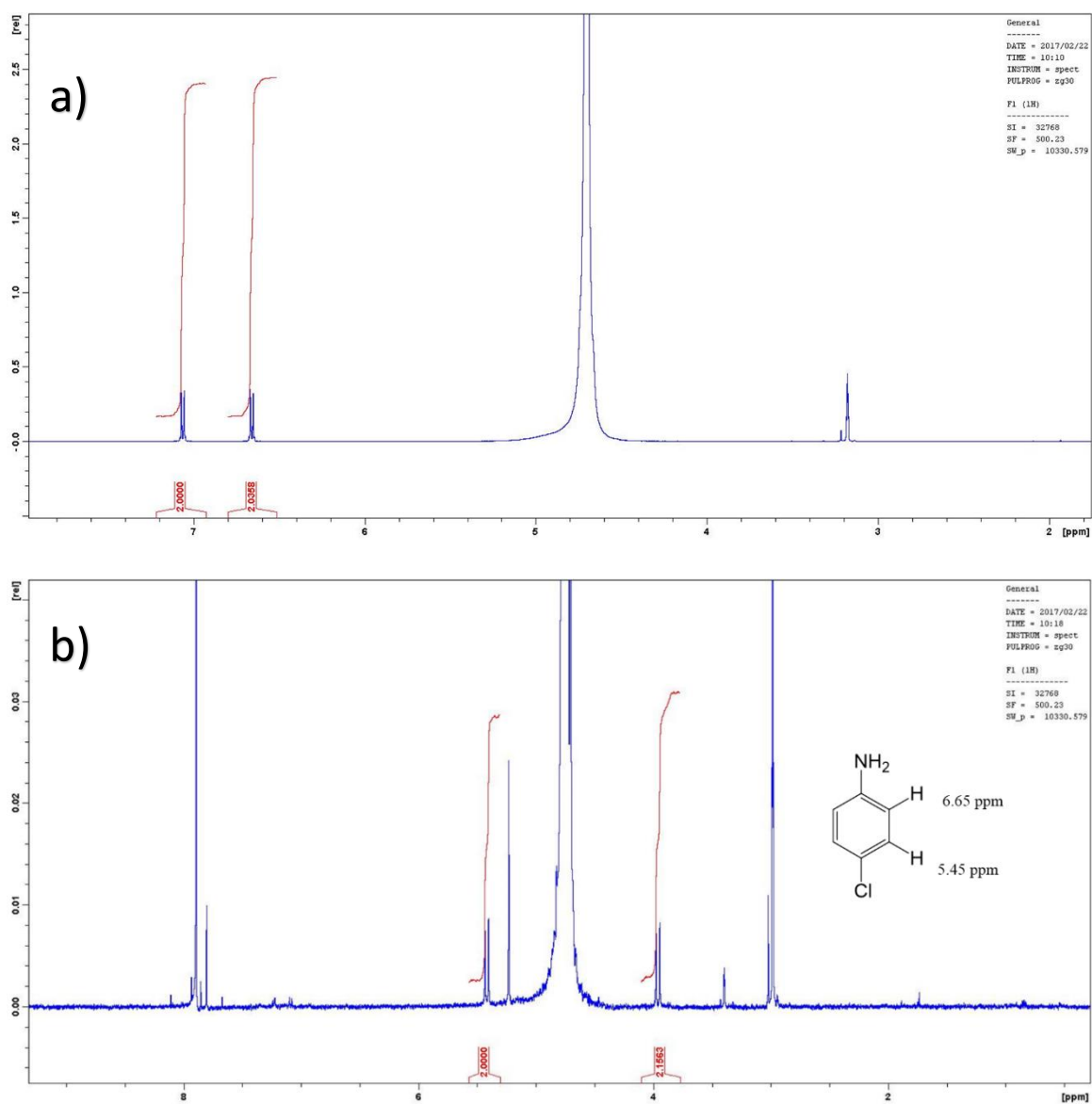


**Figure IV.2.10:**  $^1\text{H-NMR}$  spectra of (a) 4-chloroaniline and (b) an equimolar solution of 4-chloroaniline and CB[6] in  $\text{D}_2\text{O} / \text{CD}_3\text{OD}$ . Only the signals relevant to 4-chloroaniline are identified and integrated.

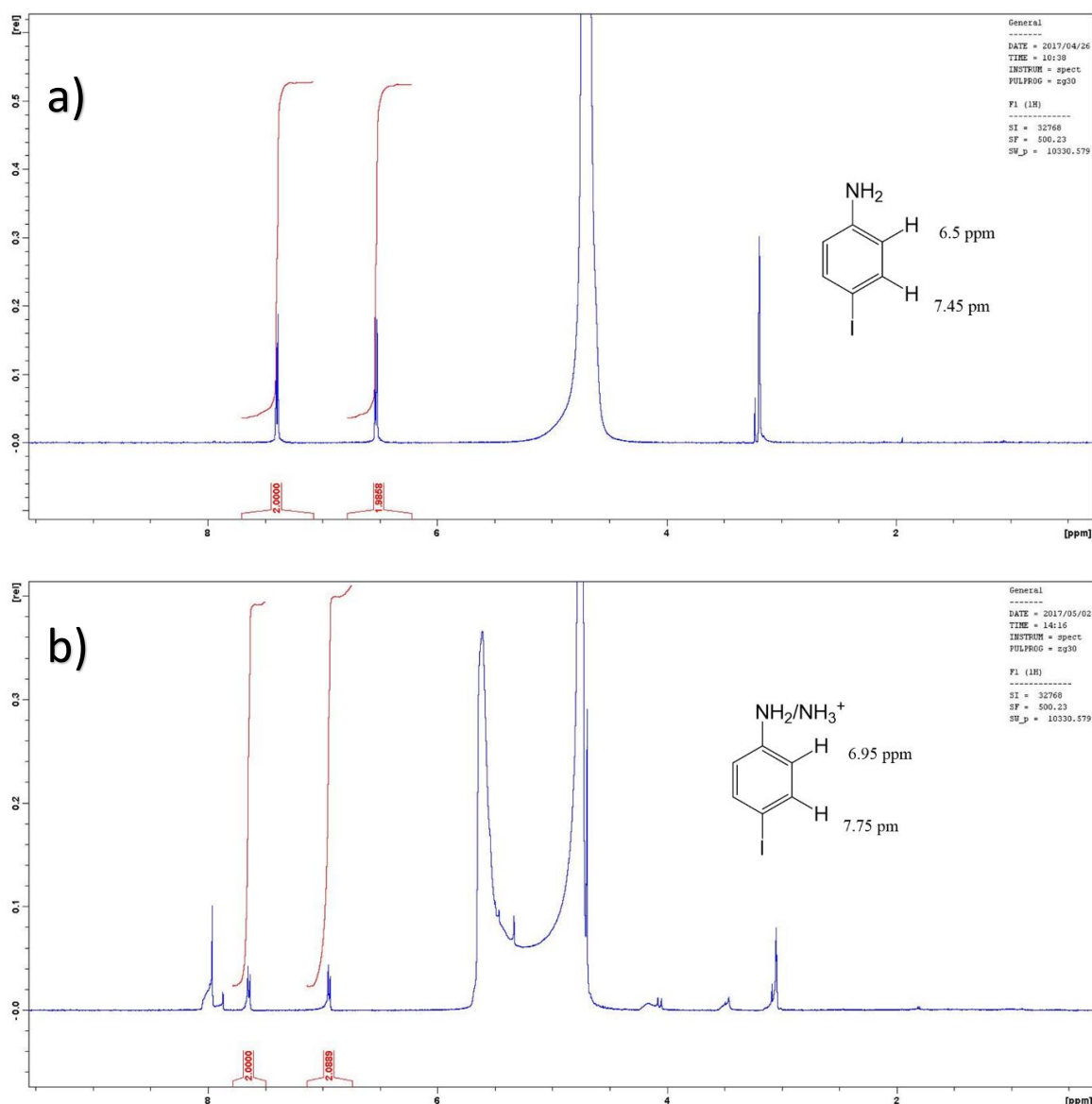


**Figure IV.2.11:**  $^1\text{H-NMR}$  spectra of (a) 4-iodoaniline and (b) an equimolar solution of 4-iodoaniline and CB[6] in  $\text{D}_2\text{O}$  /  $\text{CD}_3\text{OD}$ . Only the signals relevant to 4-iodoaniline are identified and integrated.

The calculated relative energies in **table IV.2.1** reveal that the inclusion complexes remain more stable than the exclusions ones, whatever the halogen atoms. The 4-iodoaniline situation is then straightforward to describe with the sole observation of gas phase exclusion complexes explained by the absence of inclusion complexes in the condensed phase. It is likely that the ingress of the bulky 4-iodoaniline guest within the CB[6] cavity is kinetically prohibited, even in solution.

In the case of 4-chloroaniline, we are however facing the same behavior as for aniline with partial IN-to-OUT isomerization upon ion activation. It also appears, based on the  $E_{50}$  determination (**table IV.2.1**), that the presence of the chlorine atom does not hinder the IN-to-OUT process since the  $E_{50}$  data are all around 0,8 eV, this correlates with the theoretical atom sizes and portal sizes in **figure IV.2.12**.

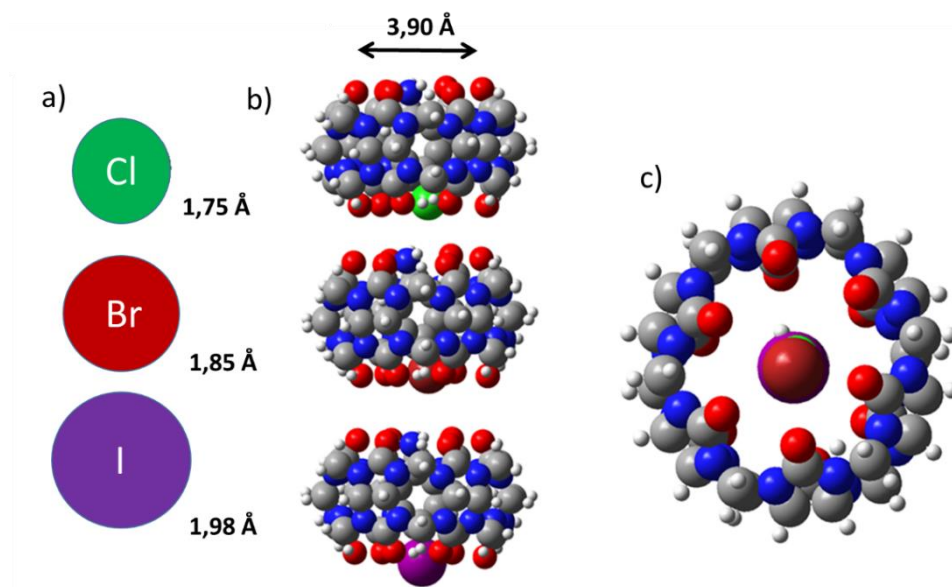


**Figure IV.2.12:** Theoretical data for the inclusion complexes associating 4-chloro/bromo/iodoaniline to CB[6] : (a) Van der Waals atom radii of the halogen atoms, (b) position of the atoms and (c) superposition of the halogen atoms in the optimized structures of the inclusion complexes (the guest phenyl ring is omitted for clarity).

#### 2.2.4 PXD•CB[6] or PXD@CB[6] as exclusion or inclusion complexes

As a final guest for the present investigation, para-xylylenediamine - PXD - has been selected based on the structural and functional compatibility with CB[6]. The PXD/CB[6] system was studied in solution and an association constant of  $5 \cdot 10^2 \text{ M}^{-1}$  has been determined by NMR spectroscopy [8]. As presented in **table IV.2.1** and **figure IV.2.13**, two topologies are detected with arrival times and CCS at, respectively, 5,08 and 5,63 ms and 202 and 219 Å<sup>2</sup>. The complexes are characterized by  $E_{50}$  of 1,98 and 0,89 eV, respectively. This unambiguously points to

the coexistence of inclusion and exclusion complex ions, namely  $\text{PXD@CB[6]}$  and  $\text{PXD}\bullet\text{CB[6]}$ . Moreover, there is a time dependence of the relative abundances of both topologies, as featured in **figure IV.2.13**.

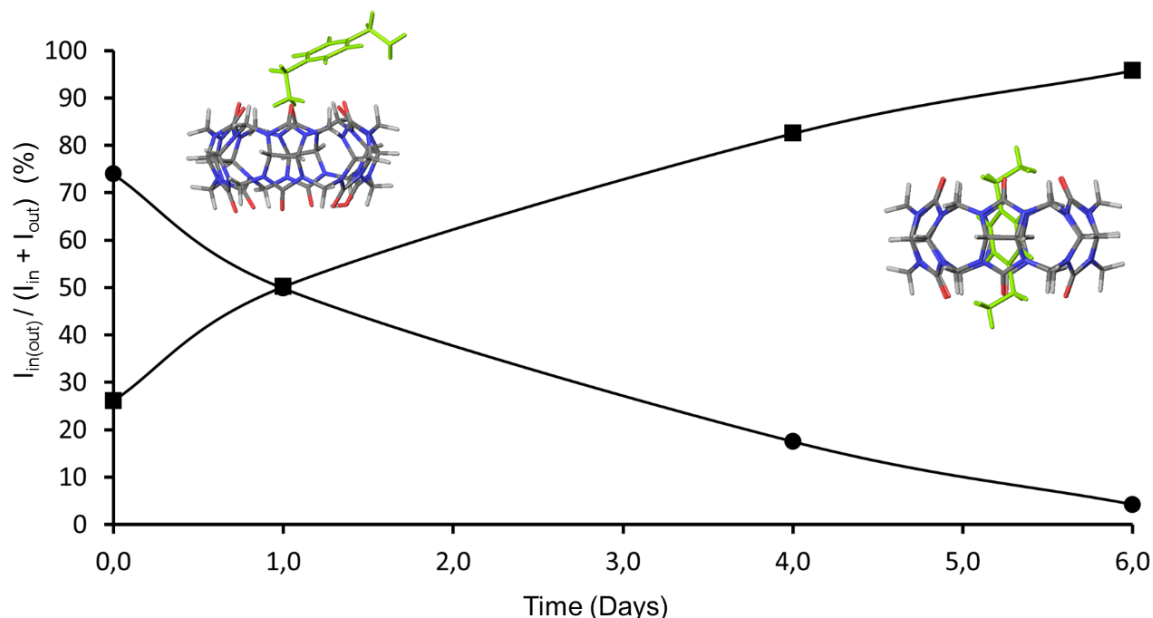


**Figure IV.2.13:** ESI-IMS-MS analysis of an equimolar solution ( $10^{-5}$  M) of CB[6] and para-xylylenediamine ( $CV = 40$  V) at different equilibration time ( $T = 5$  min to  $T = 6$  days).

We previously reported that the quantitative encapsulation of 1,4-diaminophenylene within CB[6] (starting from equimolar solution) requires 24 hours at room temperature. Here, almost 6 days are required to reach 90 % encapsulation. The extreme  $E_{50}$  value (1,98 eV) indicates that the complex ions are protected from IN-to-OUT isomerization upon ion activation. This value is also clearly associated with the need of covalent bond breaking on the way to complex ion dissociations. This is evidenced by the occurrence of a  $m/z$  120 fragment ions in the CID spectrum of the  $\text{PXD@CB[6]}$  ions (see **figure IV.2.14**), instead of the  $m/z$  136 ions for intact (mono protonated) para-xylylenediamine. This behavior mimics the CID reactions of 1,4-diaminophenylene ( $K_a=1,8\cdot 10^3$  M $^{-1}$  [8]) and 1,6-diaminohexane ( $4\cdot 10^8$  M $^{-1}$  [8]) containing complex ions.

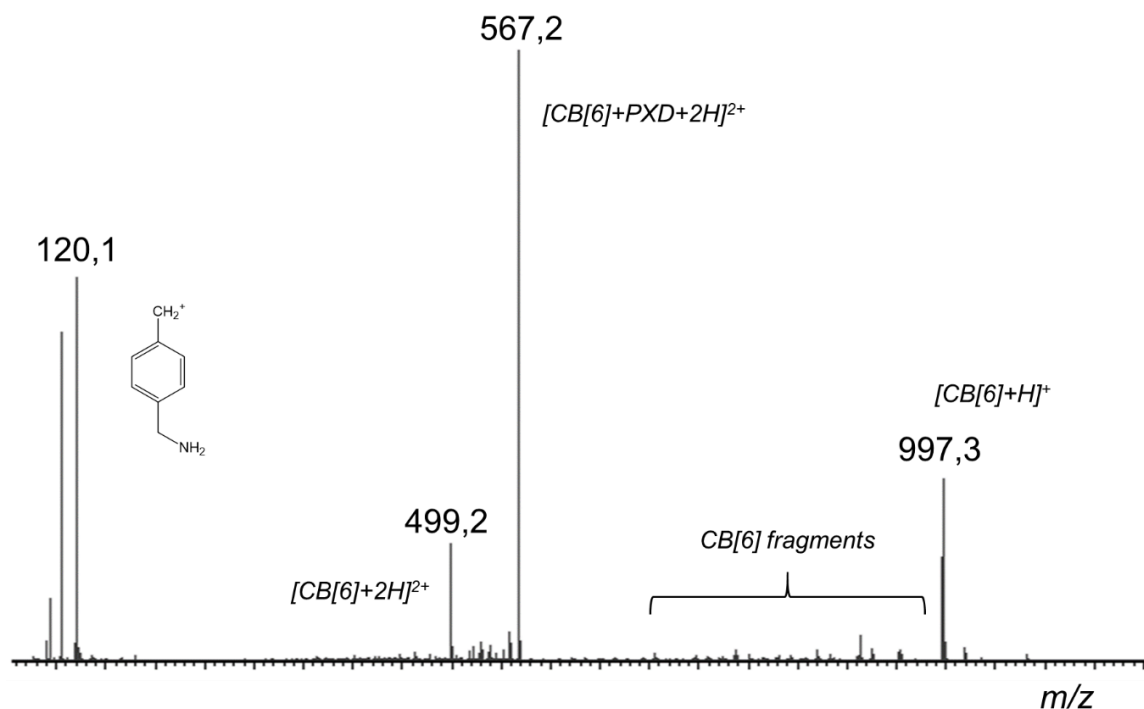


**Figure IV.2.14:** CID analysis (Trap cell) of the  $[CB[6]+PXD+2H]^{2+}$  complex ions ( $m/z$  567,2).

### 2.3 Conclusions

Aryl- and alkylammonium ions are known to strongly interact with the cucurbituril family of macrocyclic receptors. The primary interactions correspond to H-bonds created between the hydrogen atoms of the ammonium moiety and the oxygen atoms of the carbonyl groups. However, encapsulation of the guest within the cavity is often hindered or kinetically limited by steric factors since the guest molecule must enter the cavity through the small size portals. Mass spectrometry, associating Electrospray ionization, collision-induced dissociation and ion mobility, has been already advantageously used to study in the gas phase the topology of host-guest complexes associating amino compounds to cucurbituril receptors [6, 9]. In the present work, we selected a model system, extensively investigated in the condensed phase, to assess the influence of the instrumental parameters, i.e., the voltages along the ion optics, on the IN-to-OUT ratio starting from the knowledge of the condensed phase topologies. All experiments were performed on the Waters Synapt G2-Si mass spectrometer and the IN-to-OUT ratios were determined based on ion mobility experiments. We demonstrated here that,

for mono amino guest molecules, the IN-to-OUT isomerization process can be induced upon ion activation at different locations along the flight of the ions from the source to the ion mobility cell, i.e. in the stepwave (**Sample Cone voltage**) and in the Triwave<sup>®</sup> setup (**Trap DC Bias** and **TRAP CE**). On the other hand, the diammonium guest molecules entangled within the host cavity and H-bonded on both portals do not undergo the IN-to-OUT process. When increasing the internal energy, the complex ion dissociation proceeds through covalent bond breaking of the cucurbituril backbone. These results complete our previous mass spectrometry investigations on the cucurbituril systems that demonstrated the applicability of ESI, CID and ion mobility to probe the gas phase structures of complex ions – the so-called flying boxes [9]. We also previously demonstrated the influence of the equilibration time in solution on the IN/OUT nature of the detected gaseous ions [6]. In this paper, we have also highlighted the key role played by the ion optics on the topology of the supramolecular ions transferred from the solution to the gas phase upon Electrospray Ionization.



## References

1. W. L. Mock, N.-Y. Shih, *Dynamics of molecular recognition involving cucurbituril*, *J. Am. Chem. Soc.* 1989, 111, 2697–2699.
2. a) J. Lagona, P. Mukhopadhyay, S. Chakrabarti, L. Isaacs, *The cucurbit[n]uril family*, *Angew. Chem. Int. Ed.* 2005, 44, 4844–4870; *Angew. Chem.* 2005, 117, 4922–4949; b) J. W. Lee, S. Samal, N. Selvapalam, H. J. Kim, K. Kim, *Cucurbituril Homologues and Derivatives: New Opportunities in Supramolecular Chemistry*, *Acc. Chem. Res.* 2003, 36, 621–630; c) K. Kim, N. Selvapalam, Y. H. Ko, K. M. Park, D. Kim, J. Kim, *Functionalized cucurbiturils and their applications*, *Chem. Soc. Rev.* 2007, 36, 267–279; d) L. Isaacs, *The Mechanism of Cucurbituril Formation*, *Isr. J. Chem.* 2011, 51, 578–591; e) E. Masson, X. Ling, R. Joseph, L. Kyeremeh-Mensah, X. Lu, *Cucurbituril chemistry: a tale of supramolecular success*, *RSC Adv.* 2012, 2, 1213–1247.
3. a) K.I. Assaf, W.M. Nau, *Cucurbiturils: from synthesis to high-affinity binding and catalysis*, *Chem. Soc. Rev.*, 2015, 44, 394–418; b) S.J. Barrow, S. Kasera, M.J. Rowland, J. del Barrio, O.A. Scherman, *Cucurbituril-Based Molecular Recognition*, *Chem. Rev.*, 2015, 115 (22), 12320–12406.
4. W.L. Mock, N-Y Shih, *Structure and Selectivity in Host-Guest Complexes of Cucurbituril*, *J. Org. Chem.*, 1986, 51, 4440–4446.
5. C. Marquez, W.M. Nau, *Two Mechanisms of Slow Host–Guest Complexation between Cucurbit[6]uril and Cyclohexylmethylamine: pH-Responsive Supramolecular Kinetics*, *Angewandte Chemie* 2001, 40, 3155–3160.
6. [6] G. Carroy, C. Daxhelet, V. Lemaire, J. De Winter, E. De Pauw, J. Cornil, P. Gerbaux, *Influence of Equilibration Time in Solution on the Inclusion/Exclusion Topology Ratio of Host-Guest Complexes Probed by Ion Mobility and Collision-Induced Dissociation*, *Chem. Eur. J.*, 2016, 22, 4528–4534.
7. a) W.L. Mock, N-Y Shih, *Organic ligand-receptor interactions between cucurbituril and alkylammonium ions*, *J. Am. Chem. Soc.*, 1988, 110, 4706–4710.
8. S. Liu, C. Ruspic, P. Mukhopadhyay, S. Chakrabarti, P.Y. Zvalij, L. Isaacs, *The Cucurbit[n]uril Family: Prime Components for Self-Sorting Systems*, *J. Am. Chem. Soc.* 2005, 127, 15959–15967.

9. a) V. Lemaur, G. Carroy, F. Poussigue, F. Chirot, J. De Winter, L. Isaacs, P. Dugourd, J. Cornil, P. Gerbaux, *Homotropic allostereism: In-depth structural analysis of the gas-phase noncovalent complexes associating a double-cavity cucurbit[n]uril-type host and size-selected protonated amino compounds*, ChemPlusChem. 2013, 78, 959-969; b) G. Carroy, V. Lemaur, J. De Winter, L. Isaacs, E. De Pauw, J. Cornil, P. Gerbaux, *Energy-resolved collision-induced dissociation of non-covalent ions: charge- and guest-dependence of decomplexation reaction efficiencies*, Phys. Chem. Chem. Phys. 2016, 18, 12557-12568.

## Chapter 3:

Probing the cucurbituril-catalysed 1,3-cycloaddition by mass spectrometry.

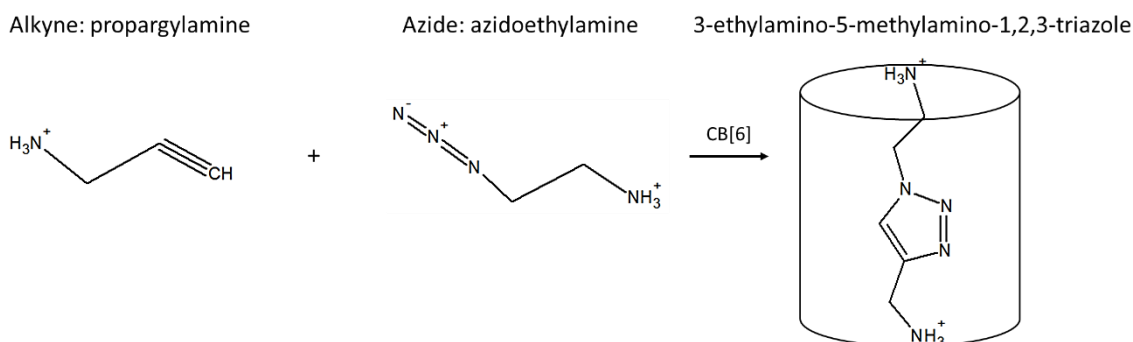
*G. Carroy, V. Lemaux, J. De Winter, E. De Pauw, J. Cornil, P. Gerbaux.*

---

### 3.1 Introduction

Cucurbit[n]urils are macrocyclic receptors made of n glycoluril repeat units hold together through methylene bridges (n=5-14) [1]. These pumpkin-shaped molecules are amphiphilic since they are made of a hydrophobic inner cavity but present two identical carbonyl hydrophilic portals, making them suitable for encapsulation of hydrophobic molecules or the hydrophobic part of molecules in aqueous media [2]. The main drawback of cucurbiturils is their low solubility in water requiring low pH or high ionic strength to ensure their dissolution upon protonation of the carbonyl portal or cationization [2]. Over the past decade, the cucurbit[n]uril (CB[n]) family of molecular containers has attracted a huge interest mainly due to their outstanding recognition properties and exceptional strength of their interaction with various guests. Cucurbiturils form stable inclusion complexes with various protonated alkyl- and aryl(di)amines [1-3]. Therefore, numerous applications have been discovered due to the encapsulation propensity of the cucurbituril family members [3].

Among those applications, cucurbiturils have been deeply studied for their remarkable catalytic properties due to their inner cavity that can be considered as a *nanoreactor* [2]. At the origin of this discovery that triazole formation by a 1,3-dipolar cycloaddition between an alkyne and an azide may occur inside the cucurbituril cavity [4]. Indeed, Mock demonstrated that a catalytic amount of cucurbit[6]uril (CB[6]) considerably accelerates ( $6 \cdot 10^4$  factor) the regiospecific formation of 1,2,3-triazole (see ***scheme IV.3.1***). The catalytic phenomenon has been explained in terms of (1) victory against the entropic constraints and (2) an activation of the substrat due to its encapsulation within the CB[6] cavity [4]. It is worth noting that, even with CB[6], several days are needed to finally reach quantitative conversion for the cycloaddition reaction [4]. This was suggested to be due to the slow egression process of the heterocyclic compound from the cavity that slow down the overall process.



**Scheme IV.3.1:** click reaction of azidoethylamine and propargylamine to form 3-ethylamino-5-methylamino-1,2,3-triazole inside the CB[6] host cavity.

Herein, we report a mass spectrometric study carried on the same reaction as the one proposed by Mock (see **scheme IV.3.1**) with a special emphasis on the in-solution time reaction prior to the ionization process. Since the final triazole product is hardly released from the CB[6] host [4], a difference should be observed on the CID fragmentations of the corresponding ionized complexes all along the reaction time. Indeed, the ternary complexes associating CB[6], propargylamine (propa) and azidoethylamine (azide) at the beginning of the reaction should present a different decomposition behavior than the final binary complexes where the synthesized triazole remains trapped inside the host cavity. Therefore, the full MS-based methods available in our laboratory (MS, MSMS, IMMS, ER-CID) have been applied to a 1:1:1 mixture between the host CB[6] and the reagents propa and azide for a total in-solution reaction time of 15 days .

### 3.2 Results and discussion

Oppositely to the reference paper of Mock [4], the mass spectrometry experiments performed in our laboratory were not realized with a catalytic amount of CB[6] but with a 1:1:1 mixture between the host and the two different guests used in this study (see **scheme IV.3.1**). The solution used for the different MS analyses presented a concentration of  $10^{-5}$ M in CB[6], propargylamine (propa) and azidoethylamine (azide) (Solvent: 80% water, 20% methanol). The stock/reaction solution ( $10^{-3}$ M) has been swirled during 15 days at 20°C. In order to monitor the time evolution of reaction medium, MS analyses have been realized each day on the Waters Synapt G2-Si.

As shown in **figure IV.3.1 a**, for an in-solution reaction time close to 0 (*just after mixing the different reagents and dissolving further the reaction solution for the MS analysis*), doubly charged non covalent complexes associating CB[6] and Propa are mostly detected in the gas phase at  $m/z$  526 for  $[\text{CB}[6]+\text{propa}+2\text{H}]^{2+}$ . Water molecule adducts are also detected amongst the gaseous complex ions (see **figure IV.3.1 a**).

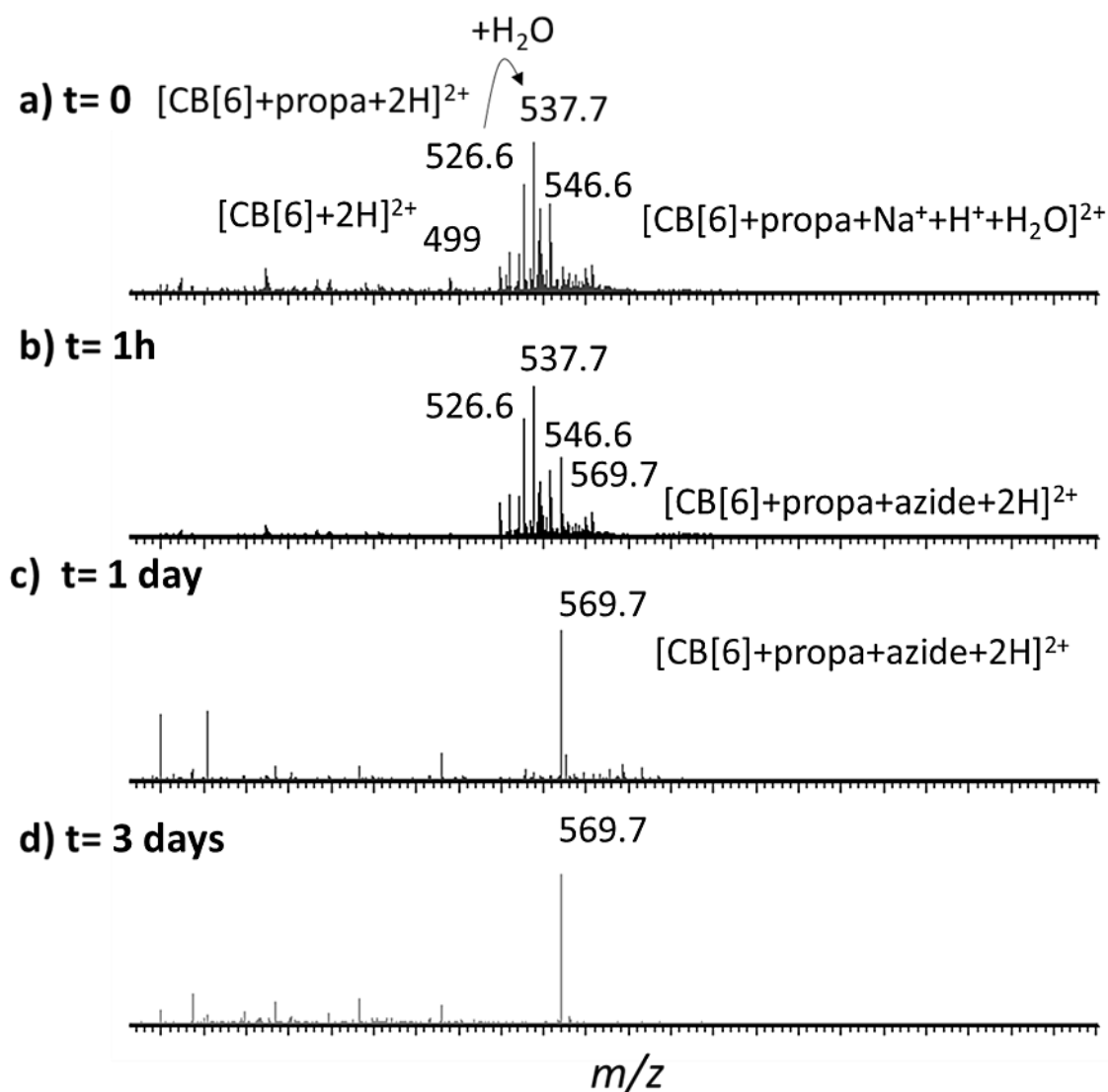


**Figure IV.3.1:** ESI-MS spectra (Waters Synapt G2-Si) of a 1:1:1 mixture between the host CB[6] and the two reagents azide and propa for different in-solution reaction time.

After 1 hour of agitation (**figure IV.3.1 b**), 2+ ions corresponding to the “ternary” complexes associating CB[6], propa and azide, say  $[\text{CB}[6] + \text{propa} + \text{azide} + 2\text{H}]^{2+}$ , starts to be detected at  $m/z$  569. The MS signal corresponding to these doubly charged complexes becomes the base peak after 24h of in-solution reaction time (**figure IV.3.1.c**). For longer reaction times, the same MS spectra are obtained regardless of the in-solution reaction time (from 2 days till 15 days). A typical example is shown in **figure IV.3.1 d** for the MS analysis after 3 days.

In addition, the experimental collisional cross sections of the ions  $m/z$  569 has been determined using ion mobility and amounts to  $204 \text{ \AA}^2$ . In comparison with our previous studies [5], we can attest that the structure of these gas phase ions should correspond to an inclusion topology. Nevertheless, we must stress out that, at this point of the study, we do not know anything yet about the presence of the cycloaddition reaction product. Indeed, the detected complexes might either be ternary complexes involving CB[6], propa and azide or binary complexes involving CB[6] and the synthesized triazole.

We then decided to expose to Collision-induced Dissociation experiments those 2+ complex ions. Indeed, the CID reactions of the ions  $m/z$  569 are likely to be different before and after the cycloaddition reaction. We also decided to follow the evolution of the CID data all along the 15 days of reaction. Interestingly, whatever the time, as soon as the  $[\text{CB}[6] + \text{propa} + \text{azide} + 2\text{H}]^{2+}$  ( $m/z$  569) complex ions are detected, their CID spectra are invariably identical. As for typical example, the MSMS spectrum presented in **figure IV.3.2** has been recorded after 15 days of in-solution reaction time. Several different fragmentations pathways are observed and are described in **scheme IV.3.2**.

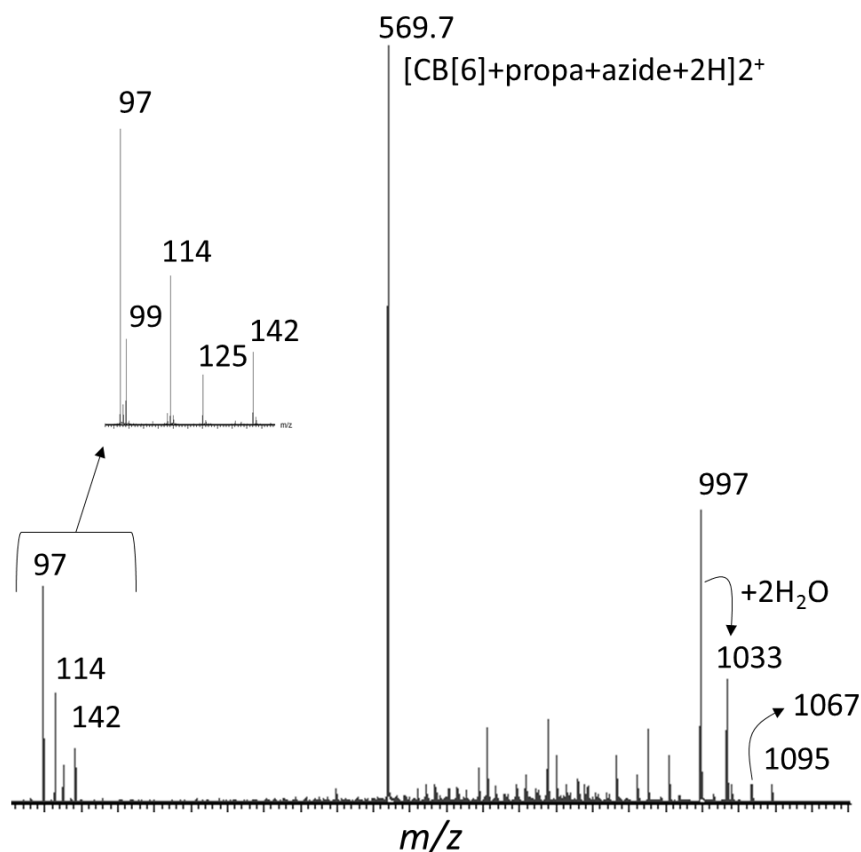


**Figure IV.3.2:** CID mass spectrum of the  $m/z$  569 ions (trapCE: 25V). The inset corresponds to a larger view of the  $m/z$  97-142 zone.

The first fragmentation pathway (**scheme IV.3.2 route a**) consists in the release of the triazole reaction product synthesized inside the CB[6] cavity leading to 1+ ions at  $m/z$  142 for protonated triazole alongside the singly charged CB[6] observed at  $m/z$  997. Consecutively, the released protonated triazole might undergo two different fragmentations, an ammonia loss ( $m/z$  125) and vinylamine loss through a 1,2-elimination reaction ( $m/z$  99). The consecutive nature of those CID fragmentation has been confirmed by recording the CID spectrum of the isolated ions  $m/z$  142 presented in **figure IV.3.3**.

The second fragmentation pathway (**scheme IV.3.2 route b**) is initiated by the 1,2-elimination reaction of the triazole product inside the CB[6] cavity leading to the detection of the 1+ ions at  $m/z$  1095. This elimination is then followed by a N<sub>2</sub> loss observed yielding the  $m/z$  1067 cations. The final step consists in the decomplexation of the protonated or neutral resulting enamine generating respectively the  $m/z$  59 and 927 ions.



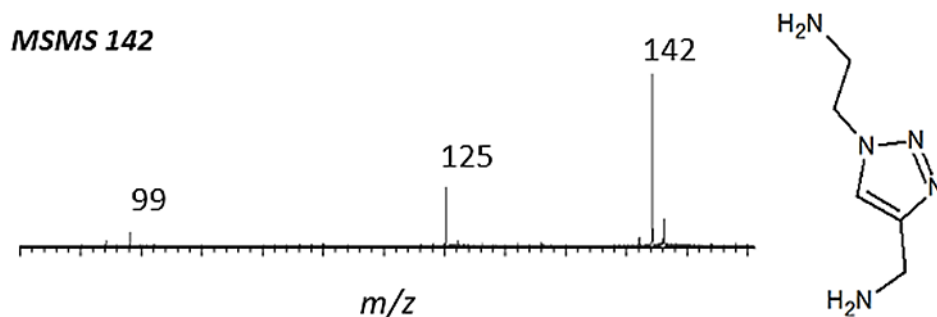
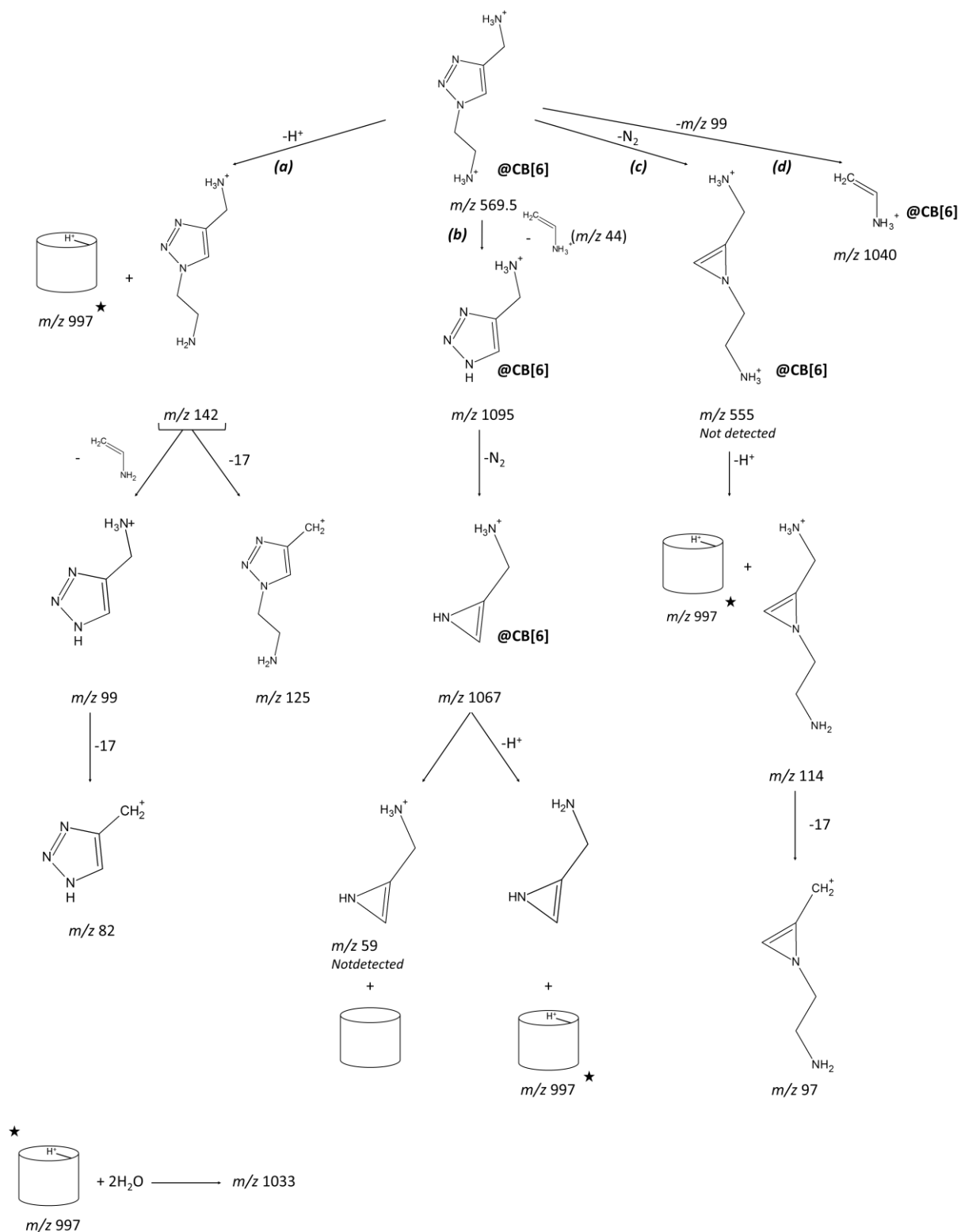


**Figure IV.3.3:** MSMS spectrum of protonated 3-ethylamino-5-methylamino-1,2,3-triazole ( $m/z$  142).

The elimination of nitrogen ( $N_2$ ) can also occur starting from the triazole ions within the host cavity (**scheme IV.3.2 route c**) leading to  $m/z$  555 ions. Protonated enamine is then expelled from the CB[6] host and two ions are detected: the protonated CB[6] ( $m/z$  997) and the protonated enamine ( $m/z$  114), which may lose ammonia to finally form the ions observed at  $m/z$  97. Interestingly when comparing the CID spectra of protonated 3-ethylamino-5-methylamino-1,2,3-triazole ( $m/z$  142 in **figure IV.3.3**) with the inset in **Figure IV.3.2**, the proposed **route c** explains the occurrence of the  $m/z$  97 ions in the low mass region.

The final decomposition route (**scheme IV.3.2 route d**) starts with the 1,2-elimination reaction leading immediately to the formation of the  $m/z$  99 ions, that were also proposed to be generated following **route a** (*vide supra*). This elimination occurs again within the CB[6] cavity and leads to the detection of the 1+ complex ions, say [CB[6]+ vinylamine + H]<sup>+</sup> ( $m/z$  1040).

## IV. Results and discussion



**Scheme IV.3.2:** CID reactions undergone by the  $m/z$  569 cations. The symbol “@CB[6]” means that the small molecule/ion is entangled within the cucurbituril cavity.

To confirm the composition of all the detected species presented in **scheme IV.3.2** and **figure IV.3.2**, HRMS measurements have been realized. The results are presented in **table IV.3.1**. For the lower masses (upper part), the signal corresponding to the protonated triazole at  $m/z$  142 has been used as internal standard – lock mass – whereas, for higher masses (bottom part), the reference ions are  $[CB[6]+H]^+$  ( $m/z$  997). Those two species have been chosen as standards since no doubts exist about their structures.

**Table IV.3.1:** HRMS measurements on the fragment ions of the complexes  $[CB[6]+propa + azide + 2H]^{2+}$  ( $m/z$  569).

HRMS reference system	Experimental $m/z$	Elemental composition	Isotopic Model $m/z$
$C_5H_{12}N_5$ $m/z$ 142.1093	97.0763	$C_5H_9N_2$	97.0766
	99.0661	$C_3H_7N_4$	99.0671
	114.1030	$C_5H_{12}N_3$	114.1031
	125.0822	$C_5H_9N_4$	125.0827
$C_{36}H_{37}N_{24}O_{12}$ $m/z$ 997.3023	1033.3253	$C_{36}H_{41}N_{24}O_{14}$	1033.3235
	1040.3381	$C_{38}H_{42}N_{25}O_{12}$	1040.3445
	1067.3596	$C_{39}H_{43}N_{26}O_{12}$	1067.3553
	1095.3601	$C_{39}H_{43}N_{28}O_{12}$	1095.3616

Finally, **figure IV.3.4** presents the energy-resolved CID curves (ER-CID) obtained on the ions  $m/z$  569 for two different in-solution reaction time: one curve has been recorded after two weeks while the other was obtained after an in-solution reaction time of one hour. As shown in **figure IV.3.4**, the ER-CID curve obtained for the “ternary” complexes at  $t=1h$  perfectly superposes the curve obtained starting from the ions observed for an in-solution reaction time of two weeks. With that observation and the similarity between the MSMS spectra already discussed in **figure IV.3.3** whatever the in-solution reaction time, we postulate that immediately both the two reagents, namely protonated propargylamine (propa) and azidoethylamine (azide), are closely associated inside the CB[6] cavity, the cycloaddition

reaction directly occurs leading to the detection of the complexes  $[\text{CB}[6] + \text{triazole} + 2\text{H}]^{2+}$  at  $m/z$  569.

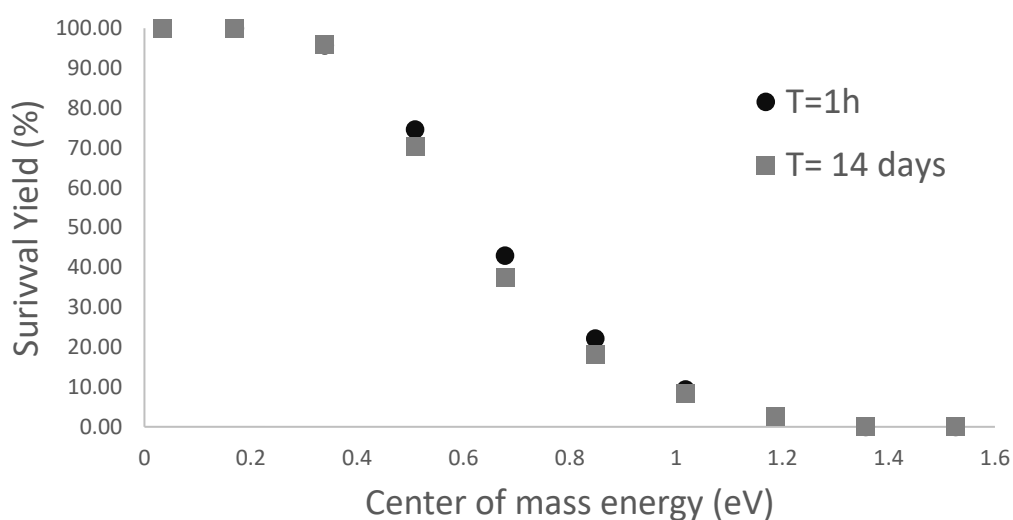


**Figure IV.3.4:** Energy-resolved (ER-CID) experiments performed on the ions  $m/z$  569 for two different in-solution reaction times.

### 3.3 Conclusion

Mass spectrometry, associating Electrospray ionization, collision-induced dissociation and ion mobility, has been already advantageously used to study the cucurbituril systems in association with different amino-compound. Those studies demonstrated the applicability of ESI, CID and ion mobility to probe the gas phase structures of complex ions – the so-called flying boxes [5]. In the present work, we reported a mass spectrometric study performed on a click reaction using the inner cavity of a cucurbit[6]uril host as a catalyzer. The use of Electrospray as ionization source renders possible the detection of gas phase ions corresponding to complexes between CB[6], Propa and Azide primarily formed in solution. According to our results using CID, ion mobility and ER-CID experiments, we observe that the cycloaddition reaction within the CB[6] cavity is an extremely fast process and that the rate determining step in the overall cycloaddition process is the encapsulation of both the reagents within the cavity. On the other hand, the cycloadduct seems to be hardly expelled from the cucurbituril cavity explain then the long reaction time monitored by Mock et al in their reference publication [4].

## References

1. a) W. L. Mock, N.-Y. Shih, *J. Am. Chem. Soc.* 1989, 111, 2697–2699.
2. a) J. Lagona, P. Mukhopadhyay, S. Chakrabarti, L. Isaacs, *Angew. Chem. Int. Ed.* 2005, 44, 4844–4870; *Angew. Chem.* 2005, 117, 4922–4949; b) J. W. Lee, S. Samal, N. Selvapalam, H. J. Kim, K. Kim, *Acc. Chem. Res.* 2003, 36, 621–630; c) K. Kim, N. Selvapalam, Y. H. Ko, K. M. Park, D. Kim, J. Kim, *Chem. Soc. Rev.* 2007, 36, 267–279; d) L. Isaacs, *Isr. J. Chem.* 2011, 51, 578–591; e) E. Masson, X. Ling, R. Joseph, L. Kyeremeh-Mensah, X. Lu, *RSC Adv.* 2012, 2, 1213–1247.
3. a) K.I. Assaf, W.M. Nau, *Chem. Soc. Rev.*, 2015, 44, 394-418; b) S.J. Barrow, S. Kasera, M.J. Rowland, J. del Barrio, O.A. Scherman, *Chem. Rev.*, 2015, 115 (22), 12320-12406.
4. a) W.L. Mock, T.A. Irra, J.P. Wepsiec, T.L. Manimaran, *J. Org. Chem.* 1983; 48:3619-3620; b) W.L. Mock, T.A. Irra, J.P. Wepsiec, M. Adhya, *J. Org. Chem.* 1989; 54: 5302-5308.
5. a) V. Lemaury, G. Carroy, F. Poussiguet, F. Chirot, J. De Winter, L. Isaacs, P. Dugourd, J. Cornil, P. Gerbaux, *ChemPlusChem.* 2013, 78, 959-969; b) G. Carroy, V. Lemaury, J. De Winter, L. Isaacs, E. De Pauw, J. Cornil, P. Gerbaux, *Phys. Chem. Chem. Phys.* 2016, 18, 12557-12568 ; c) G. Carroy, C. Daxhelet, V. Lemaury, J. De Winter, E. De Pauw, J. Cornil, P. Gerbaux, *Chem. Eur. J.*, 2016, 22, 4528 –4534.

## Chapter 4:

Homotropic allostery: in-depth structural analysis by mass spectrometry and computational chemistry of the gas-phase non covalent complexes associating a double-cavity cucurbit[n]uril-type host and size-selected protonated amino compounds.

V. lemaur, G. Carroy, F. Poussigue, F. Chirot, J. De Winter, L. Isaacs, P. Dugourd, J. Cornil, P. Gerbaux.

*ChemPlusChem*. 2013; 78: 959-969.

---

## 4.1 Introduction

A huge interest in the cucurbit[n]uril (CB[n], n=5-10) family of molecular containers has surged in recent years because of their outstanding binding capabilities.[1] Cucurbiturils are macrocyclic molecules built from glycoluril repeat units. These pumpkin-shaped molecules have a hydrophobic inner cavity and two identical carbonyl-laced portals and form stable inclusion complexes with various protonated alkyl and arylamines.[1] The relative rigidity of CB[n] host molecules and the close juxtaposition of two positively charged binding regions impart high selectivity/specificity to the CB[n] receptors.[1] Moreover, in contrast to the behavior of most synthetic receptors in aqueous solution, CB[n] molecules commonly display slow kinetics of guest association, dissociation and exchange, given the need of significant deformations of the portals of the host molecules to allow access of guest molecules to the inner cavity.[1] This peculiar property renders possible the investigation of complexation properties by NMR.[1]

Nowadays, mass spectrometry (MS) methods are increasingly used to study non-covalent complexes extracted from the solution phase to the rarefied gas phase by means of the electrospray ionization source.[2] In the gas phase, ions do not interfere with each other chemically. Consequently, dynamic processes do not play a role anymore and the properties of the supramolecular objects can be monitored, with a special interest in the determination of the composition, i.e. stoichiometry of the association. New insights can be gained from the examination of the gas phase stability and reactivity. However, huge differences can be expected when compared to the solution phase properties so that the use of MS-based methods to study non-covalent associations must be handled with great care, especially when trying to deduce from the MS data the solution properties.[2] A typical example was reported by Vouros et al when studying the non-covalent interactions between amino acids and cyclodextrin receptors and observing in the gas phase unspecific associations between polar amino acids and the host molecule in contrast to the solution.[3] MS-based methods appear nowadays more and more prone to provide fast and accurate information about supramolecular systems.[2] In recent years, numerous studies took advantages of the mass spectrometry capabilities to investigate complexation processes. For instance, several groups extensively studied the complexation properties of CB[n] and demonstrated the capabilities

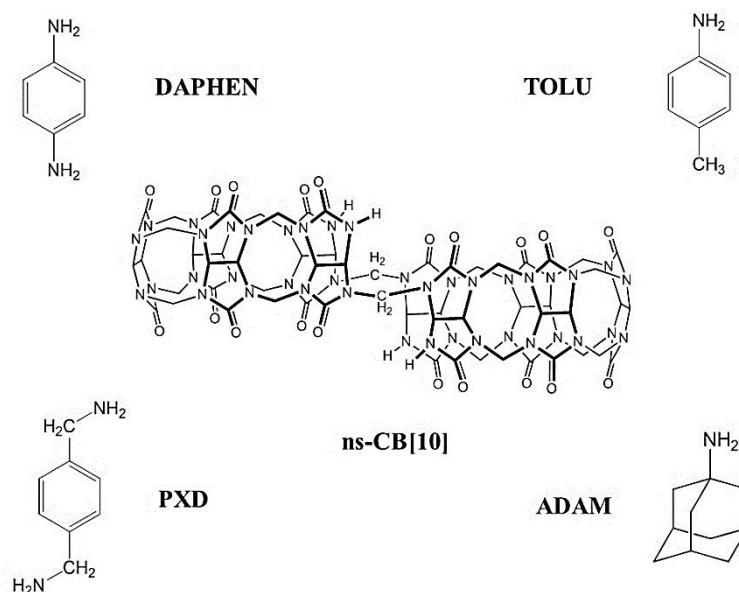
of MS methods to afford reliable data on the structure of the gas phase complexes.[4] Mass spectrometry can go far beyond the analytical characterization of the complexes in terms of their exact mass, charge state, and stoichiometry. Indeed, nowadays, mass spectrometry offers quite a large panel of methods that can provide structural information on the complexes. In particular, the “secondary structure” of the non-covalent associations, i.e. the relative position of the non-covalently bound subunits in the complex can be efficiently probed by collision-induced dissociation [5], associative ion/molecule reactions (H/D exchange)[6] and ion mobility [7] experiments. Relative binding energies of non-covalent associations in the gas phase can also be inferred by MS-based methods by performing ligand exchange reactions in the gas phase.[8] Critical energies of fragmentation for non-covalent complexes in the gas phase are also often estimated by performing energy-resolved CID experiments and determining the center-of-mass energy required for the decomposition / decomplexation reaction to occur.[9] However, such experiments do not afford any thermochemical data such as binding energies but threshold energies are estimated. Absolute binding energies for gas-phase non-covalent complexes are probably best evaluated by using computational chemistry that also yields optimized geometries to be compared to the experimental data. [8,10]

Recently, Isaacs et al reported the kinetically-controlled synthesis as well as the recognition properties of a new member of the cucurbituril family, namely nor-seco-cucurbit[10]uril (ns-CB[10], ***scheme IV.4.1***) which results from the formal extrusion of two CH<sub>2</sub> bridges from CB[10] along with bond reorganization.[11] This molecular container presents two cavities and is suitable for binding guest molecules to form ternary complexes (2:1). Several key features for the binding capabilities of this large host molecule were then described. In particular, ns-CB[10] was shown to conserve much of the binding properties of the CB[n] molecules. However, this ditopic receptor also: (i) binds larger guests than expected given that both cavities are each shaped by only five glycoluril residues, thus highlighting the structural responsiveness of the cavity; and (ii) displays homotropic allostery based on a guest size induced preorganization mechanism.

In the present study, we report a joint experimental and theoretical study by mass spectrometry and computational chemistry of the binding properties of ns-CB[10] towards selected protonated alkyl and arylamines. The underlying idea lies in a much broader context,



which aims at exploring the potentialities of MS for the study of supramolecular chemistry. Four guest molecules have been selected for this investigation, namely 1,4-diaminophenylene (DAPHEN), para-toluidine (TOLU), para-xylylenediamine (PXD) and adamantylamine (ADAM), see *scheme IV.4.1*.



**Scheme IV.4.1:** structures of the host nor-seco-cucurbit[10]uril (ns-CB[10]) and the guests under study: 1,4-diaminophenylene (DAPHEN), para-toluidine (TOLU), para-xylylenediamine (PXD) and adamantylamine (ADAM).

The X-rays structure of the ternary complex associating two DAPHEN molecules to ns-CB[10] is available [11] and represents a perfect starting point for the theoretical part of the study. The TOLU guest has been selected to probe the influence of the two amino groups of DAPHEN on the structure of the complexes. The choice of PXD as a guest molecule is driven by the presence of two aliphatic amino groups instead of two aromatic amino groups in DAPHEN. Finally, the relatively bulky and rigid structure of ADAM makes it a suitable guest to probe the homotropic allostery phenomenon described in the literature.[11] All experimental data collected in the present work rely on mass spectrometry-based methods. Namely, standard ESI-ToF analyses have been performed in order to identify the complex ions emerging from the ESI probe and to determine their charge states and stoichiometries, especially the formation of binary vs ternary complexes. The global conformations of the complexes have been further examined through ion mobility experiments. In parallel, classical molecular

mechanics and quantum-chemical Density Functional Theory (DFT) calculations have been carried out to identify the most stable geometric configuration for these systems, and particularly, the relative position of the host and guest molecules (inclusion vs exclusion complexes).

## 4.2 Results and discussion

### 4.2.1 ESI time-of-flight (TOF) measurements

#### ***PXD/ns-CB[10] interaction:***

The mass spectrum obtained following an ESI-ToF analysis (Waters QToF 2 mass spectrometer) of a solution containing  $10^{-4}$  M of ns-CB[10] and  $5 \cdot 10^{-4}$  M of PXD is presented in **figure IV.4.1 a**. This mass spectrum was obtained using a common standard cone voltage of 40 V. Different signals are observed in this spectrum at  $m/z$  120, 137, 819.3, 887.3 and 955.4 and can be attributed to the following ions:  $[\text{NH}_2\text{-CH}_2\text{-C}_6\text{H}_4\text{-CH}_2]^+$ ,  $[\text{NH}_2\text{-CH}_2\text{-C}_6\text{H}_4\text{-CH}_2\text{-NH}_3]^+$ ,  $[\text{ns-CB}[10]+2\text{H}]^{2+}$ ,  $[\text{ns-CB}[10]+\text{PXD}+2\text{H}]^{2+}$  and  $[\text{ns-CB}[10]+2\text{PXD}+2\text{H}]^{2+}$ , respectively. Beside protonated PXD ( $m/z$  137) and its fragment ions ( $m/z$  120), the other detected species correspond to doubly charged (+2) ions associating the ns-CB[10] receptor molecule to respectively 0, 1 and 2 guest molecules. The observation of free receptor ions together with binary and ternary complexes is in total contradiction with the data reported by Isaacs et al that never observed by NMR the formation of binary (1 guest) complexes concomitant with ternary (2 guests) complexes [11]. Moreover, we prepared our ns-CB[10] / PXD solution with a 2.5-fold excess in guest molecules (5:1) to avoid free receptor molecules in solution. Basically, the mass spectrum presented in **figure IV.4.1 a** is then totally inconsistent with the expectations based on the literature report [11]. Nevertheless, the occurrence in **figure IV.4.1 a** of the  $m/z$  120 fragment ions, arising from an ammonia loss from protonated PXD at  $m/z$  137, indicates that the in-source conditions are not soft enough to prevent ion decomposition, even if the selected cone voltage is reasonably low. We then tried to avoid the decomposition of the ions during their transmission between the sample cone and the extractor of the Z-spray source by: (i) decreasing the cone voltage to 20 V; and (ii) increasing the in-source

pressure by reducing the pumping speed (see experimental Section) [12]. When measuring the ESI mass spectrum with these new transmission parameters (CV 20 V, in-source pressure at 4 mbar), a significantly different ion distribution is now observed, as revealed in **figure IV.4.1 b** and summarized in **table IV.4.1**. The mass spectrum is dominated by the  $m/z$  637.2 signal that corresponds to a triply charged ternary complex, i.e.  $[\text{ns-CB}[10]+2\text{PXD}+3\text{H}]^{3+}$ . These ions are totally absent in the ESI mass spectrum of **figure IV.4.1 a**, in which only doubly charged ternary complexes,  $[\text{ns-CB}[10]+2\text{PXD}+2\text{H}]^{2+}$ , are observed at  $m/z$  955.4. In addition to these doubly and triply charged ternary complexes, 4-fold charged ions are also detected and appear at  $m/z$  478.2,  $[\text{ns-CB}[10]+2\text{PXD}+4\text{H}]^{4+}$ . Ternary complex ions are thus clearly detected from the ESI analysis but the ion population is characterized by a charge state distribution, from +2 to +4, with a higher proportion of the triply charged species at  $m/z$  637.2. It is also worth pointing to the total disappearance of the ions corresponding to free ns-CB[10] ( $m/z$  819.3) and to the binary complexes ( $m/z$  887.3). Actually, the comparison between the ESI mass spectra in **figures III.3.1 a** and **b** allows us to conclude that ternary complexes are dominant in solution and are only smoothly transmitted to the gas phase of the mass spectrometer provided really soft transmission parameters are selected. By increasing the kinetic energy of the ions between the sample and the extractor cones by augmenting the cone voltage, in-source collision induced reactions are likely to occur leading to the ion dissociation. For a given accelerating voltage, the kinetic energy of the ions is also dependent on the charge state of the ions. This explains why, only the doubly charged ternary complexes are detected under the regular source conditions, see **figure IV.4.1 a**. The  $m/z$  819.3 and  $m/z$  887.3 binary complex ions are then likely to be produced by decomposition of the ternary complex ions during their flight between the sample and the extractor cones. This will be further demonstrated on the basis of collision-induced dissociation (CID) experiments in a following part of this article. In any case, the exclusive observation of ternary complex ions in the ESI mass spectrum gives a strong confirmation that a positive cooperativity - allostereism - is operating during the complexation processes in the condensed phase.

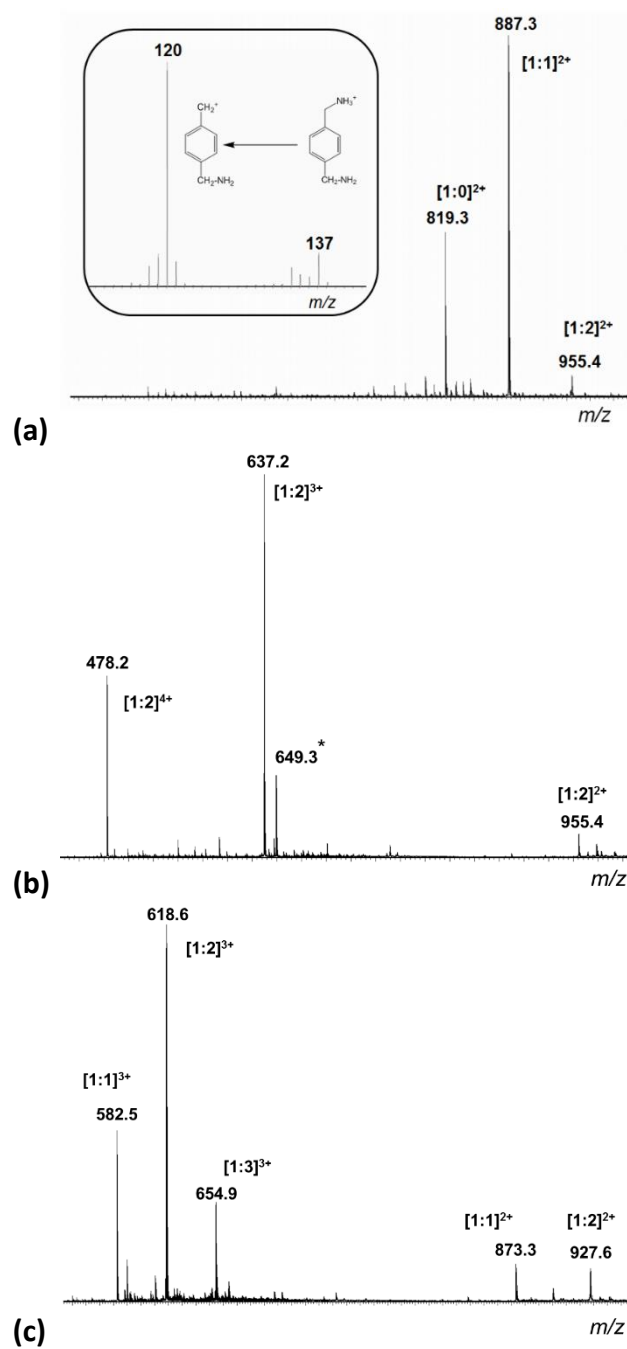


**Figure IV.4.1:** ESI-ToF mass spectra obtained on the Waters QToF 2 machine from: (a) a solution of PXD and ns-CB[10] using regular transmission conditions (see text); (b) a solution of PXD and ns-CB[10] using softer transmission conditions (see text); and (c) a solution of DAPHEN and ns-CB[10] under soft conditions. The inset of Figure IV.4.1 a represents the low  $m/z$  section of the mass spectrum.

**DAPHEN/ns-CB[10] interaction:**

Similarly, when analyzing by ESI-MS (soft conditions) a mixture of DAPHEN and ns-CB[10], triply ( $m/z$  618.6) and doubly ( $m/z$  927.6) charged ternary complex ions are observed, in agreement with the reported detection of those complexes in the condensed phase [11], see **figure IV.4.1 c** and **table IV.4.1**. Nevertheless, a significant contribution of triply charged binary complex ions,  $[\text{ns-CB}[10]+\text{DAPHEN}+3\text{H}]^{3+}$ , is observed at  $m/z$  582.5 and cannot be understood when considering the expected allosteric nature of the complexation process. In addition, the position of the third proton in those  $[\text{ns-CB}[10]+\text{DAPHEN}+3\text{H}]^{3+}$  ions is unclear, since only two basic amino groups are available on the guest DAPHEN molecule. Nevertheless, the pKa of CB[6] has been recently measured and amounts to 3.2, rendering the C=O portals probably basic enough to accommodate this additional proton [13]. We will demonstrate in a following part of this paper that these  $m/z$  582.5 ions are fragment ions from the 4-fold charged ternary complex ions,  $[\text{ns-CB}[10]+2\text{DAPHEN}+4\text{H}]^{4+}$ , which are too fragile to be transferred intact from the atmospheric pressure to the first vacuum stage of the mass spectrometer. We tried to induce even more collisional cooling by increasing the pressure between the sample cone and the extractor, but even a 11 mbar pressure was not sufficient to observe the  $[\text{ns-CB}[10]+2\text{DAPHEN}+4\text{H}]^{4+}$  ions. At this stage, it is quite clear that the triply charged ternary complex ions represent the dominant species in the ESI mass spectra for both PXD and DAPHEN. In this context, we have selected a third guest molecule that only bears one single basic amino site, namely para-toluidine (TOLU).

**TOLU/ns-CB[10] interaction:**

The base peak of the ESI mass spectrum obtained starting from a ns-CB[10]/TOLU solution also corresponds to the triply charged ternary complex ions,  $[\text{ns-CB}[10]+2\text{TOLU}+3\text{H}]^{3+}$  (**table IV.4.1**). For these ions, two protons are each associated to one guest molecule, whereas the additional proton is located somewhere on the host molecule [13]. The TOLU molecule only possesses one amino group and accordingly the doubly charged ternary complex ions are observed at  $m/z$  926.5 though the relative intensity of the corresponding signal remains weak (**table IV.4.1**). Again, the  $[\text{ns-CB}[10]+\text{TOLU}+3\text{H}]^{3+}$  ions ( $m/z$  582.2), generated by in source CID of the fragile 4-fold charged ternary complex ions, are identified in the ESI mass spectrum.

**ADAM/ns-CB[10] interaction:**

The final guest molecule selected for the present study has been chosen in the context of the demonstration of homotropic allostery [11]. Indeed, Isaacs et al observed that, when guests of different sizes compete for the complexation with ns-CB[10], the allosteric control induces the production of a mixture of both homomeric ternary complexes [11]. In contrast, mixtures of similarly sized guests result in mixtures of homomeric and heteromeric ternary complexes. These results indicate that the binding of the first guest to the receptor organizes the second cavity for binding of a guest of similar size. Adamantylamine, ADAM, then appeared as a good candidate to probe this phenomenon by mass spectrometry. Triply and doubly charged ternary complex ions are the sole species observed that incorporate the ns-CB[10] receptor. Interestingly, beside the ternary complex ions,  $[\text{ns-CB}[10]+2\text{ADAM}+2\text{H}]^{2+}$  ( $m/z$  970.3) and  $[\text{ns-CB}[10]+2\text{ADAM}+3\text{H}]^{3+}$  ( $m/z$  647.2), any binary complex ions were never observed.

**Table IV.4.1:** ESI-MS analyses on a Waters QToF 2 instrument of the ns-CB[10]/guest solutions : observed ternary and binary complex ions for the four guest molecules (see text for the experimental conditions). <sup>a</sup> Relative Intensity; <sup>b</sup> Not Detected

Charge State	TERNARY COMPLEX			BINARY COMPLEX	
	+ 2	+ 3	+ 4	+2	+3
<b>PXD</b>	$m/z$ 955.4 (5 %) <sup>a</sup>	$m/z$ 637.2 (100 %) <sup>a</sup>	$m/z$ 478.2 (55 %) <sup>a</sup>	N.D. <sup>b</sup>	$m/z$ 591.9 (5 %) <sup>a</sup>
<b>DAPHEN</b>	$m/z$ 927.6 (10 %) <sup>a</sup>	$m/z$ 618.6 (100 %) <sup>a</sup>	N.D.	$m/z$ 873.3 (10 %) <sup>a</sup>	$m/z$ 582.5 (45 %) <sup>a</sup>
<b>TOLU</b>	$m/z$ 926.5 (8 %) <sup>a</sup>	$m/z$ 617.5 (100 %) <sup>a</sup>	N.D.	$m/z$ 872.5 (3 %) <sup>a</sup>	$m/z$ 582.2 (40 %) <sup>a</sup>
<b>ADAM</b>	$m/z$ 970.3 (12 %) <sup>a</sup>	$m/z$ 647.2 (100 %) <sup>a</sup>	N.D.	N.D.	N.D.

#### 4.2.2 Collision-induced dissociation experiments

In direct connection with the observed in-source decomposition reactions and in order to gain some confirmation on the parent / daughter ion relationship, we submitted all ternary complexes to CID experiments. When subjected to collision, mass-selected 4-fold charged ternary complex ions associating two PXD and ns-CB[10], i.e.  $[\text{ns-CB}[10]+2\text{PXD}+4\text{H}]^{4+}$  ( $m/z$  478.2), expel a protonated guest molecule, yielding triply charged binary complex ions at  $m/z$  591.9 and protonated PXD at  $m/z$  137 following a charge separation process, as revealed in **figure IV.4.2 a**. The produced  $m/z$  591.9 triply charged binary complex ions consecutively decompose by losing another protonated PXD; doubly protonated empty ns-CB[10] are then generated and detected at  $m/z$  819.3.

Similarly, upon collisional activation, triply charged ternary complex ions,  $[\text{ns-CB}[10]+2\text{PXD}+3\text{H}]^{3+}$  ( $m/z$  637.2), also expel a protonated PXD (detected at  $m/z$  137) yielding doubly charged binary complex ions at  $m/z$  887.3 in **figure IV.4.2 b**. Those  $m/z$  887 ions are also produced from collisionally-excited doubly charged ternary complex ions,  $[\text{ns-CB}[10]+2\text{PXD}+2\text{H}]^{2+}$  ( $m/z$  955.4), that dissociate by losing a neutral PXD (in **figure IV.4.2 c**).

These observations allow us concluding that the binary complexes detected when analyzing by ESI the ns-CB[10]/guest solutions are undoubtedly produced by in-source CID of the corresponding ternary complex ions. When trying to identify the parent/daughter relationship in the ESI mass spectra, it must be kept in mind that 4-fold and 3-fold charged ternary complex ions dissociate by losing a protonated guest molecule, whereas the 2-fold charged ternary complex expel a neutral guest molecule. When previously analyzing the ns-CB[10]/DAPHEN (or TOLU) system by single stage ESI-MS and as already explained in a previous section of this report, 4-fold charged ternary complex ions are never observed, see **figure IV.4.1 c**. However, 3-fold charged binary complex ions are detected at  $m/z$  582.5 ions ( $m/z$  582.2 for TOLU), even if really soft transmission conditions are established. Based on the CID reactions observed for the PXD-containing ions, we can propose that those binary complex ions are fragment ions from the 4-fold charged ternary complex ions,  $[\text{ns-CB}[10]+2\text{DAPHEN (TOLU)}+4\text{H}]^{4+}$ , that are too fragile to be observed.

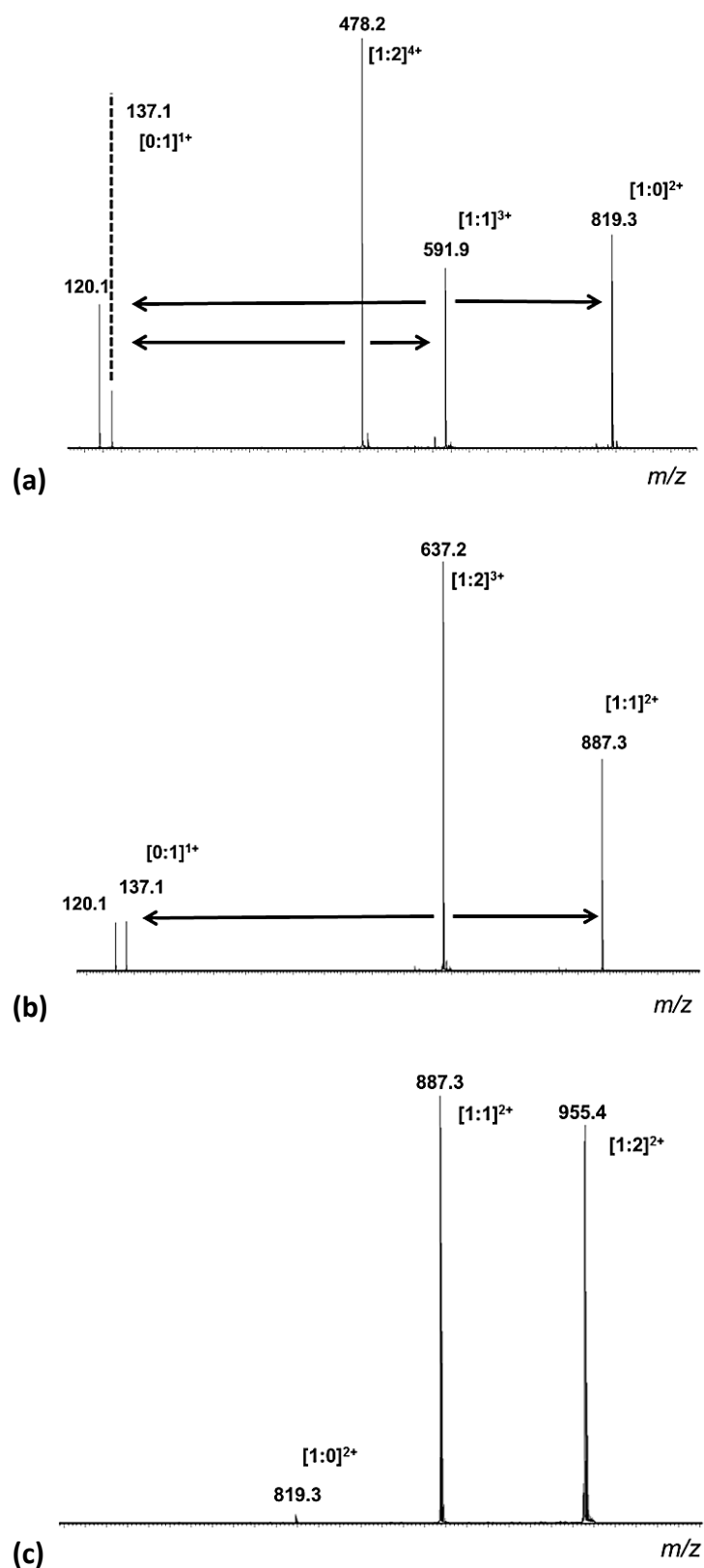


**Figure IV.4.2:** Collision-induced dissociation experiments on the ternary complexes associating two PXD molecules with one ns-CB[10] receptor: CID mass spectra of the (a) 4+, (b) 3+ and (c) 2+ complex ions.



In the following section, we will present the data obtained when subjecting the ESI-detected complex ions to ion mobility experiments. It is now well documented that ion mobility measurements can give access to the collisional cross section of ions in the gas phase [7]. Such data are definitively of prime importance in our study to obtain accurate experimental data regarding the gas-phase structures of our complex ions. In particular, the definition of the exact nature, i.e. inclusion versus exclusion, of the observed complex ions represents one of the main goals of the present study.

#### 4.2.3 Ion mobility spectroscopy experiments (IMS)

The IMS experiments were performed on a home-built instrument based on a Bruker micro-QToF mass spectrometer, see experimental Section. Given the different geometries of the ion sources between the Waters QToF 2 machine and the Bruker instrument, it is first important to confirm that similar ionic species are generated with the two machines. Note that, due to the relatively high pressure in the IMS drift-tube (13 Torr), the ion transfer to the gas phase is particularly soft using this setup, which is mandatory to observe the present complexes, as mentioned above. Overall, triply charged ternary complexes are also mainly detected on the IMS setup without any peculiar source parameter tuning. This confirms that the geometry of the transmission region of the Waters Z-spray ion source can induce extensive internal energy deposition in the ESI ions. The softer transmission conditions on the IMS machine are also confirmed since triply charged quaternary complexes, associating three guest molecules in the receptor, are detected, see **table IV.4.2**.

The collisional cross sections (CCS) extracted from our IMS measurements on different host/guest complexes are listed in **table IV.4.2** and are ranging from 297 to 368 Å<sup>2</sup>. These values lie systematically above the CCS measured for the host ns-CB[10] alone (3+ / 260 Å<sup>2</sup>). Such an increase in the cross section upon complexation is not surprising since the size of the system is likely to increase to accommodate the guests. However, it does not allow us drawing definitive conclusions on the location of the different guests, i.e., inside or outside the host cage. Indeed, both a binding of the guest at the surface of the host or a deformation of the cage upon formation of the inclusion complex could be compatible with this observation.

Nevertheless, if an inclusion complex is formed, the present results support the idea that the host cage is collapsed in the absence of guest(s).

**Table IV.4.2:** Experimental and theoretical collisional cross sections (CCS) for different systems and charge state : IMS analyses of the ns-CB[10]/guests solutions (in Å<sup>2</sup>) and calculated CCS (in Å<sup>2</sup>) for doubly and triply charged ternary homomeric complexes <sup>a</sup> Not Detected.

	IMS experiments			Theoretical values	
	TERNARY COMPLEX		QUATERNARY COMPLEX	TERNARY COMPLEX	
Homo-complexes	1:2		1:3	1:2	
Charge state	+3	+4	+3	+2	+3
TOLU	310	N.D. <sup>a</sup>	353/327	300	303
DAPHEN	297	N.D.	312	300	301
PXD	315	321	N.D.	303	310
ADAM	324	N.D.	368	319	322
<b>Host alone (+3)</b>	260			255	

Most of the observed systems are triply charged, except for the ternary complex [nsCB[10]+2PXD+4H]<sup>4+</sup> (see **table IV.4.2**). In this case, the presence of the additional charge results in a slight increase in the measured CCS (321 Å<sup>2</sup> vs 315 Å<sup>2</sup>). This increase can be intuitively understood by the fact that our relatively small and rigid systems adopt more extended structures for higher charge states in order to minimize the electrostatic repulsion between the charges. Note, however, that for compounds like peptides which exhibit polar groups, both increases and decreases in the CCS have been measured experimentally upon complexation [14]. In the following section, we will mainly discuss the triply-charged species that are dominant under our experimental conditions.

Triply-charged ternary 1:2 (one host and two guests) complexes are observed for all guests, thus allowing the investigation of the influence of the nature of the guest on the structure of the complex. As summarized in **table IV.4.2**, it appears that the different complexes are characterized by relatively close CCS, and that these CCS can be qualitatively correlated to the size of the guest rather than to its mass (TOLU is larger than DAPHEN due to the presence of one additional atom; PXD exhibits two additional CH<sub>2</sub> groups while the overall shape of ADAM makes it bulkier). The relatively small increase in the CCS when going from one guest to another suggests that they are located within the cavity of the host since larger differences would have been intuitively expected for exclusion complexes. For instance, a much larger increase in the CCS would have been expected when going from PXD to ADAM. Indeed, in the case of exclusion complexes, PXD is supposed to be more strongly bound on the host compared to ADAM as a result of the two amino groups of PXD that can promote hydrogen bonds and/or ion-dipole interactions at its two ends (**figure IV.4.3**).

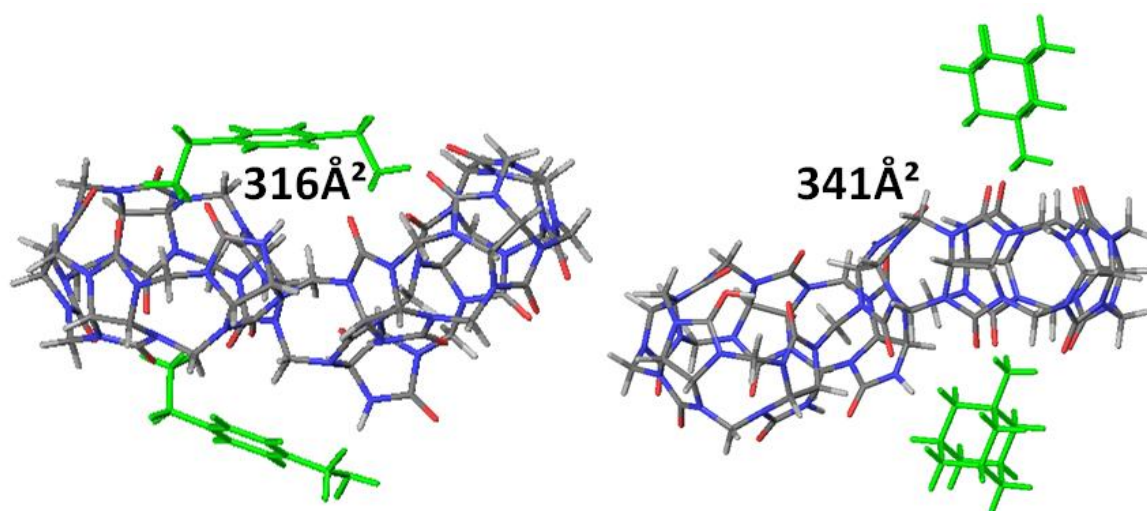


**Figure IV.4.3:** Three-dimensional structures of two specific homomeric triply charged exclusion complexes based on PXD (left) and ADAM (right) guests, as obtained among the conformers calculated at the DFT level during the last step of the conformational search procedure. The calculated collisional cross sections are reported in Å<sup>2</sup>.

In hypothetical exclusion ADAM-based complexes, ADAM is expected to point perpendicular to the host to favour hydrogen bonds therefore increasing significantly the CCS. This difference in the orientation and shape of the guest is illustrated when going to quaternary complexes in which the third guest is undoubtedly outside the host, see **table IV.4.2**. As a

matter of fact, the CCS is increased by 15 Å<sup>2</sup> when adding a third DAPHEN guest while it increases by 44 Å<sup>2</sup> upon addition of a third ADAM guest. For TOLU, two peaks corresponding to increases of 17 Å<sup>2</sup> and 43 Å<sup>2</sup> were recorded, suggesting the coexistence of species that are stuck on the host (+17 Å<sup>2</sup>) as well as perpendicular to it (+43 Å<sup>2</sup>).

#### 4.2.4 Structural analysis of the ternary complex ions (+2 / +3) by computational chemistry

In order to assist the interpretation of the IMS results, the three-dimensional structures of the different doubly and triply charged inclusion complexes have been determined at the quantum-chemical level (see Methodology section).

For doubly-charged ternary complexes, **figure IV.4.4** shows that the two protons are located on the opposite amino groups of the guests in order to minimize their electrostatic repulsion. For DAPHEN- and TOLU-based complexes, the guests are slightly tilted in the cavities. Indeed, while the ammonium groups tend to be in the center of the opposite portals, the steric hindrance between one hydrogen atom of the phenyl group in the ortho position of the ammonium and the host does not allow for a perfect vertical alignment of the guest in the cavity. For PXD-based complexes, the guests are perfectly aligned in the cavities because the additional methylene groups reduce this steric repulsion. However, for the PXD complexes, since the guests are getting closer to the center of the molecule, the interactions between the two guests increase and the two subunits of the host have to get distorted in comparison to DAPHEN- and TOLU-based complexes where the planes of both subunits are parallel. Due to the bulkiness of the ADAM molecule, the two guests are tilted such that a large part of their cage lies close to the center of the host. This part of the host is more flexible and can be strongly distorted to accommodate the large size of the ADAM molecules.

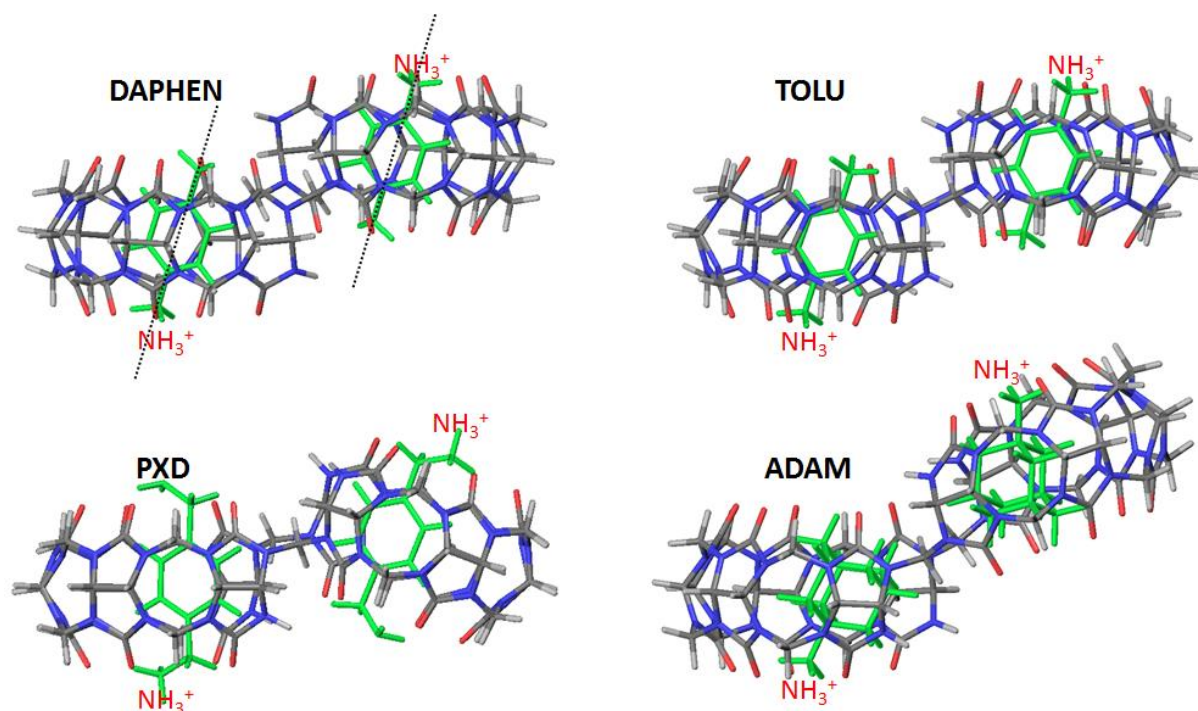
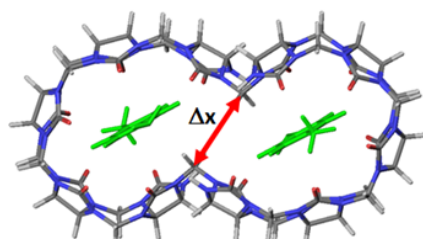


**Figure IV.4.4:** Three-dimensional structures of homomeric doubly charged ternary complexes, as calculated at the DFT level. The ammonium groups have been drawn explicitly for sake of clarity. The orientation of the two DAPHEN guests is represented by dotted black lines.

In order to quantify the impact of the size of the guest on the geometry of the host, we have listed in **table IV.4.3** the distance between the two CH<sub>2</sub> groups linking the two cavities (see also **figure IV.4.5**).

**Table IV.4.3:** Evolution of the distance between the two methylene groups bridging the two subunits of the host as a function of the size of the guest in homomeric and heteromeric doubly charged ternary complexes.



$\Delta x$ (Å)	DAPHEN	TOLU	PXD	ADAM
DAPHEN	4.45	4.46	4.69	6.40
TOLU	4.46	4.52	4.67	6.18
PXD	4.69	4.67	5.15	6.09
ADAM	6.40	6.18	6.09	7.26

The analysis of the table shows that an increase in the size of the guest in homomeric complexes promotes an increase of this geometrical parameter (4.45 Å, 4.52 Å, 5.15 Å, and 7.26 Å, for DAPHEN, TOLU, PXD, and ADAM guests, respectively). As a consequence, the hydrogen bonds and the ion-dipole interactions between the amino groups and the portals are getting weaker for larger guests. As illustrated in **figure IV.4.5**, while three hydrogen bonds are smaller than 2 Å for each of the ammonium groups in the DAPHEN-based complex, the ADAM-based complex only exhibit one short H-bond per guest.

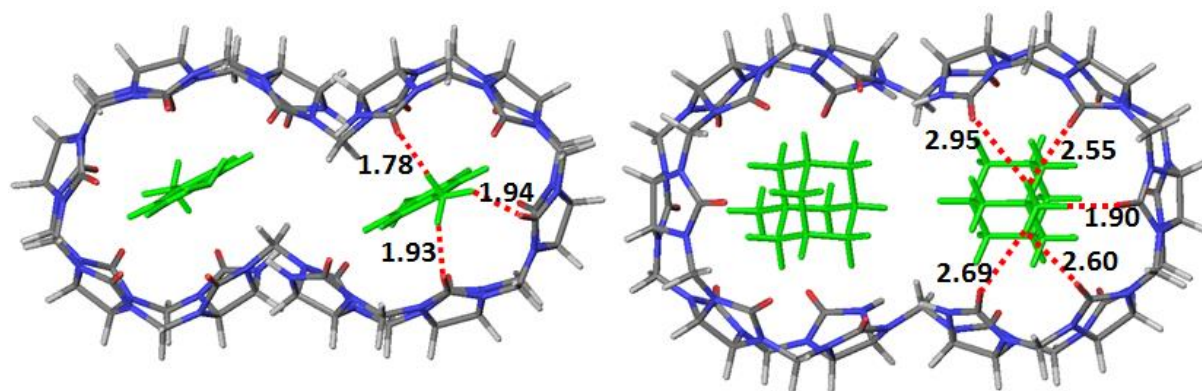


**Figure IV.4.5:** Top view of the homomeric DAPHEN and ADAM-based doubly charged ternary complexes, as optimized at the DFT level. The hydrogen bonds between the ammonium groups and the portals are displayed in red dotted lines and their lengths are listed in Å.

For the triply-charged complexes, the largest differences in the three-dimensional structures are found for the DAPHEN guest. Indeed, while the planes of both subunits are parallel for the doubly-charged complex ions, the host is getting distorted in the triply charged species (**figures III.3.4 vs III.3.6**). When adding the additional proton (going from 2+ to 3+), the nature

of the guest molecule is determinant in defining the position of the extra proton. Indeed, when the guest molecule possesses two amino groups, i.e. DAPHEN and PXD, the third proton is systematically lying on one amino group. In contrast, for TOLU and ADAM guests, the additional proton must sit on a carbonyl group of the host molecule. Interestingly, our calculations show that the most stable chemical site to add this proton is the second carbonyl group close to the center of the cavity (**figure IV.4.6**). The most pronounced geometric modifications going from a doubly charged to a triply charged complex ion are observed for the DAPHEN and PXD complexes. Whereas the axes of the guest molecules are quasi parallel inside the 2+ ions, the electrostatic repulsion created by the (second) protonation of one of the guest molecule induces a rotation of this guest molecule relative to the other, thus creating a tilt angle between the two molecular axes.

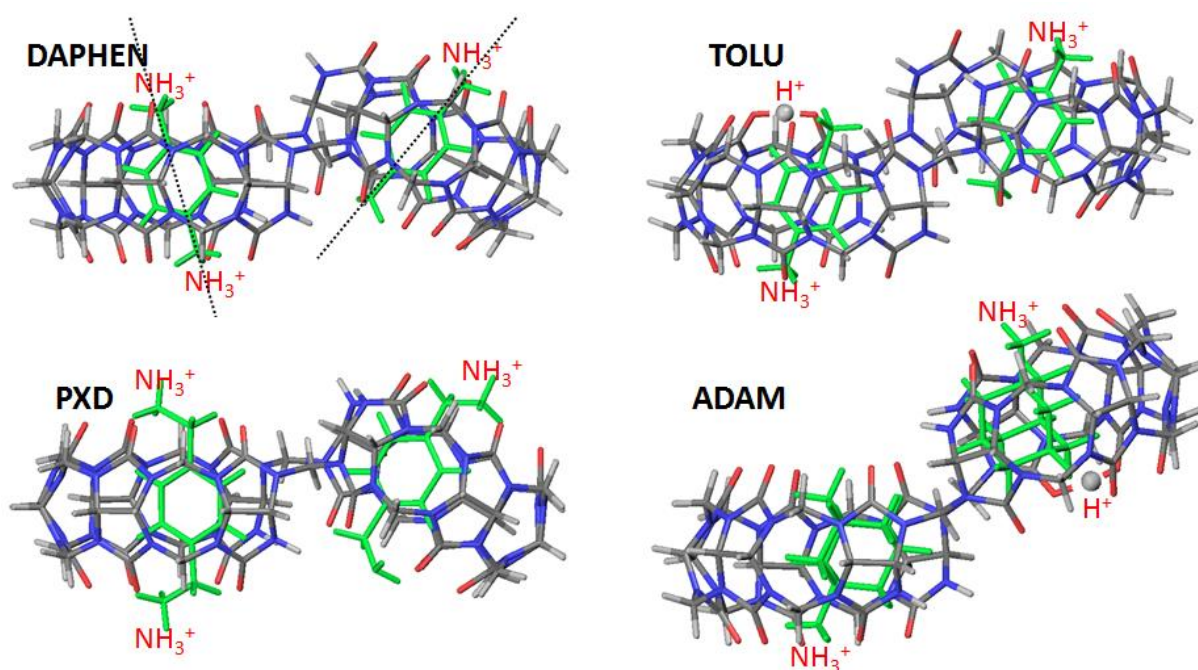


**Figure IV.4.6:** Three-dimensional structures of homomeric triply charged ternary complexes, as obtained at the DFT level. The ammonium groups and the third proton have been drawn explicitly for sake of clarity. The orientation of the two DAPHEN guests is represented by dotted black lines.

The CCS calculated on the basis of the DFT-optimized inclusion structures (**table IV.4.2**) perfectly match the experimental data. In particular, the increase in the CCS when going from a small to a more bulky guest is well reproduced. These results therefore confirm the presence

of inclusion complexes. Indeed, since  $[\text{ns-CB}[10]+2\text{DAPHEN}+2\text{H}]^{2+}$  is known to form inclusion complexes,[11] the similarity between the calculated CCS for  $[\text{ns-CB}[10]+2\text{DAPHEN}+2\text{H}^+]^{2+}$  and  $[\text{ns-CB}[10]+2\text{DAPHEN}+3\text{H}]^{3+}$  points to the formation of inclusion complexes for the triply charged ions. The calculated CCS for the reference system (host alone, ns-CB[10]) has been estimated to  $255 \text{ \AA}^2$ , showing that, in the absence of guests, the host collapses and adopts a spherical structure (see **Figure IV.4.7**).

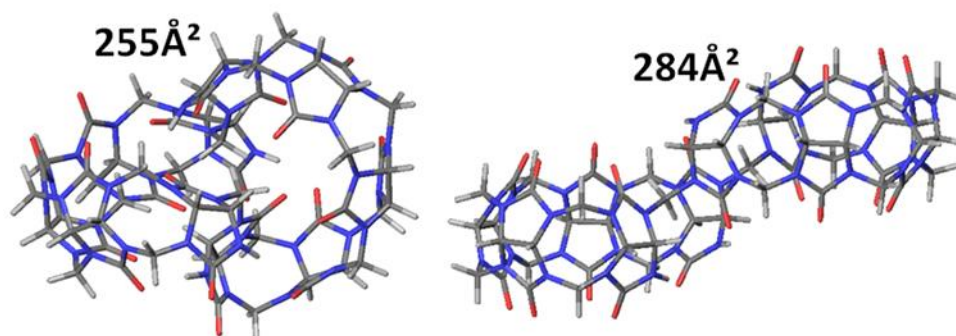


**Figure IV.4.7:** Three-dimensional structures of two conformers of a single neutral ns-CB[10] molecule. The calculated collisional cross sections are mentioned in  $\text{Å}^2$ .

We have estimated the CCS of homomeric PXD and ADAM triply-charged complexes on the basis of the optimized DFT structures, considering that the guests could be inside or outside the host. Interestingly, for exclusion complexes, while PXD are always in close contact with the host due to the presence of its two amino end groups that allows for the formation of stabilizing hydrogen bonds, ADAM is always lying perpendicular to the portals to promote hydrogen bonding, see **figure IV.4.3**. This difference in the orientation of the guest on the host can lead, for some specific conformers obtained during the conformational search procedure, to a larger increase of the CCS for the optimized exclusion complexes based on ADAM compared to those based on PXD (up to  $19 \text{ \AA}^2$  and  $6 \text{ \AA}^2$  for ADAM and PXD based-exclusion complexes, respectively, see **figure IV.4.3**).



#### 4.2.5 Experimental and theoretical investigation of the size specificity of the complexation reaction.

The results described in the previous sections reveal that the complexes detected upon ESI ionization are ternary inclusion complexes confirming that the transfer from the condensed phase to the gas phase does not modify the nature of those complexes. The specific production of such ternary complexes indicates that positive allosteric modulation is operating, i.e. the binding of one [ligand](#) enhances the attraction of another similar ligand at the second binding site. This is in perfect agreement with the observations reported by Isaacs et al [11] suggesting that the global sequence of events ultimately yielding the ternary complexes is under allosteric control. It was also proposed that the global sequence of reactions ultimately yielding the ternary complexes is under homotropic control since the binding of the first guest to ns-CB[10] pre-organizes the second cavity for binding of a similarly sized guest.

In order to assess whether ESI mass spectrometry would be able to highlight this size selectivity, three guest molecules were considered, namely DAPHEN, PXD and ADAM. DAPHEN and PXD can be considered *a priori* as reasonably similar as far as their sizes are concerned whereas ADAM definitively represents a larger guest candidate. We then prepare three different solutions, each containing an equimolar mixture of two guest molecules in excess compared to the ns-CB[10] receptor. Note that an excess in host molecules would preclude any conclusions to be drawn since competition reactions for binding are required for the present experiments. A prerequisite of such an analysis is that the ESI response factors for the homomeric and heteromeric ternary complexes are really close to each other to prevent discrepancies when using the relative proportion of ions in the gas phase to estimate the relative concentrations in the solution. It is nowadays well-known that the ESI response factors are closely related to the desolvation energies of the ions [15]. In our case, starting from the observation that all the detected gas phase ions are inclusion complexes, whatever the guest molecules, it is reasonable to make the assumption that heteromeric and homomeric ternary complexes must possess similar desolvation energies, for a given charge state.

#### IV. Results and discussion

In the ESI mass spectrum (soft conditions) recorded when analyzing the PXD/DAPHEN solution (**figure IV.4.8 a**), homomeric as well as heteromeric ternary complex ions (3+) are observed. Beside  $[\text{ns-CB}[10]+2\text{PXD}+3\text{H}]^{3+}$  ( $m/z$  637.2) and  $[\text{ns-CB}[10]+2\text{DAPHEN}+3\text{H}]^{3+}$  ( $m/z$  618.6), a really intense signal is detected and corresponds to the triply charged heteromeric ternary complex ions, namely  $[\text{ns-CB}[10]+\text{PXD}+\text{DAPHEN}+3\text{H}]^{3+}$  ( $m/z$  628.2). On the other hand, the heteromeric complex ions are less abundant in the ESI mass spectra obtained for the ADAM/PXD and ADAM/DAPHEN mixtures, as featured in **figure IV.4.8 b** and **III.3.8 c** respectively. For example, in **figure IV.4.8 b**, the signal corresponding to heteromeric complex ions at  $m/z$  642.3 is less intense than both the signals of the homomeric complexes, at respectively  $m/z$  637.2 and  $m/z$  647.2 for PXD and ADAM. Interestingly, these results also confirm the presence of inclusion complexes. Indeed, if exclusion complexes would have been prepared, no significant differences in the relative ion intensities would have been expected when comparing heteromeric and homomeric complexes since the size selectivity is likely to be a property inherent to the preparation of inclusion complexes.

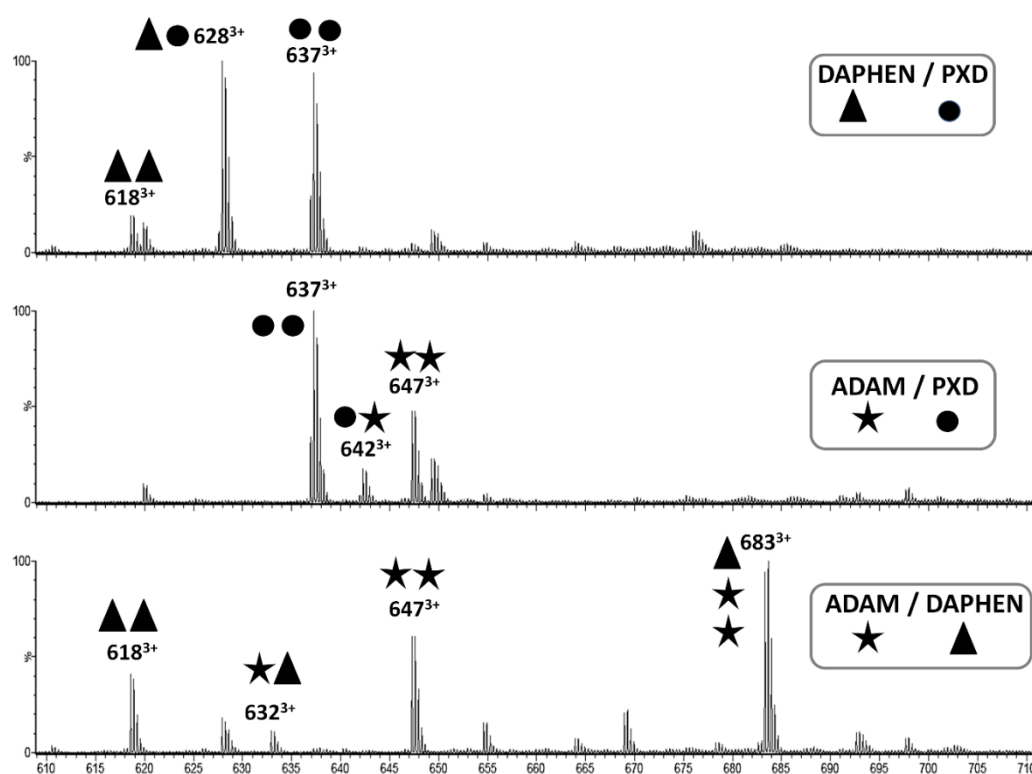


**Figure IV.4.8:** ESI-MS investigation of the size selectivity of the complexation reactions between: (a) DAPHEN and PXD, (b) ADAM and PXD, (c) ADAM and DAPHEN with ns-CB[10].

To further rationalize the origin of size selectivity when creating heteromeric complexes, all inclusion complexes based on two different guests among DAPHEN, TOLU, PXD, and ADAM have been optimized at the DFT level. Here, only doubly-charged complexes have been considered since knowing the precise localization of the third proton for heteromeric systems involving TOLU and/or ADAM guest is a very tricky issue. Nevertheless, conclusions drawn for doubly-charged complexes will also apply to triply-charged species since the geometric deformation upon addition of a proton is rather limited, see **figures III.4.4 and III.4.6**. The distance between the two methylene units bridging the two cavities has been used to characterize the ability of a guest to favor homomeric or heteromeric complexes (**table IV.4.3**). In a previous section, we have already pointed out that this geometric parameter increases with the size of the guest in homomeric complexes. For heteromeric complexes, two families of compounds exist: (i) systems containing one ADAM guest for which this parameter ranges from 6.09 Å to 6.40 Å; and (ii) complexes without an ADAM guest with distances between 4.46 Å to 4.69 Å. This points out that the shape of ADAM does not favor the formation of heteromeric complexes since the distance between the two CH<sub>2</sub> groups is so large that the loss of the other guest is expected to occur easily. In contrast, similar distances are measured for homomeric and heteromeric complexes based on DAPHEN, TOLU, and PXD, suggesting homotropic and heterotropic allosteries.

### 4.3 Conclusions

The non covalent associations between an original ditopic receptor and several guest amino compounds have been investigated by associating state-of-the-art mass spectrometry and computational methods. The host molecule, nor-seco-cucurbit[10]uril (ns-CB[10]), [11] is made of two interconnected cavities; it was previously demonstrated that ns-CB[10] retains much of the binding capabilities of the CB[n] congeners. Some additional features have been highlighted when comparing ns-CB[10] to the more rigid CB[n]-type receptors. For instance, ns-CB[10] binds larger guests than expected given that its two *open* cavities are each shaped by only five glycoluril rings conferring to the ns-CB[10] cavity a certain degree of structural responsiveness.[16] Moreover, ns-CB[10] was also demonstrated to display homotropic allostery based on a guest size induced preorganization mechanism. All those aspects render

ns-CB[10] a good candidate for our investigations focusing on the transfer of non covalent complexes from the condensed phase to the rarefied gas phase of a mass spectrometer. We have demonstrated that electrospray ionization can be advantageously exploited to transfer without decomposition the non covalent ionic complexes to the gas phase of the mass spectrometer. The quasi exclusive observation of ternary complexes, associating two guest molecules to the receptor, confirms the allosteric nature of the binding process. The gas phase structures of the ionic complexes, and especially the location of the guests (inclusion vs exclusion complexes), were elucidated by means of ion mobility spectroscopy experiments and computational chemistry. All experimental and theoretical data point to the conservation of the condensed phase structure upon desolvation and transfer to the gas phase. Carefully driven competition reactions in solution unambiguously demonstrated the size selectivity of the receptor, i.e. the binding of the first guest determines the size and the shape of the second encapsulated molecule.

## References

1. a) J. Lagona, P. Mukhopadhyay, S. Chakrabarti, L. Isaacs, *Angew.Chem., Int.Ed.*, 2005; **44**: 4844-4870; b) J.W. Lee, S. Samal, N. Selvapalam, h.J. Kim and K. Kim, *Acc. Chem. Res.*, 2003; **36**: 621-630; c) K. Kim, N. Selvapalam, Y.H. Ko, K.M. Park, D. Kim, J. Kim, *Chem.Soc.Rev.*, 2007; **36**: 267-279; d) L. Isaacs, *Isr.J.Chem.*, 2011; **51**: 578 – 591; e) E. Masson, X. Ling, R. Joseph, L. Kyeremeh-Mensah, X. Lu, *RSC Adv.*, 2012; **2**: 1213–1247; f) W. L. Mock, N. Y. Shih, *J.Org.Chem.*, 1986; **51**: 4440-4446; g) S. Liu, C. Ruspic, P. Mukhopadhyay, S. Chakrabarti, P. Y. Zavalij, L. Isaacs, *J.Am.Chem.Soc.*, 2005; **127**: 15959-15967; h) C. Márquez, R. R. Hudgins, W. M. Nau, *J.Am.Chem.Soc.*, 2004; **126**: 5806-5816; i) W. L. Mock, N. Y. Shih, *J.Am.Chem.Soc.*, 1989; **111**: 2697-2699.
2. a) C.A. Schalley, A. Springer, *Mass Spectrometry and Gas-Phase Chemistry of Non-Covalent Complexes*, John Wiley & Sons, Inc., Hoboken, New Jersey, USA, 2009; b) B. Baytekin, H.T. Baytekin, C.A. Schalley, *Org.Biomol.Chem.*, 2006; **4**: 2825–2841; c) K. Roman, M. Balabin, D. Grünstein, R. Kikkeri, V. Frankevich, P.H. Seeberger, R. Zenobi, *J.Am.Soc.Mass Spectrom.*, 2011; **22**: 1167-1177.
3. (a) J.B. Cunniff, P. Vouros, *J.Am.Soc.Mass Spectrom.*, 1995; **6**: 437-447; (b) J. Sun, E.N. Kitova, N. Sun, J.S.S Klassen, *Anal.Chem.*, 2007; **79**: 8301-8311; (c) V. Gabelica, N. Galic, E. De Pauw, *J.Am.Soc.Mass Spectrom.*, 2002; **13**: 946-953.
4. a) D.V. Daerden, T.A. Ferrell, M.C. Asplund L.W. Zilch, R.R Julian, M.F. Jarrold, *J.Phys.Chem. A*, 2009; **113**: 989–997; b) D.N. Mortensen, D.V. Dearden, *Chem.Commun.*, 2011; **47**: 6081–6083; c) K.A. Kellersberger, J.D. Anderson, S.M. Ward, K.E. Krakowiak, D.V. Dearden, *J.Am.Chem.Soc.*, 2001; **123**: 11316-11317; d) F. Yang, D.V. Dearden, *Supramol.Chem.*, 2011; **23**: 53-58; e) I. Osaka, M. Kondou, N. Selvapalam, S. Samal, K. Kim, M.V. Rekharsky, Y. Inoue, R. Arakawa, *J.Mass Spectrom.*, 2006; **41**: 201-207; f) H. Zhang, T.A. Ferrell, M.C. Asplund, D.V. Dearden, *Int.J.Mass Spectrom.*, 2007; **265**: 187-196; g) H. Zhang, E.S. Paulsen, K.A. Walker, K.E. Krakowiak, D.V. Dearden, *J.Am.Chem.Soc.*, 2003; **125**: 9284-9285; h) T. Mitkina, V. Fedin, R. Llusar, I. Sorribes, C. Vicent, *J.Am.Soc.Mass Spectrom.*, 2007; **18**: 1863-1872; i) W. Jiang, Q. Wang, I. Linder, F. Klautzsch, C.A. Schalley, *Chem.Eur.J.*, 2011; **17**: 2344-2348.
5. a) C.A. Schalley, P. Ghosh, M. Engeser, *Int.J.Mass Spectrom.*, 2004; **232**: 249-258; b) L. Wang, Y. Chai, C. Sun, D.W. Armstrong, *Int.J.Mass Spectrom.*, 2012; **323-324**: 21-27.

6. a) E. Kalenius, D. Moiani, E. Dalcanale, P. Vainiotalo, *Chem.Comm.*, 2007; 3865-3867; b) D.V. Dearden Y.J. Liang, J.B. Nicoll, K.A. Kellersberger, *J.Mass Spectrom.*, 2001; 3; 989-997; c) T. Wyttenbach, M.T. Bowers, *J.Am.Soc.Mass Spectrom.*, 1999; 10: 9-14.
7. a) H. Zhang, M. Grabenauer, M.T. Bowers, D.V. Dearden, *J.Phys.Chem.A*, 2009; 113: 1508-1517; b) J. De Winter, V. Lemaure, R. Ballivian, F. Chiro, O. Coulembier, R. Antoine, J. Lemoine, J. Cornil, P. Dubois, P. Dugourd, P. Gerbaux. *Chem.Eur.J.*, 2011; 17: 9738-9745 ; c) J.B. Renaud, E. Martineau, G.G. Mironov, M.V. Berezovski, P.M. Mayer, *Phys.Chem.Chem.Phys.*, 2012; 14: 165-172.
8. a) P. Gerbaux, J. De Winter, D. Cornil, K. Ravicini, G. Pesesse, J. Cornil, R. Flammang, *Chem.Eur.J.*, 2008; 14: 11039-11049 ; b) H. Zhang, I.H. Chu, S.Leming, D.V. Dearden, *J.Am.Chem.Soc.*, 1991; 113: 7415-7417 ; c) G. Grigorean, J. Ramirez, S. H. Ahn, C. B. Lebrilla, *Anal.Chem.*, 2000; 72: 4275 – 4281; d) E. Ventola, K. Rissanen, P. Vainiotalo, *Chem.Eur.J.*, 2004; 10: 6152 – 6162.
9. a) C. Lifshitz, *Mass Spectrom.Rev.*, 1982; 1: 309-348; b) M.B. More, D. Ray, P.B. Armentrout, *J.Am.Chem.Soc.*, 1999; 121: 417-423; c) P. Armentrout, *Int.J.Mass Spectrom.*, 2000; 200: 219–241; d) L. Wang, Y. Chai, C. Sun, D.W. Armstrong, *Int.J.Mass Spectrom.*, 2012; 323– 324: 21– 27; e) A. Revesz, D. Schröder, J. Svec, M. Wimmerova, V. Sindelar, *J.Phys.Chem.A*, 2011; 115: 11378-11386.
10. a) F. Yang, D.V. Dearden, *Isr.J.Chem.*, 2012; 51: 511-558; b) J. De Winter, V. Lemaure, O. Coulembier, J. Cornil, P. Dubois, P. Gerbaux. *J.Am.Soc.Mass Spectrom.*, 2010; 21: 1159-1168.
11. a) W-H. Huang, S. Liu, P.Y. Zavalij, L. Isaacs, *J.Am.Chem.Soc.*, 2006; 128: 14744-14745 ; b) R. Nally, L. Isaacs, *Tetrahedron*, 2009; 65: 7249-7258 ; c) J. B. Wittenberg, M. G. Costales, P. Y. Zavalij, L. Isaacs, *Chem.Comm.*, 2011; 47: 9420-9422.
12. A.J.R. Heck, R.H.H. van den Heuvel, *Mass Spectrom.Rev.*, 2004; 23: 368-389.
13. D. Ma, B. Zhang, U. Hoffmann, M. G. Sundrup, M. Eikermann, L. Isaacs, *Angew.Chem. Int. Ed.*, 2012; 51: 11358-11362.
14. C. Gill, K.R. Jennings, T. Wyttenbach, M.T. Bowers, *Int.J.Mass Spectrom.*, 2000; 196: 685-697.
15. E. Leize, A. Jaffrezic, A. Van Dorsselaer, *J.Mass Spectrom.*, 1996 ; 31 : 537-544.
16. a) D. Ma, G. Hettiarachchi, D. Nguyen, B. Zhang, J. B. Wittenberg, P. Y. Zavalij, V. Briken, L. Isaacs, *Nat.Chem.*, 2012 ; 4 : 503-510 ; b) D. Lucas, L. Isaacs, *Organic Letters*, 2011 ; 13 : 4112-4115 ; c) D. Ma, P. Y. Zavalij, L. Isaacs, *J.Org.Chem.*, 2010 ; 75 : 4786-4795.

## Chapter 5:

Energy-resolved Collision-induced Dissociation of Non-Covalent Ions: Charge- and Guest-dependence of the Decomplexation Reaction Efficiencies.

*G. Carroy, V. Lemaire, J. De Winter, L. Isaacs, E. De Pauw, J. Cornil, P. Gerbaux.*

*Phys. Chem. Chem. Phys. 2016; 18: 12557-12568.*

---

## 5.1 Introduction

Cucurbiturils are macrocyclic molecules constituted by the association of glycoluril repeat units [1]. These molecules are constituted by a hydrophobic inner cavity and two carbonyl portals and are extensively shown to form stable inclusion complexes with protonated alkyl and aryl amines [1]. One of us prepared a bitopic cucurbituril-based receptor, namely the nor-seco-cucurbit[10]uril (ns-CB[10], *scheme IV.5.1*), which results from the formal extrusion of two CH<sub>2</sub> bridges from CB[10] [2]. This molecular container presenting two cavities is consequently prone to encapsulate two guest molecules affording ternary complexes (2:1). At variance with most of the cucurbituril congeners, this flexible receptor is now able to bind large guests with the formation of the ternary complexes being under homotropic allostery control. In a recent paper [3], we used mass spectrometry (MS) and computational chemistry to investigate, at a molecular level, the binding properties of ns-CB[10] towards selected protonated alkyl and aryl amines. We have demonstrated that electrospray ionization can be advantageously exploited to transfer without decomposition the non-covalent ionic complexes to the gas phase of the mass spectrometer. The quasi exclusive observation of ternary complexes, associating two guest molecules to the receptor, was used to confirm the allosteric nature of the binding process. The gas-phase structures of the ionic complexes, and especially the location of the guests (inclusion vs exclusion complexes), were elucidated by means of ion mobility spectroscopy experiments further supported by computational chemistry. All experimental and theoretical data point to the conservation of the condensed-phase structure upon desolvation and transfer to the gas phase. Carefully driven competition reactions in solution unambiguously demonstrated the size selectivity of the receptor, i.e., the binding of the first guest determines the size and shape of the second encapsulated molecule.

The gas-phase stabilities of the non-covalent ionized complexes are often probed via collision-induced dissociation experiments [4]. In such well-known processes, when mass-selected ions collide with target gas molecules or atoms, part of the kinetic energy is converted into internal energy, by rovibrational excitations in the low-energy collision regime. After this initial step of collisional activation, it is often admitted that the internal energy is rapidly and statistically spread over all oscillators within the excited ions, ultimately leading to the unimolecular dissociation of the ions provided the internal energy excess is enough to overpass the so-called



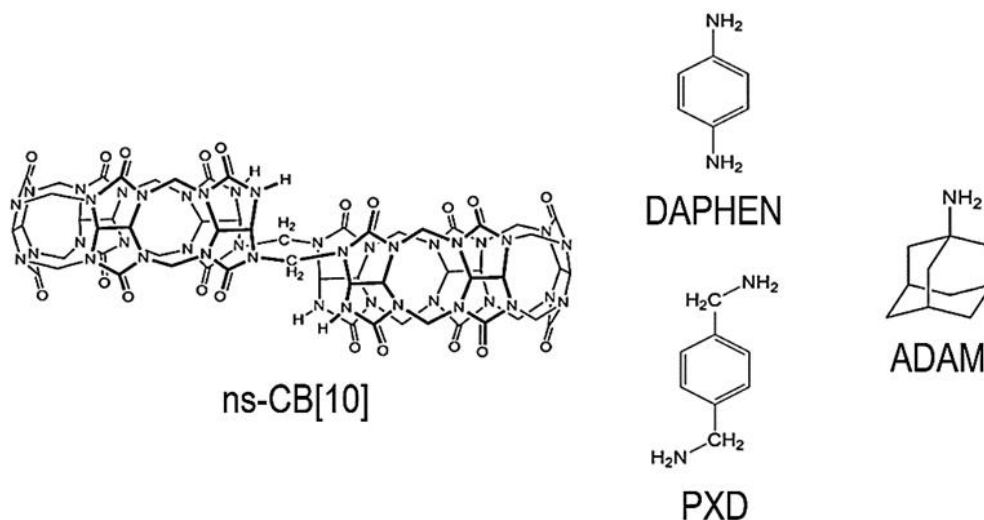
critical energy of dissociation, say the activation energy for dissociation. Since the decomposition reaction of the excited ions has to occur in the collisional cell, the ions have a finite time to decompose. When the ions become larger and more complex, the reaction time for dissociation may exceed this time, such that efficient dissociation of the ions will not be observed at the thermodynamic threshold, but will be delayed until higher energies are reached. This so-called “kinetic shift” can appear in any type of threshold measurements [5]. Moreover, the internal energy distribution within a population of parent ions after the collisional activation step is often broad, especially when the measurements are performed with a typical low-energy experimental set-up, say a hexapole or an ion trap cell, in which multiple collisions are required to progressively heat up the ions. As a consequence, several competing dissociation routes are likely to be opened, even if they usually differ with respect to the activation barriers.

In the so-called threshold-CID experiments, the CID spectra of mass-selected ions are recorded by varying the kinetic energy of the ions prior to the collisional activation step [6] in order to shed some light on the kinetic energy dependence of the decomposition reactions. The result of energy-dependent CID experiments with a given mass-selected parent ion is a breakdown curve with sigmoidal-like shape (see below) reporting the fraction of the precursor ions which survives in a CID reaction (Survival Yield) according to the reaction rate (and the residence time in the collision cell). Thermodynamic data can be extracted from these energy-resolved CID experiments when the threshold energy is set at the start of decomposition reaction. However, such measurements require a peculiar experimental set-up that is far from being commercially available nowadays and mostly relies on a single collision activation of the mass selected ions in an octopole collision cell [7]. Unfortunately, this set-up is not available in our laboratory. Nevertheless, numerous reports describe the use of energy-resolved CID experiments, carried on commercially available mass spectrometer, to access the gas-phase stability of non-covalent complexes [8]. In such cases, the non-covalent interactions are usually weak enough compared to the bonds constituting the covalent scaffold, to ultimately lead to the collision-induced decomplexation of the host-guest associations. However, counter-examples, in which the covalent bonds are preferentially broken, are well-known and occur in different specific cases, i.e. when the number of non-covalent interactions is large or

when a molecule is fully entangled within a ring molecule, such as for rotaxane or catenane associations [9].

Numerous studies dealing with mass spectrometry (MS) analysis of cucurbituril complexes are reported in the literature, most of them being performed by the groups of Dearden at the Brigham Young University, Nau at the Jacobs University Bremen and Schalley at the Freie University of Berlin [10]. In direct connection with the present study, the group of Dearden used sustained off-resonance irradiation (SORI) in their FT-ICR instrument in an energy-resolved manner to characterize fragmentation of non-covalent complexes associating alkyldiammonium to cucurbit[6]uril [11]. In particular, their experimental and theoretical data suggest that the optimum alkyldiammonium chain length for binding CB[6] in the gas phase occurs for  $n=4$ . Interestingly, such a result contrasts with the solution phase complex stability, which is maximized for  $n=6$ . This contrasting behavior was correlated with the lack of solvent stabilization of the ammonium groups in the gas phase [11]. In a recent paper, based on ion mobility and energy-resolved CID experiments, we observed that the inclusion/exclusion ratio for the 2+ complexes associating CB[6] with para-phenylenediamine is dependent of the equilibration time in solution, say the time between the preparation of the solution and the mass analysis. In other words, we demonstrated that the ion topologies in the gas phase can be affected by the equilibrium time in solution, especially for host-guest systems characterized by slow kinetics of complexation [12].

In the present report, we study the gas-phase collision-induced decomposition processes for ternary complexes combining three guest molecules (*scheme IV.5.1*), namely adamantylamine, para-phenylenediamine and para-xylylenediamine, to the bitopic ns-CB[10] receptor within a joint experimental (mass spectrometry) and theoretical (Density Functional Theory (DFT) and molecular dynamics (MD) calculations) approach.



**Scheme IV.5.1:** Host (*nor-seco-cucurbit[10]uril* (ns-CB[10], left)) and guest molecules (right): *para*-phenylenediamine (DAPHEN); *para*-xylylenediamine (PXD); adamantylamine (ADAM).

The present work has been motivated by different reasons. First, in view of the flexible nature of the receptor, covalent bond dissociation is not expected to compete with the decomplexation processes. We also already demonstrated that the ternary complexes associating the three model guest molecules are inclusion complexes [3]. Finally, for each of these ternary complexes, two charge states, 2+ and 3+, are detected, even for the adamantylamine guest that contains only one basic amino group, thus raising the question of the role of protonation of the host molecule on the decomplexation reaction processes.

## 5.2 Results and discussion

### 5.2.1 Experimental results: mass spectrometry study of the host/guest associations

In a previous study, we already demonstrated using a combination of ion mobility measurements and computational chemistry methods that the ns-CB[10] receptor encapsulates the three guest molecules, creating cationic inclusion complexes [3]. We also observed that the stabilization of these complexes relies on the creation of multiple hydrogen

bonds between the ammonium group(s) of the protonated guests and the oxygen atoms of the carbonyl portal. Interestingly, ternary complexes, i.e. one host and two guest molecules, are quasi-exclusively detected upon Electrospray ionization, thus confirming the allosteric property of the complexation reaction between the bitopic receptor and the guest molecules. Directly in line with the present paper, the ternary complexes are detected as doubly, triply and quadruply-charged species, with the triply charged species being the most abundant detected ions regardless the nature and size of the guest molecule. **Table IV.5.1** gathers all the ternary complexes detected upon ESI analysis of solutions containing ns-CB[10] and the three selected guests.

**Table IV.5.1:** ESI-MS analyses on a Waters QToF 2 instrument of the ns-CB[10]/guest solutions : observed ternary complex ions for the three guest molecules. <sup>a</sup> Collisional Cross Section from [3] and Relative intensity with the most intense peak set at 100%; <sup>b</sup> Not Detected.

	<b>Ternary complexes ([2:1])</b>		
<b>Charge State</b>	<b>+ 2</b>	<b>+ 3</b>	<b>+ 4</b>
<b>PXD</b>	$m/z$ 955.4 $303 \text{ \AA}^2 / 5 \%$ <sup>a</sup>	$m/z$ 637.2 $310 \text{ \AA}^2 / 100 \%$	$m/z$ 478.2 $321 \text{ \AA}^2 / 55 \%$
<b>DAPHEN</b>	$m/z$ 927.6 $300 \text{ \AA}^2 / 10 \%$	$m/z$ 618.6 $301 \text{ \AA}^2 / 100 \%$	N.D. <sup>b</sup>
<b>ADAM</b>	$m/z$ 970.3 $319 \text{ \AA}^2 / 12 \%$	$m/z$ 647.2 $322 \text{ \AA}^2 / 100 \%$	N.D.

In the present study, for the sake of comparison, we will mainly focus our attention on the doubly and triply charged ternary complexes that are systematically detected whatever the guest molecule (**table IV.5.1, figure IV.5.1**). When subjected to collision against argon, the mass selected ternary complexes mostly undergo collision-induced decomplexation processes, leading to binary complexes following the loss of a guest molecule. Interestingly, we observed that, during those CID experiments, the (2:1)<sup>3+</sup> complexes mainly end up into (1:1)<sup>2+</sup> fragments by elimination of a protonated guest molecule. However, when the doubly

charged species are exposed to CID, the ternary complexes mainly fragment by losing a neutral guest molecule. For the sake of information, the 4+ ternary complexes associating PXD to ns-CB[10],  $[\text{ns-CB}[10]+2\text{PXD}+4\text{H}]^{4+}$ , (see **table IV.5.1**) also exclusively expel protonated PXD upon collisional activation (**figure IV.5.2**).

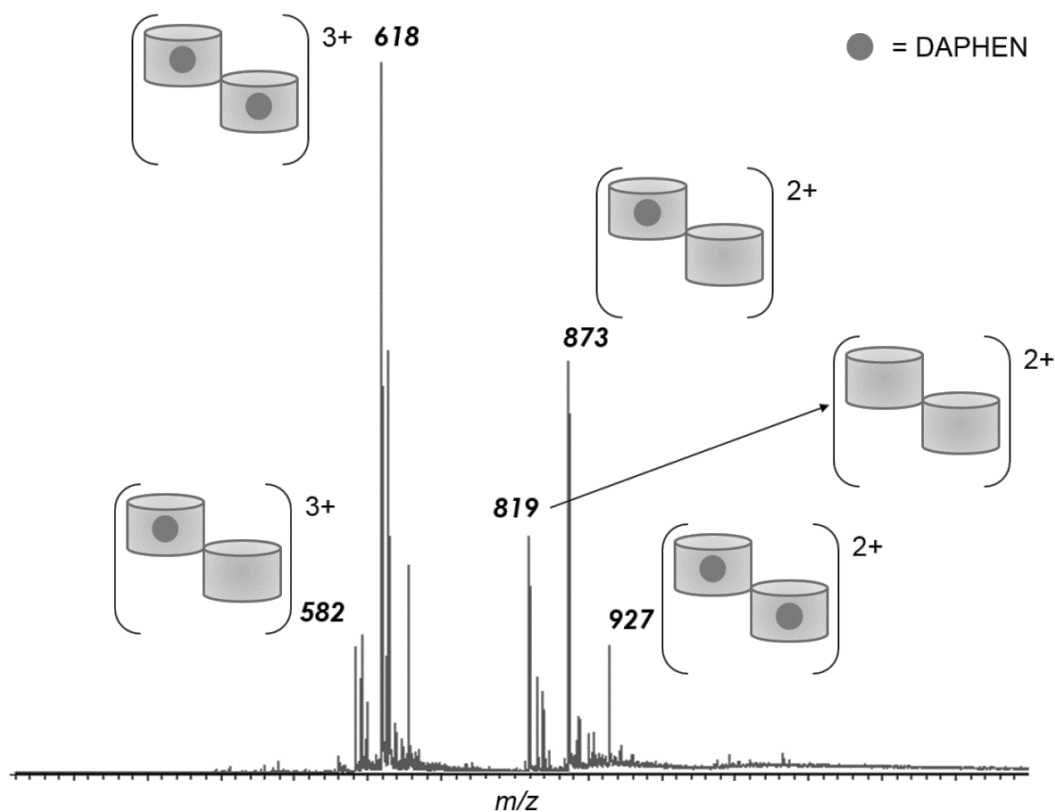
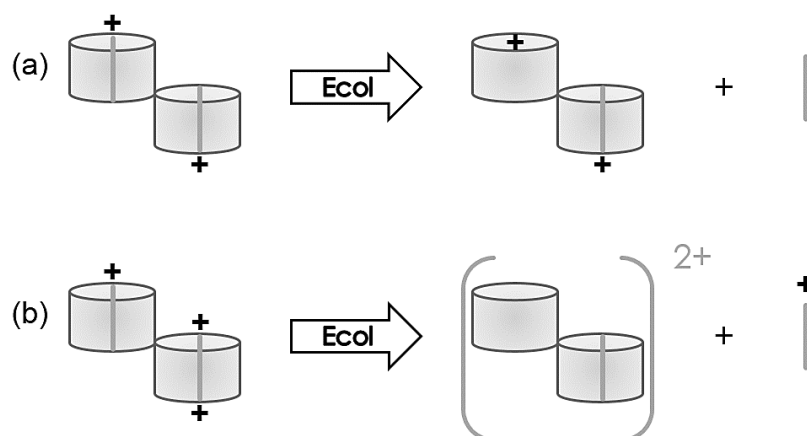


**Figure IV.5.1:** ESI-MS spectrum (Waters Q-ToF2, CV=40V, in source-pressure 6 mbar) obtained for a mixture of DAPHEN ( $5 \cdot 10^{-5} \text{M}$ ) and ns-CB[10] ( $10^{-5} \text{M}$ , solvent: water/methanol, 80/20 v/v).

The antagonistic behavior observed between the 2+ and 3+ ternary complexes is summarized in **scheme IV.5.2** and a typical example is presented in **figure IV.5.2**. The representation used for the triply charged complexes (**scheme IV.5.2 b**) will be explained later.



**Scheme IV.5.2:** Collision-induced dissociation of the ternary complexes associating one ns-CB[10] receptor to two guest molecules : CID dominant dissociations of (a) doubly charged and (b) triply charged ions.

**Figure IV.5.2** presents the CID spectra recorded when exposing  $[\text{ns-CB}[10]+2\text{DAPHEN}+3\text{H}]^{3+}$  ( $m/z$  618) (**figure IV.5.2 a**) or  $[\text{ns-CB}[10]+2\text{DAPHEN}+2\text{H}]^{2+}$  ( $m/z$  927) (**figure IV.5.2 b**) to collision against argon. As observed in **scheme IV.5.2 a**, the triply charged complexes mainly expel a protonated guest molecule, namely  $[\text{DAPHEN}+\text{H}]^+$ , affording the binary complex  $[\text{ns-CB}[10]+\text{DAPHEN}+2\text{H}]^{2+}$  ( $m/z$  873) together with protonated phenylenediamine detected at  $m/z$  109. Further decomposition of the  $m/z$  873 ions generates the doubly protonated ns-CB[10] molecule observed at  $m/z$  819. Even if the dominant CID reaction corresponds to the loss of a protonated guest molecule, the signal at  $m/z$  582 reveals that the collisionally excited  $m/z$  618 ion can also lose a neutral guest molecule, even if such a process definitively appears less favorable. Nevertheless, this neutral molecule loss becomes the prominent process in the case of the doubly charged ternary complex ions (**scheme IV.5.2 b**). Indeed, in the recorded spectrum, the reaction leading to the  $m/z$  873 doubly charged ions, namely  $[\text{ns-CB}[10]+\text{DAPHEN}+2\text{H}]^{2+}$ , clearly dominates the mass spectrum. **Table IV.5.2** summarizes all detected fragments in the CID spectra of the six ternary complexes selected for the present work. From **table IV.5.2**, we observe that, for a given ternary complex, the CID reactions appear to depend on the charge of the complex ( $2+$  versus  $3+$ ) with the  $2+$  and  $3+$  ions quasi exclusively eliminating a neutral and a protonated guest, respectively. In this context, the ADAM case really deserves a particular attention. Indeed, for the  $2+$  ions, whereas the DAPHEN and PXD containing complexes specifically expel a neutral guest, the ADAM

complexes also eliminate, though to a lower extent, protonated adamantylamine, see **table IV.5.2**. However, for the 3+ ions, only the ADAM containing complexes undergo the exclusive protonated guest elimination.

In order to further study the CID behaviors of all those six ternary complexes, we have investigated whether the nature of the guest molecule influences the CID experiments at both a qualitative (regarding the ternary compound behavior towards decomplexation) and a quantitative (by estimating theoretical energy barriers) points of view. Such an exploration will start by performing energy-resolved CID experiments to measure the kinetic energy dependence of the CID reaction efficiencies.

**Table IV.5.2:** ESI-MSMS analyses on a Waters QToF 2 instrument of the ns-CB[10]/guest ternary complexes: identification of the produced fragments. <sup>a</sup> branching ratio =  $I_{frag}/\sum I_{frag}$  (%)@ $E_{kin}$  (eV) <sup>b</sup> Not Detected.

Charge state	Guest molecules	Ternary complexes (2:1) <sup>n+</sup>	Neutral Guest Loss (1:1) <sup>n+</sup>	Protonated Guest Loss (1:1) <sup>(n-1)+</sup>
2+	DAPHEN	<i>m/z</i> 927	<i>m/z</i> 873 (100% @ 36eV) <sup>a</sup>	<i>N.D</i> <sup>b</sup>
	PXD	<i>m/z</i> 955	<i>m/z</i> 887 (100% @ 26eV)	<i>N.D</i> <sup>b</sup>
	ADAM	<i>m/z</i> 970	<i>m/z</i> 894 (97% @ 52eV)	<i>m/z</i> 1788 (3% @ 52eV)
3+	DAPHEN	<i>m/z</i> 618	<i>m/z</i> 582 (8% @ 33eV)	<i>m/z</i> 873 (92% @ 33eV)
	PXD	<i>m/z</i> 637	<i>m/z</i> 591 (1% @ 51eV)	<i>m/z</i> 887 (99% @ 51eV)
	ADAM	<i>m/z</i> 647	<i>N.D</i> <sup>b</sup>	<i>m/z</i> 894 (100% @ 33eV)

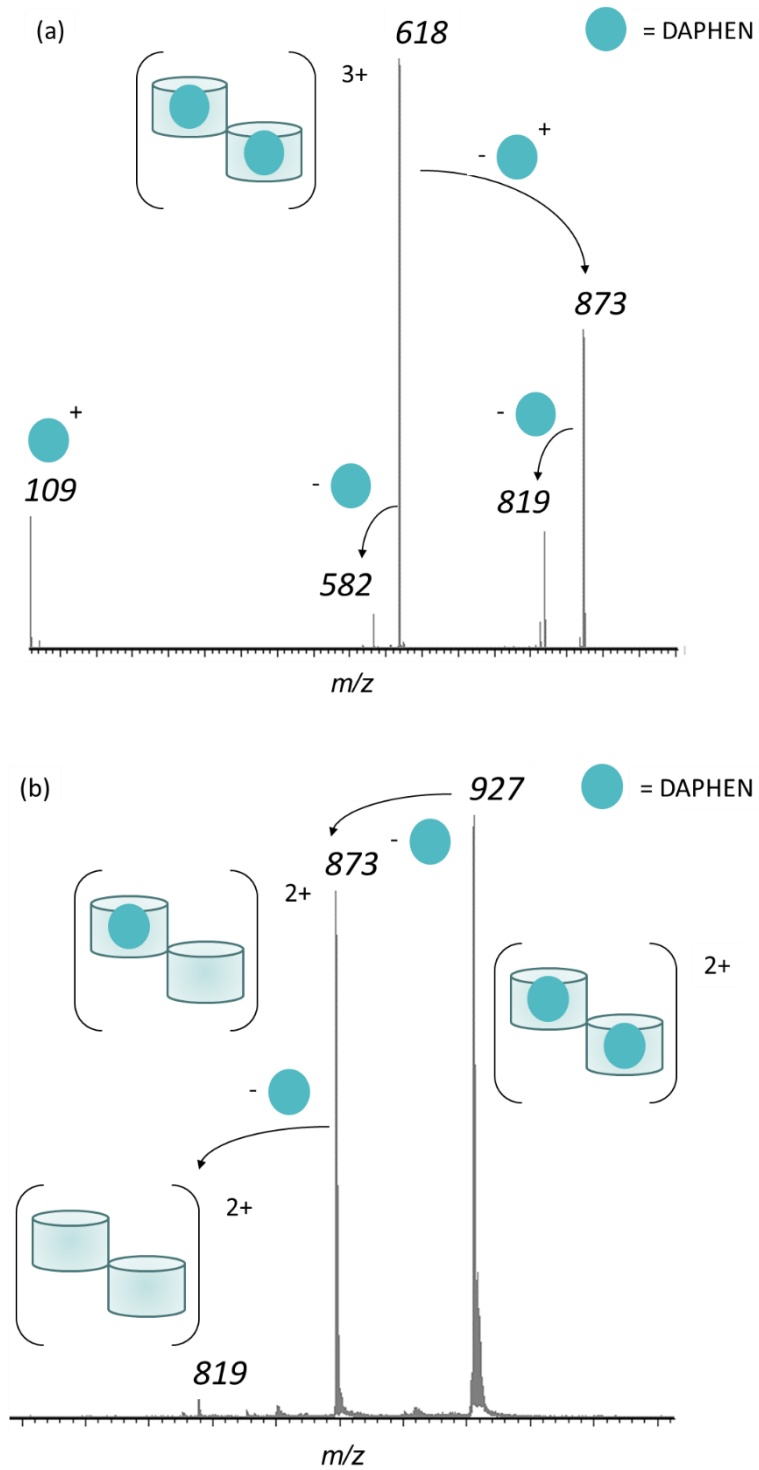


**Figure IV.5.2:** ESI-MS/MS analysis of the (a)  $m/z$  618 (Source pressure 6 mbar, CV = 20V, CE = 10V) and (b)  $m/z$  927 (Source pressure 1.2 mbar, CV = 30V, CE = 15V) ternary complexes associating *para*-phenylenediamine to the bitopic receptor.



**Figure IV.5.3** features the survival yield curves recorded for all the 2+ and 3+ ternary complexes. The underlying idea is to determine the charge and guest dependence on the CID reactions. Obviously, before undertaking such a comparative investigation, we have to normalize the kinetic energy parameter. Therefore, we will use the center-of-mass energy (ECM) of the incident ions instead of the accelerating voltage to free the energetic parameters from the mass dependence. In the experimental setup used for the present study, we are using multi-collisional conditions and it is difficult to define the relation between the internal energy distribution and the center of mass energy. However, the collision frequency at a given pressure is partly determined by the size and the shape of the ions, in other words, the average collisional cross sections (CCS) of the ions. Fortunately, we already observed on the basis of ion mobility experiments that the CCS of all investigated complex ions are similar (see **table IV.5.1**), around  $300 \text{ \AA}^2$  [3], due to the inclusion nature of all complexes regardless of the guest molecule and the charge state. As a consequence, huge differences in CID efficiencies are not likely to arise from different collision frequencies.

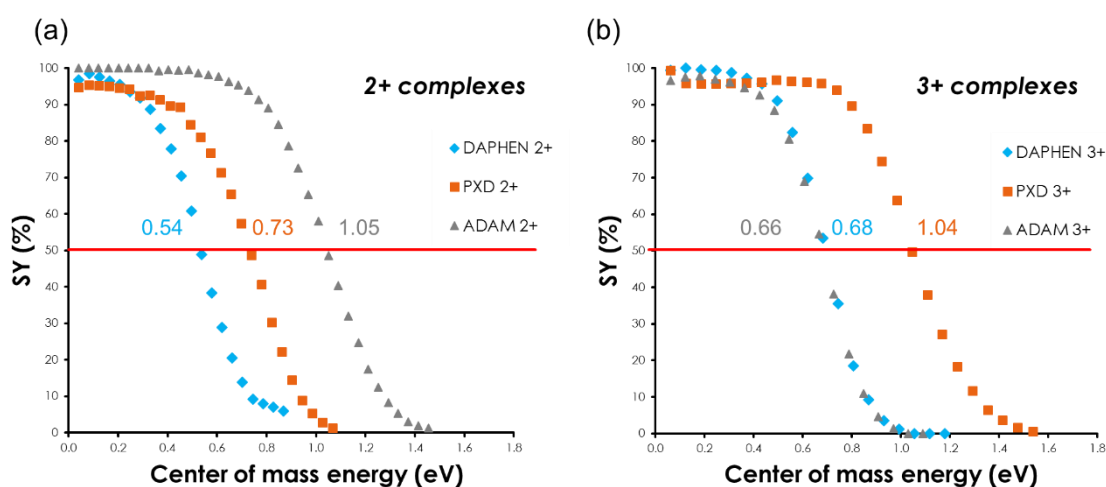


**Figure IV.5.3:** Survival Yield (SY) curves recorded for the (a) doubly charged ternary complexes and (b) triply charged ternary complexes. The corresponding values of  $E_{50}$  are reported on the graphs.

As expected, when the charged host-guest ternary complexes are exposed to increasing collision energy, the fraction of the parent ions – survival yield (SY) - that reaches the detector decreases following a sigmoidal relationship [13]. **Figure IV.5.3** presents the SY curves for (a) the doubly charged complexes and (b) the triply charged complexes. Interestingly, whatever

the charge state, it is clearly appearing that the CID efficiency is guest molecule dependent as exemplified by: (i) the separation between the different SY curves and; (ii) the difference in the  $E_{50}$  energies, i.e., the energy required to induce the decomposition of 50% of the starting parent ions. In the case of the 2+ complexes (**figure IV.5.3 a**), the  $E_{50}$  energies are 0.54, 0.73 and 1.05 eV for the ternary complexes associating the host molecule with para-phenylenediamine (DAPHEN), para-xylylenediamine (PXD) and adamantylamine (ADAM), respectively. In other words, less internal energy is required to induce the decomposition of the ternary complexes involving DAPHEN, whereas the largest interaction prevails for ns-CB[10] with ADAM. When analyzing the data for the triply charged complexes in **figure IV.5.3 b**, the three curves are also separated with  $E_{50}$  energies at 0.66, 0.68 and 1.04 eV for the complexes with adamantylamine (ADAM), para-phenylenediamine (DAPHEN) and para-xylylenediamine (PXD), respectively. When comparing the CID behaviors of the triply and doubly charged ions, it is worth highlighting the peculiar behavior of the ADAM-containing complexes, for which the  $E_{50}$  is the largest when doubly charged but the weakest when triply charged. Keeping in mind that the 2+ and 3+ ions expel a neutral and a protonated guest respectively, such a behavior of the ADAM guest can be immediately understood on the basis of the higher proton affinity of this amino-compound when compared to the other studied guests (DAPHEN 207,7 kcal/mol, PXD 214,8 kcal/mol, ADAM 218,5 kcal/mol) [14]. Indeed, since ADAM presents the highest proton affinity, leaving the cavity has a neutral compound will demand a bigger amount of energy than for the other studied guests. Nevertheless, the higher gas-phase basicity of ADAM cannot readily explain the opposite CID behaviors of the 2+ and 3+ ternary complexes. Therefore, in the following part of the paper, we will use computational chemistry to decipher the energetic reasons leading to the contrasting behaviors between the triply and doubly charged complexes.

Before entering the discussion, we must here specify that, in first approximation, the entropic effects ( $\Delta S^*$ ), associated with the pre-exponential factor in the RRKM equation [15], will not be taken into account in our study. We will only rely here on the comparison between the critical energies of fragmentation (called  $\epsilon_0$  in the RRKM theory), to explain the trends in the CID data. However, because the investigated dissociation reactions all correspond to similar decomplexation processes, the assumption that the differences among the observed kinetic data are not caused by different entropic effects is reasonable.

### 5.2.2 Estimation of the dissociation barriers

As already reminded in the introduction of this paper, the CID processes are under kinetic control. Indeed, the CID fragments are expected to be detected only if the internal energy deposited within the ions overcomes the free energy barrier of the dissociation reactions, named the critical energy for dissociation  $\epsilon_0$  [15]. When building a potential energy diagram relevant to dissociation reactions, whereas assessing the energy levels of the parent and fragment ions is nowadays a rather straightforward task using modern computational chemistry methods, the estimation of the transition state energy barriers remains challenging, especially for large systems. In the present work, we decided to develop a simplified method to estimate the critical energies for dissociation using DFT calculations. For this analysis, we started from the most stable structures of the inclusion complexes obtained at the DFT level using the B97D functional and the 6-31G(d,p) basis set (see Chapter 4 and reference [3]). These structures will be referred to as 'inclusion complexes' in the following lines.

Upon collisional activation, the first step on the way to the elimination of a guest molecule, either as neutral or protonated, corresponds to the flipping of a guest to afford an 'exclusion complex' presenting one guest outside and one guest inside the cavity. Given the high flexibility of the cage [3], we firstly hypothesize that the guest flipping reaction is not the rate-limiting step of the global decomposition reaction. To give some more support to this assumption, we submitted the different inclusion complexes to increased energies using Molecular Dynamics (MD) simulations and recorded the energy required to observe the flipping of the guest. Basically, as reported in **figure IV.5.4**, whatever the complex charge state, ADAM is always identified as the guest that needs the smallest energy to form the exclusion complex. This is of course an expected result based on the monoamine nature of ADAM, whereas both other diamino guests can hydrogen bond on both sides of the cucurbituril cavity. When confronting the MD results to the data generated from the ER-CID experiments in **figure IV.5.3**, we conclude that, if the guest flipping reaction was the rate-limiting step, the charge-state dependent behavior of the ADAM containing complexes, i.e. the most fragile complexes when triply charged and the strongest to decompose when doubly charged, could not be understood.

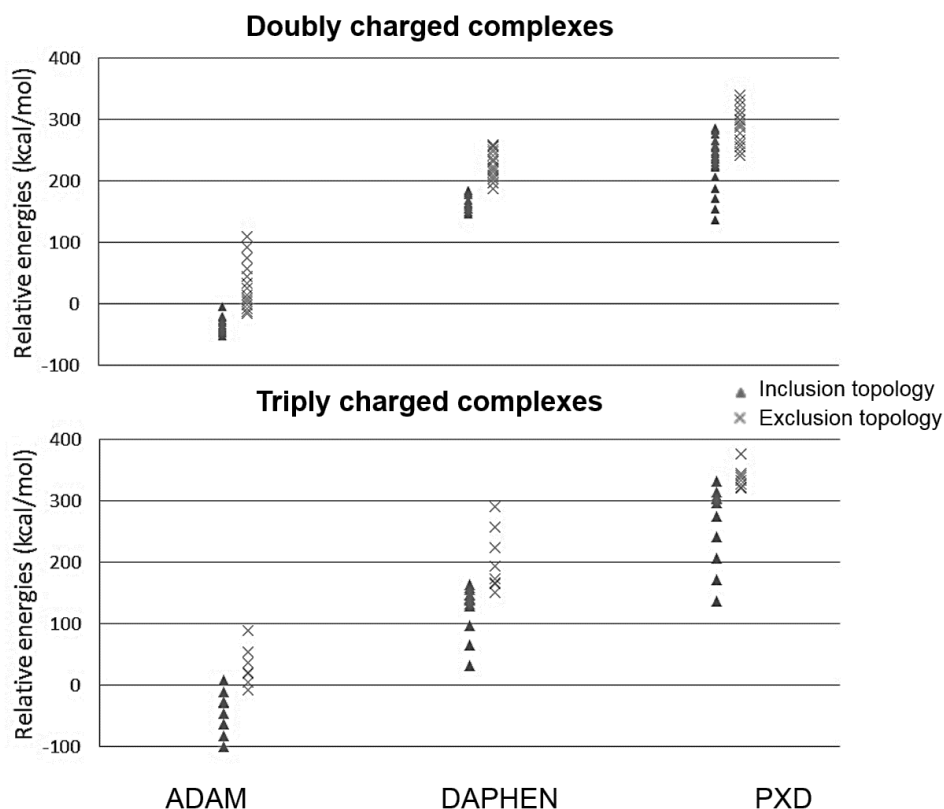


**Figure IV.5.4:** Inclusion complexes submitted to an increase energy within Molecular Dynamics simulations in order to determine the minimum energy required to observe the flipping of one guest for doubly charged and triply charged ternary complexes.

At variance with the case of the 2+ ternary complexes, see **figure IV.5.3 a**, the situation is definitively more complex when analyzing the 3+ complexes. Indeed, the presence of the third proton makes the system asymmetrical, raising the question of the nature of the molecule undergoing the flipping process. While DAPHEN and PXD are diamino compounds, ADAM only possesses one amino group, see **scheme IV.5.1**. In chapter 4, we demonstrated that, for the 3+ ternary complexes, the three protons are attached to three amino groups, except in the case of the ADAM complexes where the third proton is located on one of the oxygen atom of a carbonyl group, see **figure IV.5.5 b**, and chapter 4 for more details on the structures. We applied here Molecular Dynamics (MD) simulations on the DFT-optimized inclusion geometries to follow the flipping reaction when increasing the total energy of the triply charged complexes. For PXD and DAPHEN the triply charged ternary complexes follow the route (c) in **figure IV.5.5**, with the mono protonated guest molecule being excavated. However, for ADAM, it is observed that the guest molecule that is first rolling out comes from

the doubly charged cavity, according to route (b) in **figure IV.5.5**. These exclusion complexes will now be considered as the key intermediates on the way to the collision-induced losses of either a neutral or a protonated guest molecule. Even though we already demonstrated, see **table IV.5.2**, that the 2+ and 3+ ternary complexes present opposite behaviors upon CID, with respectively mainly the loss of a neutral or a protonated molecule, we will investigate both pathways for all complexes. Actually, one of our major interrogations is the observation of the prevalence of the loss of protonated molecules in the case of the 3+ ions knowing that charge separation processes are always characterized by large reverse activation barrier  $\epsilon_0'$ , whose dominant contribution comes from the coulombic term [16].

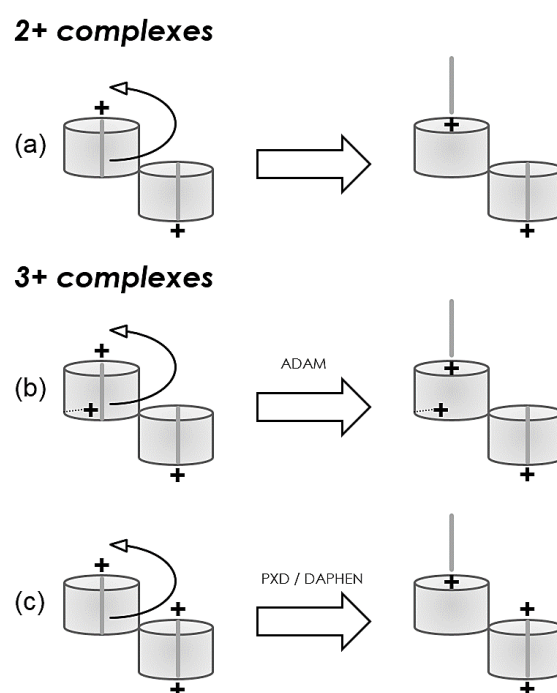


**Figure IV.5.5:** Collision-induced flip of the guest molecule from the 2+ and 3+ ternary complexes.

Before discussing the results for all studied systems, we decided to depict step by step our exclusion profile model for the case of the extraction of a neutral guest from the doubly charged ternary compound involving PXD.

To do so, we must first transfer the proton of the amino group to the closest oxygen atom of the portal in the DFT-optimized exclusion complex (note that this step is avoided for the departure of a protonated guest). All the attempts to calculate the energy required for the

proton transfer from the ammonium group to the oxygen atom of the carbonyl rim, by optimizing the non-covalent complex associating the protonated cage with the free amine ended up with the back-transfer of the proton to the more basic amino group. We thus estimated the energy for the proton transfer from the nitrogen guest atom to the closest oxygen of the carbonyl rim, by monitoring on the basis of single point calculations, the evolution of the relative energy of non-covalent complexes where the distance between the proton and the nitrogen atom is modulated while keeping constant the oxygen–nitrogen distance. This will provide the upper limit for the energy required for the proton transfer.

As a typical example of our procedure to estimate the energy involved in the proton transfer reaction, we present here the case of PXD for both the doubly and triply charged complexes. In both cases, the starting point corresponds to the exclusion structures optimized at the DFT level (B97D, 6-31G(d,p)). In those structures, all charges are carried by the PXD guests (**figure IV.5.6**).

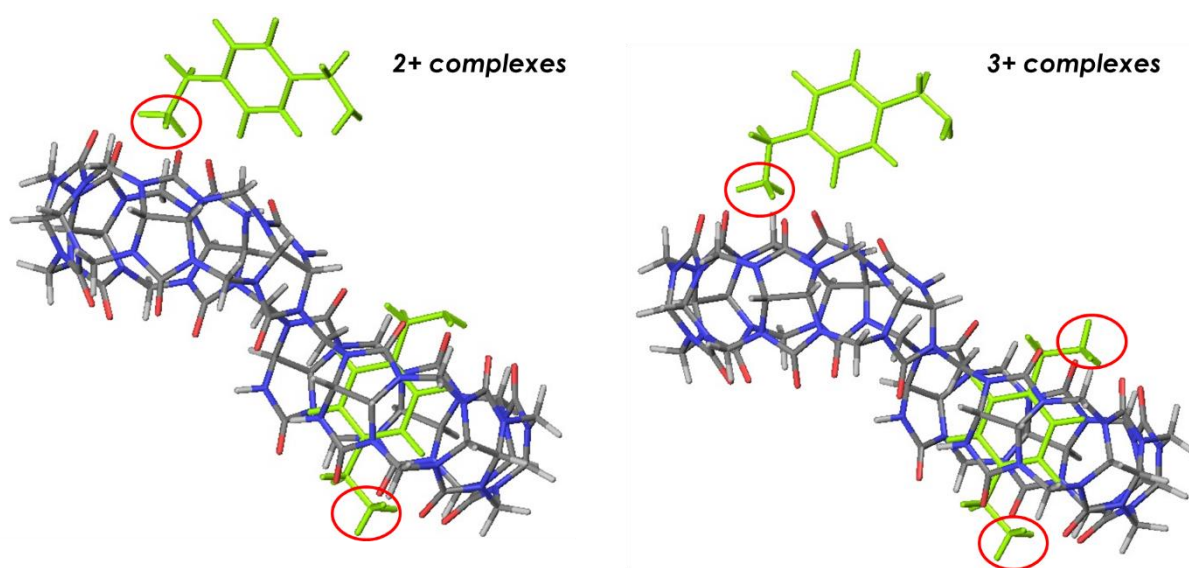


**Figure IV.5.6:** DFT-optimized structures of the doubly and triply charged exclusion complexes of PXD and ns-CB[10] (B97D, 6-31G(d,p)). Charge locations are noticed in red circles.

**Figure IV.5.7** illustrates the method used to determine the energy cost for the proton transfer. Starting from the optimized structure of the exclusion complex, single point calculations have been performed by increasing the distance between the proton and the nitrogen atom of the leaving guest amine function from the equilibrium distance up to 1 Å, upon freezing all the other atom coordinates including the O-N distance (3.1 Å) in the optimized complex (see the black arrow on **Figure IV.5.7**), with O the nearest oxygen atom.

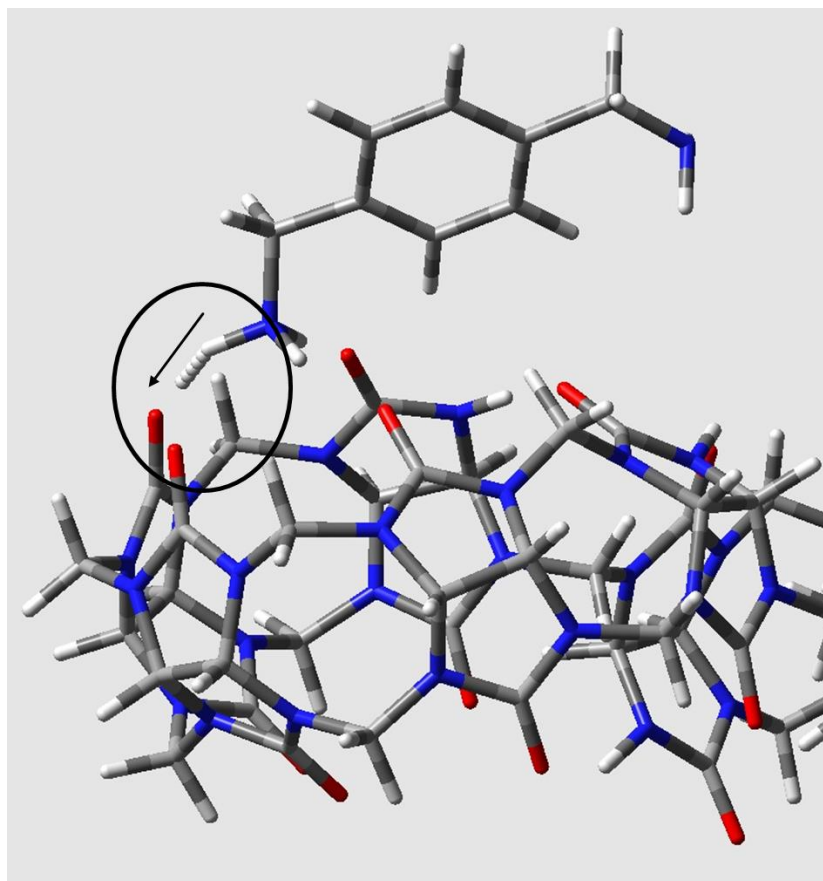


**Figure IV.5.7:** Illustration of the method used to evaluate the energy cost for a proton transfer from the guest to a cage carbonyl function (see black circle).

**Figure IV.5.8** displays the evolution of the relative energies obtained for the doubly charged and triply charged associations between ns-CB[10] and PXD as a function of the distance. The same procedure was conducted on the other complexes and the data are presented in **Table IV.5.3**. The relative energies determined by this method can be considered as the upper limit for the energy required for transferring the proton from the ammonium group to the carbonyl rim since no optimization has been performed.

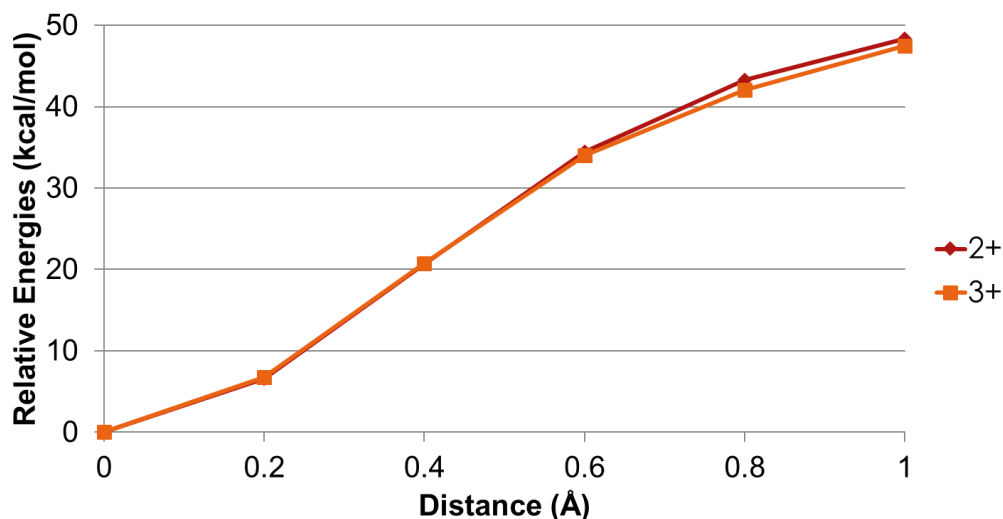


**Figure IV.5.8:** Proton transfer curves obtained with single-point calculations (DFT, B97D 6-31G(d,p)) for the doubly and triply charged complexes of PXD and ns-CB[10].

As displayed in the case of PXD (**figure IV.5.8**), the energy profile does not show an activation barrier and yields an energy difference between reactants and products of 48 kcal/mol for the 2+ complex (see **table IV.5.3**).

**Table IV.5.3:** Relative energies obtained for the proton transfer reaction for the 6 studied complexes without geometric relaxation effects thus preventing any link with the actual basicity

Guest	Maximum energy required for the proton transfer (kcal/mol)	
	2+	3+
PXD	48	47
DAPHEN	44	44
ADAM	46	50

The amount of energy presented in **table IV.5.3** (a) are reported in **figure IV.5.9** above that associated to the optimized exclusion prior to the proton transfer. Starting from this exclusion structure, we then increase the distance between the leaving neutral guest with respect to the host and build the energy profile via successive single point calculations (B97D/6-31G(d,p)). The results of those extraction procedures are presented in **figure IV.5.10** for the



2+ and 3+ complex ions and point to zero or weak reverse energy barriers, in agreement with the expected energy required to separate a neutral molecule and a charged binary complex. In the case of PXD (triangle curve), an amount of energy of about 44 kcal/mol is needed to pull away the guest from the binary complex. Such an approximation is reasonable even if a small reversed energy barrier is expected to account for the bond reorganization within both the isolated partners upon complexation; however, this amount of energy is likely to be very small and would not change any further conclusion. Consequently, the obtained energy (44 kcal/mol) is next reported on **figure IV.5.9** (b) to estimate the total energy (114 kcal/mol above the optimized inclusion complex) to fully separate the neutral PXD from the doubly charged binary complex without accounting for the structural reorganization of the cage and guest molecule. Finally, we separately optimized the structures of the neutral PXD and doubly charged binary complex at the DFT level and found that 44 kcal/mol are gained by the reorganization energy (c), leading to a final value of + 69 kcal/mol with respect to the initial inclusion complex. Since the neutral guest extraction curves do not present any barrier to cross (**figure IV.5.10**), the critical energy for fragmentation can be approximated by the dissociation energy.

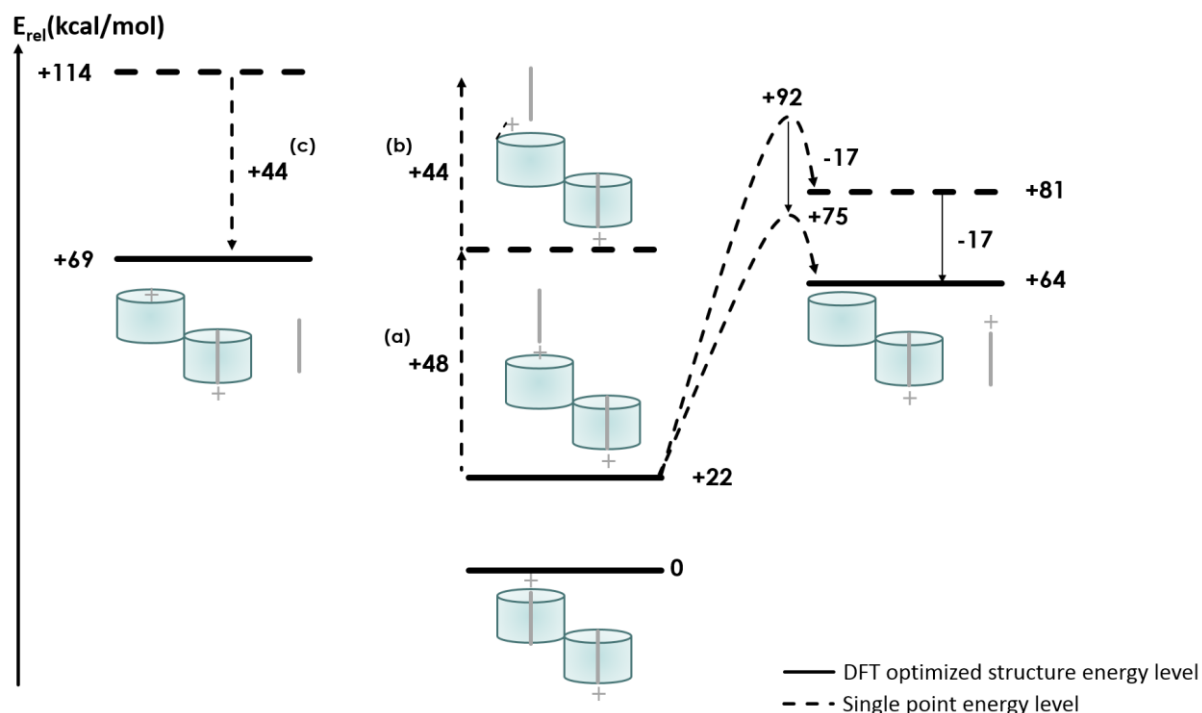


**Figure IV.5.9:** Energy diagram for the CID reaction undergone by the 2+ ternary complex

associating *ns*-CB[10] and *para*-xylylenediamine (PXD). Relative energies are given in kcal/mol.

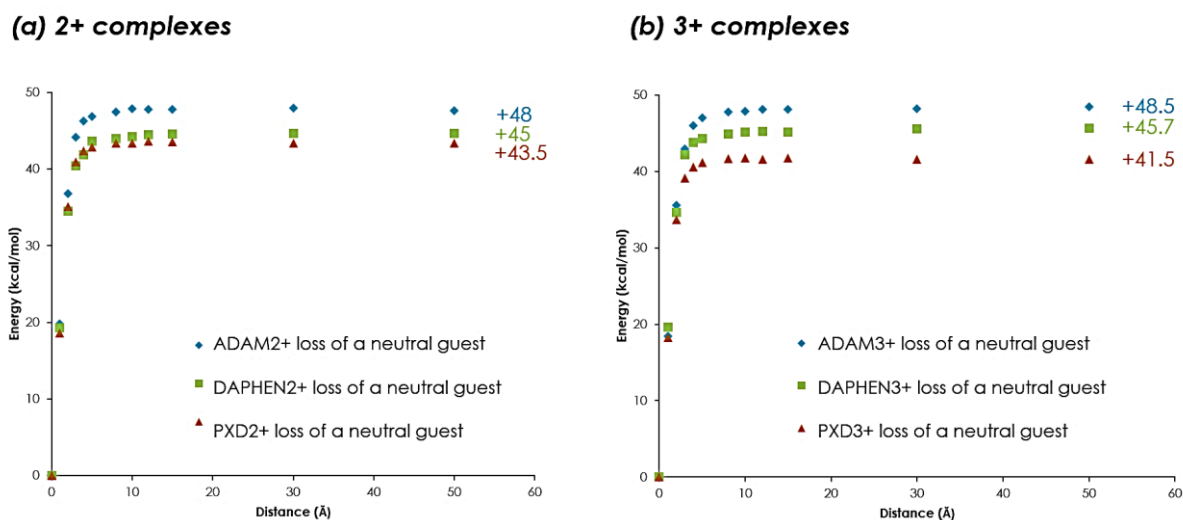


**Figure IV.5.10:** Extraction curves for the neutral guest loss from (a) the doubly charged and (b) triply charged ternary complexes. For each curve, the specified energy value corresponds to the energy difference between the equilibrium distance (0Å) and infinity.

The determination of the critical energies of dissociation is by far easier when investigating the charge separation reactions leading to the loss of a protonated guest. Indeed, in such cases, the starting point for building the extraction diagrams is clearly identified as the DFT-optimized exclusion complexes since there is no need to transfer a proton to the cage. Starting from these structures, the protonated guest is pulled away perpendicularly to the carbonyl portal and single point calculations are performed for increasing distances; see **figure IV.5.11** for the extraction curves. In the case of PXD for the doubly charged complex (**figure IV.5.11 a**, triangle curve), the activation barrier to reach the transition state amounts to 70 kcal/mol whereas an infinite separation between the two components corresponds to a relative energy level of 59 kcal/mol in regard of the starting exclusion topology. When reported to **figure IV.5.9** (right side), these energy values have to be summed to the relative energy of the exclusion complex compared to the initial inclusion structure (22 kcal/mol), leading to a total energy threshold of 92 kcal/mol to promote the dissociation and a final energy level at 81 kcal/mol. The latter does not correspond to the sum of the energies of the DFT-optimized structures of the separated binary doubly charged compound and protonated PXD since single point calculations have been made to depict the guest departure. The stabilization by nuclear

relaxation of the two separated fragments is calculated at the DFT level to be 17 kcal/mol (**figure IV.5.9**). We then assume that the same amount can be removed from the transition state to get a value of the activation barrier taking into account the reconstruction effects. Accordingly, the transition state for the departure of the protonated PXD is located 75 kcal/mol above the optimized inclusion complex.

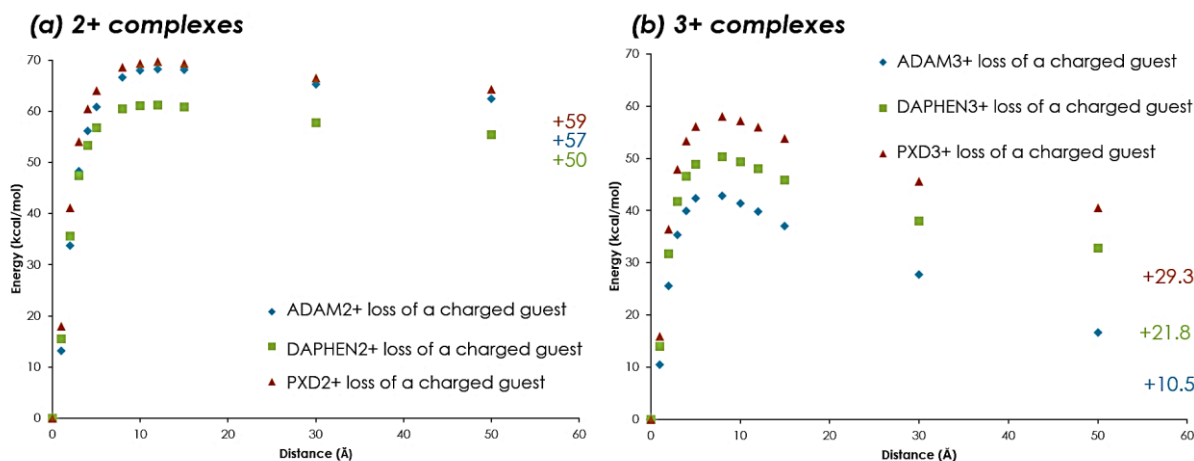
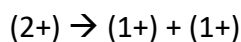


**Figure IV.5.11:** Extraction curves for the protonated guest loss from (a) the doubly charged and (b) triply charged ternary complexes. For each curve, the specified energy value corresponds to the relative energy difference between the equilibrium distance (0Å) and infinity.

As expected, our extraction procedure yields reverse activation energy barriers with the same order of magnitude as that expected for charge separation reactions. From **figure IV.5.11**, we can estimate that the reverse activation energies  $\epsilon_0^r$  amount to 11, 10 and 11 kcal/mol for the 2+ ternary complexes containing PXD, DAPHEN and ADAM respectively, as calculated from the energy difference between infinite separation and the maximum of the extraction curves. In the context of charge separation reactions, the reverse activation energies can be estimated by considering as dominant factor the Coulomb interactions, using the well-known equation suggested by March et al [16]:



$$\varepsilon_0^r = \frac{14.39}{R(\text{\AA})}$$

**Scheme IV.5.3:** Charge separation reactions: estimation of the reverse activation energy (eV), with  $R$  the separation between the charges in the transition state [16].

For the loss of a protonated molecule from the 2+ complex ions, and using as the inter-charge distance the separation  $H^+ \cdots H^+$  in the structures at the maximum of the extraction curves, the reverse activation energies are estimated from **scheme IV.5.3** to 13, 14 and 15 kcal/mol for complexes containing PXD, DAPHEN and ADAM, respectively. The slight discrepancy between the two sets of data originates from the more complex charge distribution in the structures treated at the DFT level, due in particular to the presence of the carbonyl portal.

In the following, we have combined all the calculated energetic values to build the potential energy diagrams describing the collision-induced decomposition reactions undergone by the 2+ and 3+ ternary complexes for the three different guests. Both the charge and guest dependences on the nature of the observed CID reactions (neutral versus protonated molecule loss) and CID reaction efficiencies will be discussed based on those diagrams. All energy barriers associated to the loss of a protonated guest have been corrected with the methodology used for the ternary compound associating PXD and ns-CB[10] and exemplified in **figure IV.5.9**.

### 5.2.3 CID reactions of the 2+ ternary complexes

**Figure IV.5.12** collects the energy diagram describing the CID reactions involving the doubly charged ternary complexes associating ns-CB[10] to the three selected guest molecules. The experimental results to rationalize on the basis of these diagrams are: (i) the prevalence of the neutral loss reaction; and (ii) the relative order of  $E_{50}$  with DAPHEN < PXD < ADAM.

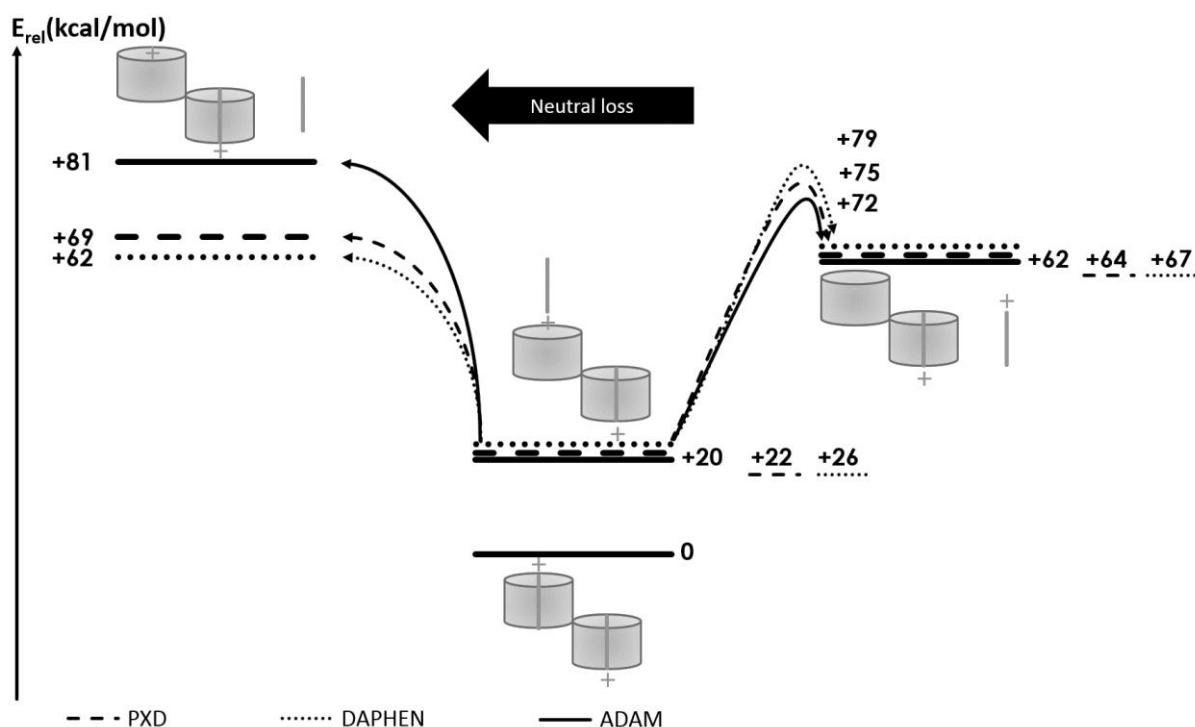


**Figure IV.5.12:** Energy diagram for the CID reactions undergone by the 2+ ternary complexes associating *ns*-CB[10] and the three selected guest molecules, *para*-xylylenediamine (PXD), *para*-phenylenediamine (DAPHEN) and adamantylamine (ADAM). Relative energies are given in kcal/mol.

While the energy cost to lose a neutral or charged guest is very similar from a thermodynamical point of view, complexes based on PXD and DAPHEN will lose preferentially a neutral fragment since, in contrast to the loss of a charged guest, this process is barrierless. In the case of the ADAM guest, the neutral and protonated adamantylamine losses require 81 and 72 kcal/mol, respectively. These theoretical data does not appear to reproduce the experimental results summarized in **table IV.5.2**, with the prevalence of the neutral loss for all 2+ complexes. Nevertheless, it is worth stressing that only in the case of the ADAM complexes is the competitive loss of the protonated guest detected. As far as the relative  $E_{50}$  values are concerned, the experimental order (**figure IV.5.3 a**) correlates very well with the theoretical values (**figure IV.5.12**), with dissociation thresholds reaching 62 kcal/mol, 69 kcal/mol and 81 kcal/mol for DAPHEN, PXD and ADAM, respectively, i.e. DAPHEN (weakest complex) < PXD < ADAM (strongest complex). This good agreement between theory and experiment validates our initial assumption that, given the high flexibility of the host, the flipping of the guest out of the cavity is not the limiting step in the CID experiments.

## 5.2.4 CID reactions of the 3+ ternary complexes

**Figure IV.5.13** summarizes all data obtained using our theoretical model for the CID behavior of the triply charged ternary complexes. It is also important to remind that the nature of the leaving protonated guest is not the same for ADAM compared to PXD and DAPHEN (see **figure IV.5.5**).

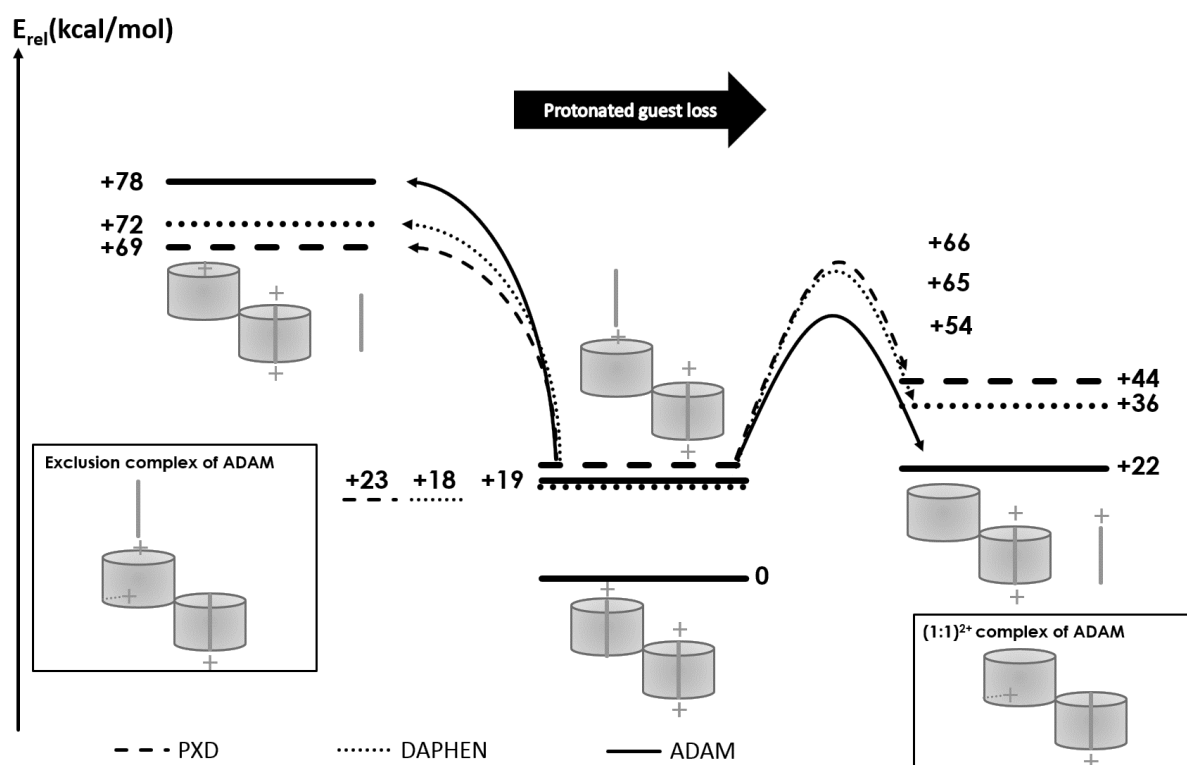


**Figure IV.5.13:** Energy diagram for the CID reactions undergone by the 3+ ternary complexes associating *ns*-CB[10] and the three selected guest molecules, *para*-xylylenediamine (PXD), *para*-phenylenediamine (DAPHEN) and adamantylamine (ADAM). Relative energies are given in kcal/mol.

We reproduce again here the order of decomplexation following the departure of a protonated guest obtained on the basis of the SY curves in **figure IV.5.3 b**, ADAM (weakest complex) < DAPHEN < PXD (strongest complex). From a thermodynamical point of view, the protonated guest loss pathway is always more favorable than the neutral guest loss reaction according to the calculated activation barriers, in full consistency with the experimental observations. The protonated ADAM loss is by far the most favorable process characterized by an energy difference of only +22 kcal/mol between the initial and final states, in line with

the experimental observations showing that the 3+ ADAM complexes exclusively eliminate a protonated ADAM (**table IV.5.2**) upon collisional activation (thus further confirming the higher basicity of ADAM). As far as the 3+ PXD (DAPHEN) complexes are concerned, the dissociation thresholds for the protonated and neutral PXD (DAPHEN) losses amount to 66 (65) and 69 (72) kcal/mol, respectively. Such a small difference rationalizes why the two fragmentation pathways are in competition based on the experimental observations made in **table IV.5.2**.

### 5.3 Conclusions

The collision energy dependence of the fragmentation pathway of ternary complexes made of ns-CB[10] and three amino compounds was studied by Electrospray ionization using tandem mass spectrometry. The use of energy-resolved CID experiments affords interesting pieces of information about the collision induced dissociation of the complexes in the gas phase. It appears that the E50 value is highly dependent on the guest molecule but also on the charge state of the complex. Indeed, adamantylamine (ADAM) was identified as the guest requiring the highest energy to be expelled from the 2+ ternary complexes and the lowest for the 3+ ternary complexes. It was also observed that the 2+ ternary complexes mainly expel a neutral molecule, whereas the CID behavior of the 3+ complexes corresponds to a charge separation process with the loss of a protonated guest. The most difficult aspect of the present work is that CID processes are by definition kinetically driven so that the activation barriers associated to the decomposition reactions must be taken into account in the analysis of such processes. Accordingly, we developed here an original method to estimate, at the DFT level (B97D/6-31G(d,p)), the critical energies for dissociation using an extraction protocol tracking the evolution of the energy of the full system when moving away the protonated or neutral guest molecule. Our model provides us a deep understanding of the observed behaviors in the CID processes, with a special emphasis on: (i) the nature (neutral or charged) of the expelled guest molecule as a function of the charge of the complex; and (ii) the nature of the guest molecule on the CID efficiency. The peculiar behavior of adamantylamine, yielding the strongest doubly charged complex and the weakest triply charged complex, was fully rationalized based on its higher basicity. Nevertheless, we suspect that the ADAM case is the most tricky to evaluate given the high basicity of the molecule especially when trying to mimic

the evolution of the proton transfer step which is probably even more poorly reproduced for such a basic compound.

However, our results also emphasize that the comprehensive description of the kinetic data for CID reactions must take into account the entropic effects, say the  $\Delta S^*$ , in addition to the determination of the critical energies of decomposition. In our case, even if the agreement between the theoretical and the experimental results are quite fair, we suspect that the pre-exponential factor that contains the entropic effects must be different between the competitive CID reactions, i.e. the neutral and the protonated guest losses. In particular, the proton transfer reaction between the ammonium group of the guest to the carbonyl rim of the cage must be affected by more favorable entropic effects given the great numbers of possibilities to transfer the proton.



## References

1. a) J. Lagona, P. Mukhopadhyay, S. Chakrabarti, L. Isaacs; *Angew. Chem. Int. Ed.* 2005; 44: 4844–4870; b) J. W. Lee, S. Samal, N. Selvapalam, H. J. Kim, K. Kim, *Acc. Chem. Res.* 2003; 36: 621–630; c) K. Kim, N. Selvapalam, Y. H. Ko, K. M. Park, D. Kim, J. Kim, *Chem. Soc. Rev.* 2007; 36: 267–279; d) L. Isaacs, *Isr. J. Chem.* 2011; 51: 578–591; e) E. Masson, X. Ling, R. Joseph, L. Kyeremeh-Mensah, X. Lu, *RSC Adv.* 2012; 2: 1213–1247; f) W. L. Mock, N. Y. Shih, *J. Org. Chem.* 1986; 51: 4440–4446; g) S. Liu, C. Ruspic, P. Mukhopadhyay, S. Chakrabarti, P. Y. Zavalij, L. Isaacs, *J. Am. Chem. Soc.* 2005; 127: 15959–15967; h) C. Marquez, R. R. Hudgins, W. M. Nau, *J. Am. Chem. Soc.* 2004; 126: 5806–5816; i) W. L. Mock, N. Y. Shih, *J. Am. Chem. Soc.* 1989; 111: 2697–2699; j) J. Kim, I-S. Jung, S-Y. Kim, E. Lee, J-K. Kang, S. Sakamoto, K. Yamaguchi, K. Kim, *J. Am. Chem. Soc.* 2000; 122 (3): 540-541; k) A. Day, A.P. Arnold, R.J. Blanch, B. Snushall, *J. Org. Chem.* 2001; 66 (24): 8094-8100; l) A. Day, R.J. Blanch, A.P. Arnold, S. Lorenzo, G.R. Lewis, I. Dance, *Angew. Chem. Int. Ed.* 2002; 41: 275-277; m) X-J. Cheng, L-L. Liang, K. Chen, N-N. Ji, X. Xiao, J-X. Zhang, Y-Q. Zhang, S-F. Xue, Q-J. Zhu, X-L. Ni, Z. Tao, *Angew. Chem. Int. Ed.* 2013; 52: 7252-7255.
2. a) W.-H. Huang, S. Liu, P. Y. Zavalij, L. Isaacs, *J. Am. Chem. Soc.* 2006; 128: 14744–14745; b) R. Nally, L. Isaacs, *Tetrahedron* 2009; 65: 7249–7258; c) J. B. Wittenberg, M. G. Costales, P. Y. Zavalij, L. Isaacs, *Chem. Commun.* 2011; 47: 9420–9422.
3. V. Lemaury, G. Carroy, F. Poussiguet, F. Chirot, J. De Winter, L. Isaacs, P. Dugourd, J. Cornil, P. Gerbaux, *ChemPlusChem.* 2013; 78: 959–969.
4. K. M. Ervin., *Chem. Rev.* 2001; 101: 391-444.
5. P.B. Armentrout, *Int. J. Mass Spectrom.* 2000; 200: 219–241.
6. a) P. B. Armentrout, *Top. Curr. Chem.* 2003; 225: 233-262; b) A. Pak, D. Lesage, Y. Gimbert, K. Vékey, J.C. Tabet, *J. Mass Spectrom.* 2008; 43: 447–455, c) T.M. Kertesz, L.H. Hall, D.W. Hill, D.F. Grant, *J. Am. Soc. Mass Spectrom.* 2009; 20: 1759–1767.
7. P. B. Armentrout, K. M. Ervin, M. T. Rodgers., *J. Phys. Chem. A* 2008; 112: 10071-10085.
8. a) L. Wang, Y. Chai, C. Sun, D.W. Armstrong, *Int. J. Mass Spectrom.* 2012; 323–324: 21–27; b) L. Wu, J.W. Denault, R.G. Cook, L. Drahos, K. Vékey, *J. Am. Soc. Mass Spectrom.* 2002; 13: 1388-1395; c) M.B. More, D. Ray, P.B. Armentrout, *J. Am. Chem. Soc.* 1999; 121: 417-423.

9. C. A. Schalley, P. Ghosh, M. Engeser., *Int. J. Mass Spectrom.* 2004; 232: 249–258.
10. a) D. V. Dearden, T. A. Ferrell, M. C. Asplund, L. W. Zilch, R. R. Julian, M. F. Jarrold, *J. Phys. Chem. A.* 2009; 113: 989–997; b) F. Yang, D. Dearden, *Isr. J. Chem.* 2011; 51: 553-558; c) T.-C. Lee, E. Kalenius, A. I. Lazar, K. I. Assaf, N. Kuhnert, C. H. Grün, J. Jänis, O. A. Scherman, W. M. Nau, *Nature Chemistry* 2013; 5: 376-382; d) K.I. Assaf, W.M. Nau, *Chem. Soc. Rev.* 2015; 44: 394-418; e) Z. Qi, T. Heinrich, S. Moorthy, C.A. Schalley, *Chem. Soc. Rev.* 2015; 44: 515-531.
11. H. Zhang, T.A. Ferrell, M.C. Asplund, D.V. Dearden, *Int. J. Mass Spectrom.* 2007; 265: 187–196.
12. G. Carroy, C. Daxhelet, V. Lemaire, J. De Winter, E. De Pauw, J. Cornil, P. Gerbaux, *Chem. Eur. J.* 2016 ; 22 : 4528-4534.
13. C. Peltz, L. Drahos, K. Vékey, *J. Am. Soc. Mass Spectrom.* 2007; 18: 2119-2126.
14. S.G. Lias, J.E. Bartmess, J.F. Liebman, J.L. Holmes, R.D. Levin, W.G. Mallard, *Journal of Physical and Chemical Reference Data* 1988, 17, supplement no.1.
15. L. Sleno, D. A. Volmer *J. Mass Spectrom.* 2004; 39: 1091-1112.
16. R.E March, R.J. Hughes, *Int. J. Mass Spectrom. and Ion Processes* 1986; 68: 167-182.

## V. Conclusion and Outlook

## Conclusion & Outlook

Throughout our thesis, mass spectrometry has been confirmed as a performant characterization tool for the study of gas phase supramolecular associations. The use of Electrospray as the ionization source permits the preservation of non-covalent interactions when host/guest associations are transferred from the solution to the gaseous phase. Furthermore, a deep study of the gas phase conformations of the corresponding ionized complexes can be conducted thanks to the complete MS-based methods (MS, CID, ER-CID, IMMS) available in the S<sup>2</sup>MOs laboratory in Mons and the MS Lab in Liège supplemented by computational chemistry results obtained at the CMN research group in Mons. Furthermore, the influence of the experimental and instrumental conditions has been treated with great care, especially the in-solution reaction time (time spent by the molecules in-solution prior the vaporization process) and the voltages applied within the Waters Synapt G2-Si prior to the ion mobility separation.

Since computational chemistry allows for the study of molecules without any influence of their environment, the association between Density Functional Theory and MS-Based methods is straightforward. In our studies, theoretical calculations are used to evaluate the guest relative binding energies for the different hosts under study but also to calculate the theoretical collisional cross sections (CCS) of the optimized structures. According to those CCS values, the gas phase topologies of host/guest complexes can be approached with comparison between those theoretical data and ion mobility mass spectrometry measurements providing experimental CCS.

In our studies, the cucurbituril macrocycle family has been selected as the model system, since cucurbiturils are mainly known to form complexes with ammonium-guests resulting in high association constants. In addition, due to the rigidity of these hosts, the guest size remains the relevant factor for encapsulation within a given cucurbituril cavity. However, researches using mass spectrometry mainly focus on the in/out character of the host/guest association involving a cucurbituril without dealing with the kinetics of the encapsulation process, which is an important factor according to the different results presented in our studies.

Firstly, we demonstrated within a joint experimental and theoretical approach that the ion topologies in the gas phase is affected by the equilibrium time in solution, especially for host-guest systems characterized by **slow kinetics of complexation**. For this study, the CB[6] host molecule in association with para-phenylenediamine (DAPHEN) have been chosen as the model system. We used ion mobility and energy-resolved CID to follow the evolution of the ion topologies as a function of time in solution prior to the ESI analysis and highlighted the overtime structure evolution. Therefore, we demonstrated the importance of **experimental conditions prior to the mass spectrometry experiment**.

Afterwards, to assess the influence of the **instrumental parameters**, we selected a model system extensively investigated in the condensed phase (Aniline@CB[6]) to study the influence of the voltages applied all along the ion optics of the mass spectrometer on the IN-to-OUT ratio of the detected ionized complexes. We demonstrated here that, for mono amino guest molecules, the IN-to-OUT isomerization process can be induced upon ion activation at different locations along the flight of the ions from the source to the ion mobility cell, i.e. in the stepwave (**Sample Cone voltage**) and in the triwave<sup>®</sup> setup (**Trap DC Bias** and **TRAP CE**).

Cucurbiturils are used in several applications but the **catalytic properties** of their inner cavity have been extensively discussed over the past years. Herein, we reported a mass spectrometric study performed on the triazole synthesis using the inner cavity of a cucurbit[6]uril host as a catalyzer. The use of Electrospray as ionization source renders possible the detection of gas phase ions corresponding to complexes between CB[6] and the two reagents primarily formed in solution. According to our results using CID, ion mobility and ER-CID experiments, we observed that the cycloaddition reaction within the CB[6] cavity is an **extremely fast process** and that **the rate determining step in the overall cycloaddition process is the encapsulation of both reagents** within the cavity. On the other hand, the cycloadduct triazole appears to be hardly expelled from the cucurbituril cavity, which explains the long reaction time monitored for this click-reaction in solution.

The last two chapters of this PhD concerned the non covalent associations between an original **ditopic receptor**, the nor-seco-cucurbit[10]uril (ns-CB[10]), and several guest amino compounds. The ionized ternary and binary complexes are investigated by associating state-of-the-art mass spectrometry and computational methods. For this study, ns-CB[10] is also

demonstrated to display **homotropic allostery** based on a guest size induced **preorganization mechanism**. Ns-CB[10] has been chosen for its peculiar ditopic structure, which makes this cucurbituril host more flexible than the rigid common cucurbiturils studied previously. Accordingly, those aspects render ns-CB[10] a good candidate for our investigations focusing on the transfer of non covalent complexes from the condensed phase to the rarefied gas phase of a mass spectrometer. We demonstrated that **Electrospray** ionization can be advantageously exploited to **transfer without decomposition** the non covalent ionic complexes to the gas phase of the mass spectrometer. The quasi exclusive **observation of ternary complexes**, associating two guest molecules to the receptor, confirms the **allosteric nature of the binding process**.

Lastly, the collision energy dependence of the fragmentation pathway of ternary complexes made of ns-CB[10] and three amino compounds was studied by Electrospray ionization using tandem mass spectrometry. The use of energy-resolved CID experiments affords interesting pieces of information about the dissociation of the complexes in the gas phase. We demonstrated the **high dependency of  $E_{50}$  value on the guest molecule but also on the charge state of the complex**. Indeed, whereas the 2+ ternary complexes mainly expel a neutral molecule, the CID behavior of the 3+ complexes corresponds to a charge separation process with the loss of a protonated guest. In this last chapter, we identified that the most difficult aspect of those CID processes is that they are **kinetically driven**. Accordingly, activation barriers are associated to the decomposition reactions and must be considered in the analysis of such processes. Therefore, we developed here an **original method** to estimate, at the DFT level (B97D/6-31G(d,p)), **the critical energies for dissociation using an extraction protocol tracking the evolution of the energy of the full system when moving away the protonated or neutral guest molecule**. Our model provides us a deep understanding of the observed behaviors in the CID processes for the doubly and triply charged ternary complexes, with a special emphasis on: (i) the nature (neutral or charged) of the expelled guest molecule as a function of the charge of the complex; and (ii) the nature of the guest molecule on the CID efficiency. However, our results also emphasized that the comprehensive description of the kinetic data for CID reactions must take into account the entropic effects, i.e.  $\Delta S^*$ .

Based on the results presented in this PhD, we can speculate some improvements that might prove useful in the study of non-covalent supramolecular associations with MS-based

methods, especially in the case of ion mobility associated to mass spectrometry. Firstly, **increasing the resolution in ion mobility** might be of great interest in order to correctly separate the different conformations/topologies, more especially shoulder peaks, detected after the mobility separation. In direct relation with that observation, we know that some brands already commercialized mass spectrometers with a better mobility separation than the Waters Synapt G2-Si (which presents a resolution of maximum 40) but also that Waters will soon commercialize a cyclic mobility cell with a mobility resolution over 500. Moreover, the possibility of adding a second ion mobility separation after the first one could be of great interest in the study of supramolecular associations in order to study isomerization phenomena or the topologies of the fragment ions generated after the first mobility separation. At the present days, such a device is not commercially available but Professor Philippe Dugourd and his team at the University of Lyon already built a homemade instrument presenting this set-up. In addition, **some studies using H/D exchange or ion cyclotron resonance (ICR)** could be used to bring additional informations on the gas phase topologies and decomposition pathways of the ionized complexes.

Concerning the molecules under study, we think that our methodology might also be applied to larger complexes involving cucurbituril hosts (such as CB[8] or even CB[14]) in order to compare the results to those obtained for CB[6]. Nevertheless, increasing the size of the host will also make them more flexible (the optimized topology of CB[14] is a loop) and therefore the need of switching the nature of the host molecules to systems that are more flexible might also be of a great interest. We can envisaged to study the calixarene family for example where each phenol unit is linked to the other by only one methylene bridge instead of two like in the cucurbituril family.

Finally, on the theoretical side, for the sake of comparison, we should try another DFT functional than B97D. Indeed, B97D refers to a DFT-D technique, where a dispersion term describes long-range interactions; lately, a new theoretical method has been developed which is called DFT-D3. In this method, it appears that dispersion forces are better described than in DFT-D though this method is more time consuming. We do not think that this new functional will deeply change the trend of our results but hope they might give us an even better description of the ion gas phase topologies

## VI. Annexes



## 1. Mass Spectrometry: additional notes

### 1.1 Tandem Mass Spectrometry

Tandem mass spectrometry, usually called MSMS, relies on at least two consecutive mass analyses. The first mass analysis consists in isolating a precursor ion (also called the parent ion) based on its  $m/z$  ratio. A fragmentation step is performed on those parent ions in order to obtain new ions called “daughter ions” and neutral species (not detected). The residual parent ions and its fragments are analyzed by a second MS analysis (**figure 1**). Accordingly, this method allows for the structural identification of ionized compounds. Theoretically, multiple successive mass analyses are doable but for sensitivity issue, tandem mass spectrometry analysis is mostly limited to two collision steps (MS<sup>3</sup>).

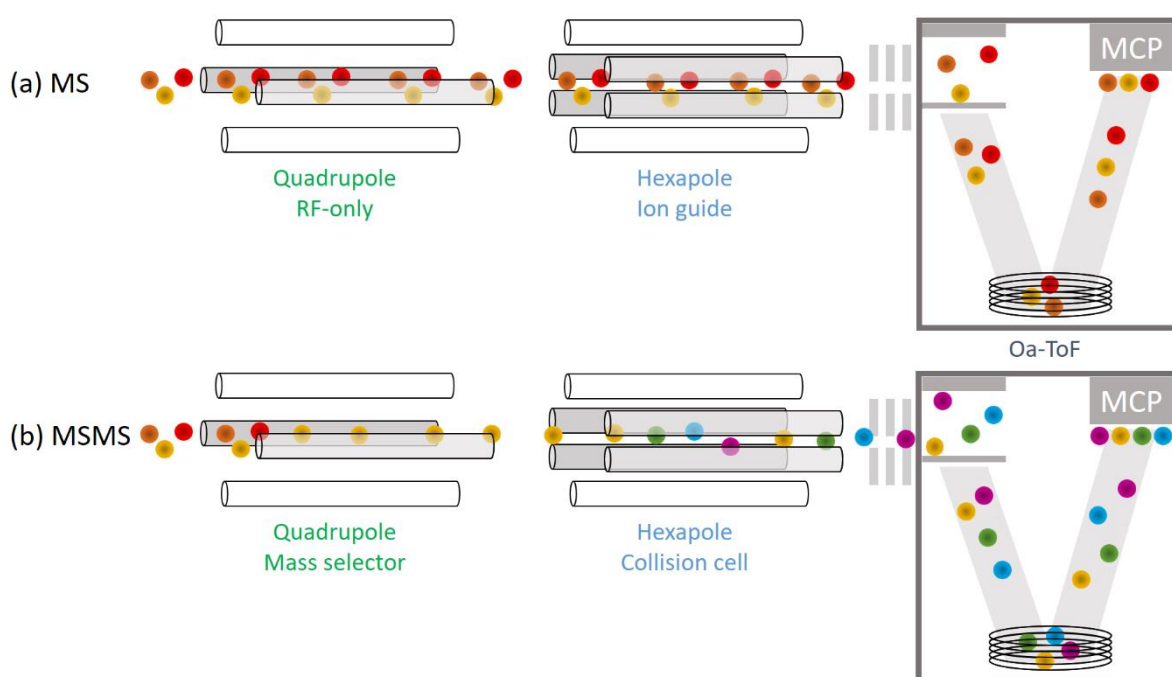


**Figure 1:** (a) scheme of a single stage mass analysis on the Waters Q-ToF US. (b) Representation of a tandem mass spectrometry analysis on the Waters Q-ToF US. Selection of the yellow ions followed by their collisional activation (in the hexapole). Daughter ions (purple, blue and green) and parent ions (yellow) are separated within the ToF analyzer.

The most common method to perform ion fragmentation is based on the activation of ions by collision with a buffer gas (Argon most of the time). Two types of activation are known depending on the energy used to accelerate the ions prior to the collision:

- Low kinetic energy (1-100 eV).
- High kinetic energy ( $\approx 1$  keV).

Therefore, fragmentations are performed within a specific region of the mass spectrometer called the collision cell. Briefly, a collision cell is filled with a buffer gas (from 2 to 5  $10^{-3}$  Torr). For the Waters Q-ToF US (**figure II.3**), the collision cell is a hexapole (section II.1.2.1) while for the Waters Synapt G2-Si (**figure II.4**), the cell is using the travelling wave technology (T-wave, more details in section II.2)). In each spectrometer, both collision cells are located after the quadrupole, which will play the role of mass selector for the first MS analysis in tandem mass spectrometry and before the ToF analyzer that will separate parent and daughter ions during the second mass analysis.

## 1.2 Triwave

The Waters Synapt G2-Si is actually equipped of three T-Wave™ ion guide units. The association of those three cells is called the Triwave™ (**figure 2**). Each unit is named as followed (from left to right): Trap, IMS cell and Transfer.

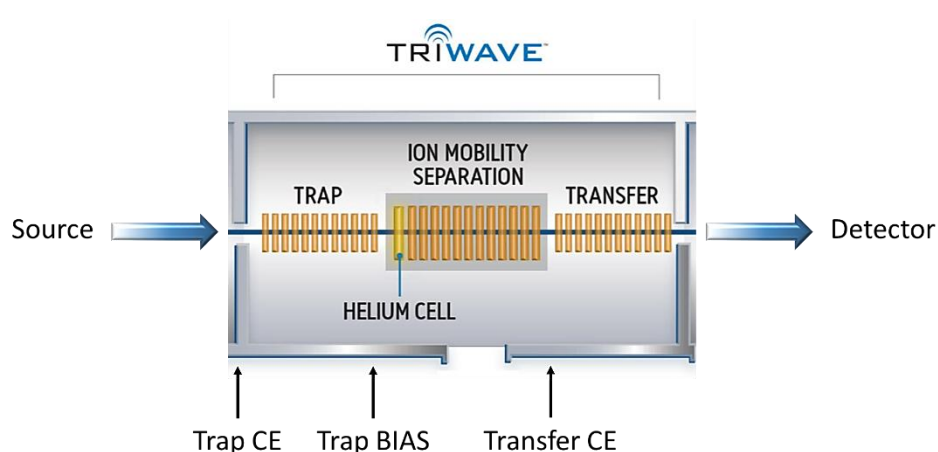


**Figure 2:** representation of the Triwave™ section of the Waters Synapt G2-Si instrument.

The purpose of the Trap cell is to stock the ions prior to their introduction inside the mobility cell. Ions are sent periodically inside the IMS-cell by a variation of the DC-potential applied on the last lens of the Trap unit. Ions might also be accelerated by the “Trap Bias” potential that is applied at the IMS-cell entrance. After separation within the mobility cell, ions will be guided towards the ToF analyzer using the Transfer ion guide unit. The purpose of this last T-wave cell is to efficiently transfer the ions while maintaining their separation.

Despite their use as ion guide, the “Trap” and “Transfer” cells can also be used as collision cells. Indeed, both Trap and Transfer are filled with a partial pressure of argon ( $\approx 10^{-2}$  mbar) which is a common gas used to activate ions through collisions (MSMS). Therefore, collision energy voltages (trap CE and transfer CE) can be adjusted in order to induce fragmentation of the ions in the Trap and/or the Transfer cell, in other words, before or after the ion mobility separation. As shown in **figure 3**, the resulting information will not be the same depending on which T-wave cell performs the ion collisional activation against argon.

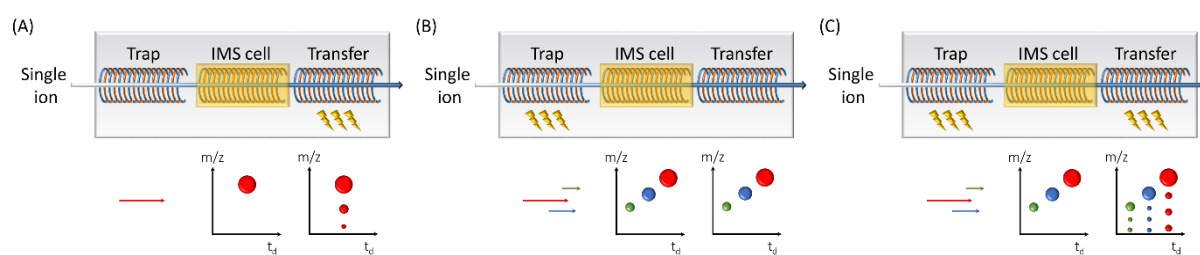


**Figure 3:** association between IMS and MSMS. A) Fragmentation in the Transfer. B) Fragmentation in the Trap C) Fragmentation in both Trap and Transfer cells.

Three different experiments can be achieved using the Triwave™ after the selection of parent ions within the quadrupole of the Waters Synapt G2-Si:

- A. MSMS achieved in the Transfer: parent ions are selected in the quadrupole, cross the ion mobility and are activated in the Transfer. Since no fragment ions have fled through the IMS cell, they will appear at the same drift-time as the parent ions (**figure II.22 a**). This set-up is particularly useful to record the CID spectra of ions with the same  $m/z$  but presenting different structures and CCS. Indeed, different structures will lead to different fragmentations that can be correlated to the appropriate parent ion separated from each other by mobility.

- B. MSMS achieved in the Trap: after CID in the Trap, the daughter ions are separated within the mobility cell (**figure II.22 b**). Accordingly, each fragment (and the remaining parent ions) will be characterized by a specific drift-time but no resolution of parent ions having the same  $m/z$  but different structures will be possible.
- C. Time-aligned parallel (TAP) fragmentation: in this mode, both Trap and Transfer T-wave cells are kept at high voltage. In the TAP mode, the parent ions will undergo first generation fragmentation in the Trap cell, and the resulting fragment ions will be separated in the ion mobility cell. The mobility-separated fragment ions will undergo further fragmentation in the Transfer, resulting in second-generation fragment ions, which are time-aligned with the first generation fragment ions [1].

## 2. Density Functional Theory

The density functional theory (DFT), whose foundations go back to 1920 [2], is a quantum chemistry calculation method for polyatomic systems where the critical parameter is the electronic density.

DFT is therefore no longer based on the search of the wave functions of an  $N$  electron system, with each electron depending on  $3N$  spatial coordinates, and  $N$  spin variables (such as in the Hartree-Fock method), but on the electronic density of the system (noted  $\rho(\mathbf{r})$ ) which only depends on 3 spatial coordinates. This theoretical approach uses the electronic density as a sufficient physical variable for the determination of the properties of polyatomic systems [3]. Accordingly, this calculation technique requires less computing time, which has greatly contributed to its popularization over the last fifty years [2].

In order to exploit this approach, the properties of a polyatomic system have to be entirely described by the electronic density. In analogy to the Hamiltonian in quantum-chemistry (**equation 1**), the electronic density  $\rho(\mathbf{r})$  gives access to (1) the total electron number of the system ( $N$ ), (2) the atomic charge ( $Z_a$ ) and (3) the position of the nuclei ( $\mathbf{R}_a$ ).

$$H = \underbrace{\sum_{j=1}^N (-\nabla^2_j)}_{\text{Electron kinetic energy}} + \underbrace{\sum_{i=1}^n (-\nabla^2_i)}_{\text{Nuclei Kinetic energy}} + \underbrace{\sum_{j=1}^N \sum_{i=1}^n \left( -\frac{Z_j}{r_{ij}} \right)}_{\text{Electrostatic attraction between nuclei and electrons}} + \underbrace{\frac{1}{2} \sum_{i=1}^n \sum_{j=1}^n \left( \frac{1}{r_{ij}} \right)}_{\text{Electrostatic repulsion between electrons}} + \underbrace{\sum_{j=1}^N \sum_{i=1}^n \left( \frac{Z_i Z_j}{r_{ij}} \right)}_{\text{Electrostatic repulsion between nuclei}}$$

**Equation 1**

Thereby,  $N$  can be obtained by integrating the electronic density over space  $\int \rho(\mathbf{r}) \cdot d(\mathbf{r}) = N$ . The position of one nucleus ( $\mathbf{R}_a$ ) corresponds to a maximum value of the distribution of  $\rho(\mathbf{r})$  while the atomic charge  $Z_a$  can be determined by the values of  $\rho(\mathbf{r})$  at the position of the atoms.

## 2.1 The Thomas-Fermi Model

The first model using the DFT approach is the Thomas and Fermi model proposed in 1927. It affords an alternative way to resolve the Schrödinger equation by expressing the energy as a function of the electronic density [4].

In this model, Thomas and Fermi (TF) split the system energy ( $E_{TF}$ ) in a kinetic and potential parts:

$$E_{TF}[\rho(r)] = \frac{3}{10} (3\pi^2)^{2/3} \int \rho^{5/3}(r) d(r) - Z \int \frac{\rho(r)}{r} d(r) + \iint \frac{\rho(r_1)\rho(r_2)}{r_{12}} dr_1 dr_2$$

**Equation 2**

In this **equation 2**, the **first term** gathers the kinetic energies of all electrons in the system (as estimated for a homogeneous electron gas) while the **second** and **third** terms correspond respectively to the nucleus-electron and electron-electron interactions that have been treated in a classic way. The principal asset of this equation is to introduce the electronic density as a parameter for all different terms. Nevertheless, the exchange/correlation energetic terms are completely ignored, which leads to dramatic errors when trying to determine the fundamental energy level of molecules.

The exchange-correlation term plays a critical role in the determination of the properties of molecules and has been introduced in the Kohn-Sham method (see section II.5.3).

## 2.2 The Hohenberg and Kohn Theorems

Pierre Hohenberg and Walter Kohn have published the two fundamental theorems validating the DFT method in 1964 [5].

The **first theorem** demonstrates that the electronic density  $\rho(r)$  is a uniquely defined parameter needed to evaluate all energetic terms of the Hamiltonian operator of a polyatomic system. Therefore, the fundamental state properties of a polyelectronic system can be

uniquely determined using the electronic density. Accordingly, the ground state energy ( $E_0$ ) is given by:

$$E_0 = T[\rho_0] + E_{Ne}[\rho_0] + E_{ee}[\rho_0]$$

**Equation 3**

Where  $\rho_0$  is the ground-state electronic density,  $T$  is the kinetic energy and  $E_{Ne}$  contains the nucleus-electron interactions while the term  $E_{ee}$  defines the electron-electron interactions in the system.

The term  $E_{Ne}[\rho_0]$  can be expressed as a function of  $\rho_0$  by  $E_{Ne} = \int v_{ext}(r)\rho_0 dr$  where  $v_{ext}$  is the external potential that only depends on the position and charge of the nuclei. The terms  $T[\rho_0]$  and  $E_{ee}[\rho_0]$  can be combined to define the Hohenberg-Kohn universal functional (noted  $F_{HK}$ ). Thereby, **equation 3** becomes **equation 4**:

$$E_0[\rho_0] = \int v_{ext}(r)\rho_0 dr + F_{HK}[\rho_0]$$

**Equation 4**

The **second theorem** proves that for a given electronic density  $\rho_{test}(r) \geq 0$  such as  $\int \rho(r) dr = N$ , the result for the system energy evaluation will always be:

$$E_0 \leq E_{\rho_{test}(r)}$$

**Equation 5**

Where  $E_0$  corresponds to the exact fundamental state energy and  $E_{\rho_{test}}$  defines the energy of the system for the tested electronic density  $\rho_{test}(r)$ .

This theorem demonstrates that the  $F_{HK}[\rho(r)]$  functional gives the fundamental energy level of a system ( $E_0$ ) only when the tested density ( $\rho_{test}(r)$ ) is exactly the fundamental state electronic density  $\rho_0$ .

Those two principles resume the philosophy hidden behind DFT, proving that the energy of a polyatomic system can be obtained using the electronic density.

Therefore, the purpose of DFT is to find the electronic density that will minimize the energy of the system. Nevertheless, this electronic density must satisfy three constraints:

- $\rho(r)$  has to be superior to zero over the whole space.
- The integration of  $\rho(r)$  over space must equal the number of electrons  $N$  of the system.
- No discontinuity !
- The DFT method has to verify the variation theorem (**equation 6**)

$$E_0 = \min \left[ \int v_{ext}(r)\rho(r)dr + F_{HK}\rho(r) \right] \quad (\text{equation 6})$$

In order to determine the electronic density in the fundamental state, a method based on the Hohenberg and Kohn theorems has been developed. This method is named the Kohn-Sham method and has been introduced in 1965 [6].

### 2.3 The Kohn-Sham Method

The electron-electron interaction term  $E_{ee}$  can be divided in two different terms: (1) a classic Coulomb term  $J(\rho)$  with a defined analytical form and (2) a non-classic part  $E_{ncl}(\rho)$  that contains the exchange interactions and the correlation effects (**equation 7**).

$$E_{ee}[\rho] = \frac{1}{2} \int \int \frac{\rho(r_i)\rho(r_j)}{r_{ij}} dr_i dr_j + E_{ncl}(\rho) = J(\rho) + E_{ncl}(\rho)$$

**Equation 7**

At this point, two terms are still problematic: the kinetic energy term  $T$  (**equation 3**) and the non-classical term (**equation 7**).

The method proposed by Kohn and Sham circumvents those problematics. Indeed, the method consists in dealing with the system in a “non-interacting” referential, where there are no electron-electron interactions ( $E_{ee}$ ). This fictitious referential possesses the same electronic density as the real system; the fictitious kinetic energy term (named  $T_s$ ) will be very easy to estimate but will differ from the real kinetic energy  $T$ .



The following relation gives the kinetic energy ( $T_S$ ) of those non-interacting particles:

$$T_S = -\frac{1}{2} \sum_i^N \langle \phi_i(r) | \nabla^2 | \phi_i(r) \rangle$$

**Equation 8**

Where  $\phi_i(r)$  are the spin-orbitals of the non-interacting system also called the Kohn-Sham orbitals.

Again, this energy does not correspond to the real system energy. Therefore, the difference between  $T$  and  $T_S$  (noted  $T_C$ ) is implemented within the non-classical term  $E_{nc}(\rho)$  in **equation 7** to give rise to **equation 9**, leading to the Kohn-Sham functional ( $F_{KS}$ ):

$$F_{KS}[\rho(r)] = T_S[\rho(r)] + J[\rho(r)] + E_{XC}[\rho(r)]$$

**Equation 9**

Where  $E_{XC}[\rho(r)]$ , called the **exchange/correlation energy**, is the sum of the non-classical electronic term and the residual kinetic energy  $T_C[\rho(r)]$  neglected before. The main challenge of the DFT method is to evaluate this energetic contribution. In DFT, these different terms are estimated with the Kohn-Sham orbitals obtained by solving the one-electron equations of the fictitious system:

$$F_{KS}[\phi_i(r)] = \varepsilon_i[\phi_i(r)]$$

**Equation 10**

With  $F_{KS}$  the one-electron Kohn-Sham operator described as:

$$F_{KS} = -\frac{1}{2} \nabla^2 + V_S(r)$$

**Equation 11**

$$\text{And } V_S(r) = \left[ \int \frac{\rho(r_2)}{r_{12}} dr_2 + V_{XC}(r_1) - \sum_A^N \frac{Z_A}{r_{1A}} \right]$$

**Equation 12**

The expression of  $V_s$  is obtained by imposing the same ground-state electronic density in the real and fictitious systems and the variational theorem to be operative in both systems.

The KS equations are solved in the LCAO approximation (Linear Combination of Atomic Orbitals) by an iterative process, which will provide after convergence the approached  $E_0$  and the energy and shape of the Kohn-Sham orbitals of the system ( $\phi_i(r)$ ).

The obtained energy  $E(\rho(r))$  is not exactly equal to  $E_0$  since the exchange/correlation potential ( $V_{xc}$ ) is always approximated following different methods.

## 2.4 Exchange-correlation Energy Assessment methods

### 2.4.1 Local Density Approximation (LDA)

This approach handles the electronic cloud of the system under study as a uniform electron gas over space. The use of this approximation is therefore validated for systems characterized by a **large electronic density and a weak polarizability** [6]. Conversely, a system characterized by a non-uniform electronic density such as molecules will be poorly described with this approximation.

The expression of the exchange-correlation term is given by:

$$E_{XC}^{LDA} = \int \rho(r) \varepsilon_{XC}(\rho(r)) dr$$

**Equation 13**

Where  $\varepsilon_{XC}(\rho(r))$  is the exchange-correlation potential of an electron that belongs to the uniform gas of density  $\rho(r)$ . It can be divided in two energetic contributions: one correlation term  $\varepsilon_c(\rho(r))$  and one exchange term  $\varepsilon_x(\rho(r))$ .

The LSDA method (Local Spin Density Approximation) is an upgraded version of the LDA method. This method differs from the LDA by taking into account two different electronic densities: one for the electrons of spin  $\alpha$  (up), and another one for the electrons of spin  $\beta$  (down).

Those approaches lay the ground for the elaboration of more accurate approximation methods allowing for a better evaluation of the exchange-correlation term.

#### 2.4.2 General Gradient Approximation (GGA)

The consideration of a homogenous electron gas is not always a good approximation since the electronic density of a system might dramatically change over space. Thereby, a correction term has to be introduced to the LDA approach.

The GGA approach introduces a density gradient (noted  $\nabla\rho(r)$ ) which reflects the heterogeneity of the system under study. Accordingly, a better estimation of the exchange-correlation term  $E_{XC}$  is given by the next equation:

$$E_{XC}^{GGA} = E_X^{GGA} + E_C^{GGA} = \int f(\rho_\alpha, \rho_\beta, \nabla\rho_\alpha, \nabla\rho_\beta) dr$$

**Equation 14**

The correction factor including the density gradient is handled in both the exchange energy ( $E_x$ ) and correlation energy ( $E_c$ ).

#### 2.4.3 Hybrid Functional

The hybrid functionals are based on a different approach regarding the description of the exchange-correlation energy. In this approach, the exchange term, which dominates over the correlation term, will be determined using both DFT and Hartree-Fock calculation methods since the exchange term is exact in the Hartree-Fock theory. Thereby, at the opposite of the two previous methods, hybrid functionals will handle the energetic contributions separately. On the one hand, the correlation energy  $E_c$  will be determined using the DFT method by mixing LDA and GGA terms. On the other hand, the exchange energy  $E_x$  will be determined both by Hartree-Fock and DFT methods

$$E_{XC} = [\alpha E_X^{HF} + (1 - \alpha) E_X^{DFT}] + E_C^{DFT}$$

**Equation 15**

Where  $\alpha$  and  $(1-\alpha)$  define respectively the fractions of the exchange energetic terms calculated either by the Hartree-Fock or DFT method.

## 2.5 The B97D Functional

The B97D functional, used during this thesis, is a GGA type functional. This functional has been introduced by the work of Axel Becke in 1997 [7].

The letter “D” indicates that the dispersion forces are explicitly taken into account. They are essential to study supramolecular associations such as those under study in this thesis. The energy of a system treated with this type of functional is expressed as two terms :

$$E_{DFT-D} = E_{KS-DFT} + E_{disp}$$

**Equation 16**

The first energetic term of **equation 16** is obtained using the Kohn-Sham method presented above (see section 5.3) while the second term  $E_{disp}$  corresponds to a correction due to dispersion forces calculated as a post treatment.

### 2.5.1 Description of the B97D energetic terms

In the functional B97D, the exchange-correlation energy is given by **equation 17**:

$$E_{XC} = E_X + E_{C\alpha\beta} + \sum_{\sigma} E_{C\sigma\sigma}$$

**Equation 17**

Where  $\sigma$  is the electron spin ( $\alpha$  or  $\beta$ ) and the terms  $E_X$  and  $E_C$  correspond respectively to the exchange and correlation terms obtained using the GGA method. Each term is defined as followed:

$$E_X^{GGA} = \sum_{\sigma} \int e_{X\sigma}^{LSDA}(\rho_{\sigma}) g X_{\sigma} (s_{\sigma}^2) d^3r$$

$$E_{C\alpha\beta}^{GGA} = \int e_{C\alpha\beta}^{LSDA}(\rho_{\alpha}, \rho_{\beta}) g_{C\alpha\beta} (s_{\alpha\beta}^2) d^3r$$

$$E_{C\sigma\sigma}^{GGA} = \int e_{C\sigma\sigma}^{LSDA}(\rho_{\sigma}) g_{C\sigma\sigma} (s_{\sigma}^2) d^3r$$

**Equation 18-20**

The term  $e^{LSDA}(\rho)$  of **equation 18 to 20** corresponds to the exchange and correlation potential of an uniform electron gas obtained using the LSDA method. The term  $s_{\alpha\beta}^2$  is given by the relation  $s_{\alpha\beta}^2 = \frac{1}{2}(s_{\alpha}^2 + s_{\beta}^2)$  while the parameter  $g$  corresponds to the gradient correction factor and is characteristic of the B97 functional parametrization. This  $g$  parameter is obtained by a series expansion of a variable  $\mu(s^2)$  such as:

$$g(s^2) = \sum_{j=0}^k c_j \mu^j (s_{\sigma}^2)$$

**Equation 21**

Where  $s_{\sigma}$  is reduced spin density gradient given by **equation 22**:

$$s_{\sigma} = \frac{\nabla \rho_0}{\rho_0^{4/3}}$$

**Equation 22**

Beck's work demonstrated that the best value for the  $k$  parameter in **equation 21** is  $k=2$  (three terms in the calculation series) [8]. This value represents the best compromise between a good robustness and a good flexibility of the B97 functional. For the determination of the  $c$  parameters, the least-square method is used [9] and the only parameter that remains undefined for each  $E_{XC}$  term is the parameter  $g$  (**equation 18-20**).

The three mathematical forms of  $g$  for each term of  $E_{XC}$  are (**equation, 23-25**):

$$\mu_{X\sigma}(s_{\sigma}^2) = \frac{0.004 s_{\sigma}^2}{1 + 0.004 s_{\sigma}^2}$$

$$\mu_{C\alpha\beta}(s_{\alpha\beta}^2) = \frac{0.006 s_{av}^2}{1 + 0.006 s_{av}^2}$$

$$\mu_{C\sigma\sigma}(s_{\sigma}^2) = \frac{0.2 s_{\sigma}^2}{1 + 0.2 s_{\sigma}^2}$$

**Equation 23-25**

### 2.5.2 Description of the dispersion forces energetic term

The energetic term that handles the dispersions forces is an empirical correction term. Its expression is given by **equation 26**:

$$E_{disp} = -S_6 \sum_{i=1}^{N_{at}-1} \sum_{j=i+1}^{N_{at}} \frac{C_6^{ij}}{R_{ij}^6} f_{dmp}(R_{ij})$$

**Equation 26**

Where  $N_{at}$  is the atom number of the system under study,  $C_6^{ij}$  is the dispersion coefficient for the atoms pair  $ij$ ,  $S_6$  is a functional intrinsic factor and  $R_{ij}$  is the interatomic distance between the atoms  $i$  and  $j$ . This expression of the dispersion energy is built to take into account the contributions of both attraction and repulsion forces that exist for each pair of atoms. The last term  $f_{dmp}(R_{ij})$  is a buffering function that prevents the physical aberrations when two atoms are too close to one another:

$$f_{dmp}(R_{ij}) = \frac{1}{1 + e^{-d(\frac{R_{ij}}{R_r}-1)}}$$

**Equation 27**

In this equation,  $R_r$  corresponds to the summation of the van Der Waals atomic radii of the atoms  $i$  and  $j$ .

## References

1. Castro-Perez J., Roddy T.P., Nibbering N.M.M., Shah V., McLaren D.G., Previs S., Attygalle A.B., Herath K., Chen Z., Wang S.P., *J. Am. Soc. Mass Spectrom.* 2011; 22: 1552–1567.
2. S.F. Sousa, P.A. Fernandes, M.J. Ramos, *J. Phys. Chem. A* 2007; 111 : 10439-10452.
3. W. Koch, M.C. Holthausen, “A Chemist’s Guide to Density Functional Theory, second edition”, 2001, Wiley.
4. E. Fermi, *Rend. Accad.* 1927; 6: 602-607.
5. P. Hohenberg, W. Kohn, *Phys. Rev. B.* 1964; 136: 864-871.
6. W. Kohn, L. Sham, *Phys. Rev. A.* 1965; 140: 1133-1138.
7. A.D. Becke, *J. Chem. Phys.* 1997; 107: 8554-8560.
8. H.L. Schmider, A.D. Becke, *J. Chem. Phys.* 1998; 108: 9624-9631.
9. S. Grimme, *J. of Computational Chemistry*, 2006; 27: 1787-1799.

## Accomplishments

### Publications

*Homotropic allostery: In-depth structural analysis of the gas-phase noncovalent complexes associating a double-cavity cucurbit[n]uril-type host and size-selected protonated amino compounds.*

V. Lemaur, G. Carroy, F. Poussigues, F. Chirot, J. De Winter, L. Isaacs, P. Dugourd, J. Cornil, P. Gerbaux,  
ChemPlusChem. 2013, 78, 959-969.

*Influence of Equilibration Time in Solution on the Inclusion/Exclusion Topology Ratio of Host-Guest Complexes Probed by Ion Mobility and Collision-Induced Dissociation.*

G. Carroy, C. Daxhelet, V. Lemaur, J. De Winter, E. De Pauw, J. Cornil, P. Gerbaux,  
Chem. Eur. J., 2016, 22, 4528–4534 (**Hot paper**).

*Energy-resolved collision-induced dissociation of non-covalent ions: charge- and guest-dependence of decomplexation reaction efficiencies.*

G. Carroy, V. Lemaur, J. De Winter, L. Isaacs, E. De Pauw, J. Cornil, P. Gerbaux,  
Phys. Chem. Chem. Phys. 2016, 18, 12557-12568.

*Flying cages in Traveling Wave Ion Mobility: insidious effect of the instrumental parameters on the topology of the host-guest complexes.*

G. Carroy, V. Lemaur, C. Henaumont, S. Laurent, J. De Winter, E. De Pauw, J. Cornil, P. Gerbaux.



In press, 2017.

## Oral communications

*Homotropic Allostery: In-Depth Structural Analysis of the Gas-Phase Noncovalent Complexes Associating a Double-Cavity Cucurbit[n]uril-Type Host and Size- Selected Protonated Amino Compounds.*

NVMS (50<sup>th</sup> anniversary)

Rolduc Abdij (NL) 04/14/2014

*Combining mass spectrometry and computational chemistry to study non covalent interactions in gas phase.*

EDT-CHIM

ULB (BE) 11/05/2014

*Flying cages in Traveling Wave Ion Mobility: insidious effect of the instrumental parameters on the topology of the host-guest complexes.*

IMMS 2017 (35<sup>th</sup> edition)

Aussois (FR) 05/09/2017

*Generalities over the study of non-covalent interactions by the association of mass spectrometry methods and computational chemistry.*

Research day of the 'Institut de Recherche en Sciences et Ingénierie des Matériaux'

Mons (BE) 07/04/2017

## Prices

### Poster:

*Supramolecular mass spectrometry: association of MS methods to computational chemistry to access, at a molecular level, systems relevant to host-guest chemistry.*

BSMS 2014

GSK Company (BE) 11/07/2014

Oral communication:

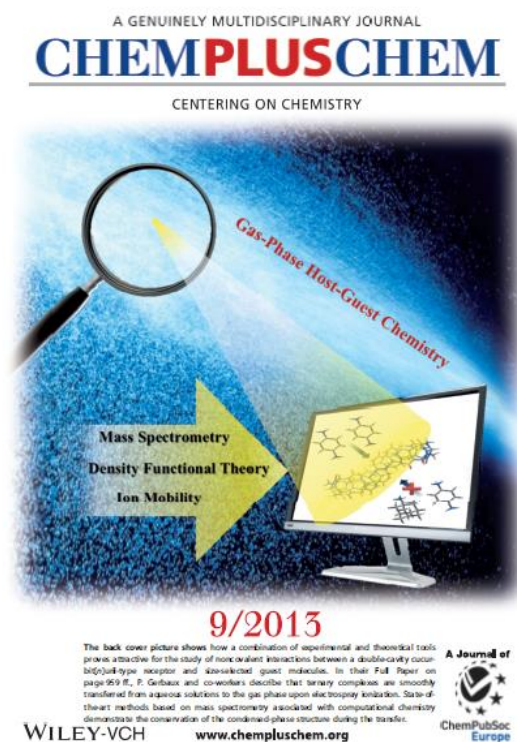
*Flying cages in Traveling Wave Ion Mobility: insidious effect of the instrumental parameters on the topology of the host-guest complexes.*

IMMS 2017 (35<sup>th</sup> edition)

Aussois (FR) 05/09/2017

Other

Cover:



Teaser:

[http://www.chemistryviews.org/details/ezine/5081761/Molecular Containers in the Gas Phase.html](http://www.chemistryviews.org/details/ezine/5081761/Molecular_Containers_in_the_Gas_Phase.html)